# Proceedings[1] of the conference on

# Compact Stars in the QCD Phase Diagram

August 2001

Nordic Institute for Theoretical Physics
(NORDITA)

Editors
R. Ouyed and F. Sannino

Organized and sponsored by NORDITA

[1]This volume was created using the LaTeX templates supplied to us by the eConf committee. The corresponding electronic version is accessible at "*www.slac.stanford.edu/econf/*".

# Foreword

This is an important collection of short articles covering the most recent theoretical ideas about the dense matter that may occupy the centers of compact stars. It is based on lectures presented at a small conference held in Copenhagen at the Nordic Institute for Theoretical Physics in the same small hall that so many famous people have gathered in ever since the days of Niels Bohr.

I wish I had been there to hear them. The novelty and sophistication of ideas for dense phases of matter is quite astonishing. And neutron stars and other compact objects may be the only laboratory available for their exploration, providing not only the high density, but also time enough and temperature enough (and not too much) for phenomena associated with these phases to develop to a potentially observable extent.

Of course, there's the rub. Many of the ideas are still in early stages of gestation and it will take some time to think what observable consequences will flow from them. Already a few have been developed and others are on the drawing boards. I am sure that this volume will speed the process.

Norman K. Glendenning
Senior Scientist Emeritus
Lawrence Berkeley National Laboratory

## Acknowledgements

First and foremost, we would like to thank the staff at NORDITA who helped with the many tasks involved in making this meeting a success. In particular, we would very much like to thank Dmitri Diakonov, Axel Brandenburg, Nils Marchal, and Paul Hoyer for their valuable contributions. Our special thanks go to Anna Maria Rey (the conference secretary) whose help and patience are inestimable. No meeting can run without sponsors, we therefore express our profound gratitude to our sponsor, NORDITA.

We are deeply indebted to our Scientific Organizing Committee: R. Casalbuoni, R. Gatto, N. K. Glendenning, R. L. Jaffe, J. Madsen, C. J. Pethick, T. Piran, K. Rajagopal, J. Schechter, F. Wilczek in supporting us at all stages of organization. We thank all the workshop participants for the stimulating atmosphere they fostered during the workshop and their contributions to the proceedings. Finally, we thank the econf committee which made the preparation of this formal book-length conference proceeding easier by providing us with the necessary LaTeX templates.

NORDITA, March 2002

R. Ouyed and F. Sannino
Organizing Committee

# Conference Organization

**International Advisory Committee**

| | |
|---|---|
| R. Casalbuoni | Firenze |
| R. Gatto | Geneva |
| N. K. Glendenning | Berkeley |
| R. L. Jaffe | MIT |
| J. Madsen | Aarhus |
| C. J. Pethick | NORDITA |
| T. Piran | Tel Aviv |
| K. Rajagopal | MIT |
| J. Schechter | Syracuse |
| F. Wilczek | MIT |

**Local Organizing Committee**

| | |
|---|---|
| R. Ouyed | NORDITA |
| F. Sannino | NORDITA |

# CONTENTS

## Color Superconductivity in Compact Stars



## The Gamma Ray Burst Connection

**Date 1930** – Left to right (first row) Klein, Oskar Benjamin - Bohr, Niels - Heisenberg, Werner Karl - Pauli, Wolfgang - Gamow, George - Landau, Lev Davidovich - Kramers, Hendrik Anton - (second row) Waller, Ivar - Hein, Piet - Peierls, Rudolf Ernst - Heitler, Walter - Bloch, Felix - Ehrenfest, Tanja - Colby, Walter Francis - Teller, Edward - (third row) Rice, Oscar - Wintner, Aurel - Moller, Christian - Pihl, Mogens - Hansen, A.J. – **Credit**: the Niels Bohr Archive.

**Date 2001** – Left to right (first row) Staff, Jan Erling - Alford, Mark - Nielsen, Holger - Son, Dam Thanh – (second row) Sannino, Francesco - Ouyed, Rachid - Bombaci, Ignazio - Hong, Deog-Ki - Nyiri, Agnes - Schechter, Joseph - Casalbuoni, Roberto (third row) Thampan, Arun - Fredriksson, Sverker - Öztaş, Ahmet Mecit - Balberg, Shmulig - Nardulli, Giuseppe (fourth row) Dobler, Wolfgang - Hoyer, Paul - Carter, Greg - Mannarelli, Massimo, (fifth row) Usov, Vladimir - Marchal, Nils (hidden) - Takanishi,Yasutaka - Motylinski, Patrick - Madsen, Jes (back row) ??? - Nordlund, Aake - Weber, Fridolin - Schaefer, Wolfgang - Hsu, Steve - Larson, Jonas - Konar, Sushan - de Val Borro, Miguel (missing) Jorgensen, Michael svart - Horvath, Jorge - Pethick, Chris - Piran, Tsvi - Beloborodov, Andrei - Bjornsson, Gunnlaugur - Dmitri, Diakonov - Heiselberg, Henning - **photographer** - Brandenburg, Axel.

# Compact Stars in the QCD Phase Diagram

# From Neutron Stars to Quark Stars

# Neutron Star Masses, Radii and Equation of State

*Henning Heiselberg*
*NORDITA*
*Blegdamsvej 17*
*DK-2100 Copenhagen O, Denmark*

## 1 Introduction

We are closing in on neutron stars both observationally and theoretically. Observationally, a number of masses (M) and a few radii (R) have been measured as well as a number of other properties. Theoretically, modern equation of states (EOS) are more reliable due to precision measurements of nucleon-nucleon interactions, detailed calculations of binding energies of light nuclei and nuclear matter which constrain three-body forces, inclusion of relativistic effects, improved many-body and Monte Carlo methods, etc.

Ultimately, we can exploit the one-to-one correspondence between the EOS and the mass-radius relation of cold stellar object:

$$P(\rho) \quad \Leftrightarrow \quad M(R) \tag{1}$$

Observing a range of neutron star M and R thus reveals the EOS (e.g., pressure P versus density $\rho$) of dense and cold hadronic matter. Possible phase transitions from nuclear matter to quark matter (either can also undergo superfluid transitions at certain densities and temperatures), hyperon matter, kaon or pion condensates, etc., would also be revealed by an anomalous/kinky function $P(\rho)$ and $M(R)$. The higher the order of the transition is, the smoother will $M(R)$ be and very accurate observations will thus be necessary. On the other hand, just one accurately measured neutron star mass and radius would already constrain the EOS significantly. Information on the EOS at high baryon densities and the presence or absence of phase transitions could guide us in solving QCD after decades of unsuccessful attempts.

In the following I shall give a brief account of the present status on neutron star observations and theory referring to [1, 2, 3, 4] for longer reviews. Subsequently, I shall attempt to recount the most likely possible phase transition in dense nuclear matter with emphasis on quark matter and its possible color superconducting states, as this is most relevant at this conference. Finally, I shall point to important developments expected in the near future.

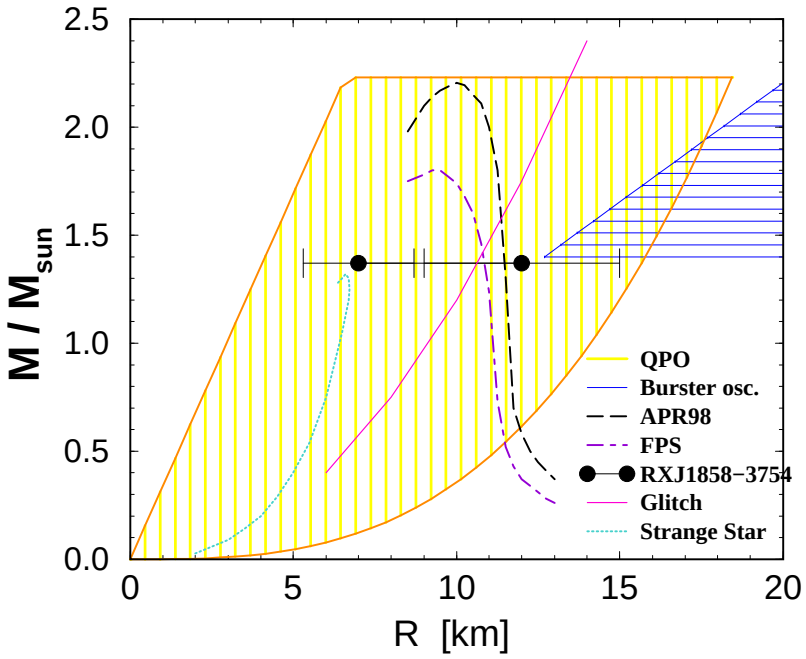


Figure 1: Neutron star masses vs. radius for modern [5] and FPS [6] EOS and strange stars [11]. The hatched areas represent the neutron star radii and masses allowed for orbital QPO frequencies 1060 Hz of 4U 1820-30 (vertical lines, [8, 9]) and for burster oscillations of 4U 1636-53 assuming $M \geq 1.4 M_\odot$ (horizontal lines, [10]) area. Models for glitches in the Vela pulsar constrain masses and radii [11] below the full line. The radii of RX J1856-3754 from Refs. [12, 13] assumes $M = 1.37 M_\odot$.

## 2 Observed neutron star masses

Only a few masses have been determined from the more than thousand neutron stars, that have been discovered so far:

**Binary pulsars:** Six double neutron star binaries are known so far, and all of them have masses in the surprisingly narrow range $1.36 \pm 0.08 M_\odot$ [14]. Neutron stars are estimated to have a binding energy of $\sim 10\%$ of their mass. Thus $\sim 1.5\ M_\odot$ of nuclei are needed to obtain a $1.35\ M_\odot$ star. It is suspicious that the Chandrasekhar mass (maximum mass before gravitational collapse sets in) for the iron core inside a large burning star is just around $\sim 1.5\ M_\odot$. It is therefore a tempting conclusion that the iron cores are the progenitors of neutron stars and that all neutron stars are simply produced with $M \simeq 1.35\ M_\odot$. Similarly, white dwarfs are formed in a narrow mass range around $M \simeq 0.6\ M_\odot$ whereas their Chandrasekhar mass is $M \simeq 1.35\ M_\odot$. The latter mass is probably reached by accretion and is responsible for supernova type

SN-1a used as standard candles in cosmology. Calculations of supernova explosions do, however, indicate that neutron stars should be formed with a wide range of masses and so the narrow binary pulsar mass range could be a selection effect in forming a double neutron star system. Whereas selection effects often are important in astrophysics the contrary is the case in particle physics, where one does not believe in accidents but invoke some underlying symmetry.

Millisecond binary pulsars with white dwarf companions have less precise mass determination. Promising progress is reported, e.g., for PSR J0437-4715 [15] where a pulsar mass of $M = (1.58 \pm 0.18) M_\odot$ (error bars are $2\sigma$) is found.

**Vela X-1** and **Cygnus X-2** are X-ray binary pulsar/burster with high/low mass companions respectively. From X-ray pulse delays, optical radial velocities and constraints from X-ray eclipse, their masses have been determined. For Vela X-1: $M = 1.87^{+0.23}_{-0.17}\ M_\odot$ [16], and for Cygnus X-2: $M = 1.8 \pm 0.4 M_\odot$ [17].

**QPO's** are neutron stars emitting X-ray's at frequencies of the orbiting accreting matter. Such *quasi-periodic oscillations* (QPO) have been found in 12 binaries of neutron stars with low mass companions. If the QPO originate from the innermost stable orbit [8, 9] of the accreting matter, their observed values imply that the accreting neutron star has a mass $\simeq 2.3 M_\odot$ in the case of 4U 1820-30. If not, the QPO's constrain the EOS as shown in Fig. 1.

# 3 Observed neutron star radii

The small size of neutron stars makes it very difficult to observe them directly and measure their radius. Estimates have been obtained using quite different methods, which has the benefit that the systematic errors are also different.

**RX J1856.5-3754** is our nearest known neutron star. It is non-pulsating and almost thermally radiating. It has been studied recently with the Hubble space telescope by Walter et al. [18]. Its surface temperature is $T \simeq 57$ eV and its distance is, from parallax measurements and circumstantial evidence, about $d \sim 61$ pc. From the measured flux

$$F = \sigma_{SB} T^4 R^2 / d^2 \tag{2}$$

one obtains a radius of $R_\infty = R/\sqrt{1 - 2GM/R} \simeq 7$ km which is incompatible with almost any EOS. Kaplan et al. [19] have reanalysed the HST data and find only half the parallax and thus twice the distance and radius $R_\infty \simeq 15$ km corresponding to $R \simeq 12$ km for $M = 1.4 M_\odot$. Its age would be almost a million years which is compatible with standard modified URCA cooling. The spectrum is, however, suppressed in the optical part as compared to the X-rays. Recent more detailed analyses of the spectrum [12, 20] attempting to model the neutron star atmosphere and its absorption, as well as including magnetic fields does not improve the spectral

fit. A much better description is obtained from a two temperature model, i.e., a small hot spot and a colder area with a larger radius $\sim 9(d/61pc)$ km.

Gravitational lensing by our nearest neutron star may be observed in june 2003, when J1856.5-3754 will pass within $\sim 0.3$ arcseconds of a background star as it flies through space with proper motion of 0.332 arcseconds per year. According to [21] (see, however, [19]) it should just be possible to measure that the 26.5 magnitude background star moves by 0.6 milliarcseconds due to the gravitational field of the neutron star. This accuracy requires that the Hubble space telescope is extended with the Advanced Camera for Surveys. If possible, its mass could be derived and our nearest known neutron star would then also be the first one with both mass and radius determined.

**X-ray bursts** are thermonuclear explosions of accreted matter on the surface of neutron stars. After accumulating hydrogen on the surface for hours, pressure and temperature become sufficient to trigger a runaway thermonuclear explosion seen as an X-ray burst that lasts a few seconds [22]. Assuming that the burst spectra are black-body one can from the resulting temperature and measured flux estimate the neutron star radius if its distance is known. Often the radius is underestimated because only a hot spot emits or the spectrum contains a hard tail. Some bursts do, however, give radii of order $\sim 12$ km with a period of almost constant (Eddington) luminosities.

**Quescent neutron stars** are non-accreting X-ray binaries of which some are emitting thermally. Recently, a few quescent neutron stars have been discovered in galactic globular clusters where the distance is known relatively accurately. CXOU 132619.7-472910.8 in NGC 5139 has $T = 66 \pm 5$ eV and $R_\infty = 14.3 \pm 2.1$ km (90% confidence limit) and similar radii although with larger uncertainties are obtained from half a dozen other quescent neutron stars [23].

**Burst oscillations** in the X-ray flux during the first seconds of the bursts have recently been exploited to determine the compactness or redshift $M/R$. Whereas the average amplitude increases with the growing size of the hot spot, the amplitude is strongly modulated by the rotational period of the neutron star. The flux does not completely disappear when the hot spot is on the back side due to bending of the light in the gravitational field. This way $M/R < 0.16$ can be extracted [10] for 4U 1636-53 and a radius $R > 12 - 13$ km is obtained for a $M = 1.4M_\odot$ neutron star (see Fig. 1). Corrections from aberration, doppler shifts, etc. are being investigated. Yet, the oscillation analyses is another new promising method by which we can obtain neutron star masses and radii.

**Absorption lines** in the neutron star photospheres should be detectable with the spectrographs on board Chandra and XMM. The gravitational redshift and pressure broadening of absorption lines determine $M/R$ and $M/R^2$ respectively and would thus complement other mass and radius information. First results were, however, disappointing. Only in RX J1856.5-3754 were there indications for one or two lines

[13] but higher resolution is required and will come with future observation time.

# 4 Modern equation of states of dense matter

The relation between $M(R)$ and $P(\rho)$ is often presented (in particular by observers) by a wide variety of curves calculated from "old" EOS thus implying that one can get anything from theory. This is very unfair as many old EOS's are inconsistent with known nucleon-nucleon interactions and/or saturation density and binding energy of nuclei/nuclear matter and should therefore not be taken seriously.

Modern microscopic EOS's are actually converging [4, 3]. The NN interaction is now well determined and constrain potential models leaving only minor differences. Relativistic effects have been included and current scattering experiments at intermediate energies will determine the NN interactions at higher momenta relevant for higher densities. Three-body interactions can be constrained in order to fit nuclear binding and saturation density as well as binding energies of light nuclei up to $A \leq 8$. Many-body and Monte Carlo techniques are now much more accurate. The resulting "modern" EOS [5] are quite reliable up to a few times nuclear saturation densities. Above they are expected to break down but can be constrained by causality conditions. It is boldly predicted [5] that neutron stars in the mass range $M \sim 0.8-1.8M_\odot$ all have radius just around $R \simeq 11.5$ km (see Fig. 1).

The uncertainties in the EOS at densities $\rho \gtrsim 3\rho_0$ affect $M(R)$ for the heavy neutron stars only. By making the EOS stiffer at high densities in a smooth way, the maximum mass can increase up to $M \lesssim 2.0-2.3M_\odot$ [4] but not much higher due to the causality ($c_s < c$) condition. Rotation can increase it by $\sim 10\%$ for the millisecond pulsars.

Phase transitions generally soften the EOS and lower the maximum mass. If the $M = 2.25M_\odot$ mass in 4U 1820-30 stands this would rule out any major phase transition and allow only the stiffest EOS.

Many other phase transitions in neutron stars have been considered. It is expected that superfluid phases of neutrons and protons exist at least in certain density regions at low temperatures although $T_c$ have not been calculated reliably for strongly interacting and correlated nuclear matter. At typical neutron star densities neutrons and protons are superfluid as well due to $^1S_0$ and, in the case of protons, also $^3P_2$ pairing [4]. These superfluid and superconducting components will have drastically different transport properties than normal Fermi liquids. Generally the resistance, specific heat, viscosities, cooling, etc. are suppressed by factors of order $\sim \exp(-\Delta_i/T)$, where $\Delta_i$ is the gap of quarks, nucleons or electrons. A superfluid neutron gas in the inner crust is assumed in the description of glitches [11] and provides constraints on the EOS (see Fig. 1).

Eventually at very high densities nucleon degrees of freedom must be replaced by quark ones but it is not known whether core densities of neutron stars are sufficient.

Such quark stars will be discussed in the following section.

More speculative phases are $\pi^0$, $\pi^-$ and $K^-$ condensates as well as hyperons ($\Sigma^-$, $\Lambda$,...). In [5] a condensate of virtual $\pi^0$ is found in a narrow density interval due to strong tensor correlations. The $K^-$ energy can be calculated at low densities and a naive extrapolation would lead to condensate at high densities $\rho \gtrsim 4\rho_0$. However, correlations in nuclear matter invalidates such an extrapolation and makes a $K^-$ condensate unlikely [3]. Hyperons are found to appear at rather low densities $\rho \gtrsim 2-3\rho_0$ in a number of models [25]. Due to limited information on hyperon-nucleon two- and three-body interactions one cannot exclude the presence of hyperons in cores of neutron stars but their effect on the binding energy and thus the EOS is minor whereas their effect on $\mu_e$ could be substantial [3].

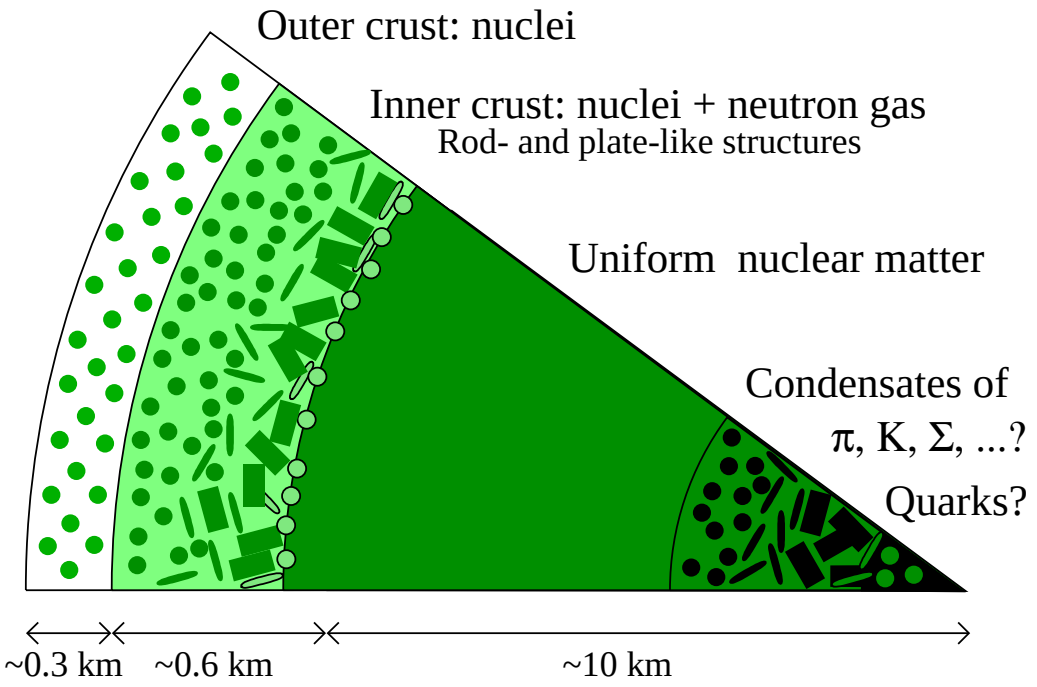


Figure 2: Cross section of a $\sim 1.4 M_\odot$ neutron star. The $\sim 1$ km thick crust consist of neutron rich nuclei in a lattice and a uniform background of electrons and, in the inner crust, also a neutron gas. The interior of the neutron star contains a nuclear liquid of mainly neutrons and $\sim 10\%$ protons at densities above nuclear matter density $n_0$ increasing towards the center. Here pressures and densities may be sufficiently high that the dense cold strongly interacting matter undergoes phase transitions to, e.g., quark or hyperon matter or pion or kaon condensates appear. Typical sizes of the nuclear and quark matter structures are $\sim 10^{-14}$ m but have been scaled up to be seen.

# 5 Quark stars

Natures marvelous variety of EOS's results in the existence of several different stable stellar objects all around one solar mass. These can be ordinary stars, white dwarfs, neutron stars, black holes - and possibly also quark stars. Quark stars come in several categories depending on the details of the nuclear to quark matter phase transition:

- The pure quark stars also called "strange" stars consist of up, down and strange quarks with electrons to fulfil charge neutrality. Possibly a crust of nuclei is suspended above the surface of the quark star. In simple bag model EOS a rather low bag constant and strange quark mass is required to make strange stars and strangelets. If the SAX J1808.4-3658 really has $R \simeq 6$ km based on accretion in magnetic fields [11] or RX J1856-1754 has $R \simeq 7$ km from the one-temperature fit in Ref. [12] that would indicate strange stars rather than normal neutron stars.

- Hybrid stars have a core of quark matter and a mantle of nuclear matter. The quark core size depends on the EOS and vanishes for large bag constants leading to a normal (nucleons only) neutron star.

- Mixed stars have a mixed phase of nuclear and quark matter over a range of density or radius. The mixed phase appear in two-component systems, where the two components: neutrons and protons or up and down quarks [26]. It is, however, required that the interface tension is sufficiently small so that the surface and Coulomb energies of the associated structures are small [27]. If not, a hybrid star results.

**A mixed phase** of quark and nuclear matter has lower energy per baryon at a wide range of densities [26] if the Coulomb and surface energies associated with the structures are sufficiently small [27, 4]. The mixed phase will then consist of two coexisting phases of nuclear and quark matter in droplet, rod- or plate-like structures (see Fig. 2) in a continuous background of electrons much like the mixed phase of nuclear matter and a neutron gas in the inner crust of neutron stars [28]. Another requirement for a mixed phase is that the length scales of such structures must be shorter than typical screening lengths of electrons, protons and quarks.

In the mixed phase the nuclear and quark matter will be positively and negatively charged respectively. $\beta$-equilibrium determines the chemical potentials and densities in the coexisting phases. Total charge neutrality

$$n_e = (1-f)n_p + f(\frac{2}{3}n_u - \frac{1}{3}n_d - \frac{1}{3}n_s)\,, \tag{3}$$

where $n_p$ is the proton density, determines the "filling fraction" $f$, i.e. the fraction of the volume filled by quark matter. For pure nuclear matter, $f = 0$, the nuclear

symmetry energy can force the electron chemical potential above $\sim 100$ MeV at a few times normal nuclear matter densities. With increasing filling fraction, however, negative charged droplets of quark matter replace some of the electrons and $\mu_e$ decreases. With increasing density and filling fraction it drops to its minimum value given $\mu_e = m_s^2/4\mu$ corresponding to pure quark matter, $f = 1$.

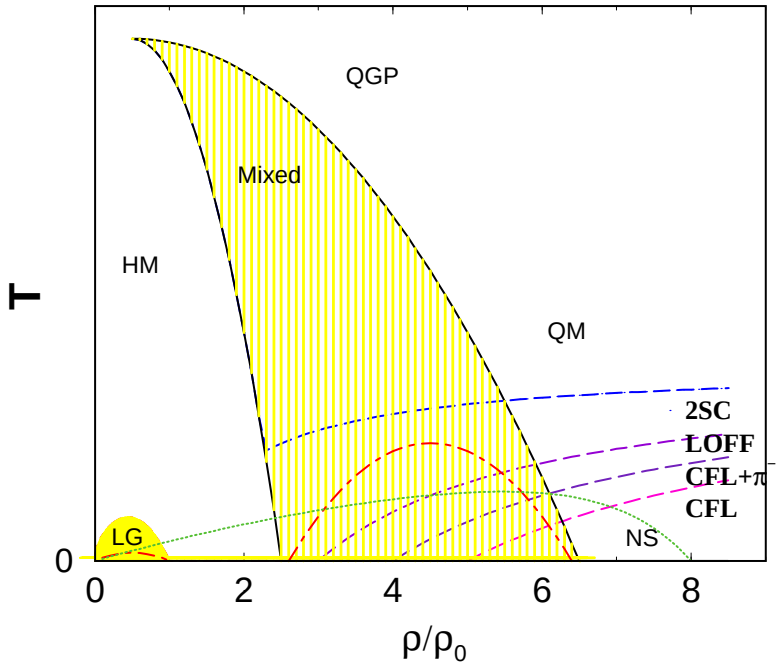


Figure 3: Sketch of the QCD phase diagram, temperature vs. baryon density *in neutron star matter*, i.e. charge neutral and in $\beta$-equilibrium containing electrons. Hatched areas indicate mixed phases of hadronic matter (HM) and quark matter (QM/QGP) as well as the nuclear liquid-gas. Dash-dotted lines indicate melting temperatures of the lattices in the mixed phase. Dashed lines separate CSC phases that may appear (see text). The trajectory of neutron star core densities during formation is shown by dotted line and densities below it exist inside neutron stars.

# 6 Color superconductivity

If quark matter exists in neutron stars or is produced in heavy-ion collisions, a condensate of quark Cooper pairs may appear at low temperatures characterized by a BCS gap $\Delta$ usually referred to as color superconductivity (CSC) [29]. The appearance of a gap through color-flavor locking (CFL) requires the gap to exceed the difference

between the $u,d,s$ quark Fermi momenta, which is not the case for sufficiently large strange quark masses or for an appreciable electron chemical potential, $\mu_e$, which is present in neutron star matter as discussed in [32].

In neutron star matter $\beta$-equilibrium relates the quark and electron chemical potentials

$$\mu_d = \mu_s = \mu_u + \mu_e \,. \tag{4}$$

Temperatures are normally much smaller than typical Fermi energies in neutron stars.

The strange quark masses and electron chemical potentials stress the system in the direction of splitting the quark chemical potentials. The pairing interaction prefer overlapping quark Fermi surfaces. We shall investigate this competition in detail below. The case where interactions between quarks are strong and the effective pairing gaps is larger than $\Delta \gtrsim \sqrt{2}|\mu_e/2 - m_s^2/8\mu|$ was shown in [30] to favor the CFL phase.

If interactions are weak, the chemical potentials are then related to Fermi momenta by $\mu_i = \sqrt{m_i^2 + p_i^2}$. If the strange quark mass $m_s$ is much smaller than the quark chemical potentials, Eq. (4) implies a difference between the quark Fermi momenta

$$p_u - p_d = \mu_e \,, \tag{5}$$

$$p_u - p_s \simeq \frac{m_s^2}{2\mu} - \mu_e \,, \tag{6}$$

$$p_d - p_s \simeq \frac{m_s^2}{2\mu} \,, \tag{7}$$

where $\mu$ is an average quark chemical potential. Strange quark masses are estimated from low energy QCD $m_s \simeq 150 - 200$ MeV and typical quark chemical potentials are typically $\mu \simeq 400 - 600$ MeV for quark matter in neutron stars [4]. Consequently, $m_s^2/2\mu \simeq 10 - 25$ MeV.

The BCS gap equation has previously been solved for pure $u,d$ and $u,d,s$ quark matter ignoring electrons and $\beta$-equilibrium and the conditions for condensates of dicolor pairs (2CS) and CFL respectively were obtained. There are three 2CS conditions

$$\Delta \gtrsim |p_i - p_j| \,, \quad i\widetilde{\chi}_j^0 = u, d, s \,. \tag{8}$$

In bulk quark matter total charge neutrality of quarks and electrons and $\beta$-equilibrium require that $\mu_e \simeq m_s^2/4\mu$. In a mixed phase of quark and nuclear matter the electron chemical potential is a decreasing function from the value in pure $\beta$-equilibrium nuclear matter $\mu_e \sim 100 - 200$ MeV down to that for bulk quark matter (if the cores of neutron stars are very dense) $\mu_e \simeq m_s^2/4\mu \simeq 5 - 10$ MeV.

We can now give a qualitative picture of the various phases that strongly interacting matter undergoes as the density increases towards the center of a cold neutron star (see Fig. 3). The inner crust will undergo several transitions as the nuclear matter and neutron gas mixed phase change dimensionality via nuclei, rods, plates, tubes,

bubbles to nuclear matter in which the neutron and protons may be superfluid. If quark matter appears at higher densities in a mixed phase with nuclear matter those structures repeat again.

Inside the quark matter part of this mixed phase the CSC phase also changes with density or $\mu_e$ depending on the size of the effective pairing interaction $\Delta$ between two quarks *i,j* (see, e.g., [29, 33]).

- If the pairing is strong $\Delta \gtrsim \sqrt{2}|\mu_e/2 - m_s^2/8\mu|$ the CFL phase is favored and no electrons appear as was shown in [30]. This condition is not likely to be fulfilled in the mixed phase with low quark filling fraction, where $\mu_e$ may be of order $100 - 200$ MeV or larger.

- If $\mu_e/2 \gtrsim \Delta \gtrsim m_s^2/2\mu$ a number of CSC phases appear. In the beginning of the mixed phase ($f \sim 0$) only (7) fulfils (30) and we have a 2CS of *d,s* quarks. A 2CS of *u,s* quarks may, however, compete at larger filling. At the end of the mixed phase ($f \sim 1$) all (5,6,7) fulfil (30) resulting in CFL. In between a crystalline LOFF phase and a CFL phase with a $\pi^-$ condensate (analogous to the CFL-$K^0$ phase in [29]) may appear.

- If the pairing interaction is weak or the strange quark mass large such that $\Delta \lesssim m_s^2/4\mu$ a number of different CSC phases such as a 2CS of *u,s* quarks or CFL-K may appear as has been discussed in [29, 31].

In the mixed phase gaps may be affected by the finite size of the quark matter structures as is the case for nuclei. Also surface and Coulomb energies generally disfavors mixed phases.

The finite temperature extension of the competing phases, calculations of the critical temperatures and densities, order of the transitions, etc. for neutron star matter should be investigated further. Probably, the superfluid phases undergo a second order phase transition to the normal phase with increasing temperature at constant baryon density. However, transitions between competing phases might also occur as indicated in Fig. 3.

Temperatures in neutron stars, $T \lesssim 10^6 K \simeq 10^{-4}$ MeV after cooling, are typically much lower than lattice melting temperatures, $T_{melt} \simeq Z^2 e^2/170a$ where $a$ is the lattice spacing (see Fig. 3). Thus the quark matter structures would be solid frozen and the cores of neutron stars would be crystalline and possibly also CSC. Lattice vibration will couple electrons at the Fermi surface with opposite momenta and spins via phonons and lead to a "standard" BCS gap for electrons. The isotopic masses are similar but as densities and Debye frequencies are larger, we can expect considerably larger BCS gaps for electrons. The electrical superconductivy affect magnetic fields through the Meissner effect and magnetic field decay.

# 7 Outlook

A number of promising developments have been mentioned above that may provide new information on neutron star masses, radii, EOS and possible phase transitions in high density matter.

On the observational front more and better masses and radii are determined by a number of different methods (thus with different systematic errors). On the theoretical front the uncertainties in the EOS are reduced by improved two- and three-body forces, relativistic effects and manybody calculations leading to socalled modern EOS. A number of phase transitions are still possible at high densities and can lead to marvelous structured phases and condensates.

We can hope for additional information from other directions as well:

**Gamma ray bursters**. The discovery of afterglow in *Gamma Ray Bursters* (GRB) allows determination of their very high redshifts ($z \geq 1$). They imply that GRB have an enormous energy output $\sim 10^{53}$ ergs which requires some central engine more powerful than ordinary supernovae [23]. These could be a special class of type Ic supernova (*hypernovae*) where cores collapse to black holes, or binary neutron stars merging, or some major phase transition to, e.g., quark matter [35]. Also soft GRB may be explained by accretion on strange stars [36].

**Neutrinos** from the formation of a "proto-neutron star" will be detected from the predicted 1-3 supernovae explosions in our and neighboring galaxy per century. In the case of the recent 1987A in LMC 19 neutrinos were detected on earth and with the upgraded neutrino detectors many thousand neutrinos are expected. The neutrinos can test the SN models, the neutron star EOS and early cooling. During the first second rapid cooling takes place and a phase transitions to, e.g., quark matter or CSC may occur. This may result in a delayed neutrino blimps [37].

**Gravitational wave** ground based interferometic detectors currently under commission will improve sensitivity significantly. Detectable candidate sources are inspiralling binary neutron stars or black holes merging which may be responsible for gamma ray bursts. R-mode instabilities in rapidly rotating neutron stars may also be detectable [38, 39].

**Relativistic heavy-ion collisions** are probing the high temperature and low baryon density part of the QCD phase diagram at the opposite end to neutron stars. The phase transition from hadronic matter to a quark-gluon plasma is searched for though the transition may well be a smooth cross over. Some "anomalous" effects, i.e. deviations from predictions based on hadronic theory, have been found and are currently studied intensively at RHIC. It has been speculated that one might find a critical point at high temperatures which would then indicate that the smooth cross over changes to a first order transition at higher baryon densities. That would be valuable information for neutron stars although it would not tell at which density the transition would occur at low temperatures.

**Superfluidity in cold fermionic atomic systems** will, due to the rapid progress in cooling and trapping techniques, soon be discovered. The great advantage of atomic traps is that one can vary the number of particles, their density and interaction strength as well as the number of spin states, masses, etc. Measuring the size of the pairing gap and varying these parameters provides a testing ground for analytical calculations in the dilute or weakly interacting limit [40]. This would be very useful for gap calculations in neutron and nuclear matter as well as quark matter.

*The future* of neutron star observations looks bright as new windows are about to open. A new fleet of X- and Gamma-ray satellites have and will be launched. With upgraded ground based observatories and detectors for neutrinos and gravitational waves [39] our knowledge of neutron star properties will be greatly improved. Heavy-ion physics at RHIC and LHC may add further to our understanding of the QCD phase diagram.

Thanks to R. Ouyed and F. Sannino for organizing this conference and comments on the manuscript.

# References

[1] J.M. Lattimer and M. Prakash, Phys. Rep. **333**, 121 (2000).

[2] S. Balberg, S.L. Shapiro, astro-ph/0004317.

[3] H. Heiselberg and V.R. Pandharipande, Ann. Rev. Nucl. Part. sci. **50**, 481 (2000).

[4] H. Heiselberg and M. Hjorth-Jensen, Phys. Rep. **328**/5-6, 237-327 (2000).

[5] A. Akmal, V. R. Pandharipande, D. G. Ravenhall, Phys. Rev. C **58**, 1804 (1998).

[6] B. Friedman and V.R. Pandharipande, *Nucl. Phys.* A361, 502 (1981).

[7] X.-D. LI, I. Bombaci, M. Dey, J. Dey and E.P.J. van den Heuvel, Phys. Rev. Lett. **83**, 3776 (1999); I. Bombaci, astro-ph/0201369.

[8] W. Zhang, T. E. Strohmayer and J. H. Swank, Ap. J. **482**, L167 (1997).

[9] M. C. Miller, F. K. Lamb and D. Psaltis, Ap. J. **508**, 791 (1998).

[10] N.R. Nath, T.E. Strohmayer and J.H. Swank, astro-ph/0102421 astro-ph/0102421. T.S. Olson, Phys. Rev. C **63**, 015802 (2001); astro-ph/0201099. C.M. Miller, priv. comm.

[11] B. Link, R. I. Epstein, J. M. Lattimer, Phys. Rev. Lett. **83**, 3362 (1999).

[12] J. A. Pons et al., ApJ 564, (2002), in press.

[13] M.H. van Kerkwijk, astro-ph/0110336.

[14] S.E. Thorsett and D. Chakrabarty, Ap. J. **512**, 288 (1999).

[15] W. van Straten et al., astro-ph/0108254.

[16] O. Barziv et al., astro-ph/0108237. M. H. van Kerkwijk, astro-ph/0001077 (2000).

[17] J.A. Orosz and E. Kuulkers, Mon. Not. R. Astron. Soc., **305**, 1320 (1999).

[18] F.M. Walter and L.D. Metthews, Nature 389, 358 (1997); F.M. Walter, S.J. Wolk, and R. Neuhäuser, Nature 379, 233 (1996).

[19] D.L. Kaplan, M.H. van Kerkwijk, J. Anderson, astro-ph/0111174.

[20] V. Burwitz et al., astro-ph/0109374.

[21] B. Paczynski, astro-ph/0107443.

[22] L. Bildsten and T. Strohmayer, Physics Today, Feb., p. 40, (1999).

[23] E. F. Brown, L. Bildsten and R. E. Rutledge, Ap. J., 504, L95 (1998); astro-ph/0105405.

[24] V.R. Pandharipande et al., Phys. Rev. Lett. **75**, 4567 (1995); Phys. Rev. C **63**, 017603 (2001).

[25] N. Glendenning and J. Schaffner, Phys. Rev. Lett. **81**, 4564 (1998).

[26] F. Weber, astro-ph/0112058. N.K. Glendenning, Phys. Rev. D 46, 1274 (1992).

[27] H. Heiselberg, C.J. Pethick, E.F. Staubo, *Phys. Rev. Letts.* **70**, 1355 (1993).

[28] C.P. Lorenz, D.G. Ravenhall and C.J. Pethick, *Phys. Rev. Lett.* **70**, 379 (1993).

[29] See, e.g., M. Alford, K. Rajagopal, S. Reddy, F. Wilczek, Phys.Rev. D64, 074017 (2001), and refs. therein. M. Alford, hep-ph/0102047, hep-ph/0110150. D.T. Son, hep-ph/0108260 .

[30] K. Rajagopal, F. Wilczek, Phys. Rev. Lett. **86**, 3492 (2001).

[31] K. Splittorff, D.T.Son, M.A. Stephanov, Phys.Rev. **D64**, 016003 (2001). J.B. Kogut, D. Toublan, Phys.Rev. **D64**, 034007 (2001).

[32] H. Heiselberg, hep-ph/9912419.

[33] J.E. Horvath et al., astro-ph/0112159. D. Blaschke, S. Fredriksson, A.M. Oztas, astro-ph/0111587.

[34] T. Piran, astro-ph/0111314.

[35] D.K. Hong, S.D.H. Hsu, F. Sannino, Phys.Lett. B516 (2001) 362-366. R. Ouyed and F. Sannino, astro-ph/0103022; hep-ph/0112013.

[36] V.V. Usov, astro-ph/0111442.

[37] G. Carter, hep-ph/0111353

[38] J. Madsen, hep-ph/0111417.

[39] See, e.g., K. Belczynski et al., astro-ph/0111452, for a discussion of LIGO candidates.

[40] H. Heiselberg et al., Phys. Rev. Letters, **85**, 2418 (2000); Phys. Rev. **A63** 043606 (2001)

# From Neutron Stars to Strange Stars

*Fridolin Weber*
*Department of Physics*
*225 Nieuwland Science Hall*
*University of Notre Dame*
*Notre Dame, IN 46556-5670, USA*

## 1 Introduction

It is generally agreed that the tremendous densities reached in the centers of neutron stars provide a high pressure environment in which numerous particles processes are likely to compete with each other. These processes range from the generation of hyperons to quark deconfinement to the formation of kaon condensates and H-matter [1]. Another striking possibility concerns the formation of absolutely stable strange quark matter, a configuration of matter even more stable than the most stable atomic nucleus, iron. In the latter event all neutron stars would in fact be strange (quark matter) stars [2], objects largely composed of pure strange quark matter, eventually enveloped in a thin nuclear crust made up of ordinary, hadronic matter.

There has been much recent progress in our understanding of quark matter, culminating in the discovery that if quark matter exists it will be in a color superconducting state [3, 4, 5, 6]. The phase diagram of such matter appears to be very complex [5, 6]. At asymptotic densities the ground state of QCD with a vanishing strange quark mass is the color-flavor locked (CFL) phase. This phase is electrically neutral in bulk for a significant range of chemical potentials and strange quark masses [7]. If the strange quark mass is heavy enough to be ignored, then up and down quarks may pair in the two-flavor superconducting (2SC) phase. Other possible condensation patters are the recently discovered CFL–$K^0$ phase [8] and the color-spin locked (2SC+s) phase [9]. The magnitude of the gap energy lies between $\sim 50$ and 100 MeV. Color superconductivity thus modifies the equation of state (eos) at the order $(\Delta/\mu)^2$ level, which is only a few percent. Such small effects can be safely neglected in present determinations of models for the eos of neutron stars and strange quark matter stars. There has been much recent work on how color superconductivity in neutron stars could affect their properties [5, 6, 10, 11, 12]. These studies revealed that possible signatures include the cooling by neutrino emission, the pattern of the arrival times of supernova neutrinos, the evolution of neutron star magnetic fields, rotational (r-mode) instabilities, and glitches in rotation frequencies. In this review I shall complement this

list by reviewing several, most intruigung astrophysical implications connected with the possible absolute stability of strange quark matter. (Surface properties of strange matter are discussed in Usov's paper elsewhere in this volume.) This is followed by a discussion of two astrophysical signals that may point at the existence of quark matter in both isolated neutron stars as well as in neutron stars in low-mass x-ray binaries (LMXBs). We recall that a convincing discovery of quark matter in neutron stars would demonstrate that strange quark matter is not absolutely stable, ruling out the absolute stability of strange quark matter and the existence of strange quark stars, for it is not possible for neutron stars to contain quark matter cores and strange matte quark stars to both be stable [5].

## 2 Nuclear crusts on strange matter stars

Since stars in their lowest energy state are electrically charge neutral to very high precision, any net positive quark charge must be balanced by leptons. As a general feature, there is only very little need for leptons, since charge neutrality can be achieved essentially among the quarks themselves. (This is specifically the case for superconducting CFL quark matter in the asymptotic limit.) If electrons form a component of absolutely stable strange quark matter, their presence is crucial for the possible existence of a nuclear curst on such matter [13, 14]. The reason being that the electrons, which are bound to strange matter by the Coulomb force rather than the strong force, extend several hundred fermi beyond the surface of strange matter. Associated with this electron displacement is a very strong electric dipole layer which can support, out of contact with the surface of the strange matter, a crust of nuclear material, which it polarizes. The maximal possible density at the base of the crust (inner crust density) is determined by neutron drip, $\epsilon_{\rm drip} = 4.3 \times 10^{11}$ g/cm$^3$, at which neutrons begin to drip out of the nuclei and form a free neutron gas. Being electrically charge neutral, the neutrons do not feel the repulsive Coulomb force and hence would gravitate toward the quark matter core, where they become converted into strange matter. Neutron drip thus sets a strict upper limit on the crust's maximal inner density. The actual value may be slightly smaller though [15]. The somewhat complicated situation of the structure of a strange matter star with crust can be represented by a proper choice of eos [16], which consists of two parts. At densities below neutron drip it is represented by the low-density eos of charge-neutral nuclear matter, for which we use the Baym-Pethick-Sutherland eos. The star's strange matter core is described by the bag model.

# 3 Complete sequences of strange matter stars

Since the nuclear crusts surrounding the cores of strange stars are bound by the gravitational force rather than confinement, the mass-radius relationship of strange matter stars with crusts is qualitatively similar to the one of purely gravitationally bound stars, neutron stars and white dwarfs, as illustrated in Fig. 1 [17, 18]. The

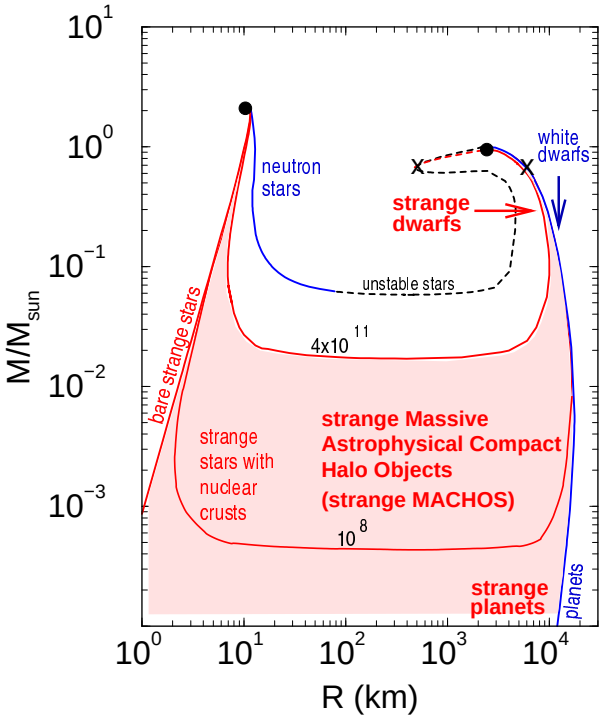


Figure 1: Classification of stellar objects in the mass-radius plane. Bare strange stars obey $M \propto R^3$. Nuclear crusts on them give way to an expansive range of novel stellar configurations (shaded area). These range from strange MACHOS to strange dwarfs to strange planets. The labels $10^8$ and $4 \times 10^{11}$ refer to inner crust densities in g/cm$^3$.

strange star sequences are computed for the maximal possible inner crust density, $\epsilon_{\rm crust} = \epsilon_{\rm drip}$, as well as for an arbitrarily chosen, smaller value of $\epsilon_{\rm crust} = 10^8$ g/cm$^3$, which may serves to demonstrate the influence of less dense crusts on the mass-radius relationship [17]. From the maximum mass star (dot in the upper left corner), the central density decreases monotonically through the sequence in each case. The stars located along the dashed line represent unstable configurations [17, 18]. The fact that strange stars with crusts tend to possess somewhat smaller radii than neutron stars implies smaller mass shedding (Kepler) periods $P_{\rm K}$ for the former. This is already indicated by the classical expression $P_{\rm K} = 2\pi\sqrt{R^3/M}$ and carries over to the full

general relativistic determination of $P_{\rm K}$ [1],

$$P_{\rm K} = 2\pi \left( \omega + \frac{\omega'}{2\psi'} + e^{\nu-\psi} \sqrt{\frac{\nu'}{\psi'} + \left( \frac{\omega'}{2\psi'} e^{\psi-\nu} \right)^2} \right)^{-1} . \quad (1)$$

This expression is to be computed simultaneously in combination with Einstein's field equations for a rotating compact body [1],

$$R^{\kappa\lambda} - \frac{1}{2}\, g^{\kappa\lambda}\, R = 8\,\pi\, T^{\kappa\lambda}(\epsilon, P(\epsilon)) . \quad (2)$$

It is found that, due to the smaller radii of strange stars, the complete sequence of such objects, and not just those close to the mass peak as is the case for neutron stars, can sustain extremely rapid rotation [17]. In particular, model calculations indicate for a strange star with a typical pulsar mass of $\sim 1.45\, M_\odot$ Kepler periods in the range of 0.55 msec$\lesssim$P$_{\rm K}\lesssim$0.8 msec, depending on the thickness of the nuclear curst and the bag constant [16, 17]. This range is to be compared with $P_{\rm K} \sim 1$ msec obtained for neutron stars of the same mass.

The minimum-mass configurations of the sample strange star sequences in Fig. 1 have masses of about $\sim 0.017\, M_\odot$ (about 17 Jupiter masses) and $10^{-4}\, M_\odot$, depending on the valuer of $\epsilon_{\rm crust}$. For inner crust densities smaller than $10^8$ g/cm$^3$ one obtains stable strange matter stars that can be by orders of magnitudes lighter than Jupiters. If abundant enough, these light strange stars could be seen by the gravitational microlensing searches [19]. Strange stars located to the right of the minimum mass configuration of each sequence consist of small strange cores, typically smaller than about 3 km, surrounded by nuclear crusts (ordinary white dwarf matter) that are thousands of kilometers thick. Such objects are called strange dwarfs. Their cores have shrunk to zero at the crossed points. What is left are ordinary white dwarfs with central densities equal to the inner crust densities of the former strange dwarfs. A stability analysis of strange stars against radial oscillations [17] shows that all strange dwarf sequences that terminate at stable ordinary white dwarfs are stable against radial oscillations. Strange stars that are located to the left of the mass peak of ordinary white dwarfs (solid dot in upper right corner), however, are unstable against oscillations and thus cannot exist in nature. So, in sharp contrast to neutron stars and white dwarfs, the branches of strange stars and strange dwarfs are stably connected with each other [17, 18]. Finally we would like to stress that strange dwarfs with $10^9$ g/cm$^3$ $< \epsilon_{\rm crust} < 4 \times 10^{11}$ g/cm$^3$ form entire new classes of stars that contain nuclear material up to $\sim 4 \times 10^4$ times denser than in ordinary white dwarfs of average mass, $M \sim 0.6\, M_\odot$ (central density $\sim 10^7$ g/cm$^3$). The entire family of such strange stars owes its stability to the strange core. Without the core they would be placed into the unstable region between ordinary white dwarfs and neutron stars [18].

Until recently, only rather vague tests of the theoretical mass-radius relation of white dwarfs have been possible. This has changed because of the availability of new

data emerging from the Hipparcos project [20]. These data allow the first accurate measurements of white dwarf distances and, as a result, establishing the mass-radius relation of such objects empirically. Figure 2 shows a comparison of several data from

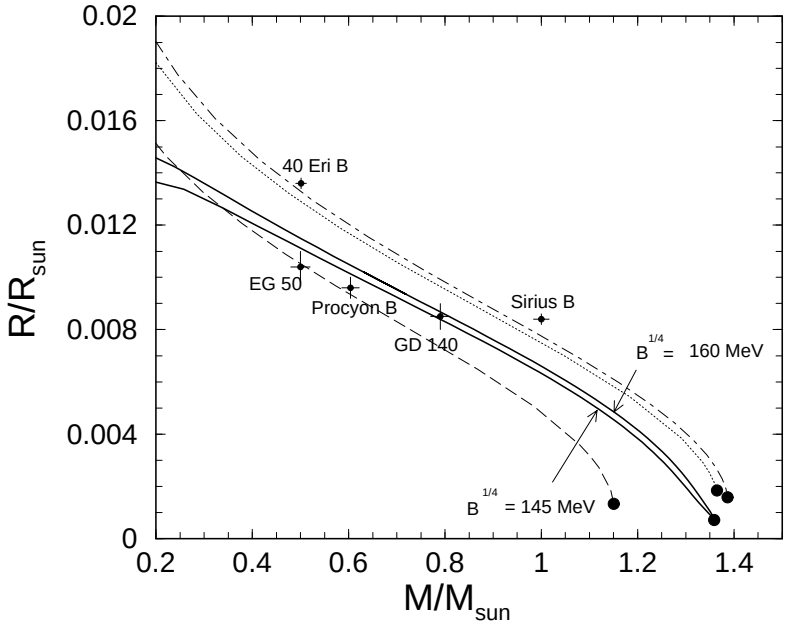


Figure 2: Comparison of theoretical mass-radius relationships of strange dwarfs ($\epsilon_{\rm crust} = \epsilon_{\rm drip}$) and several ordinary white dwarf stars [21] ($^{12}$C dwarfs: dot-dashed, $^{24}$Mg: dotted, $^{56}$Fe: dashed double-dotted) with data from the Hipparcos project.

the Hipparcos project with the mass-radius relationships of strange dwarfs (solid lines) and ordinary white dwarfs computed for different compositions.

# 4 Post-glitch behavior of strange stars

Ordinary neutron stars older than a few months have crusts made of a crystal lattice or an ordered inhomogeneous medium reaching from the surface down to regions with a density of $2 \times 10^{14}$ g/cm$^3$. This crust contains only a few percent of the total moment of inertia. Strange stars, in contrast, can only support a crust with a density below neutron drip ($4.3 \times 10^{11}$ g/cm$^3$), for reasons discussed in section 2. Such a strange star crust contains at most $\sim 10^{-5}$ of the total moment of inertia. This is an upper bound, since the strange star may have no crust at all, depending on its prior evolution. The difference in the moment of inertia stored in the crust of neutron stars and strange stars seems to pose significant difficulties for explaining the glitch phenomenon observed in radio pulsars with models based on strange stars. Glitches

are observed as sudden speed-ups in the rotation rate of pulsars. The fractional change in rotation rate $\Omega$ is $\Delta\Omega/\Omega \approx 10^{-6} - 10^{-9}$, and the corresponding fractional change in the spin-down rate $\dot{\Omega}$ is of order $\Delta\dot{\Omega}/\dot{\Omega} \approx 10^{-2} - 10^{-3}$. In [16] it has been demonstrated that strange stars with crusts obey

$$\frac{\Delta\Omega}{\Omega} \simeq (10^{-5} \text{ to } 10^{-3})\ f\,, \qquad (0 < f < 1)\,, \tag{3}$$

where $f$ represents the fraction of the crustal moment of inertia that is altered in the quake, $|\Delta I| = f I_{\rm crust}$. Since observed glitches have relative frequency changes of $\Delta\Omega/\Omega \simeq 10^{-9}$ to $10^{-6}$, a change in the crustal moment of inertia by less than 10% would cause a giant glitch ($\Delta\Omega/\Omega \sim 10^{-6}$) even in the least favorable case. Of course there remains the question of whether there can be a sufficient build up of stress and also of the recoupling of crust and core which involves the healing of the pulsar period. This is probably a very complicated process that does not simply involve the recoupling of two homogeneous substances. For $\Delta\dot{\Omega}/\dot{\Omega}$ we established that [16]

$$\frac{\Delta\dot{\Omega}}{\dot{\Omega}} > (10^{-1} \text{ to } 10)\ f\,, \tag{4}$$

yielding a small $f$ value as before, namely $f < 10^{-4}$ to $10^{-1}$. We have used measured values of the ratio $(\Delta\Omega/\Omega)/(\Delta\dot{\Omega}/\dot{\Omega}) \sim 10^{-6}$ to $10^{-4}$ for the Crab and Vela pulsars respectively. So the observed range of the fractional change in $\dot{\Omega}$ is consistent with the crust having the small moment of inertia calculated and the quake involving only a small fraction, $f$, of that, just as in Eq. (3). Nevertheless, without undertaking a study of whether the nuclear solid crust on strange stars could sustain a sufficient buildup of stress before cracking to account for such a sudden change in relative moment of inertia, or whether the healing-time and intervals between glitches can be understood, one cannot say definitely that strange stars with a nuclear solid crust can account for any complete set of glitch observations for a particular pulsar.

# 5 Formation of strange dwarfs

At present there is neither a well-studied model for the formation of hypothetical strange dwarfs, nor exists a study that determines their abundance in the universe. One possible scenario would be the formation of strange dwarfs from main sequence progenitors that have been contaminated with strange nuggets over their lifetimes. We recall that the capture of strange matter nuggets by main sequence stars is an inevitable consequence if strange matter were more stable than hadronic matter [22] because then the Galaxy would be filled with a flux of strange nuggets which would be acquired by every object they come into contact with, i.e. planets, neutron stars, white dwarfs, and main sequence stars. Naturally, due to the large radii of the latter,

they arise as ideal large-surface long integration time detectors for the strange matter flux. Nuggets that are accreted onto neutron stars and white dwarfs, however, never reach their centers, where the gravitational potential is largest, because they are stopped in the lattice close to the surface due to the large structural energy density there. This prevents such stars from building up a cores of strange matter. The situation is different for main sequence stars which are diffuse in comparison with neutron stars and white dwarfs. In this case the accreted nuggets may gravitate to the star's core, accumulate there and form a strange matter core that grows with time until the star's demise as a main sequence star. Another plausible mechanism has to do with primordial strange matter bodies. Such bodies of masses between $10^{-2}$ and $1\,M_\odot$ may have been formed in the early universe and survived to the present epoch [23]. Such objects will occasionally be captured by a main sequence star and form a significant core in a single and singular event. The core's baryon number, however, cannot be significantly larger than $\sim 5{\times}10^{31}\ (M/M_\odot)^{-1.8}$ where $M$ is the star's mass. Otherwise a main sequence star is not capable of capturing the strange matter core [2, 24]. Finally we mention that in the very early evolution of the universe lumps of hot strange matter will evaporate nucleons which are plausibly gravitationally bound to the lump. The evaporation will continue until the quark matter has cooled sufficiently. Depending on the original baryon number of the quark lump, a strange star or dwarf, both with nuclear crusts will have been formed.

# 6 Quark matter in isolated neutron stars

Whether or not quark deconfinement occurs in neutron stars makes only very little difference to their static properties, such as the range of possible masses and radii, which renders the detection of quark matter in such objects extremely complicated. This turns out to be strikingly different for rotating neutron stars (i.e. pulsars) which develop quark matter cores in the course of spin-down. The reason being that as such stars spin down, because of the emission of magnetic dipole radiation and a wind of electron-positron pairs, they become more and more compressed. For some rotating neutron stars the mass and initial rotational frequency may be just such that the central density rises from below to above the critical density for dissolution of baryons into their quark constituents. This effects the star's moment of inertia dramatically [25], as shown in figure 3. Depending on the ratio at which quark and normal matter change with frequency, the moment of inertia can decrease very anomalously, and could even introduce an era of stellar spin-up lasting for $\sim 10^8$ years [25]. Since the dipole age of millisecond pulsars is about $10^9$ years, we may roughly estimate that about 10% of the $\sim 25$ solitary millisecond pulsars presently known could be in the quark transition epoch and thus could be signaling the ongoing process of quark deconfinement! Changes in the moment of inertia reflect themselves in the braking

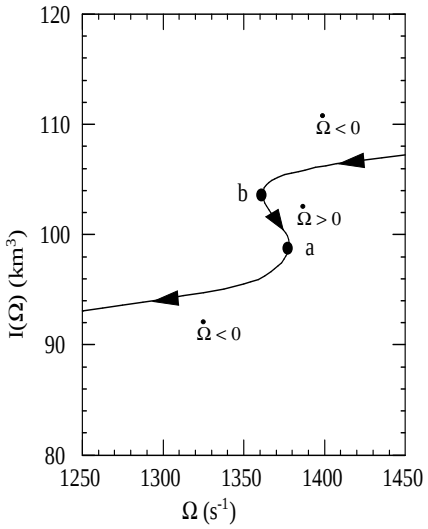


Figure 3: Moment of inertia versus frequency. The generation of quark matter causes a "backbending" of $I$ for frequencies between $a$ and $b$ [1, 25].

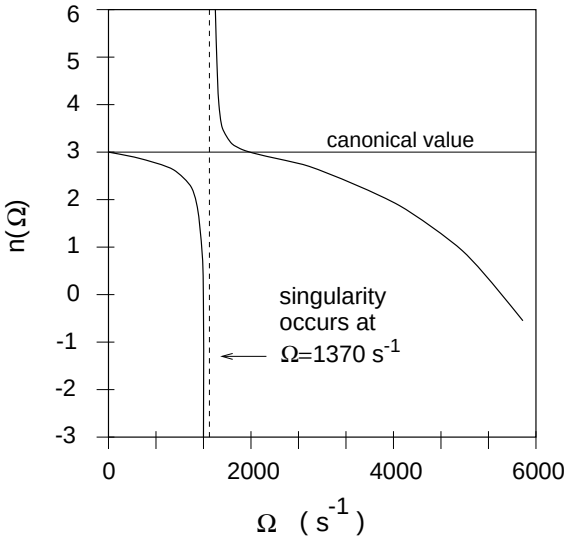


Figure 4: Anomaly in braking index caused by generation of quark matter.

index, $n$, of a rotating neutron star, as can be seen from ($I' \equiv \mathrm{d}I/\mathrm{d}\Omega$, $I'' \equiv \mathrm{d}^2I/\mathrm{d}\Omega^2$)

$$n(\Omega) \equiv \frac{\Omega\,\ddot{\Omega}}{\dot{\Omega}^2} = 3 - \frac{3\,I'\,\Omega + I''\,\Omega^2}{2\,I + I'\,\Omega}\,. \tag{5}$$

The right-hand-side of this expression reduces to the well-known canonical constant $n = 3$ if $I$ is independent of frequency. Evidently, this is not the case for rapidly rotating neutron stars, and it fails completely for stars that experience pronounced internal changes (phase transitions) which alter the moment of inertia significantly. Figure 4 illustrates this for the moment of inertia of the neutron star of Fig. 3. Because of the changes in $I$, caused by the gradual transition of hadronic matter into quark matter, the braking index deviates dramatically from 3 at the transition frequency, when pure quark matter is generated. Such dramatic anomalies in $n(\Omega)$ are not known for conventional neutron stars, because their moments of inertia appear to vary smoothly with $\Omega$ [1]. The future astrophysical observation of such anomalies in the braking behavior of pulsars may thus be interpreted as a signal for quark deconfinement in neutron stars.

# 7 Quark matter in accreting x-ray neutron stars

Accreting x-ray neutron stars provide a very interesting contrast to the spin-down of isolated neutron stars discussed in sect. 6. These x-ray neutron stars are being spun up

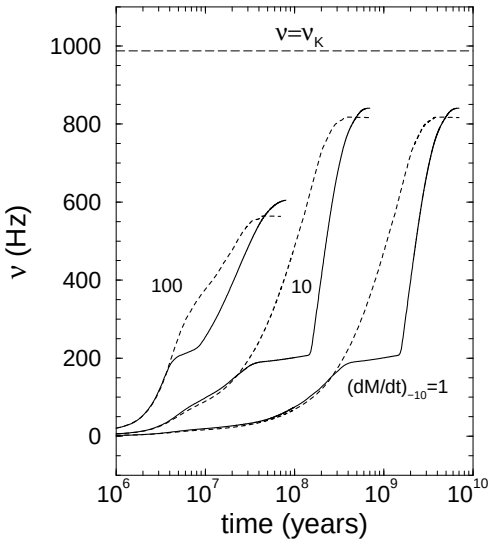


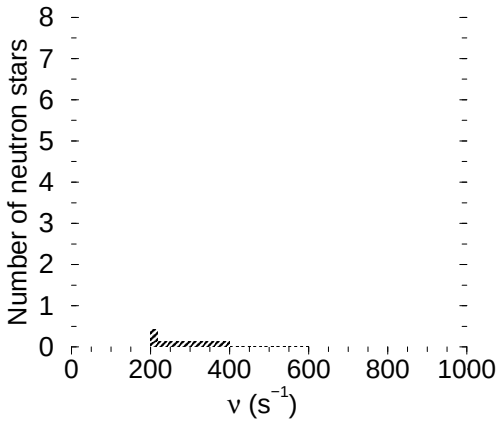


Figure 5: Evolution of spin frequencies of accreting x-ray neutron stars with (solid curves) and without (dashed curves) quark deconfinement [26]. The spin plateau around 200 Hz signals the ongoing process of quark reconfinement in the stellar centers [26].

matter is defined by $r_{\rm A} = \mu^{4/7}(2M\dot{M}^2)^{-1/7}$. The rate of change of a star's angular frequency $\Omega = 2\pi/\nu$ $(= J/I)$ then follows from Eq. (6) as

$$I(t)\frac{d\nu(t)}{dt} = \frac{\dot{M}\tilde{l}(t)}{2\pi} - \nu(t)\frac{dI(t)}{dt} - \kappa\,\mu(t)^2\,r_{\rm c}(t)^{-3}\,, \tag{7}$$

with the explicit time dependences as indicated. Evidently, the second term on the right-hand-side of Eq. (7) depends linearly on $\Omega$ while the third terms grows quadratically with $\Omega$. The temporal change of the moment of inertia of accreting neutron stars which undergo phase transitions is crucial [26, 27]. This also renders the calculation of the moment of inertia, given by [1]

$$I(t) = 2\pi\int_0^\pi d\theta\int_0^{R(\theta;t)} dr\,e^{\lambda+\mu+\nu+\psi}\frac{\epsilon+P}{e^{2\nu-2\psi}-(\omega-\Omega)^2}\frac{\Omega-\omega}{\Omega}\,, \tag{8}$$

very cumbersome, for each quantity on the right-hand-side varies accordingly during stellar spin-up. (We assume rigid body rotation, which renders the star's frequency $\Omega$ constant throughout the star.) The solution of equation (7) is shown in Fig. 6. The result is most striking. One sees that quark matter remains relatively dormant in the stellar core until the star has been spun up to frequencies at which the central density is about to drop below the threshold density at which quark matter exists. As known from Fig. 3, this manifests itself in a significant increase of the star's moment of inertia. The angular momentum added to a neutron star during this phase of evolution is therefore consumed by the star's expansion, inhibiting a further spin-up until the quark matter has been converted into a mixed phase of matter made up of hadrons and quarks. Such accreters, therefore, tend to spend a greater length of time in the critical frequencies than otherwise. There will be an anomalous number of accreters that appear at or near the same frequency, as shown in Fig. 6. This is what was found recently with the Rossi x-ray Timing Explorer (shaded area in Fig. 6). Quark deconfinement constitutes an attractive explanation for this anomaly [26, 27, 28], though alternative explanations were suggested too [29, 30].

**Acknowledgments:** I am grateful to the organizers of Compact Stars in the QCD Phase Diagram, R. Ouyed and F. Sannino.

# References

[1] F. Weber, *Pulsars as Astrophysical Laboratories for Nuclear and Particle Physics*, High Energy Physics, Cosmology and Gravitation Series (IOP Publishing, Bristol, Great Britain, 1999).

[2] J. Madsen, Lecture Notes in Physics **516** (1999) 162, (`astro-ph/9809032`).

[3] M. Alford, K. Rajagopal, and F. Wilczek, Phys. Lett. **422B** (1998) 247.

[4] R. Rapp, T. Schäfer, E. V. Shuryak, and M. Velkovsky, Phys. Rev. Lett. **81** (1998) 53.

[5] K. Rajagopal and F. Wilczek, *The Condensed Matter Physics of QCD*, At the Frontier of Particle Physics / Handbook of QCD, ed. M. Shifman, (World Scientific) (2001), (`hep-ph/0011333`).

[6] M. Alford, *Color superconducting quark matter*, to appear in Ann. Rev. Nucl. Part. Sci. (2001), (`hep-ph/0102047`).

[7] K. Rajagopal and F. Wilczek, Phys. Rev. Lett. **86** (2001) 3492.

[8] P. F. Bedaque and T. Schäfer (`hep-ph/0105150`).

[9] T. Schäfer, Phys. Rev. D **62** (2000) 094007.

[10] K. Rajagopal, Acta Physica Polonica B **31** (2000) 3021.

[11] M. Alford, J. Bowers, and K. Rajagopal, Phys. Rev. D **63** (2001) 074016.

[12] M. Alford, J. A. Bowers, and K. Rajagopal, J. Phys. G **27** (2001) 541.

[13] C. Alcock, E. Farhi, and A. V. Olinto, Astrophys. J. **310** (1986) 261.

[14] Ch. Kettner, F. Weber, M. K. Weigel, and N. K. Glendenning, Phys. Rev. D **51** (1995) 1440.

[15] O. G. Benvenuto and L. G. Althaus, Astrophys. J. **462** (1996) 364.

[16] N. K. Glendenning and F. Weber, Astrophys. J. **400** (1992) 647.

[17] N. K. Glendenning, Ch. Kettner, and F. Weber, Astrophys. J. **450** (1995) 253.

[18] N. K. Glendenning, Ch. Kettner, and F. Weber, Phys. Rev. Lett. **74** (1995) 3519.

[19] C. Alcock et al., Astrophys. J. **542** (2000) 281.

[20] J. L. Provencal, H. L. Shipman, E. Hog, and P. Thejll, Astrophys. J. **494** (1998) 759.

[21] Computed by B. C. O'Gorman, Univ. of Notre Dame (2001).

[22] J. Madsen, Phys. Rev. Lett. **61** (1988) 2909.

[23] W. N. Cottingham, D. Kalafatis, and R. Vinh Mau, Phys. Rev. Lett. **73** (1994) 1328.

[24] J. Madsen, *Physics and Astrophysics of Strange Quark Matter*, Proc. of the 2nd International Conference on Physics and Astrophysics of Quark-Gluon Plasma, ed. by B. Sinha, Y. P. Viyogi, and S. Raha (World Scientific, Singapore, 1994) p. 186.

[25] N. K. Glendenning, S. Pei, and F. Weber, Phys. Rev. Lett. **79** (1997) 1603.

[26] N. K. Glendenning and F. Weber, Astrophys. J. **559** (2001) L119.

[27] N. K. Glendenning and F. Weber, *Signal of Quark Deconfinement in Millisecond Pulsars and Reconfinement in Accreting X-ray Neutron Stars* (to appear in the Springer Lecture Notes on Neutron Star Interiors), (Spring-Verlag 2001) (`astro-ph/0106054`).

[28] G. Poghosyan, H. Grigorian, D. Blaschke, Astrophys. J. **551** (2001) L73.

[29] L. Bildsten, Astrophys. J. **501** (1998) L89.

[30] N. Andersson, D. I. Jones, K. D. Kokkotas, and N. Stergioulas, Astrophys. J. **534** (2000) L75.

[31] N. K. Glendenning and Ch. Kettner, Astron. & Astrophys. **353** (2000) L9.

# Discussion

**S. Balberg (Hebrew University):** The "anomalous" behavior in spin down (up) of an isolated (pair in a LMXB) neutron star attributed to the quark phase is really a feature of the equation of state, not of quark matter in itself. In other words, we need a relatively sharp feature in the equation of state to get a significant change in the moment of inertia, which would, in principle be due to other phenomena as well.

**Weber:** One needs a pronounced feature in the equation of state in order to get an anomaly in the breaking index (spin-up). Hyperons and meson condensates lead to features in the equation of state that seem to be way to week to cause such a striking anomaly [1]. A softening alone, as caused by hyperons and/or bosons, is not sufficient. What is really required is a softening followed by a gradual stiffening at higher densities which is naturally obtained for hadron-quark matter gradually compressed to higher densities.

**H. Heiselberg (NORDITA):** How does $M(R)$ look for your quark matter star?

**Weber:** Glendenning and Kettner demonstrated the existence of non-identical neutron star twins, depending on whether or not the low-density sequence of neutron stars terminates at central densities that fall close to the end of the mixed phase of quarks and hadrons [31].

# Strange star candidates

*Ignazio Bombaci*
*Dipartimento di Fisica "Enrico Fermi"*
*via Buonarroti, 2*
*I-56127 Pisa, ITALY*

## 1 Introduction

One of the most exciting aspects of modern astrophysics is the possible existence of a new family of compact stars, which are made entirely of deconfined *u,d,s* quark matter (*strange quark matter* (SQM)). These strange quark matter stars are called in the scientific literature *strange stars* (SS). They differ from neutron stars, where quarks are confined within neutrons, protons, and eventually within other hadrons (hadronic matter stars). The possible existence of SS is a direct consequence of the so called *strange matter hypothesis* [1]. According to this hypothesis, SQM (in equilibrium with respect to the weak interactions) could be the true ground state of matter. In other words, one assumes the energy per baryon of SQM (at the baryon density where the pressure is equal to zero) to be less than the lowest energy per baryon found in nuclei, which is about 930 MeV for $^{56}$Fe. According to the strange matter hypothesis, the ordinary state of matter, in which quarks are confined within hadrons, is a metastable state [1, 2]. The strange matter hypothesis does not conflict with the existence of atomic nuclei as conglomerates of nucleons, or with the stability of ordinary matter [2, 3, 4].

From a basic point of view the equation of state for SQM should be calculated solving QCD at finite density. As we know, such a fundamental approach is presently not doable. Therefore one has to rely on phenomenological models. In this work, we use two simple phenomenological models for the equation of state (EOS) of strange quark matter. One is a model [2] which is related to the MIT bag model for hadrons. The other is a model proposed by Dey *et al.* [20].

## 2 The mass–radius relation for compact stars

To distinguish whether a compact star is a neutron star or a strange star, one has to find a clear observational signature. There is a striking qualitative difference in the mass–radius (MR) relation of SS with respect to that of neutron stars (see Fig. 1).

For SS with "small" ($M << M_{max}$) gravitational mass, $M$ is proportional to $R^3$. In contrast, neutron stars have radii that decrease with increasing mass. This is a consequence of the underlying interaction between the stellar constituents which makes "low" mass SS self-bound objects (see *e.g.* ref.[6]) contrary to the case of neutron stars which are bound by gravity. As we know, there is a minimum mass for a neutron star ($M_{min} \sim 0.1\ M_\odot$). In the case of a strange star, there is essentially no minimum mass. As the central density $\rho_c \to \rho_s$ (surface density), a strange star (or better a strangelet for very low baryon number) is a self–bound system, until the baryon number becomes so low that finite size effects destabilize it.

The transient X-ray burst source SAX J1808.4-3658 was discovered in September 1996 by the BeppoSAX satellite. Two bright type-I X-ray bursts were detected, each lasting less than 30 seconds. Analysis of the bursts in SAX J1808.4-3658 indicates that it is 4 kpc distant and has a peak X-ray luminosity of $6 \times 10^{36}$ erg/s in its bright state, and a X-ray luminosity lower than $10^{35}$ erg/s in quiescence [7]. Coherent pulsations at a period of 2.49 milliseconds were discovered [8]. The binary nature of SAX J1808.4-3658 was firmly established with the detection of a 2 hour orbital period [9] as well as with the optical identification of the companion star. SAX J1808.4-3658 is the first pulsar to show both coherent pulsations in its persistent emission and X-ray bursts.

A mass–radius (MR) relation for the compact star in SAX J1808.4-3658 has been obtained by Li *et al.* [10] using the following two requirements. (*i*) Detection of X-ray pulsations requires that the inner radius $R_0$ of the accretion flow should be larger than the stellar radius $R$. In other words, the stellar magnetic field must be strong enough to disrupt the disk flow above the stellar surface. (*ii*) The radius $R_0$ must be less than the so-called co-rotation radius $R_{\rm c}$, *i.e.* the stellar magnetic field must be weak enough that accretion is not centrifugally inhibited: $R_0 \lesssim R_{\rm c} = [GMP^2/(4\pi^2)]^{1/3}$. Here $G$ is the gravitation constant, $M$ is the mass of the star, and $P$ is the pulse period. The inner disk radius $R_0$ is generally evaluated in terms of the Alfvén radius $R_{\rm A}$, at which the magnetic and material stresses balance [11]: $R_0 = \xi R_{\rm A} = \xi[B^2R^6/\dot{M}(2GM)^{1/2}]^{2/7}$, where $B$ and $\dot{M}$ are respectively the surface magnetic field and the mass accretion rate of the pulsar, and $\xi$ is a parameter of order of unity almost independent [12] of $\dot{M}$. Since X-ray pulsations in SAX J1808.4-3658 were detected over a wide range of mass accretion rate (say, from $\dot{M}_{\rm min}$ to $\dot{M}_{\rm max}$), the two conditions (*i*) and (*ii*) give $R \lesssim R_0(\dot{M}_{\rm max}) < R_0(\dot{M}_{\rm min}) \lesssim R_{\rm c}$. Next, we assume that the mass accretion rate $\dot{M}$ is proportional to the X-ray flux $F$ observed with RXTE. This is guaranteed by the fact that the X-ray spectrum of SAX J1808.4-3658 was remarkably stable and there was only slight increase in the pulse amplitude when the X-ray luminosity varied by a factor of $\sim 100$ during the 1998 April/May outburst [13, 14, 15]. Therefore, Li *et al.* [10] get the following upper limit of the stellar radius:

$R < (F_{min}/F_{max})^{2/7} R_{\rm c}$, or

$$R < 27.5 \Big(\frac{F_{min}}{F_{max}}\Big)^{2/7} \Big(\frac{P}{2.49\ {\rm ms}}\Big)^{2/3} \Big(\frac{M}{M_\odot}\Big)^{1/3}\ {\rm km}, \qquad (1)$$

where $F_{\rm max}$ and $F_{\rm min}$ denote the X-ray fluxes measured during X-ray high- and low-state, respectively, $M_\odot$ is the solar mass. Note that in writing inequality (1) it is assumed that the pulsar's magnetic field is basically dipolar [1].

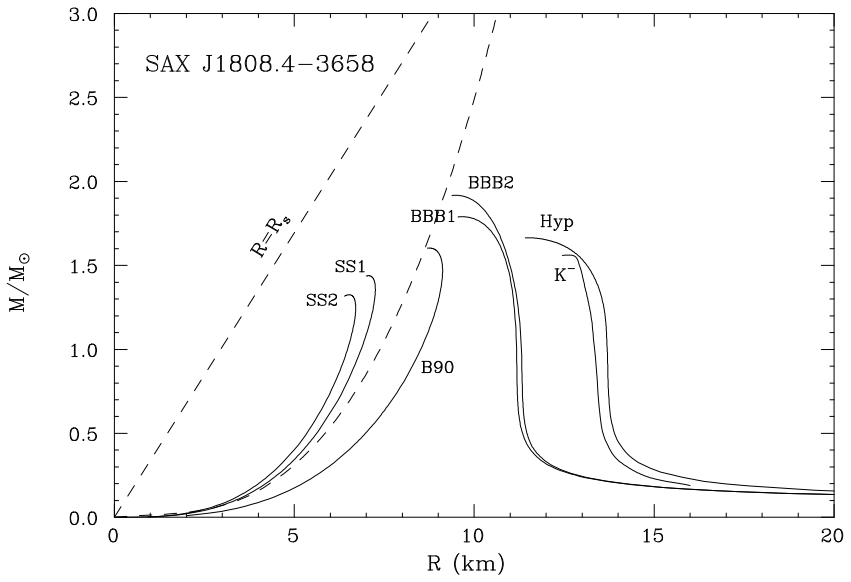


Figure 1: Comparison of the MR relation of SAX J1808.4 -3658 determined from RXTE observations with theoretical models of neutron stars and of SS. The solid curves represents theoretical MR relations for neutron stars and strange stars.

Given the range of X-ray flux at which coherent pulsations were detected, inequality (1) defines a limiting curve in the MR plane for SAX J1808.4-3658, as plotted in the dashed curve in Fig. 1. The authors of ref.[10] adopted the flux ratio $F_{\rm max}/F_{\rm min} \simeq 100$ from the measured X-ray fluxes with the RXTE during the 1998 April/May outburst [14, 15]. The dashed line $R = R_{\rm s} \equiv 2GM/c^2$ represents the Schwartzschild radius - the lower limit of the stellar radius to prevent the star collapsing into a black hole. Thus the allowed range of the mass and radius of SAX J1808.4-3658 is the region confined by these two dashed curves in Fig. 1.

[1] see ref.[10] for arguments to support this hypothesis. See also ref.[15] for a study of the influence on the MR relation for SAX J1808.4-3658 of a quadrupole magnetic moment, and of a *non-standard* disk–magnetosphere interaction model.

In the same figure, we report the theoretical MR relations (solid curves) for neutron stars given by some recent realistic models for the EOS of dense matter (see ref.[10] for references to the EOS models). Models BBB1 and BBB2 are relative to "conventional" neutron stars (*i.e.* the core of the star is assumed to be composed by an uncharged mixture of neutrons, protons, electrons and muons in equilibrium with respect to the weak interaction). The curve labeled Hyp depicts the MR relation for a neutron star in which hyperons are considered in addition to nucleons as hadronic constituents. The MR curve labeled $K^-$ is relative to neutron stars with a Bose-Einstein condensate of negative kaons in their cores. It is clearly seen in Fig. 1 that none of the neutron star MR curves is consistent with SAX J1808.4-3658. Including rotational effects will shift the $MR$ curves to up-right in Fig. 1 [16], and does not help improve the consistency between the theoretical neutron star models and observations of SAX J1808.4-3658. Therefore SAX J1808.4-3658 is not well described by a neutron star model. The curve B90 in Fig. 1 gives the MR relation for SS described by the schematic EOS of ref. [2] for massless non-interacting quarks with B = 90 MeV/fm$^3$. The two curves SS1 and SS2 give the MR relation for SS calculated with the EOS of Dey *et al.*[20] for two parameterizations which give absolutely stable SQM according to the strange matter hypothesis. Clearly a strange star model is more compatible with SAX J1808.4-3658 than a neutron star one.

Stringent constraints on the MR relation have been also obtained for the compact star in the X-ray source 4U 1728-34 ($M < 1.0\ M_\odot$ and $R < 9$ km) [17], for the isolated compact star RX J1856-37 ($M = 0.9 \pm 0.2\ M_\odot$ and $R = 6^{+2}_{-1}$ km) [18] (see also [19]) and for the X-ray pulsar Her X-1 ($M = 1.1 - 1.8\ M_\odot$ and $R = 6.0 - 7.7$ km) [20]. Clearly it is very difficult to model the MR relation for these compact objects (see *e.g.* Fig. 1) using any realistic EOS for neutron star matter.

# 3 Astrophysical implications and final remarks

If the strange matter hypothesis is true, then a neutron star could "decay" to a strange star (NS→SS conversion) once a "seed" of SQM forms in the neutron star's core or it comes from the galactic space [20]. The conversion of the whole star occurs in a very short time [21], in the range 1 ms – 1 s, and liberates a total energy [22] of a few $10^{53}$ erg. The NS→SS conversion has been proposed [22] as a possible energy source to power $\gamma$-ray bursts at cosmological (redshift $z \sim 1 - 3$) distances [23].

Strange stars are the natural site for a color superconducting state of quark matter [24, 25]. Particularly, there could be a region inside a strange star where quark matter is in a crystalline ("LOFF"[4]) superconducting phase [24, 25]. This raises the possibility to successfully model pulsar glitches with strange stars [25].

A very unpleasant consequence of the strange matter hypothesis could be the possible formation of stable negatively charged strangelets during heavy ion collisions

at RHIC or at LHC. In fact, it has been pointed out [27] that these "dangerous" negatively charged strangelets may trigger the disruption of our planet. Luckily, there are various theoretical as well as experimental arguments [27] to rule out this "Disaster Scenario".

The main result of the present work (*i.e.* the likely existence of strange stars) is based on the analysis of observational data for the X-ray sources SAX J1808.4-3658. The interpretation of these data is done using *standard* models for the accretion mechanism, which is responsible for the observed phenomena. The present uncertainties in our knowledge of the accretion mechanism, and the disk–magnetosphere interaction, do not allow us to definitely rule out the possibility of a neutron star for this X-ray source. For example, making *a priori* the *conservative* assumption that the compact object in SAX J1808.4-3658 is a neutron star, and using a MR relation similar to our eq.(1), Psaltis and Chakrabarty [15] try to constrain disk–magnetosphere interaction models or to infer the presence of a quadrupole magnetic moment in the compact star.

SAX J1808.4-3658, 4U 1728-34, RX J1856-37, and Her X-1 are not the only X-ray sources which could harbour a strange star. Recent studies have shown that the compact objects associated with the X-ray burster 4U 1820-30 [28] and the bursting X-ray pulsar GRO J1744-28 [10] are likely strange star candidates. For each of these X-ray sources (strange star candidates) the conservative assumption of a neutron star as the central accretor would require some particular (possibly *ad hoc*) assumption about the nature of the plasma accretion flow and/or the structure of the stellar magnetic field. On the other hand, the possibility of a strange star gives a simple and unifying picture for all the systems mentioned above.

# References

[1] A. R. Bodmer, Phys. Rev. D **4**, 1601 (1971); H. Terazawa, INS Rep. **336** (Univ. Tokyo, INS) (1979); E. Witten, Phys. Rev. D **30**, 272 (1984).

[2] E. Farhi and R. L. Jaffe, Phys. Rev. D **30**, 2379 (1984).

[3] J. Madsen, Lecture Notes in Physics, Springer Verlag, **516** (1999).

[4] I. Bombaci, *Strange Quark Stars: structural properties and possible signatures for their existence*, in "Physics of Neutron Stars Interiors", Eds. D. Blaschke, *et al.*, Lecture Notes in Physics, Springer Verlag, **578**, (2001).

[5] M. Dey, I. Bombaci, J. Dey, S. Ray, and B.C. Samanta, Phys. Lett. B **438**, 123 (1998); erratum, Phys. Lett. B **467**, 303 (1999).

[6] I. Bombaci, Neutron stars' structure and nuclear equation of state, Ed. M. Baldo, in *Nuclear methods and the nuclear equation of state*, World Scientific (1999).

[7] J.J.M. in't Zand, *et al.*, Astron. Astrophys. **331**, L25 (1998).

[8] R. Wijnands, and M. van der Klis, Nature **394**, 344 (1998).

[9] D. Chakrabarty, and E.H. Morgan, Nature **394**, 346 (1998).

[10] X.-D. Li, I. Bombaci, M. Dey, J. Dey, and E.P.J. van den Heuvel, Phys. Rev. Lett. **83**, 3776 (1999).

[11] D. Bhattacharya and E. P. J. van den Heuvel, Phys. Rep. **203**, 1 (1991).

[12] X.-D. Li, Astrophys. J. **476**, 278 (1997).

[13] M. Gilfanov *et al.*, Astron. Astrophys. **338**, L83 (1998).

[14] W. Cui, E.H. Morgan,and L. Titarchuk, Astrophys. J. **504**, L27 (1998).

[15] D. Psaltis, and D. Chakrabarty, Astrophys. J. **521**, 332 (1999).

[16] B. Datta, A.V. Thampan, and I. Bombaci, Astron. Astrophys. **334**, 943 (1998).

[17] X.-D. Li, S. Ray, J. Dey, M. Dey, and I. Bombaci, Astrophys. J. **527**, L51 (1999).

[18] J. A. Pons *et al.*, Astrophys. J. (submitted); astro-ph/0107404.

[19] D.L. Kaplan *et al.*, astro-ph/0111174; S. M. Ransom *et al.*, astro-ph/0111339.

[20] C. Alcock, E. Farhi, and A. Olinto, Astrophys. J. **310**, 261 (1986).

[21] J.E. Horvath, and O.G. Benvenuto, Phys. Lett. B **213**, 516 (1988).

[22] I. Bombaci, and B. Datta, Astrophys. J. **530**, L69 (2000).

[23] S.R. Kulkarni, *et al.*, Nature 393, 35 (1998).

[24] G. Nardulli, proceedings of this Conference, hep-ph/0111178.

[25] M.Alford, J.A. Bowers, and K. Rajagopal, hep-ph/0008208; hep-ph/0009357; K. Rajagopal, and F. Wilczek, hep-ph/0011333.

[26] A.I. Larkin, and Yu.N. Ovchinnikov, Zh. Eksp. Teor. Fiz. **47**, 1136 (1964), translation: Sov. Phys. JETP 20, 762 (1965); P. Fulde, and R.A. Ferrell, Phys. Rev. **135**, A550 (1964).

[27] A. Dar, A. De Rújula, and U. Heinz, Phys. Lett. B 470, 142 (1999); R.L. Jaffe, W. Busza, J. Sandweiss, and F. Wilczek, Rev. Mod. Phys. **72**, 1125 (2000); J. Madsen, Phys. Rev. Lett. **85**, 4687 (2000).

[28] I. Bombaci, Phys. Rev. C **55**, 1587 (1997).

[29] K.S. Cheng, Z.G. Dai, D.M. Wai, and T. Lu, Science **280**, 407 (1998).

# The observational appearance of strange stars

*Vladimir V. Usov*
*Department of Condensed Matter Physics*
*Weizmann Institute of Science*
*Rehovot 76100, ISRAEL*

## 1 Introduction

Strange stars that are entirely made of strange quark matter (SQM) have been long ago proposed as an alternative to neutron stars (e.g., [1, 2]). The possible existence of strange stars is a direct consequence of the conjecture that SQM composed of roughly equal numbers of up, down, and strange quarks plus a smaller numbers of electrons (to neutralize the electric charge of the quarks) may be the absolute ground state of the strong interaction, i.e., absolutely stable with respect to $^{56}$Fe [1, 3]. The bulk properties (size, moment of inertia, etc.) of models of strange and neutron stars in the observed mass range ($1 < M/M_{\odot} < 2$) are rather similar, and it is very difficult to discriminate between strange and neutron stars [4].

SQM with the density of $\sim 5 \times 10^{14}$ g cm$^{-3}$ might exist up to the surface of strange stars [2, 4]. Such a bare strange star differs qualitatively from a neutron star which has the density at the stellar surface (more exactly at the stellar photosphere) of about $0.1 - 1$ g cm$^{-3}$. This opens observational possibilities to distinguish bare strange stars from neutron stars.

## 2 Thermal emission from bare strange stars

At the bare SQM surface of a strange star the density changes abruptly from $\sim 5\times10^{14}$ g cm$^{-3}$ to zero. The thickness of the SQM surface is about 1 fm $= 10^{-13}$ cm, which is a typical strong interaction length scale. Since SQM at the surface of a bare strange star is bound via strong interaction rather than gravity, such a star is not subject to the Eddington limit in contrast to a neutron star [2, 5]. Below, we discuss the thermal emission of photons and $e^+e^-$ pairs from the SQM surface of a hot bare strange star.

## 2.1 Emission of photons

Hot SQM is filled with electromagnetic waves in thermodynamic equilibrium with quarks. The dispersion relation of these waves may be written in the following simple form $\omega^2 = \omega_{\rm p}^2 + k^2c^2$, where $\omega$ is the frequency of electromagnetic waves, $k$ is their wavenumber, and $\omega_{\rm p}$ is the plasma frequency of quarks [2]. This equation is the familiar dispersion relation for a plasma, and its conventional interpretation may be applied to SQM. Propagating modes exist only for $\omega > \omega_{\rm p}$. Therefore, there is the lower limit on the energy of electromagnetic photons that are in thermodynamic equilibrium with quarks, $\varepsilon_\gamma = \hbar\omega > \hbar\omega_{\rm p} \simeq 18.5(n_{\rm b}/n_0)^{1/3}$ MeV, where $n_{\rm b}$ is the baryon number density of SQM, and $n_0 = 0.17$ fm$^{-3}$ is normal nuclear matter density. At the SQM surface where the pressure is zero, we expect $n_{\rm b} \simeq (1.5-2)n_0$ and $\hbar\omega_{\rm p} \simeq 20-25$ MeV. i.e., the spectrum of thermal equilibrium photons radiated from the bare SQM surfaces of strange stars is very hard, $\varepsilon_\gamma > \hbar\omega_{\rm p} \simeq 20-25$ MeV [2].

The energy flux emitted from the unit surface of SQM in thermal equilibrium photons is [5, 6]

$$F_{\rm eq} = \frac{\hbar}{c^2}\int_{\omega_{\rm p}}^{\infty} d\omega\, \frac{\omega\,(\omega^2-\omega_{\rm p}^2)\,g(\omega)}{\exp\left(\hbar\omega/k_{\rm B}T_{\rm S}\right)-1}\,, \tag{1}$$

where

$$g(\omega) = \frac{1}{2\pi^2}\int_0^{\pi/2} d\vartheta\,\sin\vartheta\,\cos\vartheta\,D(\omega,\vartheta)\,, \tag{2}$$

$k_{\rm B}$ is the Boltzmann constant, $T_{\rm S}$ is the surface temperature, $D(\omega,\vartheta)$ is the coefficient of radiation transmission from SQM to vacuum, $D = 1-(R_\perp + R_\parallel)/2$, and

$$R_\perp = \frac{\sin^2(\vartheta-\vartheta_0)}{\sin^2(\vartheta+\vartheta_0)}\,,\quad R_\parallel = \frac{\tan^2(\vartheta-\vartheta_0)}{\tan^2(\vartheta+\vartheta_0)}\,,\quad \vartheta_0 = \arcsin\left[\sin\vartheta\sqrt{1-\left(\frac{\omega_{\rm p}}{\omega}\right)^2}\right]. \tag{3}$$

Figure 1 shows the ratio of the equilibrium photon emissivity of the bare SQM surface to the blackbody surface emissivity, $\xi_{\rm eq} = F_{\rm eq}/F_{\rm BB}$, where $F_{\rm BB} = \sigma T_{\rm S}^4$, and $\sigma$ is the Stefan-Boltzmann constant. From Figure 1 we can see that at $T_{\rm S} \ll \hbar\omega_{\rm p}/k_{\rm B} \sim 10^{11}$ K the equilibrium photon radiation from the bare surface of a strange star is very small, compared to the blackbody one.

Low energy photons ($\varepsilon_\gamma < \hbar\omega_{\rm p}$) may leave SQM if they are produced by a non-equilibrium process in the surface layer with the thickness of $\sim c/\omega_{\rm p} \simeq 10^{-12}$ cm. The upper limit on the emissivity of SQM in non-equilibrium photons at low energies is $\xi_{\rm neq} = F_{\rm neq}/F_{\rm BB} \leq 10^{-4}$ [6].

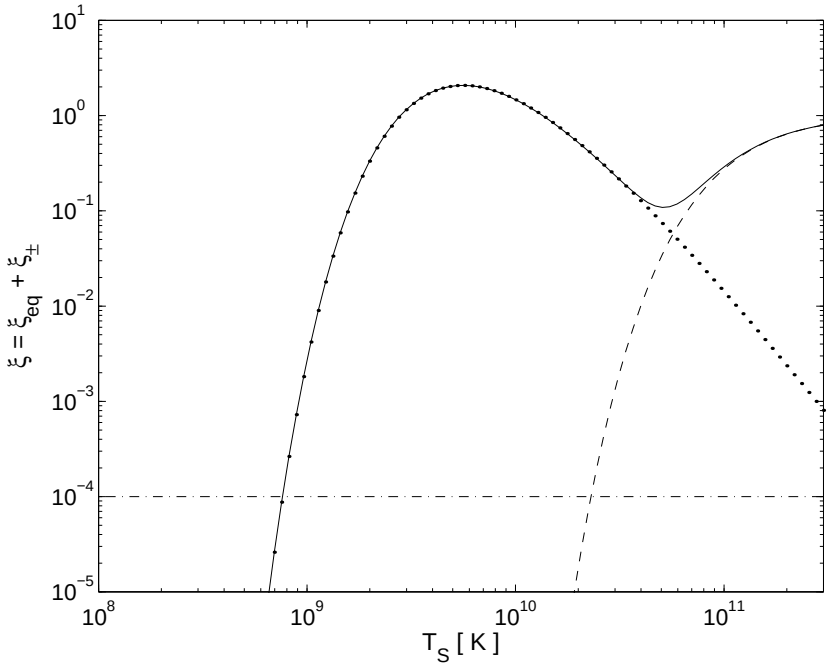


Figure 1: Total emissivity of bare SQM surface (solid line), which is the sum of emissivities in equilibrium photons (dashed line) and $e^+e^-$ pairs (dotted line), divided by the blackbody emissivity, $\xi = \xi_{\rm eq} + \xi_{\pm}$. The value of $\xi$ is valid at least for the surface temperature $T_{\rm s} \geq 8 \times 10^8$ K when $\xi$ is more than the upper limit on $\xi_{\rm neq}$, $\xi_{\rm neq} \leq 10^{-4}$, which is shown by the dot-dashed line.

## 2.2 Emission of $e^+e^-$ pairs

It was pointed out [7] that the bare surface of a hot strange star may be a powerful source of $e^+e^-$ pairs which are created in an extremely strong electric field at the quark surface and flow away from the star. The electric field is generated because there are electrons with the density $n_{\rm e} \simeq (10^{-3} - 10^{-4}) n_{\rm b}$ in SQM to neutralize the electric charge of the quarks (e.g., [2, 4]). The point is that the electrons, being bound to SQM by the electromagnetic interaction alone, are able to move freely across the SQM surface, but clearly cannot move to infinity because of the bulk electrostatic attraction to the quarks. The electron distribution extends up to $\sim 10^3$ fm above the quark surface, and a strong electric field is generated in the surface layer to prevent the electrons from escaping to infinity, counterbalancing the degeneracy and thermal pressure. The typical magnitude of the electric field at the SQM surface is $\sim 5 \times 10^{17}$ V cm$^{-1}$ [2]. This field is a few ten times higher than the critical field $E_{\rm cr} = m^2c^3/e\hbar \simeq 1.3 \times 10^{16}$ V cm$^{-1}$ at which vacuum is unstable to creation of $e^+e^-$ pairs. In such a strong electric field, $E \gg E_{\rm cr}$, in vacuum, the pair creation rate is

extremely high, $W_{\pm} \simeq 1.7 \times 10^{50} (E/E_{\rm cr})^2$ cm$^{-3}$ s$^{-1}$. At $E \simeq 5 \times 10^{17}$ V cm$^{-1}$, we have $W_{\pm} \simeq 2.5 \times 10^{53}$ cm$^{-3}$ s$^{-1}$. The high-electric-field region is, however, not a vacuum. The electrons present fill up states into which would-be-created electrons have to go. This reduces the pair-creation rate from the vacuum value. At zero temperature the process of pair creation is suppressed altogether because there is no free levels for electrons to be created [7].

At finite temperatures, $T_{\rm s} > 0$, in thermodynamical equilibrium electronic states are only partly filled, and pair creation by the Coulomb barrier becomes possible. Since the rate of pair production when electrons are created into the empty states is extremely high, the empty states below the pair creation threshold, $\varepsilon \leq \varepsilon_{\rm F} - 2m_{\rm e}c^2$, are occupied by created electrons almost instantly, where $\varepsilon_{\rm F} = \hbar c (\pi^2 n_{\rm e})^{1/3} \simeq 20$ MeV is the Fermi energy of electrons in SQM, and $m_{\rm e}$ is the electron mass [7]. Then, the rate of pair creation by the Coulomb barrier is determined by the process of thermalization of electrons which favors the empty-state production below the pair creation threshold. The thermal energy of SQM is, in fact, the source of energy for the process of pair creation.

The flux of $e^+e^-$ pairs from the unit surface of SQM is [5]

$$f_{\pm} \simeq 10^{39} \left( \frac{T_{\rm s}}{10^9 \ {\rm K}} \right)^3 \exp \left[ -11.9 \left( \frac{T_{\rm s}}{10^9 \ {\rm K}} \right)^{-1} \right] J(\zeta) \ \ {\rm cm}^{-2} \, {\rm s}^{-1} \, , \qquad (4)$$

where

$$J(\zeta) = \frac{1}{3} \frac{\zeta^3 \ln (1 + 2\zeta^{-1})}{(1 + 0.074\zeta)^3} + \frac{\pi^5}{6} \frac{\zeta^4}{(13.9 + \zeta)^4} \, , \qquad \zeta = 2 \sqrt{\frac{\alpha}{\pi}} \frac{\varepsilon_{\rm F}}{k T_{\rm s}} \simeq 0.1 \frac{\varepsilon_{\rm F}}{k T_{\rm s}} \, , \qquad (5)$$

and $\alpha = e^2/\hbar c = 1/137$ is the fine structure constant.

The energy flux from the unit surface of SQM in $e^+e^-$ pairs created by the Coulomb barrier is $F_{\pm} \simeq \varepsilon_{\pm} f_{\pm}$, where $\varepsilon_{\pm} \simeq m_{\rm e}c^2 + k_{\rm B} T_{\rm s}$ is the mean energy of created particles [7]. Figure 1 shows the ratio of the SQM surface emissivity in $e^+e^-$ pairs to the blackbody surface emissivity, $\xi_{\pm} = F_{\pm}/F_{\rm BB}$, versus the surface temperature $T_{\rm s}$. Creation of $e^+e^-$ pairs by the Coulomb barrier is the main mechanism of thermal emission from the surface of SQM at $8 \times 10^8 < T_{\rm s} < 5 \times 10^{10}$ K, while the equilibrium radiation dominates at extremely high temperatures, $T_{\rm s} > 5 \times 10^{10}$ K.

## 2.3 The thermal luminosity of a hot bare strange star

At $T_{\rm s} > 8 \times 10^8$ K, when the thermal emission from the SQM surface in both equilibrium photons and $e^+e^-$ pairs prevail, the total thermal luminosity of a bare strange star is

$$L = L_{\rm eq} + L_{\pm} = 4\pi R^2 (F_{\rm eq} + F_{\pm}) \,, \tag{6}$$

where $R \simeq 10^6$ cm is the radius of the strange star. Figure 2 shows the value of $L$ as a function of the surface temperature $T_{\rm s}$.

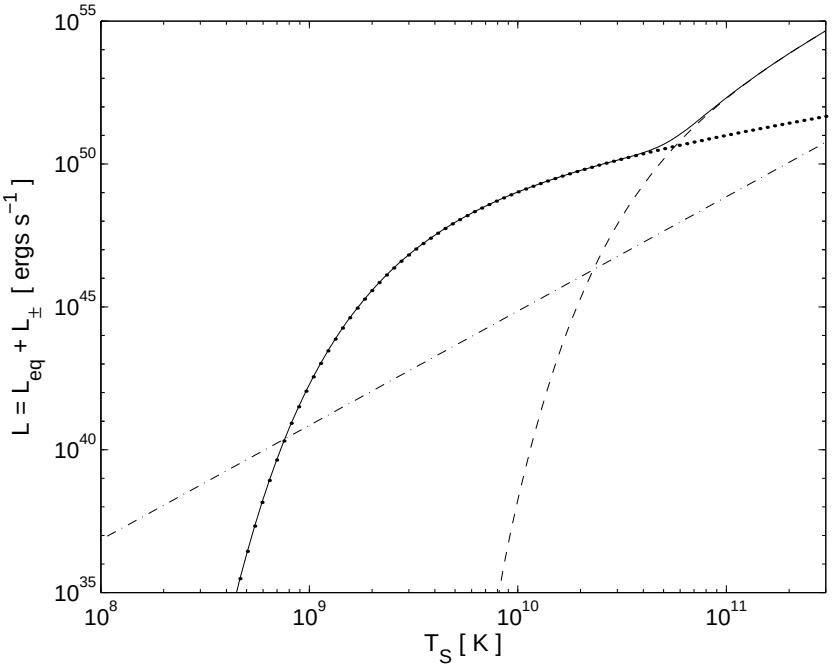


Figure 2: The total luminosity of a bare strange star $L = L_{\rm eq} + L_{\pm}$ (solid line), where $L_{\rm eq}$ and $L_{\pm}$ are the luminosities in thermal equilibrium photons (dashed line) and $e^+e^-$ pairs (dotted line), respectively. The upper limit on the luminosity in non-equilibrium photons, $L_{\rm neq} < 10^{-4} 4\pi R^2 F_{\rm BB}$, is shown by the dot-dashed line.

At $T_{\rm s} > 8 \times 10^8$ K the luminosity in $e^+e^-$ pairs created by the Coulomb barrier at the SQM surface is very high, $L_{\pm} > 10^{40}$ ergs s$^{-1}$ (see Fig. 2), that is at least four orders of magnitude higher than

$$L_{\pm}^{\rm max} \simeq 4\pi m_{\rm e} c^3 R/\sigma_{\rm T} \simeq 10^{36} \text{ ergs s}^{-1} \,, \tag{7}$$

where $\sigma_{\rm T}$ is the Thomson cross-section. In this case, the time-scale $t_{\rm ann} \sim (n_{\pm}\sigma_{\rm T} c)^{-1}$ for annihilation of $e^+e^-$ pairs is much shorter than the time-scale $t_{\rm esc} \sim R/c$ for their escape, $t_{\rm ann}/t_{\rm esc} \simeq L_{\pm}^{\rm max}/L_{\pm} < 10^{-4} \ll 1$, and $e^+e^-$ pairs outflowing from the stellar surface mostly annihilate in the vicinity of the strange star, $r \sim R$ (e.g., [8]). The luminosity in $e^+e^-$ pairs at the distance $r \gg R$ cannot be significantly more than $L_{\pm}^{\rm max}$. Therefore, far from a bare strange star with the surface temperature

$T_{\rm s} > 8 \times 10^8$ K the photon luminosity dominates irrespective of $T_{\rm s}$ and practically coincides with the total luminosity given by equation (6). At $T_{\rm s} < 8 \times 10^8$ K the total luminosity $L = L_{\pm} + L_{\rm neq}$ is somewhere between $\sim 4\pi 10^{-4} R^2 F_{\rm BB}$ and $\sim L_{\pm}$.

Till now, we assumed tacitly that SQM at the surface of the strange star is in the normal (nonsuperconducting) state. Recently, it was argured that SQM may be a color superconductor if its temperature is below some critical value (for a review, see [9]). In the classic BCS model, the critical temperature is $T_c \simeq 0.57\Delta_0/k_{\rm B}$, where $\Delta_0$ is the energy gap at zero temperature. The value of $\Delta_0$ is in the range from $\sim 0.1 - 1$ MeV [10] to $\sim 50 - 10^2$ MeV [9]. Color superconductivity can suppress the nonequilibrium radiation discussed in [6] significantly (if not completely). In this case, equation (6) may be used at $T_{\rm s} < 8 \times 10^8$ K as well. If SQM at the stellar surface is a color superconductor in the color-flavor locked (CFL) phase the process of $e^+e^-$ pair creation at the SQM surface may be turned off at $T \ll T_c$. This is because cold SQM in the CFL phase is electrically neutral, and no electrons are required and none are admitted inside CFL quark matter [11].

The energy spectrum of photons far from the strange star depends on the total thermal luminosity. At $L > 10^{43}$ ergs s$^{-1}$, the photon spectrum is nearly blackbody with the temperature $T \simeq T_0 (L/10^{43}$ ergs s$^{-1})^{1/4}$, where $T_0 \simeq 2 \times 10^8$ K [16]. For intermediate luminosities, $10^{42} < L < 10^{43}$ ergs s$^{-1}$, the effective temperature of photons is more or less constant, $T \sim T_0$ [17]. At $L_{\rm th} < 10^{42}$ ergs s$^{-1}$, the hardness of the photon spectrum increases when $L$ decreases. This is because photons that form in annihilation of $e^+e^-$ pairs cannot reach thermodynamical equilibrium before they escape from the strange star vicinity. When the photon luminosity decreases from $\sim 10^{42}$ ergs s$^{-1}$ to $\sim 10^{36}$ ergs s$^{-1}$, the mean energy of photons increases from $\sim 100$ keV to $\sim 500$ keV while the spectrum of photons changes eventually into a very wide ($\Delta E/E \sim 0.3$) annihilation line of energy $E \sim 500$ keV [17]. Such a behavior of photon spectra offers a good observational signature of hot bare strange stars. Super-Eddington luminosities are another finger print of such stars.

# 3 Thermal emission from non-bare strange stars

"Normal" matter (ions and electrons) may be at the quark surface of strange stars. The ions in the inner layer are supported against the gravitational attraction to the underlying strange star by a very strong electric field of the Coulomb barrier. There is an upper limit to the amount of normal matter at the quark surface, $\Delta M \leq 10^{-5} M_{\odot}$ [2, 12]. Such a massive envelope of normal matter with $\Delta M \sim 10^{-5} M_{\odot}$ completely obscures the quark surface. However, a strange star at the moment of its formation is very hot. The temperature in the interior of a nascent strange star is expected to be as high as a few $\times 10^{11}$ K [13]. The rate of mass ejection from an envelope of such a hot strange star is very high [14]. Besides, the high surface temperature leads to a

considerable reduction of the Coulomb barrier, which favors the tunneling of nuclei toward the quark surface [15]. Therefore, it is natural to expect that in a few seconds after formation of a strange star the normal-matter envelope is either blown away by radiation pressure or quarkonized, and the stellar surface is completely bare. The SQM surface remains bare until the thermal luminosity of the strange star is more than the Eddington limit, $L > L_{\rm Edd} \simeq 1.3 \times 10^{38} (M/M_\odot)$ ergs s$^{-1}$.

## 3.1 Low-mass normal-matter atmospheres

At $L < L_{\rm Edd}$ the normal-matter atmosphere forms because of gas accretion onto the strange star. The presence of the atmosphere may restore the ability of the stellar surface to radiate soft photons (this is like painting with black paint on a silver surface).

The strange star acts on the atmosphere as a heat reservoir. At $T_{\rm s} > 10^7$ K when the hot gas emits mainly due to bremsstrahlung radiation, the thermal structure of the low-mass normal-matter atmosphere and its photon radiation were considered in [18] by solving the heat transfer problem with $T = T_{\rm s}$ as a boundary condition at the inner layer. It was shown that if the atmosphere mass $\Delta M$ is smaller than

$$\Delta M_1 \simeq 7 \times 10^{11} \frac{A}{Z^2} \left( \frac{T_{\rm s}}{10^8 \, {\rm K}} \right)^{3/2} \left( \frac{R}{10^6 \, {\rm cm}} \right)^2 \, {\rm g} \, , \tag{8}$$

the atmosphere is nearly isothermal, and its photon luminosity is

$$L_{\rm a} \simeq \frac{4 \times 10^{33} Z^3}{A(1+Z)} \left( \frac{R}{10^6 \, {\rm cm}} \right)^{-4} \left( \frac{M}{M_\odot} \right) \left( \frac{T_{\rm s}}{10^8 \, {\rm K}} \right)^{-1/2} \left( \frac{\Delta M}{10^{12} \, {\rm g}} \right)^2 \, {\rm ergs \, s^{-1}} \, , \tag{9}$$

where $A$ is the mass number of ions and $Z$ is their electrical charge.

At $\Delta M_1 < \Delta M < \Delta M_2$, convection develops in the atmosphere, and the photon luminosity is $\tilde{L}_{\rm a} = 4\gamma L_{\rm a}/(3\gamma + 1)$, where

$$\Delta M_2 \simeq \frac{4 \times 10^{12} A}{Z^2 \mu^{1/2}} \left( \frac{T_{\rm s}}{10^8 \, {\rm K}} \right) \left( \frac{R}{10^6 \, {\rm cm}} \right)^2 \, {\rm g} \, , \tag{10}$$

$\mu = A/(1+Z)$ is the mean molecular weight, and $\gamma$ is the ratio of the specific heats at constant pressure and at constant volume [18]. For a rarefied totally-ionized plasma we have $\gamma = 5/3$ and $\tilde{L}_{\rm a} = (10/9) L_{\rm a}$. The difference between $L$ and $\tilde{L}$ is within the accuracy of our calculations which is $\sim 20\%$.

At $\Delta M > \Delta M_2$, both thermal conductivity and convection are not able to account for the cooling of atmospheric matter, and a thermal instability develops in the atmosphere [18]. As a result, the atmosphere cannot be in hydrostatic equilibrium during a time larger than the characteristic cooling time, and it has to be strongly

variable on a timescale of $\sim (10^{-4} - 10^{-3})(T_{\rm s}/10^8\,{\rm K})^{1/2}$ s. This variability of the strange-star atmosphere and its photon luminosity are known poor. Most probably, at $\Delta M > \Delta M_2$ the tendency of the photon luminosity to increase with increase of $\Delta M$ holds up to $L_{\rm a} \simeq L_{\rm Edd}$ if $T_{\rm s} > 3 \times 10^7$ K [18].

The photon emission from the low-mass normal-matter atmosphere of a hot ($T_{\rm s} > 3 \times 10^7$ K) strange star is hard. The spectrum of this emission is similar to the spectrum of thermal emission of optically thin plasma at $k_{\rm B}T$ up to $\sim 10^2$ keV [18]. This differs significantly from the photon emission of neutron stars.

### 3.2 Massive normal-matter envelopes with $\Delta M \sim 10^{-5} M_\odot$

If the age of a neutron star is $t > 10^2$ yr, the stellar interior may be divided into two regions: the isothermal core with density $\rho > \rho_e \sim 10^{11}$ g cm$^{-3}$ and the outer envelope with $\rho < \rho_e$ (e.g., [19]). Since the density of the normal-matter envelope with $\Delta M \sim 10^{-5} M_\odot$ at the quark surface of a strange star is about $\rho_e$, the temperature variation between the quark surface and the surface of the normal-matter envelope is more or less the same as the core-to-surface temperature variation of a neutron star for a fixed temperature at the stellar center. The cooling behavior of the quark core of strange stars depends on many factors and may be more or less similar to the cooling behavior of the isothermal core of neutron stars [20]. Therefore, from observations of thermal X-ray emission from not too young ($t > 10^2$ yr) compact objects it is difficult to distinguish strange stars with massive ($\Delta M \sim 10^{-5} M_\odot$) normal-matter envelopes from neutron stars (cf. [21]).

## 4 Soft $\gamma$-ray repeaters may be bare strange stars

Bare strange stars can radiate at the luminosities greatly exceeding the Eddington limit (see §2). The mean energy of radiated photons is a few ten keV or higher. Therefore, bare strange stars are reasonable candidates for soft $\gamma$-ray repeaters (SGRs) that are the sources of brief ($\sim 0.1$ s), intense [$\sim (10^3 - 10^4) L_{\rm Edd}$] outbursts with soft $\gamma$-ray spectra (for a review on SGRs, see [22]). The bursting activity of SGRs may be explained by fast heating of the SQM surface of bare strange stars up to the temperature of $\sim (1 - 2) \times 10^9$ K (see Fig. 2) and its subsequent thermal emission [5, 23]. The heating mechanism may be either impacts of comets onto bare strange stars [23, 24] or fast decay of superstrong ($\sim 10^{14} - 10^{15}$ G) magnetic fields [25].

Two giant flares were observed on 5 March 1979 and 27 August 1998 from SGR 0526-66 and SGR 1900+14, respectively. The peak luminosity of these remarkable flares was as high as $\sim 10^{45}$ ergs s$^{-1}$, 7 orders of magnitude in excess of the Eddington limit for a solar-mass object [26]. This luminosity is about ten times higher than the luminosity of our Galaxy. Recently, it was shown that the light curves of the two

giant outbursts may be easily explained in the following model [23]. A comet-like object with the mass $M_c \sim 10^{25}$ g falls onto a bare strange star. The total duration of the accretion is $\Delta t \sim 10^2 - 10^3$ s. The accreted matter sinks into the strange star and quarkonizes [2]. During the accretion, $t < \Delta t$, the surface layers of the strange star are heated, while their thermal radiation is completely suppressed by the falling matter. The total thermal energy accumulated in the surface layers at the moment $t = \Delta t$ is $Q \simeq 0.1 M_c c^2 \sim 10^{45}$ ergs. When the accretion is finished and the strange star vicinity is transparent for radiation, some part of the energy $Q$ is emitted from the quark surface and observed as a giant burst. Figure 3 shows the light curve expected in this model for $Q = 9.2 \times 10^{44}$ ergs and $\Delta t = 370$ s [23]. This light curve is in good agreement with the light curve observed for the 5 March 1979 event [26]. The spectrum of this event may be also explained by the thermal emission from the strange star [17].

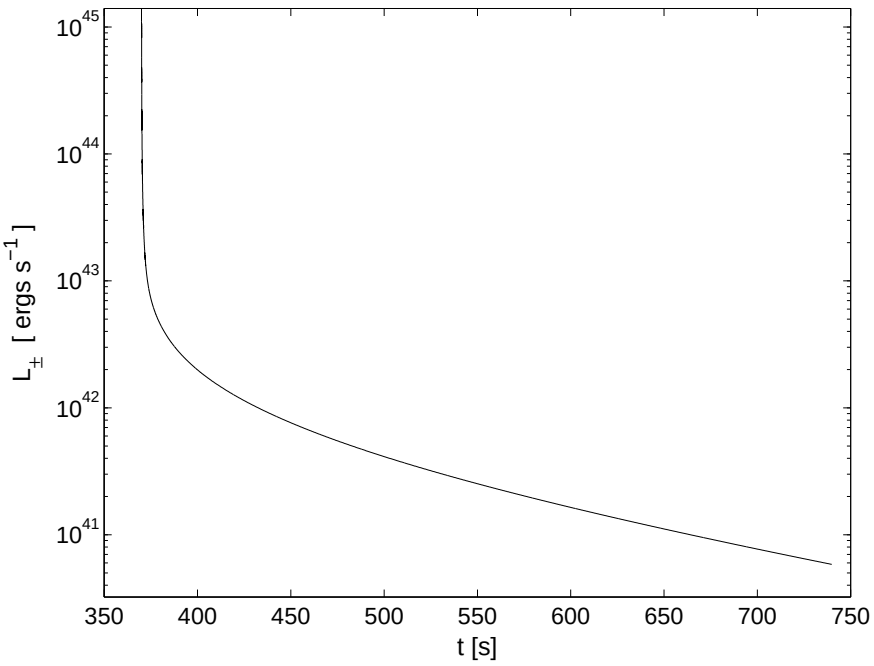


Figure 3: The light curve expected for $Q = 9.2 \times 10^{44}$ ergs and $\Delta t = 370$ s.

The light curve of the 27 August 1998 event may be fitted fairly well in our model for $Q = 6.4 \times 10^{44}$ ergs and $\Delta t = 270$ s [23].

One of the sources of matter that falls onto a strange star producing a SGR could be debris formed in collisions of planets orbiting the star in nearly coplanar orbits [27]. In this particular model, there appear two typical masses ($\sim 10^{25}$ g and $\sim 10^{22}$ g) available for prompt infall. Accretion of comet-like objects with the masses of $\sim 10^{25}$ g

and $\sim 10^{22}$ g may result in the giant and typical flares of SGRs, respectively.

It is worth to note that the distribution of temperature in the surface layers at the moment $t = \Delta t$, when the accretion is just finished and the powerful radiation from the stellar surface just starts, completely determines the subsequent radiation from the strange star at $t \geq \Delta t$. If the surface layers of a bare strange star are heated very fast ($< 10^{-3}$ s) to this temperature distribution by any other mechanism, for example by decay of superstrong ($\sim 10^{14} - 10^{15}$ G) magnetic fields [25], the light curve of the subsequent radiation coincides with the light curve shown by Figures 3.

Recently, the response of a bare strange star to the energy input onto the stellar surface was studied numerically [28]. In these simulations, the energy input started at the moment $t = 0$, and it was spherical and steady at $t \geq 0$. A wide range of the rate of the energy input was considered, $10^{38}$ ergs s$^{-1}$ $\leq L_{\rm input} \leq 10^{45}$ ergs s$^{-1}$. The rise time of the thermal radiation from the strange star was calculated for both normal and superconducting SQM. For giant outbursts ($L_{\rm input} \sim 10^{45}$ ergs s$^{-1}$), the rise time is $< 10^{-3}$ s irrespective of whether SQM is a superconductor or not. This time is consistent with available data on the two giant outbursts. For typical outbursts ($L_{\rm input} \sim 10^{41} - 10^{42}$ ergs s$^{-1}$) the rise time is $\sim 10^{2} - 10^{4}$ s for SQM in the normal state and $\sim 10^{-1} - 10^{-3}$ s for SQM in the superconducting state with the energy gap $\Delta_0 \geq 1$ MeV. Therefore, for typical outbursts the observed rise times ($\sim 10^{-1} - 10^{-3}$ s) may be explained in our model only if SQM is a superconductor with the energy gap of more than $\sim 1$ MeV.

This work was supported by the Israel Science Foundation of the Israel Academy of Sciences and Humanities.

# References

[1] E. Witten, Phys. Rev. D **30**, 272 (1984).

[2] C. Alcock, E. Farhi and A. Olinto, Astrophys. J. **310**, 261 (1986).

[3] D. Bodmer, Phys. Rev. D **4**, 1601 (1971).

[4] N.G. Glendenning, *Compact Stars: Nuclear Physics, Particle Physics, and General Relativity* (Springer, New York, 1997).

[5] V.V. Usov, Astrophys. J. Lett. **550**, L179 (2001).

[6] T. Chmaj, P. Haensel and W. Slomiński, Nucl. Phys. B **24**, 40 (1991).

[7] V.V. Usov, Phys. Rev. Lett. **80**, 230 (1998).

[8] A.M. Beloborodov, Astron. Astrophys. **305**, 181 (1999).

[9] M. Alford, K. Rajagopal and F. Wilczek, Phys. Lett. B **422**, 247 (1998); M. Alford, J. Berges and K. Rajagopal, Nucl. Phys. B **558**, 219 (1999); R.D. Pisarski and D.H. Rischke, Phys. Rev. D **61**, 051501 (2000); M. Alford, J. Berges and K. Rajagopal, Phys. Rev. D **63**, 074016 (2001).

[10] D. Bailin and A. Love, Phys. Rep. **107**, 325 (1984).

[11] K. Rajagopal and F. Wilczek, Phys. Rev. Lett. **86**, 3492 (2001).

[12] N.K. Glendenning and F. Weber, Astrophys. J. **400**, 647 (1992).

[13] P. Haensel, B. Paczyński and P. Amsterdamski, Astrophys. J. **375**, 209 (1991); K.S. Cheng and Z.G. Dai, astro-ph/0105164 (2001).

[14] S.E. Woosley and E. Baron, Astrophys. J. **391**, 228 (1992); A. Levinson and D. Eichler, Astrophys. J. **418**, 386 (1993); S.E. Woosley, Astron. Astrophys. **97**, 205 (1993).

[15] Ch. Kettner, F. Weber, M.K. Weigel, N.K. Glendenning, Phys. Rev. D **51**, 1440 (1995).

[16] B. Paczyński, Astrophys. J. **363**, 218 (1990); M. Lyutikov and V.V. Usov, Astrophys. J. Lett. **543**, L129 (2000).

[17] A.G. Aksenov, M. Milgrom and V.V. Usov, Astrophys. J., in preparation.

[18] V.V. Usov, Astrophys. J. Lett. **481**, L107 (1997).

[19] E.H. Gudmundsson, C.J. Pethick and R.I. Epstein, Astrophys. J. **272**, 286 (1983); M.E. Schaaf, Astron. Astrophys. **227**, 61 (1990).

[20] Ch. Schaab, F. Weber, M.K. Weigel and N.K. Glendenning, Nucl. Phys. A **605**, 531 (1996).

[21] P.M. Pizzochero, Phys. Rev. Lett. **66**, 2425 (1991).

[22] C. Kouveliotou, Astrophys. Space Sci. **231**, 49 (1995).

[23] V.V. Usov, Phys. Rev. Lett. **87**, 021101 (2001).

[24] B. Zhang, R.X. Xu and G.J. Qiao, Astrophys. J. Lett. **545**, L127 (2000).

[25] V.V. Usov, Astrophys. Space Sci. **107**, 191 (1984); C. Thompson and R.C. Duncan, Mon. Not. R. Astron. Soc. **275**, 255 (1995); J.S. Heyl and S.R. Kulkarni, Astrophys. J. **506**, L61 (1998).

[26] E.E. Fenimore, R.W. Klebesadel and J.G. Laros, Astrophys. J. **460**, 964 (1996); K. Hurley *et al.*, Nature (London) **397**, 41 (1999); E.P. Mazets *et al.*, Astron. Lett. **25**, 635 (1999); M. Feroci *et al.*, Astrophys. J. Lett. **515**, L9 (1999).

[27] J.I. Katz, H.A. Toole and S.H. Unruh, Astrophys. J. **437**, 727 (1994).

[28] V.V. Usov, Astrophys. J. Lett. **559**, L135 (2001).

# Discussion

**A. Thampan (IUCAA):** Won't general relativity modify (qualitatively) the temperature profile ($T$ versus $x$) that you have got?

**Usov:** The effects of general relativity do not change qualitatively the distribution of temperature in the surface layers of the strange star. These effects can lead only to rather small ($\sim 20\%$) corrections. In our calculations, the effects of general relativity were ignored because many input parameters (for example, the thermal emission from the SQM surface) are known within a factor of 2 or so.

**D.K. Hong (Pusan National University):** In the case of SQM, why the rise time does not change much as the energy gap changes a lot?

**Usov:** This is because when the energy gap is higher than about 1 MeV both the specific heat of the quark subsystem of SQM and its thermal conductivity are strongly suppressed. In this case, the heat transport is mostly determined by the electron subsystem, and it practically does not depend on the energy gap.

**J.E. Horvath (Sao Paulo University):** Did you attempt spectral comparisons of the model with the outburst of SGR 1900+14 Aug. 9? In that case the light curve has shown evidence for several periods $\sim$ fractions of a second. Is there any "natural" room for them in this model?

**Usov:** I have compared the theoretical and observed spectra for the 5 March 1979 outburst and found that they are consistent with each other. Since the spectra of other outbursts do not differ qualitatively, I think that these spectra may be explained as well. Our consideration of the short-time structure of the light curves is just started, and we have no even preliminary results yet.

# Structure of rapidly rotating strange stars: salient differences from neutron stars

*Arun V. Thampan*
*SISSA,*
*via Beirut n.2–4,*
*Trieste 34014,*
*ITALY*

## 1 Introduction

The existence of a third class of compact objects (apart from white dwarfs and neutron stars) has been debated for some time now (e.g. [1]). Attention may be drawn, particularly, to suggestions of "bare" strange stars as the candidates [2]. Although an important question in this regard would be the formation mechanisms for such objects, an issue of equal import is that of observationally distinguishing these objects from neutron stars and black holes. In this work, we juxtapose the parameters of structure of compact stars ("bare" strange stars and neutron stars) in an attempt to glean the salient differences between these two classes of compact object - a first step in proving (or disproving) the existence of strange stars.

The discussion presented here is, therefore, expected to have relevance when modelling future sensitive observational data from low mass X–ray binaries (LMXBs). LMXBs are compact objects in binary orbit with an evolved low mass or dwarf companion star. The closeness of the orbit permits the compact object to peel off the outer layer of the companion star. Owing to it possessing substantial angular momentum, the matter so accreted (or peeled off), forms an accretion disk around the compact star.

Astrophysical models of LMXBs (in particular, the X–ray burst sources) play an important role in the constraining the equation of state of high density matter of the central object. It is, therefore, imperative that the models so constructed be realistic. Including general relativisitic effects is inescapable. General relativity not only decides the internal structure of compact stars, but also their external spacetime.

General relativity implies the existence of an innermost marginally stable orbit around compact objects with a radius $r_{\rm in}$. For non–rotating (Schwarzschild) compact objects, $r_{\rm in} = 3GM/c^2$. For rotating compact objects, the $r_{\rm in}$ decreases (for a given

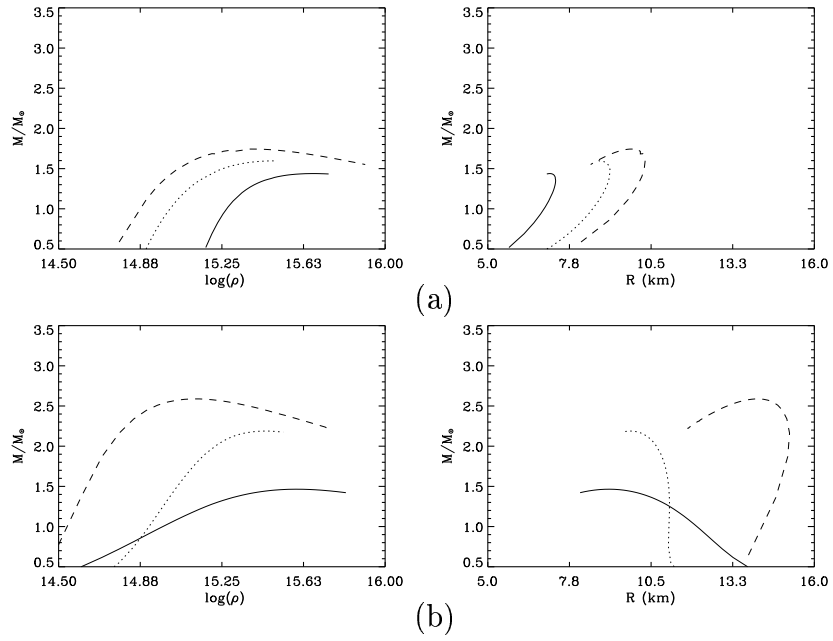


Figure 1: Structure parameters for non–rotating compact stars. The upper panel corresponds to strange stars and the lower to neutron stars. The curves correspond to: Upper Panel: EOS A (solid), B (dotted), C (dashed) and Lower Panel: EOS BPAL12 (solid), WFFII (dotted) and SBD (dashed) respectively.

rest mass) with increasing angular momentum. Accretion disks around compact objects will have an inner–edge located at $r = r_{\rm in}$. Neutron stars as well as strange stars may have radii $R > r_{\rm orb}$.

The matter spiralling in from the inner–edge of the accretion disk, transfers angular momentum to the compact star, spinning it up to high rotation rates ($\sim$ millisecond periods) over dynamical timescales. Realistic astrophysical models must incorporate the effects of rotation of the accreting compact object.

In this work, we point out some of the salient differences between rotating neutron and strange stars. We refer the reader to [3], [4], [5], for details on the results presented here.

## 2 Rotating compact stars

The first calculation of the structure of non–rotating bare strange stars [2], established the mass-radius relationship to be the chief difference between the structure of non–

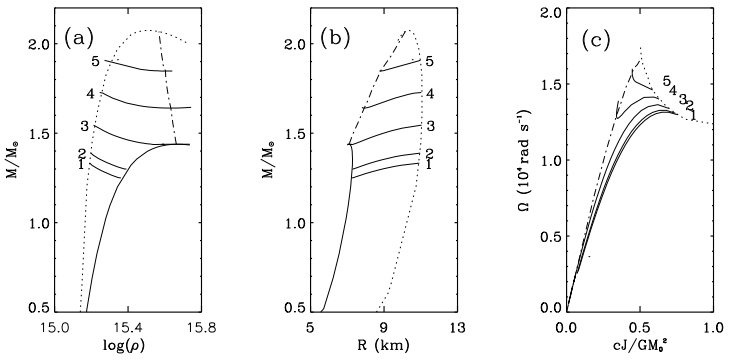


Figure 2: Rapidly rotating strange star structure parameters. EOS model used is EOS A. Labels 1–5 correspond to $M_0$ = 1.59, 1.66, 1.88, 2.14, 2.41 (where $M_0$ is the baryonic mass and the numbers are in units of solar mass $M_\odot$ : $1.9 \times 10^3 3$ gms) respectively.

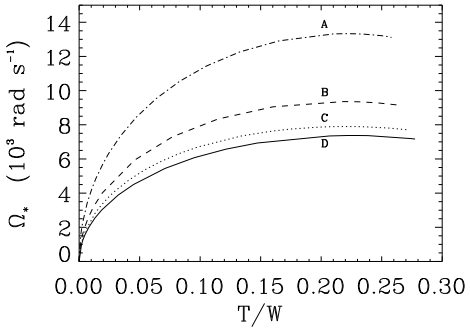


Figure 3: Strange star rotation rate as a function of the ratio of rotational kinetic energy to the total gravitational energy. The labels on curves correspond to the strange star EOS models used. All curves correspond to gravitational mass sequence $M = 1.4\ M_\odot$ .

rotating strange stars and neutron stars (Fig. 1). In the calculations reported here, we make use of 4 equations of state (EOS) models for strange stars (in what follows $B$, $\alpha_{\rm c}$, $m_{\rm s}$, $m_{\rm u}$, $m_{\rm d}$ refer to the Bag constant, QCD structure constant, and masses of strange, up and down quarks respectively): EOS A: [6], and MIT Bag model [7] with EOS B: $B = 90$ MeV/fm$^3$, EOS C: $B = 60$ MeV/fm$^3$, $\alpha_{\rm c} = 0$, $m_{\rm s} = 200$ MeV and $m_{\rm u} = m_{\rm d} = 0$, EOS D: $B = 60$ MeV/fm$^3$, $\alpha_{\rm c} = 0$ and 3 EOS models for neutron stars: BPAL12 [8]; WFFII [9]; SBD [10]. NSEOS model SBD is a very stiff EOS,

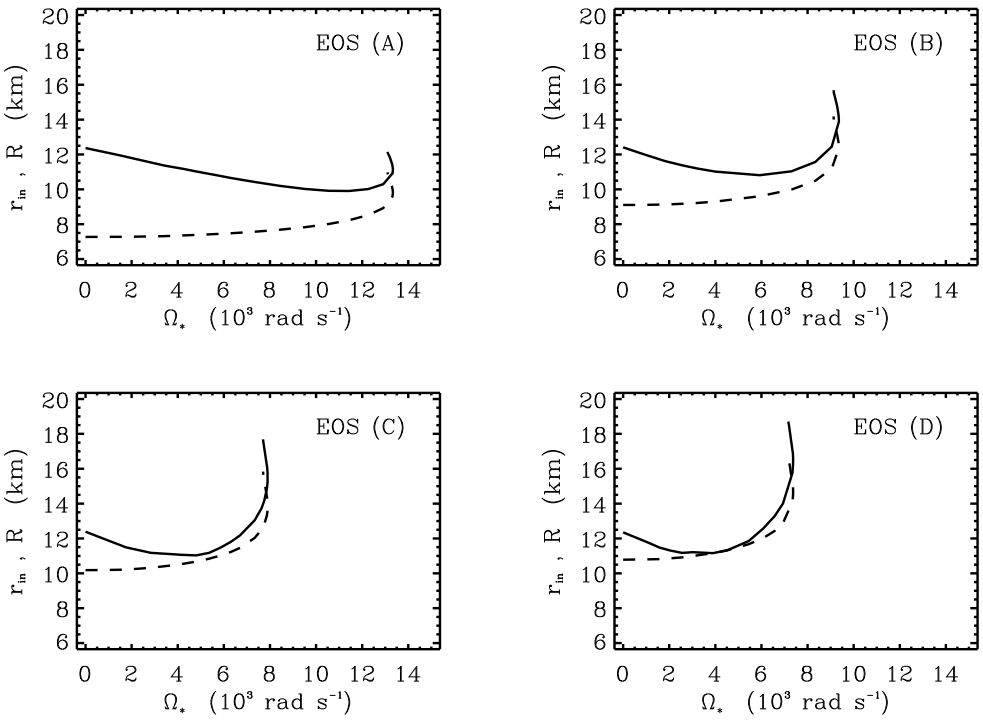


Figure 4: Strange star radii ($R$) and innermost stable circular orbit radii ($r_{\rm in}$) variations with rotation rate for graviational mass sequences corresponding to $M = 1.4$ $M_\odot$ .

while WFFII is moderate in stiffness and BPAL12 is very soft. In addition to these EOS models, we also use (for displaying the effect of EOS on Kepler frequencies) a strange star EOS model due to [11].

To construct rapidly rotating strange stars, we perform numerical computations based on the formalism by [12]. We construct sequences all the way from the static limit to mass–shed limit where centrifugal forces balance the inward gravitational pull. We also construct constant gravitational mass ($M$) and constant baryonic mass ($M_{\rm B}$) sequences. The results of our calculations, for one SSEOS: ... is shown in Fig. 2: the thick solid curve is the non–rotating limit, the dotted curve is the mass shed limit and the horizontally directed curved lines are constant baryonic mass sequences.

The constant gravitational mass sequences help studying the effect of spin on the strange stars. From Fig. 3, we notice that there exists a maximum rotation rate for the strange stars, with a value that is higher than the rotation rate at mass shed (an effect that is absent in neutron stars: [13]). This maximum occurs at $T/W \sim 0.2$, indicating that such angular velocities are perhaps not attainable in strange stars due

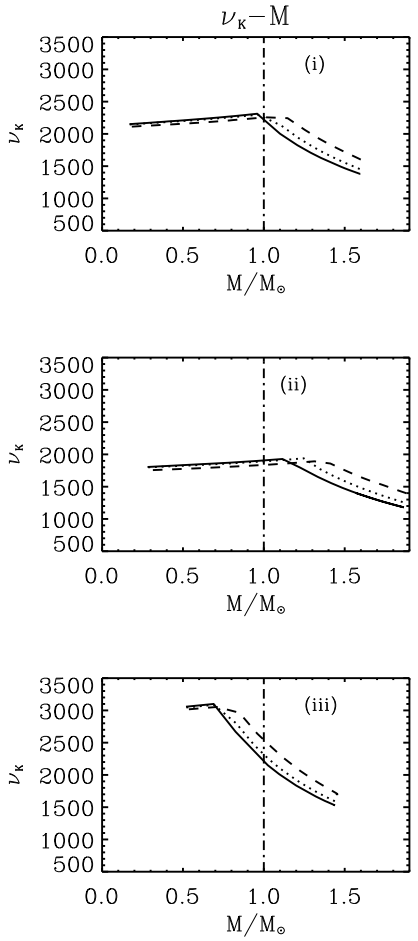


Figure 5: Kepler frequencies of test particles around rotating strange stars. The panel (i) corresponds to EOS B, and panel (iii) to A. Panel (ii) corresponds to EOS model due to [11]. The curves in each of these panel correspond to strange star rotation rates of 0 (solid), 200 (dotted) and 580 (dashed) Hz. The vertial dot–dashed lines in the panel represents a 1 $M_\odot$ configuration.

to triaxial instabilies [14].

Fig. 4 showing $r_{\rm in}$ v/s $\Omega$ for constant gravitational mass sequences imply that $r_{\rm in}$ decreases with increasing $\Omega_*$ for low values of the rotation rate (similar to Kerr black holes and rotating neutron stars), but reaches a minimum and increases for higher rotation rates. The increase in $r_{\rm in}$ with rotation is purely an effect of the large quadrupole moment of the strange star [15].

We also compute the Kepler frequencies of test particles around rotating strange stars (Fig. 5). On comparing these with the Kepler frequencies expected for neutron

stars (see [16]), we see that frequencies in the range (1.9 - 3.1) kHz if observed in future in X–ray burst sources, can be understood in terms of strange stars rather than neutron stars.

Acknowledgements: The results presented in this paper was obtained at Inter–University Centre for Astronomy and Astrophysics (IUCAA), Pune, India.

# References

[1] N. K. Glendenning in Compact Stars, (Springer-Verlag, New York, 2000), 399

[2] C. Alcock, E. Farhi, A. Olinto, Astrophys. J., **310**, 261 (1986)

[3] I. Bombaci, A.V. Thampan, B. Datta, Astrophys. J. **541**, L71 (2000)

[4] B. Datta, A.V. Thampan, I. Bombaci, Astron. Astrophys. **355**, L19 (2000)

[5] S. Bhattacharyya, A.V. Thampan, I. Bombaci, Astron. Astrophys., **372**, 925 (2001)

[6] M. Dey, I. Bombaci, J. Dey, S. Ray, B.C. Samanta, Phys. Lett. B, **438**, 123 (1998), erratum Phys. Lett. B, **467**, 303

[7] E. Farhi, R.L. Jaffe, Phys. Rev. D, **30**, 2379 (1984)

[8] I. Bombaci in Perspectives on Theoretical Nuclear Physics, I. Bombaci, A. Bonaccorso, A. Fabrocini et al. eds. (ETS, Pisa, 1995) p223

[9] R.B. Wiringa, V. Fiks, A. Fabrocini, Phys. Rev. C, **38**, 1010 (1993)

[10] P.K. Sahu, R. Basu, B. Datta, Astrophys. J., **416**, 267 (1993)

[11] A. Goyal, J.D. Anand, Phys. Rev., **D42**, 992 (1990)

[12] G.B. Cook, S.L. Shapiro, S.A. Teukolsky, Astrophys. J., **424**, 823 (1994)

[13] S. Bhattacharyya, A.V. Thampan, R. Misra, B. Datta, Astrophys. J., **542**,473 (2000)

[14] E. Gourgoulhon, P. Haensel, R. Livine, E. Paluch, et al., Astron. Astrophys., **349**, 851 (1999)

[15] P. Amsterdamski, T. Bulik, D. Gondek-Ronsinska, W. Kluźniak, `astro-ph/0012547`, (2000)

[16] A.V. Thampan, D. Bhattacharya, B. Datta, Mon. Not. Royal Astron. Soc. **302**, L69 (1999)

# Tensor Correlations and Pions in Dense Nuclear Matter

*Emma Olsson*[1,2] *and Chris J. Pethick*[2]

[1] *Uppsala Astronomical Observatory, Sweden*
[2]*NORDITA, Denmark*

## 1 Introduction

Despite concerted efforts by many groups over a period of more than three decades, the problem of stellar collapse, supernova production, and neutron star formation is still not understood. The basic physical inputs required for calculations of stellar collapse are, apart from an initial stellar model, the equation of state of hot dense matter, and the rates of neutrino production, absorption, and scattering processes. There are tantalizing hints that, if the microscopic physical input differed from what is presently used in simulations, the "delayed" mechanism [1], in which the outgoing shock wave is revived by deposition of energy by neutrinos streaming out of the stellar core, could account for core collapse supernovae and the formation of neutron stars in the collapse of a massive star.

One such hint comes from a relatively old calculation in which it was found that the allowance for pion-like excitations in the equation of state led to an increase in the explosion energy [2]. This indicates the importance of performing improved calculations of the equation of state in which pionic degrees of freedom are treated realistically. A second hint comes from parametric studies of core-collapse models, which indicate that the outcome of stellar collapse is sensitive to modest changes (a factor of two, say) in the neutrino opacity [3]. The effects of some parts of the nucleon-nucleon interactions on rates of neutrino processes in stellar collapse have been investigated by a number of groups, but so far the tensor part of the interaction has received scant attention, except in the work of Raffelt and colleagues [4]. Given what is known about the role of the tensor force in finite nuclei, there is reason to believe that its effect on neutrino processes in stellar collapse could be significant.

Numerical simulations of stellar collapse provide motivation for taking up the question of how important tensor correlations are in nuclear and neutron matter. In

[1]Uppsala Astronomical Observatory, Box 515, SE-75120 Uppsala, SWEDEN
[2]NORDITA, Blegdamsvej 17, DK-2100 Copenhagen, DENMARK

addition, theoretical investigations of the equation of state of cold dense matter point to there being strong pionic correlations at densities only slightly above that of saturated nuclear matter [5]. In the latter work it was found that a state resembling a neutral pion condensate was energetically favorable compared with one that did not, contrary to the view accepted for the past quarter of a century that pion condensation is ruled out at such densities by the strong central part of the nucleon-nucleon interaction in the spin-isospin channel. The pionic correlations give rise to maxima in the static longitudinal structure factor for the nuclear spin in neutron matter, and for the nucleon spin-isospin in nuclear matter, as shown in Fig. 1. The definition of the structure factor is given in Eq. (10) below. All these pieces of evidence point to

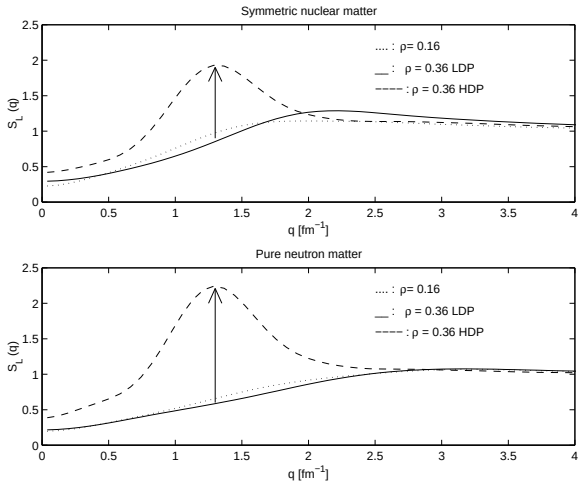


Figure 1: Static structure factor for the longitudinal spin operator in neutron matter and for the longitudinal spin-isospin operator in symmetric nuclear matter as a function of wave number, $q$. (After Ref. [5]).

the importance of investigating anew tensor correlations in dense matter.

The aspect we shall focus on most here is that of neutrino processes, and how they are affected by non-central forces, of which the pion-exchange interaction between nucleons is an example. Our aim is to provide a general framework within which to describe neutrino processes, including production, scattering and absorption. We shall make connections to Landau's theory of normal Fermi liquids, and indicate how the usual formulation, which assumes that the interaction is invariant under rotation of the spins of the particles, needs to be extended.

## 2 Neutrino processes

Rates of neutrino processes in dense matter are affected significantly by nucleon-nucleon interactions. Among early works on this subject we mention Refs. [6] and [7] on neutrino scattering processes in degenerate matter. Rates of neutrino processes in dense matter were calculated with allowance for the effect of nucleon-nucleon interactions on the energies of the quasiparticles in Ref. [8]. In addition, the influence of the finite lifetime of excitations in the nuclear medium on rates of neutrino processes has been considered in Refs. [4] and [9]. In the latter calculations, the non-central character of the nucleon-nucleon interaction plays an important role. Finally, in Ref. [10], the calculations of Refs. [6] and [7] have been extended to allow for partial degeneracy of the nucleons, and for non-zero momentum transfers. In the latter work the screening of the weak interaction matrix elements by the central part of the nucleon-nucleon interaction was taken into account. Tensor correlations play an important role in determining the rates of neutrino processes in dense matter, both for the neutrino processes of importance in stellar collapse, as we shall explain in greater detail below, as well as for the modified Urca process which is important for the cooling of neutron stars.

Since the weak coupling constant is small, it is generally an excellent approximation to calculate the rate of neutrino processes in dense matter using the standard golden-rule result for the transition rate. Furthermore, the effects of other interactions, such as electromagnetic ones, between leptons and hadrons are generally small, and the expression for the rate $Q$ of transitions may be written in the form [9]

$$Q \sim {G_F}^2 \; n \int \frac{d^3\mathbf{q} d\omega}{(2\pi)^4} S_{\mu\nu}(\mathbf{q},\omega) N^{\mu\nu}(\mathbf{q},\omega) \tag{1}$$

where $G_F$ is the weak coupling constant, $n$ is the baryon density, $S_{\mu\nu}(\mathbf{q},\omega)$ is a dynamical structure factor for the hadron system, and $N^{\mu\nu}(\mathbf{q},\omega)$ is a function that depends only on the leptons. The quantity $\mathbf{q}$ denotes the momentum transfer to the nucleon system, and $\omega$ the energy transfer. The weak interaction has the form of a product of current operators, either the vector current or the axial vector one, for the leptonic and hadronic systems. For definiteness, let us assume that the hadron system consists of non-relativistic nucleons. In this case, the leading contribution to a current is the time component which, for the vector current, is proportional to the nucleon density and, for the axial vector current, to the spin density. More generally one must include relativistic effects, such as weak magnetism (see e.g. Ref. [11]), and other hadronic degrees of freedom.

## 2.1 Neutral-current processes

To illustrate the qualitative effects of a non-central interaction, such as the tensor interaction, on neutrino processes, we consider as an example scattering of neutrinos by the weak neutral-current interaction. The structure factor of interest in calculating the rate of the process is then the one for the spin density. The tensor interaction has three qualitatively different effects. These are conveniently examined for processes in which the momentum and energy transfers are small compared with the typical energies and momenta of a nucleon in the medium. One effect is to change the expectation value of the spin of an excitation in the nuclear medium to a value different from that for an isolated nucleon. This effect is well-known in the context of nuclear magnetic moments, where the spin-orbit and tensor components of the nucleon-nucleon interaction modify the nuclear moment [12]. A second effect is to introduce into the effective interaction between nucleon-like excitations a non-central component – this modifies screening phenomena. A third effect is that the spin operator, which, if one neglects contributions due to exchange currents, is a one-body operator when expressed in terms of nucleon degrees of freedom, acquires two- and higher-body contributions for the excitations in the nuclear medium.

## 2.2 Landau theory

To illustrate the effects of non-central interactions described above, we consider the special case of long wavelengths, and temperatures low compared with the Fermi temperature. In this regime the concepts and machinery of Landau's theory of normal Fermi liquids may be applied [13]. We shall examine the form of the spin response for a one-component system. As we mentioned above, this is relevant for calculating the rates of neutral-current processes that proceed via the axial vector contribution of the interaction. If interactions are central, the static magnetic susceptibility of an interacting Fermi liquid with a single fermion component may be expressed in the form

$$\frac{\chi}{\chi_0} = \frac{m^*/m}{1+G_0} \tag{2}$$

where $\chi_0$ is the susceptibility of a non-interacting Fermi gas of the same density, $m^*$ is the effective mass of a quasiparticle, and $G_0$ is the Landau parameter describing the isotropic part of the spin-dependent component of the interaction. When there are non-central forces, this expression must be modified, and we shall consider the three effects mentioned above in turn.

When the interaction has tensor components, which are non-central, application of a magnetic field will tend to polarize quasiparticles in a direction different from that of the applied field. The magnetic moment of a quasiparticle is then described

by a tensor which, from the requirement of rotational invariance, must have the form

$$\mu_{ij}(\mathbf{p}) = \mu_0\delta_{ij} + (3/2)\mu_2(\hat{p}_i\hat{p}_j - \delta_{ij}/3), \tag{3}$$

where $\hat{\mathbf{p}}$ is a unit vector in the direction of the momentum, and $\mu_0$ and $\mu_2$ are coefficients. The interaction between two quasiparticles $f_{\mathbf{p}\boldsymbol{\sigma},\mathbf{p}'\boldsymbol{\sigma}'}$ may be written in the general form

$$f_{\mathbf{p}\boldsymbol{\sigma},\mathbf{p}'\boldsymbol{\sigma}'} = f_{\mathbf{p}\mathbf{p}'} + g_{\mathbf{p}\mathbf{p}'}\boldsymbol{\sigma}\cdot\boldsymbol{\sigma}' + t_{\mathbf{p}\mathbf{p}'}(3\boldsymbol{\sigma}\cdot\hat{\mathbf{k}}\,\boldsymbol{\sigma}'\cdot\hat{\mathbf{k}} - \boldsymbol{\sigma}\cdot\boldsymbol{\sigma}'), \tag{4}$$

where there is tensor contribution in addition to the usual expression for a central interaction. Here $\hat{\mathbf{k}}$ is a unit vector in the direction of $\mathbf{p}-\mathbf{p}'$. If we assume that we may neglect all but the isotropic parts of the quasiparticle interaction, one finds for the magnetic susceptibility the result [14]

$$\chi = \frac{{\mu_0}^2 N(0)}{1+G_0-{K_0}^2/8} - \frac{\mu_0\mu_2 N(0)K_0}{1+G_0} + \frac{1}{2}N(0){\mu_2}^2 + \chi_{\rm M}, \tag{5}$$

where $K_0 = N(0)t$ is the tensor Landau parameter, $N(0)$ being the density of quasiparticle states at the Fermi surface, $G_0 = N(0)g$ and $\chi_M$ is the multipair contribution to the susceptibility. In this expression, the effects of tensor interactions have been included only to second order in all but the first term. The first term in Eq. (5) corresponds to the result derived in Ref. [15] if renormalization of the magnetic moment is neglected.

One reason for the great success of Landau Fermi-liquid theory for liquid $^3$He and for electrons in metals is that the forces between particles are central to a good first approximation. In addition, the quantities of greatest physical interest are the particle number density and the spin density. What the result for the static susceptibility demonstrates is that many more parameters are needed to characterize the long-wavelength properties of a normal Fermi liquid with non-central forces, compared with the two needed for a liquid with only central forces.

## 2.3 Kinematics of neutrino processes

Now let us consider scattering of neutrinos by dense matter. For the simultaneous conservation of momentum and energy in the process, the magnitude of the energy transfer $\omega$ to the neutrino must be less than $cq$, where $\mathbf{q}$ is the momentum transfer. In other words, the four-momentum transfer from the nuclear medium to the neutrino must be space-like. For production of neutrino-antineutrino pairs via neutral-current processes, the requirements are the opposite, since the total energy of the pair must be greater than $cq$, $\mathbf{q}$ in this case being the total momentum of the pair, or the four-momentum transfer must be time-like. It is therefore of interest to explore which sorts of transitions in the nuclear medium can contribute to the various classes of neutrino

process. For simplicity, let us again consider momentum transfers small compared with the Fermi momentum of the nucleons, and temperatures low compared with the Fermi temperature. The energy of a single quasiparticle-quasihole pair is given by $\omega = \epsilon_{\mathbf{p}} - \epsilon_{\mathbf{p}-\mathbf{q}} \approx \mathbf{v}_{\mathbf{p}} \cdot \mathbf{q}$, where $\mathbf{v}_{\mathbf{p}} = \boldsymbol{\nabla}_{\mathbf{p}} \epsilon_{\mathbf{p}}$ always has a magnitude less than $v_{\mathrm{F}} q$, where $v_{\mathrm{F}}$ is the velocity of a quasiparticle at the Fermi surface. Thus single pair excitations in the nuclear medium always have space-like four momentum. Consequently annihilation of a single quasiparticle-quasihole pair cannot create a neutrino-antineutrino pair, while it can contribute to scattering of a neutrino. This clearly indicates the important role that excitations containing two or more quasiparticle-quasihole states play in neutrino pair emission.

## 2.4 Relative importance of single-pair and multipair states

The discussion above indicates the different roles that single-pair and multipair states play, and here we investigate their relative strength. One simple result may be obtained for operators $\mathcal{O}$ that satisfy a local conservation law of the usual form

$$\frac{\partial \mathcal{O}(\mathbf{r})}{\partial t} + \boldsymbol{\nabla} \cdot \mathbf{j}(\mathbf{r}) = 0, \tag{6}$$

where $\mathbf{j}(\mathbf{r})$ is the associated current density. On taking the matrix element of this equation between an excited state $j$ and the ground state and Fourier transforming in space, one finds

$$\omega_{j0} (\mathcal{O}_{\mathbf{q}})_{j0} = \mathbf{q} \cdot (\mathbf{j}_{\mathbf{q}})_{j0}. \tag{7}$$

This shows that the matrix element of the density satisfies the condition

$$(\mathcal{O}_{\mathbf{q}})_{j0} = \frac{\mathbf{q} \cdot (\mathbf{j}_{\mathbf{q}})_{j0}}{\omega_{j0}}. \tag{8}$$

Thus for an excited state with non-zero energy, the matrix element of the operator tends to zero as $q$ tends to zero, provided only that the matrix element of the current remains finite. Therefore, since the vector current is conserved, there will be no multipair contributions to the time component of the current. However, the axial current is not conserved, and consequently multipair contributions will be present in general.

To determine how large these multipair contributions are, a number of approaches are possible. One is to calculate them directly from a nucleon-nucleon interaction and microscopic many-body theory. Another is to make use of sum rules to put bounds on multipair contributions. To illustrate the latter method, let us look at the structure function, defined by

$$S(q, \omega) = \sum_j | < j | \mathcal{O}_{\mathbf{q}} | 0 > |^2 \delta(\omega - \omega_{j0}) = -\mathrm{Im}\chi(q, \omega)/\pi. \tag{9}$$

In the limit $q \to 0$, only multipair states contribute to the static structure factor

$$S(q) = \frac{1}{n} \sum_j | < j|\mathcal{O}_{\mathbf{q}}|0 > |^2, \tag{10}$$

and to the energy-weighted sum

$$W(q) = \sum_j | < j|\mathcal{O}_{\mathbf{q}}|0 > |^2 \omega_{j0}. \tag{11}$$

Another moment of interest is the static response function, $\chi(q,0)$, which is given by

$$\chi(q,0) = \sum_j 2| < j|\mathcal{O}_{\mathbf{q}}|0 > |^2/\omega_{j0}. \tag{12}$$

Let us denote the multipair contribution to the structure function by $S_{\rm M}(q,\omega)$. From the fact that the integrand is positive for positive $\omega$, it follows that

$$\int_0^\infty \frac{S_{\rm M}(q,\omega)}{\omega} \left(\omega - \overline{\omega}\right)^2 \geq 0, \tag{13}$$

where the mean excitation energy $\overline{\omega} = W(q)/S(q)$. This leads to the following condition on the multipair contribution to the static response function $\chi_{\rm M}$:

$$\chi_{\rm M}(0) \geq 2 \, \frac{nS(q)}{\overline{\omega}}. \tag{14}$$

If one were to take the $q \to 0$ limit of the calculations of the static spin structure factor and the energy-weighted sum calculated in Ref. [5], one would be led to the conclusion that multipair excitations make up more than $\sim$60% of the total static response function. This estimate is surprisingly large, but we should stress that the calculations in Ref. [5] were designed to shed light on correlations at non-zero wave numbers, where pionic correlations were found to enhance the static structure factor, and not to give accurate results for the long-wavelength response. It is possible that the calculations of Ref. [5] overestimate the structure factor at small wave numbers. Consequently, improved calculations of the static structure function are needed before it will be possible to place better bounds on the magnitude of multipair contributions to the response.

# 3 Concluding remarks

From the discussion above it is apparent that tensor correlations potentially play an important role in the microscopic physics needed as input to simulations of stellar

collapse and supernovae. Similar conclusions apply to other processes that we do not have space to consider here, among them charged current processes, such as the modified Urca process [16], which is important for the cooling of neutron stars.

Many open problems remain. With respect to neutrino processes, improved expressions are needed for the modification of axial vector matrix elements in a nuclear medium, and for the Landau parameters [17]. To obtain an improved equation of state, the effects of pionic correlations need to be included in a realistic manner.

We are grateful to A. Akmal for supplying us with tables of his results for the static structure factor and average excitation frequencies, and to S. Fantoni and V. R. Pandharipande for valuable discussions. Part of this work was carried out while the authors enjoyed the hospitality of the Institute of Nuclear Theory at the University of Washington. E.O. thanks the school on Advanced Instrumentation and Measurements (AIM) and the EU Marie Curie Training Site at NORDITA for financial support.

# References

[1] J. R. Wilson, in *Numerical Astrophysics*, Ed. J. M. Centrella, J. M. LeBlanc and R. L. Bowers (Jones and Bartlett, Boston, 1985) pp. 422-434. H. A. Bethe and J. R. Wilson, Ap. J. **295**, 14 (1985).

[2] R. W. Mayle, M. Tavani, and J. R. Wilson, Ap. J. **418**, 398 (1993).

[3] H.-T. Janka, Astr. Astroph. **368**, 527 (2001).

[4] G. Raffelt and D. Seckel, Phys. Rev. D **52**, 1780 (1995); G. Raffelt, D. Seckel and G. Sigl, Phys. Rev. D **54**, 2784 (1996); G. Raffelt and G. Sigl, Phys. Rev. D **60**, 023001 (1999).

[5] A. Akmal and V. R. Pandharipande, Phys. Rev. C **56**, 2261 (1997).

[6] R. F. Sawyer, Phys. Rev. D **11**, 2740 (1975).

[7] N. Iwamoto and C. J. Pethick, Phys. Rev. D **25**, 313 (1982).

[8] S. Reddy, M. Prakash and J. M. Lattimer, Phys. Rev. D **58**, 013009 (1998).

[9] G. Raffelt *Stars as Laboratories for Fundamental Physics*, The University of Chicago Press, Chicago (1996) Sec. 4.3.

[10] A. Burrows and R. F. Sawyer, Phys. Rev. C **58**, 554 (1998).

[11] C. J. Horowitz, Phys.Rev. D **65**, 043001 (2002).

[12] A. Arima, K. Shimizu, W. Bentz, and H. Hyuga, Adv. Nucl. Phys. **18**, 1 (1987).

[13] L. D. Landau, Sov. Phys. JETP **3**, 920 (1957); **5**, 101 (1957).

[14] E. Olsson and C. J. Pethick, in preparation.

[15] P. Haensel and A. J. Jerzak, Phys. Lett. B **112**, 285 (1982).

[16] See, e.g., B. L. Friman and O. V. Maxwell, Ap. J **232**, 541 (1979), C. Hanhart, D. R. Phillips, and S. Reddy, Phys. Lett. B **499**, 9 (2001) and A. E. L. Dieperink, E. N. E. Dalen, A. Korchin, and R. Timmermans, nucl-th/0012073.

[17] A. Schwenk, G. E. Brown, and B. Friman, Nucl. Phys. A **703**, 745 (2002).

# The QCD Phase Diagram

# The QCD Phase Diagram and Explosive Astrophysics

*Stephen D. H. Hsu*
*Department of Physics*
*University of Oregon*
*Eugene, OR USA*

## 1 Introduction

I was asked by the organizers to give an overview of the QCD phase diagram, geared towards a mixed audience of astrophysicists and particle theorists. I chose to emphasize the phase transition(s) from the normal nuclear phase to the color superconducting and chirally symmetric phases at high density and low temperature[1]. I did so because it is possible that these transitions might occur during violent astrophysical phenomena such as supernovae or neutron star mergers [1], with potentially dramatic consequences. If so, these astrophysical events could provide a window into the physics of QCD.

This contribution is organized as follows. In section 2 I summarize our current understanding of the QCD phase diagram. In section 3 I discuss the phase transition characteristics most relevant to astrophysics, such as critical temperature and latent heat. In section 4 I discuss supernova core collapse and argue that conditions at core bounce might lead to the crossing of a QCD phase boundary. I also briefly discuss neutron star mergers and hypernovae. I conclude with some discussion from the conference.

## 2 QCD phase diagram

Figure 1 (taken from Rajagopal and Wilczek's excellent review in [1]) shows a possible QCD phase diagram as a function of temperature and chemical potential. The region at low temperature and density (lower left) is the normal nuclear matter phase (the small spur at the bottom is the phase boundary for the formation of nuclear matter). At sufficiently high density and low temperature (lower right) it has recently been

[1]By low temperature here I mean low relative to the QCD scale, or $\sim 100$ MeV; by astrophysical standards supernova temperatures of tens of MeV are obviously quite high.

established that the ground state of quark matter exhibits Color Superconductivity (CSC), resulting from the Cooper pairing of quark quasiparticles near the Fermi surface [1] – [19]. At high temperature and low density (upper left, extending to the upper right) we expect to find the quark-gluon plasma. I will comment on the more specific features of the diagram below.

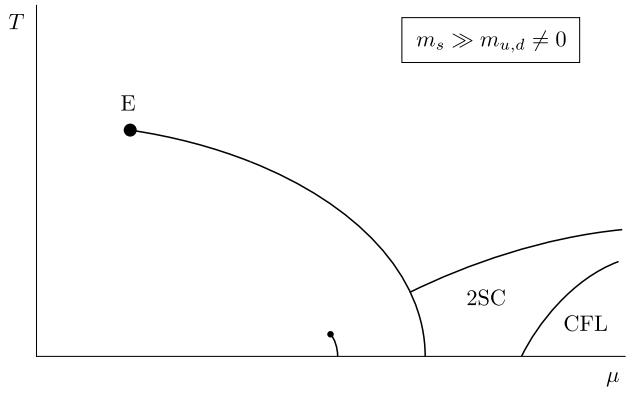


Figure 1: QCD phase diagram (simplified) in the density-temperature plane.

Let me try to give you some flavor of the recent results on color superconductivity. Recall that Cooper pairing (as in ordinary superconductors) involves excitations near the Fermi surface, but with equal and opposite momenta (figure 2). In QCD the excitations have quark quantum numbers, and hence there is a directly attractive channel due to gluon exchange in the anti-triplet ($\overline{3}$) color representation. In the case of electrons in a metal photon exchange is repulsive, and the attractive channel is due to the exchange of phonons (lattice vibrations).

What is common between quark matter and an ordinary metal is the existence of a Fermi surface. The Pauli exclusion principle requires that fermions like quarks or electrons occupy distinct quantum states, hence at zero temperature the ground state consists of filled levels up to some energy (this boundary is the Fermi surface). The lowest energy excitations of this system, called quasiparticles, are states just above the Fermi surface. Now, a Fermi surface is unstable with respect to attractive interactions in the Cooper pairing channel. That is, even an arbitrarily weak interaction in this channel can lead to pairing of quasiparticles, which reduces the overall energy of the system. Heuristically, the spherical symmetry of the Fermi surface (in momentum space, the energy of a quasiparticle only depends on its distance from the surface, and not on its angular position) reduces the pairing dynamics to that of a 1+1 dimensional system, where even weak interactions lead to pairing.

Now, recall that QCD exhibits a property called asymptotic freedom, which means that short distance (large momentum transfer) interactions are weak, whereas long distance (small momentum transfer) interactions are strong. At very high quark

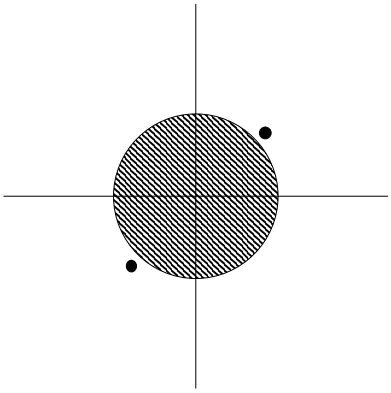

Figure 2: Excitations on opposite sides of the Fermi surface.

densities, most interactions occur over short distances, and we therefore have very good control over calculations. However, at quark densities likely to be found in a neutron star, roughly a few per cubic Fermi, the typical interactions are quite strong, precluding reliable quantitative results. Nevertheless, the indications of at least an *instability* to the formation of Cooper pairs is still evident, even if we can't say more about the details.

In figure 1 there are two distinct CSC phases displayed, the 2SC and CFL phases. In the former, the up and down quarks pair in the isosinglet channel, and the strange quark is left to pair with itself in an exotic (possibly spin 1) channel. In the latter, the flavor and color orientations of all three quarks are correlated in a non-trivial way (see figure 3): pairing in a particular flavor channel corresponds to a particular orientation in color space. In this talk I will assume that figure 1 is correct in that the 2SC phase has the lowest energy at intermediate density. The transition from nuclear matter to the 2SC phase is likely to be first order [18], as we will discuss further below.

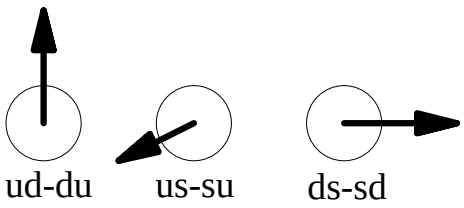


Figure 3: Di-quark orientation in the CFL phase. The arrow represents a $\overline{3}$ orientation in color space.

Before leaving the subject of the QCD phase diagram, let me discuss another transition – the chiral phase transition – that is likely to occur as we increase the

baryon number density. Chiral symmetry has to do with unitary rotations among different flavors of quarks:

$$q_i^{L,R} \to U_{ij} q_j^{L,R} \quad , \tag{1}$$

where i labels the flavor (i = up, down, strange) and $U$ is a unitary matrix. L and R label whether the quark is left handed or right handed. Chiral symmetry reflects the fact that, in the limit of small quark masses, the strong interactions (gluons) can't tell the difference between different flavors of left and right handed quarks.

These symmetries are broken by quark condensation in the QCD ground state:

$$\langle \overline{q}_L q_R \rangle \neq 0 \quad ,$$

but are restored in the 2SC phase and in the quark-gluon plasma. (However, in the CFL state chiral symmetries do remain broken at high density.) Their restoration involves a phase transition, again at quark densities of roughly a few per cubic Fermi. What can we say about this transition?

Because it occurs at a density where the effective coupling is strong, we can't make quantitative predictions. However, we can learn something about the order of the transition from something called "universality". The logic is as follows: if the transition is second order (or higher), then at the precise point of transition there must be very long wavelength excitations in the system. A heuristic way to understand this is to visualize the effective potential near the transition. In a second order transition the potential becomes very flat as the second derivative changes sign from positive to negative. (In contrast, in a first order transition the system tunnels or fluctuates out of the disfavored vacuum while the second derivative is still positive.)

Technically, a second order transition implies fluctuations of infinite wavelength (or equivalently, zero mass excitations). There are not very many models which describe such low-energy dynamics. To be self-consistent they need to exhibit something called an infrared fixed point in the renormalization group evolution of the coupling constant. Roughly speaking, the low-energy dynamics must become almost scale invariant as the correlation length diverges. The candidate models describing the low-energy dynamics must possess the same symmetry properties as the underlying system, but otherwise can be quite simple. In some cases, there are no candidate models with the right symmetries and low-energy particle content that exhibit an infrared fixed point. In this case the transition is predicted to be first order. Based on this kind of analysis, both the 2SC and chiral phase transition at finite density are likely to be first order [17, 18].

So, we have two candidate phase transitions which, as we discuss below, might have astrophysical implications. Obviously, a number of issues are still unresolved. For example, are there two separate phase transitions, or does chiral symmetry restoration coincide with color superconductivity? The renormalization group analysis of color superconductivity [8, 11] suggests that once the effective excitations start

to look like quarks, there is a pairing instability and the system is likely to be superconducting. However, one could also imagine a chirally restored phase with nucleonic excitations, so chiral symmetry does not necessarily imply CSC. In any case, both transitions are likely to occur at temperatures and densities that might be achieved by astrophysical phenomena.

# 3 Phase transition parameters

At asymptotic density, the nature of the CSC order parameter, the binding energy density and the critical temperature are all precisely calculable. Less is known about intermediate densities of several times nuclear density. However, there are strong indications of a Cooper pairing instability, and estimates of the resulting gap are of order $\Delta \sim$ 40-120 MeV at a quark chemical potential $\mu$ of $\approx 400$ MeV. The nature of the chiral phase transition is similarly poorly determined, although as we discussed in the previous section it is likely to be first order. Rather than discuss the two transitions separately, we will focus on the CSC transition, keeping in mind that if a first order chiral boundary is crossed, the consequences should be similar.

Consider the possible implications of CSC for the collapse and explosion of massive stars ($M > 8M_{\odot}$). We will argue that it is quite likely that at the moment of maximum compression of the collapsing Fe core, the densest part of the star crosses the critical density into the phase where CSC is energetically favored. The release of latent energy has the potential to generate an explosive shockwave which powers the resulting supernova (SN). Current simulations of supernovae are generally unable to reproduce the explosive behavior observed in nature: the shockwave generated by the mechanical bounce of the nuclear core stalls before reaching the surface, unless an appeal is made to neutrino reheating combined with non-spherical phenomena such as rotation or convection [20, 21]. We also note that the energy liberated in a CSC phase transition is potentially sufficient to power hypernovae (HN) [22], which have been linked to gamma ray burst events [23].

First, let us summarize some results on CSC from the recent literature. Precise results are only valid at asymptotic densities where the effective QCD coupling is small, however they should still be useful guide when dealing with intermediate densities. In any case, our qualitative results will be insensitive to factors of 2 in these formulas:

- Gap size: $\Delta \sim$ 40 - 120 MeV
- Critical temperature: $T_c \simeq .57\Delta$
- At asymptotic density the binding energy density is $E_{CSC} = \frac{5.8}{4\pi^2}\Delta^2\mu^2$. Simple dimensional analysis (given the absence of any small parameter) also suggests a value in this range. Note that we are interested here in the latent *energy* associated with

the first order transition to the CSC phase (or any other transition that occurs as the baryon density is increased beyond several times nuclear density). The baryon density changes on astrophysical timescales, or very slowly on the timescale of QCD dynamics, and the vacuum state at zero temperature (or at $T << T_c$) is found by minimizing the energy in the sector of the Hilbert space with fixed baryon number. Studies such as [19], which involve the free energy $\Omega$ at finite chemical potential (but not fixed density) are appropriate for determining pressure equilibrium between nuclear and CSC matter in circumstances in which baryon number can flow across a boundary (e.g. in a neutron star), but do not address a possible SN transition. (See discussion for further remarks.)

• Phase diagram: the normal nuclear phase is separated from the CSC phase (most likely the 2SC two flavor condensate phase, although possibly the CFL phase [17, 18, 19]) by a first order boundary.

# 4 Astrophysics of Core Collapse

Now let us review the standard scenario of Fe core collapse which is believed to lead to type II supernovae [20]. Nuclear burning during the $10^7$ year lifetime of the star leads to a shell structure, with the inner core eventually consisting of Fe ash. Because iron cannot participate in further exothermic nuclear reactions, there is an eventual cooling and collapse of the Fe core, whose mass is likely to be $(1-2)\ M_\odot$ (or, roughly the Chandresekhar mass). The collapse of this core is only halted by neutron degeneracy, which leads to a stiffening of the equation of state. The resulting bounce produces a shockwave, whose energy of $\sim 10^{51}$ ergs is a small fraction of the total available gravitational binding energy released by the collapse:

$$E_b \sim 3 \cdot 10^{53} \text{ergs} \left(\frac{M_{core}}{M_\odot}\right)^2 \left(\frac{R}{10\text{km}}\right)^{-1} . \quad (2)$$

Most of this energy escapes in the form of neutrinos during the supernova, as was observed in the case of SN1987a.

The pressure in the collapsed core at the instant of the bounce is most likely *greater* than the corresponding pressure in any remnant neutron star. In order to cause a bounce, the kinetic energy $E_b$ of the infalling material (which is a sizeable fraction of a solar mass!) must be momentarily stored as compressional potential energy in the (sub)nuclear matter. This additional mechanical squeezing at the bounce suggests that if the critical density for CSC is ever reached in a neutron star, it will be reached at this instant.

Simulations of the core bounce result in densities of at least several times nuclear density $(5 - 10 \cdot 10^{14} \text{g/cm}^3)$, and temperatures of roughly 10-20 MeV [20]. This

temperature is likely less than $T_c$ for CSC, possibly much less[2], and hence the core of the star traverses the phase diagram horizontally in the density-temperature plane, crossing the critical density boundary into the CSC phase. It is important to note that the core region at bounce is probably *cooler* than post-bounce, since degenerate neutrinos tend to heat the proto-neutron star as they diffuse out [24]. Studies quoting larger SN temperatures such as $T \sim 30$ MeV generally refer to this later stage [25].

Once the core crosses into the CSC part of the phase diagram, the transition proceeds rapidly, on hadronic timescales. Because the transition is first order, it proceeds by nucleation of bubbles of the CSC phase in the normal nuclear background. The rate of bubble nucleation will be of order $(\text{fm})^4$ ($\text{fm} = 10^{-13}$cm.), due to strong coupling. (In a system governed by a dimensional scale $\Lambda$, the nucleation rate is given by $\Gamma \sim \Lambda^4 e^{-S}$, where $S$ is the action of the Euclidean bounce solution interpolating between the false (normal nuclear) vacuum and a bubble of critical size. At strong coupling, $S$ is of order one, so there is no large exponential suppression of the nucleation rate. The scale $\Lambda$ is of the order of $\Delta$ or $\mu = 400$ MeV.)

Causality requires that the mechanical bounce of the core happen over timescales larger than the light crossing time of the core, or at least $10^{-4}s$. Hence, the phase transition occurs instantaneously on astrophysical timescales. A nucleated bubble of CSC phase expands relativistically – liberated latent heat is converted into its kinetic energy – until it collides with other bubbles. Because the system is strongly coupled, these collisions lead to the rapid production of all of the low energy excitations in the CSC phase, including (pseudo)Goldstone bosons and other hadrons. The resulting release of energy resembles an explosion of hadronic matter.

To estimate the total CSC energy released in the bounce, we use the result that the ratio of CSC binding energy density to quark energy density is of order $\left(\frac{\Delta}{\mu}\right)^2$. For $\mu \sim 400$ MeV, and $\Delta \sim$ 40-120 MeV, this ratio is between .01 and .08, or probably a few percent.

$$E \sim \left(\frac{\Delta}{\mu}\right)^2 M_{core} \ . \tag{3}$$

In other words, the total energy release could be a few percent of a solar mass, or $10^{52}$ ergs! This is significantly larger than the energy usually attributed to the core shockwave, and possibly of the order of the gravitational collapse energy $E_b$. The implications for SN simulations are obviously quite intriguing.

In [26] it was suggested that strange matter formation might overcome the energetic difficulties in producing type-II supernova explosions. While there are strong arguments that the CSC transition should be first order, and reasonable order of mag-

[2]It is conceptually easier to think about the case where $T$ is much less than $T_c$, since in this case the Free energy ($F = U - TS$) liberated by the transition is predominantly energy, with only a small component related to entropy. The relevant dynamics is governed by energetics rather than Free energetics.

nitude estimates of the latent heat [1, 19], it is not clear to us why there would be supercooling in a strange matter transition. The conversion of up quarks to strange quarks must proceed by the weak interactions, but the rate is still much faster than any astrophysical timescale. Thus, the population of strange quarks is likely to track its chemical equilibrium value as the pressure of the core increases. There may be an important effect on the nuclear equation of state from strangeness (e.g. a softening of the pressure-density relationship), but we do not see why there should be explosive behavior.

Our results are also relevant to hypernovae [22], which are observed to have ejecta kinetic energies 10-100 times larger (of order $10^{52-53}$ ergs) than those of ordinary type II supernovae. Accounting for this extra kinetic is extremely challenging in standard scenarios. However, for exceptionally massive stars with $M < 35 M_{\odot}$ (for $M > 35 M_{\odot}$ the hydrogen envelope is lost during H-shell burning, and the core size actually decreases [27]) there is a large core mass which leads to a larger release of CSC binding energy. In fact, the released energy might depend nonlinearly and sensitively on the star's mass at the upper range. For example, the fraction of $M_{core}$ which achieves critical density might be a sensitive function of the mass of the star.

Another alternative is that hypernovae are the result of neutron star mergers rather than the explosion of an individual star. This possibility has been examined in relation to hypernovae as the engines of gamma ray bursts (GRBs) [23]. It seems quite plausible that in the merger of two cold neutron stars a significant fraction of the stars' mass undergoes the CSC transition (i.e. crosses the critical pressure boundary for the first time; in this case the temperature is probably negligible relative to the CSC scale $\Delta$). This provides a substantial new source of energy beyond gravitational binding, and may solve the "energy crisis" problem for this model of GRBs [23].

Finally, we note that the trajectory of the SN core in the temperature-density phase diagram might be rather complicated. The parameters suggest a density transition (at $T < T_c$), but subsequent reheating of the core due to the explosion, or to neutrino diffusion [24] might raise the temperature above $T_c$, and lead to additional transitions across the temperature boundary [25]. When $T \sim T_c$, the Free energies ($F = U - TS$) of the normal and CSC phases are comparable, due to the larger entropy of the normal phase. The evolution of bubbles in this regime is governed by relative Free energies rather than energetics alone, and the transition is presumably less explosive than the pressure transition at $T << T_c$.

# 5 Summary

Our understanding of QCD at high density has evolved dramatically over the past two years, leading to remarkable progress in understanding the QCD phase diagram and the color superconducting state of quark matter. We have argued here that

phase transitions at high density and low temperature (relative to the QCD scale) might play a role in violent astrophysical phenomena. In particular, the densities and temperatures associated with core collapse in massive stellar evolution suggest that CSC could play an important role in type II supernovae, or possibly hypernovae (GRBs).

Our assumptions concerning key parameters are conservative, and taken from distinct (and heretofore independent) regimes of inquiry: stellar astrophysics and dense quark matter. Yet, they point to the interesting possibility that supernova explosions are powered by CSC binding energy. It is well established that the shock-wave energy from core collapse is insufficient to produce an explosion, and recent results incorporating Boltzman transport of neutrinos show that neutrino reheating is also insufficient unless non-spherical phenomena such as rotation or convection are taken into account [21]. We are optimistic that future progress in simulations will tell us much about whether and how latent energy from QCD plays a role in stellar explosions.

**Acknowledgements**
I would like to thank F. Sannino and R. Ouyed for organizing this very stimulating workshop. The work of S.H. was supported in part under DOE contract DE-FG06-85ER40224 and by the NSF through the Korean-USA Cooperative Science Program, 9982164.

# References

[1] D.K. Hong, S.D.H. Hsu and F. Sannino, Phys. Lett. B516, 362,2001.

[2] For a review see K. Rajagopal, F. Wilczek hep-ph/0011333; S.D.H. Hsu, Proceedings of TMU - Yale Symposium on Dynamics of Gauge Fields, hep-ph/0003140; D. K. Hong, hep-ph/0101025; M. Alford, hep-ph/0102047.

[3] S. C. Frautschi, Asymptotic freedom and color superconductivity in dense quark matter, in: Proceedings of the Workshop on Hadronic Matter at Extreme Energy Density, N. Cabibbo, Editor, Erice, Italy (1978).

[4] B. Barrois, Nucl. Phys. B, 129, 390 (1977).

[5] D. Bailin, and A. Love, Phys. Rept., 107, 325 (1984).

[6] M. Alford, K. Rajagopal, and F. Wilczek, Phys. Lett. B, 422, 247 (1998).

[7] R. Rapp, T. Schäfer, E.V. Shuryak, M. Velkovsky, Phys. Rev. Lett., 81, 53 (1998).

[8] N. Evans, S. Hsu and M. Schwetz, Nucl. Phys. B**551**, 275 (1999); Phys. Lett. B**449**, 281 (1999). S. Hsu and M. Schwetz, Nucl.Phys.B**572**, 211 (2000).

[9] N. Evans, J. Hormuzdiar, S. Hsu and M. Scwhetz, Nucl.Phys.B**581**, 391 (2000).

[10] D.T. Son, Phys. Rev. D**59**, 094019 (1999).

[11] T. Schäfer and F. Wilczek, Phys. Rev. Lett. **82** , 3956 (1999).

[12] D. K. Hong, Phys. Lett. B **473**, 118 (2000); Nucl. Phys. B **582**, 451 (2000). D. K. Hong, T. Lee and D. Min, Phys. Lett. B**477**, 137 (2000). D. K. Hong, V. A. Miransky, I. A. Shovkovy and L. C. R. Wiejewardhana, Phys. Rev. D**61**, 056001 (2000).

[13] R.D. Pisarski and D.H. Rischke, Phys. Rev. **D61**, 051501 (2000);Phys. Rev. **D61**, 074017 (2000).

[14] R. Casalbuoni and R. Gatto, Phys. Lett. B**464**, 11 (1999); Phys. Lett. B**469**, 213 (1999).

[15] F. Sannino, Phys. Lett. B**480**, 280, (2000). S. Hsu, F. Sannino and M. Schwetz, hep-ph/0006059.

[16] R. Casalbuoni, Z. Duan and F. Sannino, Phys. Rev. D**62**, 094004, (2000). R. Casalbuoni, Z. Duan and F. Sannino, hep-ph/0011394. R. Casalbuoni, Z. Duan and F. Sannino, Phys. Rev. D63, 114026, 2001. R. Ouyed, F. Sannino hep-ph/0103168, to appear in Phys. Lett. B.

[17] S.D.H. Hsu and M. Schwetz, Phys.Lett.B432:203,1998.

[18] R. Pisarski and D. Rischke, Phys.Rev.Lett.83:37,1999.

[19] M. Alford, K. Rajagopal, S. Reddy and F. Wilczek, hep-ph/0105009.

[20] S. L. Shapiro, and S.A. Teukolsky, Black Holes, White Dwarfs, and Neutron Stars: the physics of compact objects (Wiley-Interscience, 1983); B. Cooperstein and E. Baron, in Supernovae, edited by A. Petschek (Springer-Verlag, 1990).

[21] For recent reviews on the status of supernova simulations, see H.T. Janka, K. Kifonidis and M. Rampp, astro-ph/0103015; A. Mezzacappa, astro-ph/0010579.

[22] T. Galama et al, Nature 395, 670 (1998); Q. Daniel Wang, ApJ 517, L27 (1999).

[23] Piran, T. 1999b, in Gamma-Ray Bursts: The first three minutes, ASP Conference Series, Vol. 190, eds. J. Poutanen and R. Svensson, p3.

[24] J.M. Lattimer, in Supernova Shells and Their Birth Events, edited by W. Kundt (Springer-Verlag, 1988). A. Burrows, T.J. Mazurek and J.M. Lattimer, Ap. J. **251**, 325 (1981); A. Burrows and J.M. Lattimer, Ap. J. **307**, 178 (1986).

[25] G.W. Carter and S. Reddy, hep-ph/0005228.

[26] O.G. Benvenuto and J. Horvath, Phys. Rev. Lett.**63**, 716 (1989).

[27] G. E. Brown, C. H. Lee and H. A. Bethe, New Astron. **4**, 313 (1999).

# Discussion

**Student:** How does one identify the order of a phase transition? What is the difference between first and second order?

**Hsu:** Formally speaking, the order refers to the level of discontinuity exhibited by thermodynamic quantities (in the infinite volume limit) at the transition. In an Nth order transition, the Nth derivative of the free energy (with respect to, e.g., temperature or density) is discontinuous, while lower order derivatives are continuous. So, in a first order transition the derivative of the free energy itself is discontinuous, whereas in a second order transition the first derivative of the free energy is continuous and the second derivative is not. One can imagine even smoother transitions where only some high derivative of the free energy is discontinuous. Alternatively, one can distinguish by noting that the order parameter exhibits a jump in the first order case, but evolves smoothly in the 2nd and higher order cases. Of course, it is only first order transitions (with nonzero latent heat) that can lead to the explosive phenomena considered here.

**Mark Alford (University of Glasgow):** (paraphrasing) In our recent investigations of a model of the nuclear matter–quark matter interface in neutron stars, we find that while the free energy of the quark phase is lower, the energy density of the quark core is actually higher than in the nuclear phase. If this is the case, how does the phase transition proceed?

**Hsu:** In this discussion I assumed that there is a high density state (either the CSC or chirally restored phase) with lower energy than the normal nuclear phase. Note that I really mean energy here, not free energy: $F = H - \mu N = -P$. If we consider the phase diagram as a function of baryon density (not baryon chemical potential), the existence of a new phase implies a state with lower energy than the normal nuclear phase at the same density. If the transition is first order, there is the possibility of

latent energy release. In a core bounce, the baryon density is increased on a timescale too short for bulk baryon number flow. So, the relevant question is what happens when you cross a boundary in the baryon density direction. The system will try to tunnel into the lower energy phase, and the release of latent energy powers the explosion.

On the other hand, if the compression is slow enough for significant rearrangement of baryon number, then it is governed by free energetics, or $F$. In the model you considered, the quark matter phase has lower free energy, but higher energy and baryon density than the nuclear phase. The system can only form the quark phase by aggregating baryon number, and there is probably not enough time for this to happen during a supernova core bounce. The conversion from nuclear to quark phases also requires energy input, which presumably has to come from gravitational collapse.

# Introduction to Effective Lagrangians for QCD

*Joseph Schechter*
*Department of Physics*
*Syracuse University*
*Syracuse, New York 13244-1130, USA*

A brief introduction to the effective Lagrangian treatment of QCD (in the sense of using fields representing physical particles rather than quarks and gluons) will be given. The historical evolution of the subject will be discussed. Some background material related to a recent model for Gamma Ray Bursters will be given. Finally, some recent work on low energy strong interactions will be mentioned.

## 1 Need for an effective Lagrangian; historical background

There is little doubt that, at least up to energies probed by present accelerators, QCD is the correct theory of strong interactions. It contains the three light spin 1/2 quark fields u, d and s as well as the three heavy quark fields c, b and t. We will focus attention completely on the light quarks here. The dynamics is governed by an SU(3) Yang Mills [1] theory; roughly this means that the strong force has a general similarity to the ordinary QED force which involves the exchange of a gauge field (photon). However there are eight "photons" rather than a single one in QCD. They may be put into a traceless $3 \times 3$ matrix, $A_\mu$ and the interaction term in the fundamental Lagrangian for, say, the $u$ quark is $ig\overline{u}\gamma_\mu A_\mu u$, where $g$ is a coupling constant. Notice that $u$ is a column vector with unwritten "color" indices. Unlike the QED case, the QCD "photons" have self- interaction terms with the structures $-igTr(\partial_\mu A_\nu [A_\mu, A_\nu]) + \frac{g^2}{4} Tr([A_\mu, A_\nu][A_\mu, A_\nu])$. These have the consequence at the first loop order of perturbation theory that the effective energy dependent coupling constant behaves as

$$\frac{g^2(E)}{4\pi} \sim 1/ln(\frac{E}{\Lambda}), \tag{1}$$

where $E$ is the energy scale at which the theory is being applied and $\Lambda$ is a fixed number of order 250 MeV characterizing QCD. At high energies (above several GeV) $g$ is small and perturbation theory is good. However at low energies, where we want

to discuss topics like binding of quarks to make mesons, interactions of light mesons, CP violation in K meson decays, Nuclear Physics, etc. etc., g is large so QCD is non perturbative. Then one must adopt some other approach. It seems reasonable to hope that this strong coupling at low energies tightly binds the quarks into mesons which interact weakly enough among themselves to be described by the perturbative treatment of an *effective Lagrangian* constructed from the light meson fields [1] rather than the quarks and gluons. This hope turns out to be realized.

The crucial idea in constructing the effective Lagrangian is to mock up the symmetries observed in nature (and which are displayed by the more fundamental QCD Lagrangian). Apart from the Lorentz and discrete space-time symmetries of the strong interaction, the starting point is the imposition of Wigner's isotopic spin symmetry, now denoted $SU(2)_V$. The proton and neutron belong to a spinor of $SU(2)_V$ while three pion fields representing linear combinations of the three pion charge states belong to a vector. The corresponding transformations are:

$$SU(2)_V: \quad N = \begin{pmatrix} p \\ n \end{pmatrix} \rightarrow U_V N \quad \text{and} \quad \phi = \frac{1}{\sqrt{2}} \boldsymbol{\pi} \cdot \boldsymbol{\tau} \rightarrow U_V \phi U_V^{\dagger}, \tag{2}$$

where $U_V$ is a two dimensional unitary unimodular matrix. The subscript $V$ stands for vector. Yukawa's original theory implies an effective Lagrangian with the $SU(2)_V$ invariant interaction terms:

$$i g_Y \overline{N} \phi \gamma_5 N + \lambda [Tr(\phi^2)]^2. \tag{3}$$

Here $g_Y$ is the Yukawa coupling constant while $\lambda$ is the coupling constant for a term which gives $\pi\pi$ scattering.

Does the Yukawa Lagrangian actually work? If it is to be a reasonable effective Lagrangian it should, like QED, give reasonable results already at tree level. Now the value of $g_Y$ has been known for about 60 years (determined from the long distance part of the nucleon nucleon force due to pion exchange). Around 50 years ago pions were made in accelerators and pion nucleon scattering measured. At tree level, the amplitude for this scattering process should correspond to nucleon "exchange" and be proportional to $g_Y^2$. Unfortunately it turns out, near the scattering threshold, to be more than an order of magnitude larger than experiment. This would appear to doom the Yukawa theory as the basis for a perturbative treatment. However, there is a small modification which saves it.

Before getting to this modification we note that the discovery of strange particles indicated that the isotopic symmetry group $SU(2)_V$ is too small and that it should be upgraded to $SU(3)_V$ while the meson matrix $\phi$ in eq.(2) should be upgraded [3] to a $3 \times 3$ matrix. The mesons are now pictured as composites, $q\overline{q}$ of a quark and

[1] Baryons can either be included directly or observed to emerge as solitons[2] in the effective meson theory.

anti-quark [4, 5]. Similarly the baryons are regarded as composites $qqq$. At the fundamental quark level the $SU(3)_V$ symmetry is realized as:

$$q = \begin{pmatrix} u \\ d \\ s \end{pmatrix} \to U_V q, \tag{4}$$

where $U_V$ is now a $3 \times 3$ unitary matrix. It was understood from the beginning [4, 6] that the symmetry group $SU(3)_V$ has to be an approximate one; it could only be exact in a world in which the nucleons and strange baryons like the $\Lambda$ are degenerate.

The desired modification of the Yukawa theory which saves the perturbative pion nucleon scattering prediction arises from the extension of the isotopic spin symmetry in another direction. This may be motivated by consideration of the "V-A" theory of beta decay type interactions, discovered [7] a little more than forty years ago. In that well confirmed model, which displays maximal parity violation, the fundamental fermion fields (then nucleons but now quarks) enter into the interaction only through their projection: $q_L = \frac{1+\gamma_5}{2} q$ . For a massless fermion, this corresponds to a left handed helicity state (momentum vector opposite to spin vector). The strong interaction, which conserves parity, of course, requires the inclusion also of the right handed projection $q_R = \frac{1-\gamma_5}{2} q$. What this seems to be telling us is that Nature likes to employ the projected (chiral) fields. Around that time, well before QCD was known, it raised the question as to whether Nature also chooses to realize isotopic type symmetries on the chiral components. The chiral (for generality) $U(3)_L \times U(3)_R$ symmetry corresponds to demanding invariance under the transformations:

$$q_{L,R} \to U_{L,R} q_{L,R}, \tag{5}$$

where $U_L$ and $U_R$ are two separate $3 \times 3$ unitary matrices. This symmetry is an approximate one since it is manifestly broken by non zero fundamental fermion masses. The vector symmetry corresponds to the special choice $U_L = U_R = U_V$. In order to implement the chiral symmetry in the usual manner it is necessary to further enlarge the meson multiplet. In the simplest version which uses $SU(2)_L \times SU(2)_R$ it means adding to the three pion field components an isosinglet scalar field called the sigma [8], whose coupling to the nucleon is correlated with that of the pion. We will discuss this more soon but for the moment just note that it modifies the pion nucleon scattering diagrams to those shown in Fig 1. The new sigma exchange diagram almost completely cancels the contribution of the nucleon exchange diagrams. The much smaller answer agrees at low energies with experiment to about 15 per cent, if the mass of the sigma is considerably heavier than that of the pions. Other similarly good strong interaction predictions can be made by the same model. Thus it seems that chiral symmetry has "saved" the Yukawa theory as the effective description of strong interactions at low energies.

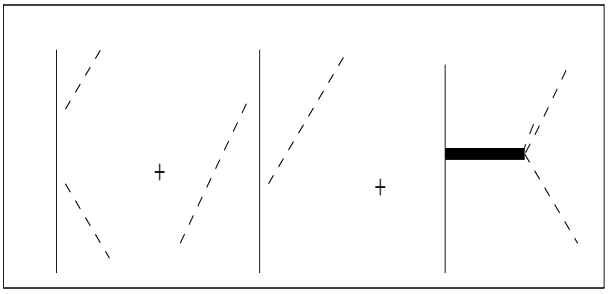

Figure 1: Nucleon=full line,pion=dashed line, sigma=heavy line.

## 2 Effective Lagrangian of mesons

One of the many questions raised by the remarks above concerns the consistency of the requirement that the mass of the sigma be appreciably greater than the mass of the pion, with the requirement that they both belong to the same chiral multiplet and hence should be, at least approximately, degenerate in mass. To investigate this further it is easier to focus just on the mesons. The same problem of too large predicted low energy scattering is displayed by pi pi scattering and the solution of including sigma exchanges is also the same.

The meson field multiplet, $M_{ab}$ with the correct chiral properties is schematically constructed from the underlying quark fields as:

$$\overline{q}_{Rb} q_{La} \sim M_{ab} = S_{ab} + i\phi_{ab}. \tag{6}$$

where the decomposition of $M$ into pseudoscalar, $\phi = \phi^\dagger$ and scalar, $S = S^\dagger$ pieces is shown. M has the transformation properties

$$U(3)_L \times U(3)_R : \quad M \to U_L M {U_R}^\dagger, \quad \text{parity} : \quad M(\mathbf{x}) \to M^\dagger(-\mathbf{x}). \tag{7}$$

One may check these by noting that the Yukawa like term $\overline{q}_L M q_R + h.c.$ is invariant. The simplest Lagrangian made from $M$ is:

$$\mathcal{L}_{meson} = -\frac{1}{2} Tr(\partial_\mu M \partial_\mu M^\dagger) - V_0(M, M^\dagger) + \sum A_a (M_{aa} + {M^\dagger}_{aa}). \tag{8}$$

The first term is the standard kinetic term while the second term might as well be taken to be the most general non derivative function of the independent chiral $SU(3)_L \times SU(3)_R$ invariants $I_1 = Tr(MM^\dagger)$, $I_2 = Tr[(MM^\dagger)^2]$, $I_3 = Tr[(MM^\dagger)^3]$ and $I_4 = 6(detM + detM^\dagger)$. The last term provides the required chiral as well as flavor (vector) type symmetry breaking, with the real numbers $A_a$ being proportional to the masses $m_a$ of the light quarks. It turns out [9] that many of the most interesting consequences of eq.(8) at tree level are independent of the specific form of $V_0$; only its

symmetry properties are needed. The consequences of chiral symmetry are relations between $n$ and $n-1$ point vertices; for example, trilinear vertices are related to masses while masses are related to "decay constants". Another point of interest is that the presence of the quantity $I_4$ in $V_0$ spoils the invariance under "axial baryon number" or $U(1)_A$ transformations of the form $M \to phase \times M$. If this extra symmetry were allowed to remain it would force [10] one of the eta type mesons to be degenerate with the pi, in clear contradiction to nature.

The names of the 18 particles belonging to $M$, which comprises a basis for the irreducible representation $(3, 3^*) + (3^*, 3)$ of $SU(3)_L \times SU(3)_R$ and parity, are listed in Table 1.

It is helpful to first consider the two flavor case wherein M is just a $2 \times 2$ matrix. This corresponds to keeping the eight particles in the first two columns of Table 1. However a further simplification is possible since, for only $N = 2$, the fundamental representation of $SU(N)$ is equivalent to its complex conjugate. Using the fact that $U\tau_2 = \tau_2 U^*$ for any 2 dimensional unitary, unimodular matrix, $U$ we observe that under an $SU(2)_L \times SU(2)_R$ transformation, $\tau_2 M^* \tau_2 \to U_L(\tau_2 M^* \tau_2) U_R{}^\dagger$. This is the same transformation as in eq.(7) so we have the following two linear combinations which each transform irreducibly under $SU(2)_L \times SU(2)_R$:

$$\frac{1}{\sqrt{2}}(M + \tau_2 M^* \tau_2) = \sigma + i\boldsymbol{\pi} \cdot \boldsymbol{\tau}, \quad \frac{1}{\sqrt{2}}(M - \tau_2 M^* \tau_2) = i\eta + \mathbf{a}_0 \cdot \boldsymbol{\tau}. \tag{9}$$

Thus it is consistent to construct a theory using just the $\sigma$ and $\pi$ fields; this is the choice made in the Gell-Mann Levy model [8] discussed above.

The chiral invariant potential in the Gell-Mann Levy model is taken to be:

$$V_0 = -b(\sigma^2 + \boldsymbol{\pi}^2) + \lambda(\sigma^2 + \boldsymbol{\pi}^2)^2, \tag{10}$$

where $b$ and $\lambda$ are real, positive constants. Because of the "wrong sign" quadratic term, the parity conserving minimum of the potential will occur for $\boldsymbol{\pi} = 0$ and $(\sigma)_{min} \widetilde{\chi}_0^0$. Once the Lagrangian is rewritten in terms of new "small oscillation" fields defined as deviations from their values at the potential minimum, it is evident that the resulting theory no longer has the full chiral symmetry. This is the familiar phenomenon of spontaneous symmetry breakdown. The remaining symmetry is just isospin invariance ($SU(2)_V$) and, neglecting the quark masses for simplicity, the pion

| $spin^{parity}$ | $I = 1$ | $I = 0$ | $I = 1/2$ | $I = 0$ |
|---|---|---|---|---|
| $0^-$ | $\boldsymbol{\pi}$ | $\eta$ | $K's$ | $\eta'$ |
| $0^+$ | $\mathbf{a}_0$ | $\sigma$ | $\kappa's$ | $\sigma'$ |

Table 1: States represented by $M$.

is forced to become a Nambu Goldstone boson (i.e. to have zero mass). On the other hand the mass of the sigma is a free parameter. This solves the problem of degenerate pion and sigma, mentioned at the beginning of this section.

At the level of fundamental (idealized to be massless) fermions, it was pointed out [11] that the origin of $(\sigma)_{min}\widetilde{\chi}_0^0$ is, analogously to the theory of superconductivity, a pairing force between (in modern language) $q_L$ and $\overline{q}_R$. This leads to a ground state $|0>$ which is a "condensate" of such pairs and their conjugates, characterized by $<0|\overline{q}_a q_a|0>\widetilde{\chi}_0^0$.

It is interesting to discuss the pi pi scattering amplitude in this model. There is a $\sigma\phi\phi$ interaction as well as the four pion self interaction term shown in eq.(3). The amplitude for any particular choice of pion charges is conventionally specified by a suitable linear combination of the single function $A(s,t,u)$ and its permutations under the interchange of the Mandelstam variables $s$, $t$ and $u$. At tree level one has:

$$A(s,t,u) = \frac{2}{F_\pi^2}(m_\sigma^2 - m_\pi^2)(\frac{m_\sigma^2 - m_\pi^2}{m_\sigma^2 - s} - 1), \tag{11}$$

where the first term represents the sigma exchange piece and the second term, the contact interaction piece. Furthermore the quantity $F_\pi$ ($= \sqrt{2}(\sigma)_{min}$ in the model) is identifiable as the hadron factor of the amplitude for $\pi^- \to \mu^-\overline{\nu}_\mu$ and is numerically, 0.131 GeV. At low energies (i.e. just above $s = 4m_\pi^2$ ) and considering $m_\sigma$ to be considerably larger than $m_\pi$, eq.(11) becomes,

$$A(s,t,u) = \frac{2}{F_\pi^2}(s - m_\pi^2), \tag{12}$$

a formula due to Weinberg [12]. It is in reasonable agreement with experiment and can be noted to emerge from the difference of the two terms in eq.(11) which are each about twenty times larger than the final result.

While this numerical result is very encouraging, from the standpoint of making a perturbation expansion it is not nice that it arises from the near cancellation of two large quantities. Also, historically the sigma meson has been hard to identify from experiment. For the latter reason it was proposed already in [8] to "integrate out" the sigma by imagining its mass to go to infinity. This may be done from the equation of motion $\partial_\mu\partial_\mu\sigma = \frac{\partial V_0}{\partial\sigma}$. For an infinitely heavy particle we neglect the kinetic term so the equation of motion just becomes $0 = \frac{\partial V_0}{\partial\sigma}$, neglecting, at first, the "quark mass terms". Then eq.(10) can be solved for $\sigma$:

$$\sigma = \sqrt{F_\pi^2/2 - \boldsymbol{\pi}^2}. \tag{13}$$

Substituting back into the two flavor version of eq.(8) yields the Gell-Mann Levy non linear sigma model:

$$\mathcal{L} = -\frac{1}{2}(\partial_\mu\boldsymbol{\pi})^2 - \frac{1}{2}(\partial_\mu\sqrt{F_\pi^2/2 - \boldsymbol{\pi}^2})^2. \tag{14}$$

Notice that the substitution of eq.(13) replaces the potential of eq.(10) by a constant. All the interactions in eq.(14) involve only pions and are of derivative type. This reproduces the desired result eq.(12) directly without any need to mention the sigma.

It is possible to give a slightly more convenient form for this model, which was obtained independently [13] of ref. [8]. In terms of the unitary matrix "chiral field" $U = exp(2i\phi/F_\pi)$ just write:

$$\mathcal{L} = -\frac{F_\pi^2}{8} Tr(\partial_\mu U \partial_\mu U^\dagger). \tag{15}$$

Of course, the matrix, $U$ is defined by its power series expansion. In order to verify the equivalence of eqs.(14) and (15) one may make use of Chisholm's theorem [14]. This states that the transformation (analog of a point transformation in classical mechanics):

$$\chi_a = \phi_a + \gamma_{abc}\phi_b\phi_c + \gamma_{abcd}\phi_b\phi_c\phi_d + \cdots \tag{16}$$

between the sets of scalar fields $\phi_a$ and $\chi_a$ leads to equivalent results at tree level. An advantage of this formulation is that it can straightforwardly be extended to the three flavor case just by considering $\phi$ in eq.(15) to be the $3\times 3$ matrix of pseudoscalar fields. Notice that $U$ transforms in the same (linear) way $M$ does in eq.(7); this forces $\phi$ to transform non-linearly, which give the model its name.

A quick mnemonic for going from the three flavor linear model in eq.(8) to the three flavor non-linear model is to first make the "polar decomposition", $M = BU$ with $B$ hermitian and $U$ unitary, and then replace $B$ by the the assumed $SU(3)$ symmetric "vacuum" value $< B >= \frac{F_\pi}{2} diag(1,1,1)$. Substituting this form into eq.(8) yields finally:

$$\mathcal{L} = -\frac{F_\pi^2}{8} Tr(\partial_\mu U \partial_\mu U^\dagger) + function(detU) + \frac{F_\pi}{2}\sum A_a(U_{aa} + U_{aa}^\dagger). \tag{17}$$

The second term will be non-trivial only if there are nine rather than eight pseudoscalars (i.e. the $\eta'$ is included) so that $detU\tilde{\chi}_1^0$. The quantities $A_a$, proportional to the quark masses, can be related, by using eq.(17) or eq.(8), to the meson masses. In this way one can recapture the initially surprising result [15] for the strange to non-strange quark mass ratio:

$$\frac{A_3}{(A_1 + A_2)/2} = \mathcal{O}(25). \tag{18}$$

This may be contrasted with the value of about 1.4 expected in the qualitatively successful non-relativistic quark model. Similarly one gets [16] for the corresponding iso-spin violating quark mass ratio:

$$\frac{A_2 - A_1}{(A_1 + A_2)/2} = \mathcal{O}(\frac{1}{2}), \tag{19}$$

which may be compared with a value about 0.01 expected in the non-relativistic quark model. These results suggest that the first three (and especially the first two) quark masses are very small. Since these quark masses are the source of the intrinsic chiral $SU(3)_L \times SU(3)_R$ symmetry breaking in the Lagrangian, the goodness of the low energy chiral Lagrangian predictions becomes understandable. In the present picture the non-relativistic quark model masses are identified as arising from the spontaneous breakdown of chiral symmetry; they would be non-zero even if the true quark masses referred to above were zero.

# 3 QCD ingredients and Gamma Ray Bursters

So far, the arguments leading to eq.(17) were the ones used before QCD was discovered; they are general, based only on flavor symmetries of the strong interaction, and do not need to be changed. Of course QCD has strengthened their acceptance and led to many new insights. In the present context, for example, the violation of the $U(1)_A$ symmetry noted after eq.(8) has been clarified. Even though the QCD Lagrangian written at the classical level obeys this symmetry, it is illusory since quantum corrections (called the Adler Bell Jackiw [17] anomaly) spoil the conservation of the would be symmetry current in the full color gauge theory.

A related phenomenon may be used to throw some light on the ground state of the strong gauge theory and provide the basis for certain semi-quantitative estimates. Neglecting the light quark masses, the QCD Lagrangian written at the classical level is invariant under scale transformations, $x_\mu \to \lambda x_\mu$. Classsically, this implies the existence of a corresponding Noether current $D_\mu$ satisfying the conservation law, $\partial_\mu D_\mu = 0$. However this conservation law is also illusory due to quantum corrections. It must be replaced by [18],

$$\partial_\mu D_\mu = -\frac{\beta(g)}{g} Tr(F_{\mu\nu} F_{\mu\nu}) = H, \tag{20}$$

where $\beta(g)$ is the QCD beta function and $F_{\mu\nu}$ is the field strength tensor of QCD. $H$ is a convenient abbreviation for the right hand side. Several authors [19, 1] have considered the possibility of restricting the effective Lagrangian to mock up this equation. This requires the potential term, $V_0$ of eq.(8) to contain the scalar glueball field, $H$ and to satisfy,

$$H = dTr(M\frac{\partial V_o}{\partial M} + M^\dagger \frac{\partial V_0}{\partial M^\dagger}) + 4H\frac{\partial V_0}{\partial H}) - 4V_0, \tag{21}$$

where $d$ is the scale dimension of $M$. In order to see how this works let us focus on the simple case in which the quark fields are absent (pure color gauge theory). We

assume that the whole theory is approximated by the self interactions of the single scalar glueball $H$. Then the appropriate effective Lagrangian is,

$$\mathcal{L}_H = -\frac{a}{2}H^{-3/2}(\partial_\mu H)^2 - \frac{1}{4}Hln(\frac{H}{\Lambda^4}), \tag{22}$$

where $a$ is a dimensionless constant and $\Lambda$ is a QCD energy scale. The first term is a scale invariant kinetic type term while the second term provides the solution of the anomaly condition eq.(21). It is easily seen that the minimum of the potential in eq.(22) occurs for $< H >= \Lambda^4/e$, at which point the vacuum energy density takes the negative value $< V >= -\Lambda^4/(4e)$. In fact, a negative value is required in the bag model picture [21] of quark confinement. In that model, if a "bubble" of non-perturbative, zero energy vacuum is made it would tend to collapse to lower the total energy. However, if quarks or gluons are put inside the bubble, their kinetic energy opposes this effect and results in a stable state. To study the glueball field, $h$ in the simple model of eq.(22) we set $H = \Lambda^4/e + Zh$ and expand. For a given scale $\Lambda$, both $Z$ and $a$ may be gotten by specifying the mass $m_h$.

It may be amusing to note that an effect of electromagnetism can be added to the model through its contribution to the scale anomaly. One should replace the second term in eq.(22) by $-\frac{1}{4}(H + H_{EM})ln(\frac{H}{\Lambda^4})$, where $H_{EM} = -\frac{\alpha}{2\pi}\sum Q_a^2 \mathcal{A}_{\mu\nu}\mathcal{A}_{\mu\nu}$. Here $\mathcal{A}_{\mu\nu}$ is the electromagnetic field strength tensor and the $Q_a$ are the quark charges. This would give an estimate of the glueball decay into two photons in the approximation that it dominates the energy momentum tensor. Of course this model is oversimplified for ordinary QCD since, unlike the case of the pseudoscalar mesons, the glueball will not have low mass.

At this conference many interesting talks were presented on the treatment of QCD at high density (large chemical potential $\mu$). This is a fascinating field [22] since it gives rise to exotic new phases of matter whose properties may be computed perturbatively at large $\mu$. These new phases may be neatly described by effective Lagrangians similar to the one describing ordinary QCD. Possible applications may include matter in compact stars. As an example, Ouyed and Sannino have recently proposed a very imaginative model [23] to understand the puzzling behaviors of Gamma Ray Bursters. They argue it is possible that under the crust of a "quark star" there is a surface layer which could be in the so-called 2SC (two flavor superconducting) phase. In this phase the $SU(3)_C$ color gauge symmetry is spontaneously broken to $SU(2)_C$ and a two flavor chiral symmetry $SU(2)_L \times SU(2)_R$ is preserved in the massless quark limit. They go on to show that the lightest physical hadronic states should actually be glueballs and that the effective Lagrangian is given by an appropriate modification of eq.(22). The gamma ray emissions are born in the $H \to 2\gamma$ process mentioned above. Finally an ingenious mechanism in which the state of the surface layer shuttles between the 2SC and QGP (quark gluon plasma) phases is proposed to explain the observed episodic character of the gamma ray emissions.

# 4 Going away from threshold.

Gasser and Leutwyler [24] have worked out a systematic procedure for treating eq.(17) beyond tree level (neglecting the second term). Since it is a non-renormalizable theory new counter terms have to be added at every order to cancel divergences. There are ten such terms at one loop order (Two examples : $c_3 Tr(\partial_\mu U \partial_\mu U^\dagger \partial_\nu U \partial_\nu U^\dagger)$ and $c_5 Tr(\partial_\mu U \partial_\mu U^\dagger A(U + U^\dagger))$ where $A = diag(A_1, A_2, A_3)$). If one counts $\mathcal{O}(A/F_\pi) = \mathcal{O}(E^2)$, then the tree diagrams are $\mathcal{O}(E^2/F_\pi^2)$, the one loop diagrams are $\mathcal{O}(E^4/F_\pi^4)$ and so forth. Thus if $E$ is sufficiently small the higher terms in the expansion should be suppressed. This procedure has worked very well to correlate a large number of experimental results near threshold. It should be remarked that the counter terms also contain arbitrary finite pieces, which are adjusted to fit the data.

How far up in energy can this chiral perturbation approach practically take us? To get an idea consider the experimental points shown in Fig. 2 for the real part, $R_0^0(s)$ of the $I = J = 0$ pi pi partial wave amplitude. The chiral perturbation series should essentially give a polynomial fit to this shape, which up to 1.0 GeV is crudely reminiscent of one cycle of the sine curve. Of course,

$$sin(x) = x - \frac{x^3}{3!} + \frac{x^5}{5!} - \frac{x^7}{7!} + \frac{x^9}{9!} - \frac{x^{11}}{11!} + \frac{x^{13}}{13!} - \frac{x^{15}}{15!} + \cdots . \tag{23}$$

By using MAPLE or a similar program it will only take a minute to convine yourself that the number of terms needed to get a decent approximation to one cycle of the sine curve is that just shown. This suggests that something like 7 loop chiral perturbation theory would be required to explain pi pi scattering up to about 1 GeV. An alternative approach, as the data itself suggests, is to explicitly include resonances. For example the fit shown in Fig. 2 was computed [25] using a unitarized tree amplitude from a chiral Lagrangian in which scalar mesons and vector mesons have been consistently added. The sigma, which was earlier "sent to infinity", now turns out to be a broad resonance of mass about 560 MeV. There has been a lot of work [26] in this area recently and it seems exciting, though still in progress. Generalization to a full nonet of scalars suggests [27] the light scalars actually are more likely to be of $qq\overline{qq}$ type [28] than of $q\overline{q}$ type. Probably an even better approximation is to include [29] mixing between $qq\overline{qq}$ and $q\overline{q}$ states.

I would like to thank the organizers for a very stimulating conference. This work has been supported in part by the US DOE under contract DE-FG-02-85ER40231.

# References

[1] C.Yang and R. Mills, Phys. Rev. **96**, 191 (1954). Note that these authors gauged the "flavor" indices differentiating the proton and neutron instead of, as later turned out to be appropriate, their "color" indices.

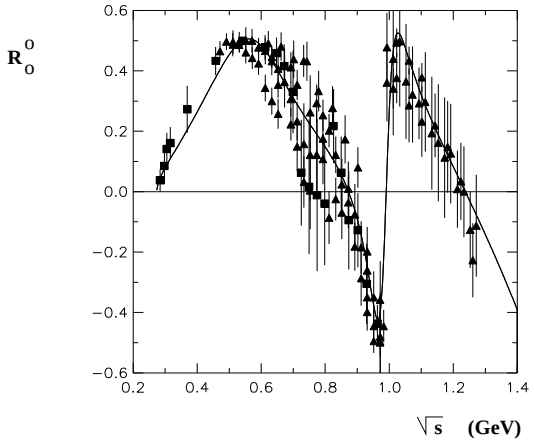


Figure 2: Pi Pi scattering amplitude.

[2] T.Skyrme, Proc. Roy. Soc. (London)**A260**, 127(1961).

[3] M. Ikeda, S. Ogawa and Y. Ohnuki, Prog. Theor. Phys. Suppl. No. **19**, 44 (1961).

[4] M. Gell-Mann, Phys. Lett. **8**, 214 (1964); Phys. Rev. **125**, 1067 (1962).

[5] G. Zweig, CERN preprint 8182/Th401 (1964).

[6] S. Okubo, Prog. Theor. Phys. **27**, 949 (1962).

[7] E. Sudarshan and R. Marshak, Proc. Padua-Venice conf. on mesons and recently discovered particles (1957); R. Feynman and M. Gell-Mann, Phys. Rev. **109**, 193 (1958); J. Sakurai, Nuovo Cimento **7**, 1306 (1958).

[8] M. Gell-Mann and M. Levy, Nuovo Cimento **16**, 705 (1960). See also J. Schwinger, Ann. Phys., **2**,407 (1957).

[9] See for example J. Schechter and Y. Ueda, Phys. Rev.**D3**, 2874(1971).

[10] See the Appendix of J. Schechter and Y. Ueda, Phys. Rev. **D3**, 168(1971).

[11] Y. Nambu and G.Jona-Lasinio, Phys. Rev. **122**, 345 (1961); **124**, 246 (1961).

[12] S. Weinberg, Phys. Rev. Lett. **17**, 616 (1966).

[13] K. Nishijima, Nuovo Cimento **11**, 698 (1959); F. Gursey, Nuovo Cimento **16**, 230 (1960). For the three flavor extension see J. Cronin, Phys. Rev. **161**, 1483 (1967).

[14] J. Chisholm, Nucl. Phys. **26**, 469 (1961).

[15] M. Gell-Mann, R. Oakes and B. Renner, Phys. Rev. **175**, 2195 (1968); S. Glashow and S. Weinberg, Phys. Rev. Lett. **20**, 224 (1968).

[16] J. Schechter and Y. Ueda, Phys. Rev. **D4**, 733(1971).

[17] S. Adler, Phys. Rev, **177** 2426(1969); J. Bell and R. Jackiw, Nuovo Cimento **60A**, 47 (1969).

[18] J. Crewther, Phys. Rev. Lett. **28**, 1421 (1972); M. Chanowitz and J. Ellis, Phys. Rev. **7**, 2490 (1973); S. Adler, J. Collins and A. Duncan, *ibid* **15**, 1712 (1977); N. Nielsen, Nucl. Phy. **B210**, 212 (1977); J. Collins, A. Duncan and S. Joglekar, Phys. Rev. **D16**, 438 (1977).

[19] J. Schechter, Phys. Rev. **D21**, 3393 (1980); A. Salomone, J. Schechter and T. Tudron, *ibid* **23**, 1143 (1981); H. Gomm, P. Jain, R. Johnson and J. Schechter, *ibid* **D33**, 801 (1986).

[20] A. Migdal and M. Shifman, Phys. Lett. **114B**, 445 (1982); J. Cornwall and A. Soni, Phys. Rev. **D32**, 764(1985).

[21] J. DeGrand, R. Jaffe, K. Johnson and J. Kiskis, Phys. Rev. **D12**, 2066 (1975).

[22] Recent reviews are given in K. Rajagopal and F. Wilczek, hep-ph/0011333; M. Alford, hep-ph/0102047; S. Hsu, hep-ph/0003140; D. Hong, hep-ph/0101025; D. Rischke and R. Pisarski, nucl-th/0004016.

[23] R. Ouyed and F. Sannino astro-ph/0103022; hep-ph/0103168.

[24] J. Gasser and H. Leutwyler, Ann. Phys. **158**, 142(1984); Nucl. Phys. **B250**, 465 (1985).

[25] M. Harada, F. Sannino and J. Schechter, Phys. Rev. **D54**, 1991 (1996).

[26] See the conference proceedings, S. Ishida et al "Possible existence of the sigma meson and its implication to hadron physics", KEK Proceedings 2000-4, Soryushiron Kenkyu 102, No. 5, 2001.

[27] D. Black, A. Fariborz, F. Sannino and J. Schechter, Phys. Rev. **D59**, 074026 (1999).

[28] R. Jaffe, Phys. Rev. **D15**, 267 (1977).

[29] D. Black, A. Fariborz and J. Schechter, Phys. Rev.**D61**, 074001 (2000); D. Black, A. Fariborz, S. Moussa, S. Nasri and J. Schechter, Phys. Rev. **D64**, 014031 (2001); T. Teshima, I Kitamura and N. Morisita, hep-ph/010507.

# Effective description of QCD at high density

*Roberto Casalbuoni*
*Dipartimento di Fisica dell'Universita'*
*Sezione INFN di Firenze*
*I-50125 Firenze, ITALY*

## 1 Introduction

Ideas about color superconductivity go back to almost 25 years ago [1], but only recently this phenomenon has received a lot of attention (for recent reviews see refs. [2, 3]). The naive expectation is that at very high density, due to the asymptotic freedom, quarks would form a Fermi sphere of almost free fermions. However, Bardeen, Cooper and Schrieffer proved that the Fermi surface of free fermions is unstable in presence of an attractive, arbitrary small, interaction. Since in QCD the gluon exchange in the $\overline{3}$ channel is attractive one expects the formation of a coherent state of particle/hole pairs (Cooper pairs). An easy way to understand the origin of this instability is to remember that the Fermi energy distribution for free fermions at zero temperature is given by $f(E) = \theta(\mu - E)$ and therefore, the maximum value of the energy (Fermi energy) is $E_F = \mu$. Then consider the grand-potential $F = E - \mu N$. Adding or subtracting a particle (or adding a hole) to the Fermi surface does not change $F$, since $F \to (E \pm E_F) - \mu(N \pm 1) = F$. We see that the Fermi sphere of free fermions is highly degenerate. This is the origin of the instability, because if we add to the Fermi sphere two particles bounded with a binding energy $E_B$, the grand potential decreases, since $F - F_B = -E_B < 0$. Therefore in presence of an arbitrarily small attractive interaction, it is energetically more favorable for fermions to pair and form condensates.

We will discuss the methods for the quantitative evaluation of the condensates via a toy model. We will present also the results for the 2SC and CFL phases. Then we will introduce the effective lagrangian describing the low energy degrees of freedom of the CFL phase, that is the Goldstone bosons associated to the global symmetry breaking. We will then show how to formulate in a convenient way the idea of quasi-particles near the Fermi surface, introducing a formalism similar to the one used in heavy quark effective theory [4]. Next we will couple the quasi-particles to the Goldstone bosons in such a way to obtain the right gap term in the fermionic lagrangian. Using a weak coupling expansion, justified by asymptotic freedom, we will be able to evaluate the self-energy of the Goldstone bosons. The expansion at

low momenta will allow us to get some of the couplings appearing in the low-energy effective lagrangian. The remaining couplings are then obtained through an analogous evaluation of the gluon self-energy.

## 2 Color condensation

Thee physics of fermions at finite density and zero temperature can be treated in a systematic way by using Landau's idea of quasi-particles. An example is the Landau theory of Fermi liquids. A conductor is treated as a gas of almost free electrons. However these electrons are dressed ones, where the dressing takes into account the interactions which are neglected in this description. According to Polchinski [5] this procedure just works because the interactions can be integrated away in the usual sense of the effective theories. Of course, this is a consequence of the special nature of the Fermi surface, which is such that there are practically no relevant or marginal interactions. In fact, all the interactions are irrelevant except for the four-fermi couplings between pairs of opposite momentum. Quantum corrections make the attractive ones relevant, and the repulsive ones irrelevant. This explains the instability of the Fermi surface of free fermions against attractive four-fermi interactions, but we would like to understand better the physics underlying the formation of the condensates and how the idea of quasi-particles comes about. To this purpose we will make use of a toy model involving two Fermi oscillators describing, for instance, spin up and spin down. Of course, in a finite-dimensional system there is no spontaneous symmetry breaking, but this model is useful just to illustrate the main points. We assume our dynamical system to be described by the following Hamiltonian containing a quartic coupling between the oscillators

$$H = \epsilon(a_1^\dagger a_1 + a_2^\dagger a_2) + G a_1^\dagger a_2^\dagger a_1 a_2. \tag{1}$$

We will study this model by using a variational principle. We start introducing the following normalized trial wave-function $|\Psi\rangle$

$$|\Psi\rangle = \left(\cos\theta + \sin\theta\, a_1^\dagger a_2^\dagger\right)|0\rangle. \tag{2}$$

The di-fermion operator, $a_1 a_2$, has the following expectation value

$$\Gamma \equiv \langle\Psi|\, a_1 a_2 |\Psi\rangle = -\sin\theta\cos\theta. \tag{3}$$

Then we determine the value of $\theta$ by looking for the minimum of the expectation value of $H$ on the trial state

$$\langle\Psi|H|\Psi\rangle = 2\epsilon\sin^2\theta - G\Gamma^2. \tag{4}$$

We get

$$2\epsilon \sin 2\theta + 2G\Gamma \cos 2\theta = 0 \longrightarrow \tan 2\theta = -\frac{G\Gamma}{\epsilon}. \tag{5}$$

By using the expression (3) for $\Gamma$ we obtain the gap equation

$$\Gamma = -\frac{1}{2}\sin 2\theta = \frac{1}{2}\frac{G\Gamma}{\sqrt{\epsilon^2 + G^2\Gamma^2}}, \tag{6}$$

or

$$1 = \frac{1}{2}\frac{G}{\sqrt{\epsilon^2 + \Delta^2}}, \tag{7}$$

where $\Delta = G\Gamma$. Therefore the gap equation can be seen as the equation determining the ground state of the system, since it gives the value of the condensate. We can now introduce the idea of quasi-particles in this particular context. Let us write the hamiltonian $H$ as the sum of two pieces, a quadratic one, plus another piece containing the interaction term defined in such a way to have zero expectation value on the ground state $|\Psi\rangle$. We have

$$H = H_0 + H_{\rm res}, \tag{8}$$

with

$$H_0 = \epsilon(a_1^\dagger a_1 + a_2^\dagger a_2) - G\Gamma(a_1 a_2 - a_1^\dagger a_2^\dagger), \tag{9}$$

and

$$H_{\rm res} = G(a_1^\dagger a_2^\dagger + \Gamma)\,(a_1 a_2 - \Gamma)\,, \tag{10}$$

where we have neglected a constant term $G\Gamma^2$. Let us now look for a transformation on the Fermi oscillator variables such that $H_0$ acquires a canonical form (Bogoliubov transformation). Such a transformation is

$$A_1 = a_1 \cos\theta - a_2^\dagger \sin\theta, \quad A_2 = a_1^\dagger \sin\theta + a_2 \cos\theta, \tag{11}$$

and we get

$$H_0 = (\epsilon - \sqrt{\epsilon^2 + \Delta^2}) + \sqrt{\epsilon^2 + \Delta^2}(A_1^\dagger A_1 + A_2^\dagger A_2). \tag{12}$$

Furthermore we can check that

$$A_{1,2}|\Psi\rangle = 0. \tag{13}$$

Therefore the operators $A_i^\dagger$ create out of the vacuum quasi-particles of energy

$$E = \sqrt{\epsilon^2 + \Delta^2}. \tag{14}$$

We see that the condensation gives rise to the fermionic energy gap, $\Delta$. The Bogoliubov transformation realizes the dressing of the original operators $a_i$ and $a_i^\dagger$ to the quasi-particle ones $A_i$ and $A_i^\dagger$. Of course, the interaction is still present, but part of

it has been absorbed in the dressing process, and the hope is that in such a way one is able to get a better starting point for a perturbative expansion. As we have said this point of view has been very fruitful in the Landau theory of conductors.

Let us now discuss what have been done in order to determine the gap in QCD at high density (see [2]). At asymptotically high-density one can, in principle, perform the calculation starting from first principles, since QCD is weakly coupled [6] (for a more complete list of references see [2]). However the actual calculations are unlikely to be extrapolated below a chemical potential of order $10^8\ GeV$ [7]. Since the interesting density regime for neutron stars and heavy ions is for $\mu \leq 500\ MeV$, one has to use phenomenological interactions known to capture the essential features of QCD. In the case of two massless flavors one can use the instanton vertex producing a four-fermi interaction. For more flavors use has been made of the one-gluon exchange approximation or, again, of a four-fermi interaction with color, flavor, and spin structure identical to the one gluon exchange case. A practical way to arrive at the gap equation is to write down the Schwinger-Dyson equation for the case at hand, ignoring vertex corrections. One gets an equation of the type

$$\Sigma(k) = -\frac{1}{2\pi^4}\int d^4q\, G^{-1}(q)V(k-q), \tag{15}$$

where $G^{-1}(q)$ is the full propagator and $V(p)$ is the vertex function, momentum independent for a point-like interactions. This is an integral equation for the self-energy which appears on the right-hand side in $G^{-1}(q)$. Since one expects a diquark condensate it is convenient to introduce the Nambu-Gorkov fields

$$\Psi = \begin{pmatrix} \psi \\ \overline{\psi}^T \end{pmatrix}, \tag{16}$$

The wave operator is then postulated of the form

$$G(q) = G(q)_{\rm free} + \Sigma = \begin{pmatrix} \not{q} + \mu\gamma_0 & \gamma_0\Delta\gamma_0 \\ \Delta & (\not{q} - \mu\gamma_0)^T \end{pmatrix}, \tag{17}$$

equivalent to introduce in the lagrangian a mass gap term of the type $\psi^T C\Delta\psi$. For a four-fermi interaction $\Delta$ is a matrix in color-flavor-spin space. In the gluon-exchange case there is also a momentum dependence. The typical gap equation for a four-fermi interaction (neglecting antiparticle contribution) is

$$\Delta = 4G\int_0^\Lambda \frac{d^4p}{(2\pi)^4}\Big(\frac{\Delta}{p_0^2 + (|\vec{p}| - \mu)^2 + \Delta^2}\Big). \tag{18}$$

When the interaction strength, $G \to 0$, and $\Delta \ll \mu$, $\Lambda$, one finds

$$\Delta \propto \Delta\mu^2\, G\log(\mu/\Delta) \to \Delta \propto \mu\exp(-c/(G\mu^2)). \tag{19}$$

Replacing the effective four-fermi interaction with one-gluon exchange one expects

$$\Delta \propto \mu \exp(-c/g^2). \tag{20}$$

But taking into account the gluon propagator one gets a double-log contribution due to a collinear infrared divergence arising from the gluon propagator. This divergence is regulated, for $q \to 0$, by the inverse of the penetration length, which turns out to be of order $\Delta$ [8]. In the weak coupling limit one gets [6]

$$\Delta \propto \Delta g^2 (\log(\mu/\Delta))^2 \to \Delta \propto \mu \exp(-c/g). \tag{21}$$

The gap at large $\mu$ is much larger in QCD than in the case of a point-like interaction. If the coupling $g$ is evaluated at $\mu$ and we assume $1/g^2 \approx \log \mu$ the exponential gives a very weak suppression and for $\mu \to \infty$ we have $\Delta \to \infty$ and $\Delta/\mu \to 0$. Color superconductivity is bounded to dominate physics at high density.

The phase structure of QCD at high density depends on the number of flavors and there are two very interesting cases, corresponding to two massless flavors (2SC) [1, 5] and to three massless flavors (CFL) [10, 11] respectively. In this talk we will be mainly concerned with the latter case. The two cases correspond to very different patterns of symmetry breaking. If we denote left- and right-handed quark fields by $q^\alpha_{iL(R)}$ with $\alpha = 1, 2, 3$, the $SU(3)_c$ color index, and $i = 1, \cdots, N_f$ the flavor index ($N_f$ is the number of massless flavors), in the 2SC phase the previous calculations give the following color-flavor-spin structure for the condensate

$$\langle q^\alpha_{iL(R)}(\vec{p}) C q^\beta_{jL(R)}(-\vec{p}) \rangle = \frac{\Delta}{G} \epsilon_{ij} \epsilon^{\alpha\beta 3}. \tag{22}$$

Here $C = i\gamma^2\gamma^0$ is the charge-conjugation matrix. The resulting symmetry breaking pattern (barring $U(1)$ factors) is [1, 5]

$$\begin{array}{c} SU(3)_c \otimes SU(2)_L \otimes SU(2)_R \\ \downarrow \\ SU(2)_c \otimes SU(2)_L \otimes SU(2)_R \end{array} \tag{23}$$

The color group $SU(3)_c$ breaks down to the subgroup $SU(2)_c$ but no global symmetry is broken. Although the baryon number, $B$, is broken, there is a combination of $B$ and of the broken color generator, $T_8$, which is unbroken in the 2SC phase. Therefore no massless Goldstone bosons are present in this phase. On the other hand, five gluon fields acquire mass whereas three are left massless. It is worth to notice that for the electric charge the situation is very similar to the one for the baryon number. Again a linear combination of the broken electric charge and of the broken generator $T_8$ is unbroken in the 2SC phase. The condensate (22) gives rise to a gap, $\Delta$, for quarks of

color 1 and 2, whereas the two quarks of color 3 remain un-gapped (massless). The resulting effective low-energy theory has been described in [12].

Numerically, by choosing a cutoff $\Lambda = 800\ MeV$ (see eq. (18)), and fixing the coupling $G$ in such a way to reproduce correctly the physics at zero density and temperature, one finds [2]

$$\begin{aligned} \mu &= 400\ MeV \Rightarrow \Delta = 106\ MeV, \\ \mu &= 500\ MeV \Rightarrow \Delta = 145\ MeV. \end{aligned} \tag{24}$$

In this contribution we will be mainly interested in the formulation of the effective theory for three massless quarks. An analysis similar to the previous one for this case leads to the condensate [10, 11]

$$\langle q^i_{\alpha L}(\vec{p}) C q^j_{\beta L}(-\vec{p})\rangle = \frac{1}{G} P^{ij}_{\alpha\beta}, \tag{25}$$

with

$$P^{ij}_{\alpha\beta} = \frac{1}{3}(\Delta_8 + \frac{1}{8}\Delta_1)\delta^i_\alpha\delta^j_\beta + \frac{1}{8}\Delta_1\delta^i_\beta\delta^j_\alpha. \tag{26}$$

This originates the breaking

$$SU(3)_c \otimes SU(3)_L \otimes SU(3)_R \otimes U(1)_B \otimes U(1)_A$$

$$\downarrow \tag{27}$$

$$SU(3)_{c+L+R} \otimes Z_2 \otimes Z_2 \tag{28}$$

The $U(1)_A$ symmetry is broken at the quantum level by the anomaly, but it gets restored at very high density since the instanton contribution is suppressed [13, 14, 15]. Again, for $\Lambda = 800\ MeV$, a convenient choice for $G$ and $\mu = 400\ MeV$, one gets [2]

$$\Delta_8 = 80\ MeV, \quad \Delta_1 = -176\ MeV. \tag{29}$$

The condensate can also be written in the form

$$\langle q^\alpha_{iL(R)}(\vec{p}) C q^\beta_{jL(R)}(-\vec{p})\rangle \propto \epsilon^{ijX}\epsilon_{\alpha\beta X} + \kappa(\delta^i_\alpha\delta^j_\beta + \delta^i_\beta\delta^j_\alpha). \tag{30}$$

Notice that $\kappa = 0$ corresponds to $\Delta_1 = -2\Delta_8$. Due to the Fermi statistics, the condensate must be symmetric in color and flavor. As a consequence the two terms appearing in eq. (30) correspond to the $(\overline{\mathbf{3}}, \overline{\mathbf{3}})$ and $(\mathbf{6}, \mathbf{6})$ channels of $SU(3)_c \otimes SU(3)_{L(R)}$. It turns out that $\kappa$ is small [10, 14, 16] and therefore the condensation occurs mainly in the $(\overline{\mathbf{3}}, \overline{\mathbf{3}})$ channel (see also eq. (29)). The expression (30) shows that the ground state is left invariant by a simultaneous transformation of $SU(3)_c$ and $SU(3)_{L(R)}$. This is called Color Flavor Locking (CFL). The $Z_2$ symmetries arise since the condensate is left invariant by a change of sign of the left- and/or right-handed fields. As for the

2SC case the electric charge is broken but a linear combination with the broken color generator $T_8$ annihilates the ground state. On the contrary the baryon number is broken. Therefore there are $8+2$ broken global symmetries giving rise to 10 Goldstone bosons. The one associated to $U(1)_A$ gets massless only at very high density. The color group is completely broken and all the gauge particles acquire mass. Also all the fermions are gapped.

# 3 Effective theory for the CFL phase

We start introducing the Goldstone fields as the phases of the condensates in the $(\overline{\mathbf{3}},\overline{\mathbf{3}})$ channel [17, 18]

$$X^i_\alpha \approx \epsilon^{ijk}\epsilon_{\alpha\beta\gamma}\langle q^j_{\beta L} q^k_{\gamma L}\rangle^*, \quad Y^i_\alpha \approx \epsilon^{ijk}\epsilon_{\alpha\beta\gamma}\langle q^j_{\beta L} q^k_{\gamma L}\rangle^*. \tag{31}$$

Since quarks belong to the representation $(\mathbf{3},\mathbf{3})$ of $SU(3)_c\otimes SU(3)_{L(R)}$ and transform under $U(1)_B\otimes U(1)_A$ according to

$$qq_L \to e^{i(\alpha+\beta)}q_L, \quad q_R \to e^{i(\alpha-\beta)}q_R, \quad e^{i\alpha}\in U(1)_B, \quad e^{i\beta}\in U(1)_A, \tag{32}$$

the transformation properties of the fields $X$ and $Y$ under the total symmetry group $G = SU(3)_c\otimes SU(3)_L\otimes SU(3)_R\otimes U(1)_B\otimes U(1)_A$ are ($g_c\in SU(3)_c$, $g_{L(R)}\in SU(3)_{L(R)}$)

$$X \to g_c X g_L^T e^{-2i(\alpha+\beta)}, \quad Y \to g_c Y g_R^T e^{-2i(\alpha-\beta)}. \tag{33}$$

The fields $X$ and $Y$ are $U(3)$ matrices and as such they describe $9+9=18$ fields. Eight of these fields are eaten up by the gauge bosons, producing eight massive gauge particles. Therefore we get the right number of Goldstone bosons, $10 = 18-8$. These fields correspond to the breaking of the global symmetries in $G$ (18 generators) to the symmetry group of the ground state $H = SU(3)_{c+L+R}\otimes Z_2\otimes Z_2$ (8 generators). For the following it is convenient to separate the $U(1)$ factors in $X$ and $Y$ in order to get new fields belonging to $SU(3)$

$$X = \hat{X}e^{2i(\phi+\theta)}, \quad Y = \hat{Y}e^{2i(\phi-\theta)}, \quad \hat{X},\hat{Y}\in SU(3). \tag{34}$$

The fields $\phi$ and $\theta$ can be also described in an a more invariant way through the determinants of $X$ and $Y$

$$d_X = \det(X) = e^{6i(\phi+\theta)}, \quad d_Y = \det(Y) = e^{6i(\phi-\theta)}, \tag{35}$$

with transformation properties under $G$

$$\hat{X} \to g_c\hat{X}g_L^T, \quad \hat{Y} \to g_c\hat{Y}g_R^T, \quad \phi\to\phi-\alpha, \quad \theta\to\theta-\beta. \tag{36}$$

The breaking of the global symmetry can be discussed in terms of gauge invariant fields $d_X$, $d_Y$ and

$$\Sigma^i_j = \sum_\alpha (\hat{Y}^j_\alpha)^* \hat{X}^i_\alpha \to \Sigma = \hat{Y}^\dagger \hat{X}. \tag{37}$$

The $\Sigma$ field describes the 8 Goldstone bosons corresponding to the breaking of the chiral symmetry $SU(3)_L \otimes SU(3)_R$, as it is made clear by the transformation properties of $\Sigma^T$,

$$\Sigma^T \to g_L \Sigma^T g_R^\dagger. \tag{38}$$

That is $\Sigma^T$ transforms exactly as the usual chiral field. The other two fields $d_X$ and $d_Y$ provide the remaining two Goldstone bosons corresponding to the breaking of the $U(1)$ factors.

In order to build up an invariant lagrangian it is convenient to define the following currents

$$J^\mu_X = \hat{X} D^\mu \hat{X}^\dagger = \hat{X}(\partial^\mu \hat{X}^\dagger + \hat{X}^\dagger g^\mu), \quad J^\mu_Y = \hat{Y} D^\mu \hat{Y}^\dagger = \hat{Y}(\partial^\mu \hat{Y}^\dagger + \hat{Y}^\dagger g^\mu), \tag{39}$$

with $g_\mu = i g_s g^a_\mu T^a/2$ the gluon field and $T^a = \lambda_a/2$ the $SU(3)_c$ generators. These currents have simple transformation properties under the full symmetry group $G$,

$$J^\mu_{X,Y} \to g_c J^\mu_{X,Y} g_c^\dagger. \tag{40}$$

The most general lagrangian, up to two derivative terms, invariant under $G$, the rotation group $O(3)$ (Lorentz invariance is broken by the chemical potential term) and the parity transformation defined as

$$\hat{X}(\vec{x},t) \leftrightarrow \hat{Y}(-\vec{x},t), \quad \phi(\vec{x},t) \to \phi(-\vec{x},t), \quad \theta(\vec{x},t) \to -\theta(-\vec{x},t), \tag{41}$$

is [17]

$$\begin{aligned} \mathcal{L} = & -\frac{F_T^2}{4}\mathrm{Tr}\left[(J^0_X - J^0_Y)^2)\right] - \alpha_T \frac{F_T^2}{4}\mathrm{Tr}\left[(J^0_X + J^0_Y)^2)\right] + \frac{1}{2}(\partial_0\phi)^2 + \frac{1}{2}(\partial_0\theta)^2 \\ + & \frac{F_S^2}{4}\mathrm{Tr}\left[\left(\vec{J}_X - \vec{J}_Y)^2\right)\right] + \alpha_S \frac{F_S^2}{4}\mathrm{Tr}\left[\left(\vec{J}_X + \vec{J}_Y)^2\right)\right] - \frac{v_\phi^2}{2}|\vec{\nabla}\phi|^2 - \frac{v_\theta^2}{2}|\vec{\nabla}\theta|^2. \end{aligned} \tag{42}$$

Using $SU(3)_c$ color gauge invariance we can choose $\hat{X} = \hat{Y}^\dagger$, making 8 of the Goldstone bosons disappear and giving mass to the gluons. The properly normalized Goldstone bosons, $\Pi^a$, are given in this gauge by

$$\hat{X} = \hat{Y}^\dagger = e^{i\Pi^a T^a/F_T}. \tag{43}$$

Expanding eq. (42) at the lowest order in the fields we get

$$\mathcal{L} \approx \frac{1}{2}(\partial_0\Pi^a)^2 + \frac{1}{2}(\partial_0\phi)^2 + \frac{1}{2}(\partial_0\theta)^2 - \frac{v^2}{2}|\vec{\nabla}\Pi^a|^2 - \frac{v_\phi^2}{2}|\vec{\nabla}\phi|^2 - \frac{v_\theta^2}{2}|\vec{\nabla}\theta|^2, \tag{44}$$

with $v = F_s/F_T$. The gluons $g_0^a$ and $g_i^a$ acquire Debye and Meissner masses given by

$$m_D^2 = \alpha_T g_s^2 F_T^2, \quad m_M^2 = \alpha_S v^2 g_s^2 F_T^2. \tag{45}$$

It should be stressed that these are not the true rest masses of the gluons, since there is a large wave function renormalization effect making the gluon masses of the order of the gap $\Delta$ (see later) [8]. Since this description is supposed to be valid at low energies (we expect much below the gap $\Delta$), we could also decouple the gluons solving their classical equations of motion neglecting the kinetic term. The result from eq. (42) is

$$g_\mu = -\frac{1}{2}\left(\hat{X}\partial_\mu \hat{X}^\dagger + \hat{Y}\partial_\mu \hat{Y}^\dagger\right). \tag{46}$$

It is easy to show that substituting this expression in eq. (42) one gets [8]

$$\mathcal{L} = \frac{F_T^2}{4}\left(\mathrm{Tr}[\dot{\Sigma}\dot{\Sigma}^\dagger] - v^2\mathrm{Tr}[\vec{\nabla}\Sigma\cdot\vec{\nabla}\Sigma^\dagger]\right) + \frac{1}{2}\left(\dot{\phi}^2 - v_\phi^2|\vec{\nabla}\phi|^2\right) + \frac{1}{2}\left(\dot{\theta}^2 - v_\phi^2|\vec{\nabla}\theta|^2\right). \tag{47}$$

The first term is nothing but the chiral lagrangian except for the breaking of the Lorentz invariance. This is a way of seeing the quark-hadron continuity, that is the continuity between the CFL and the nuclear matter in three flavor QCD. The identification is perfect if one realizes that in nuclear matter the pairing may occur in such a way to give rise to a superfluid due to the breaking of the baryon number as it happens in CFL [19].

# 4 Fermions near the Fermi surface

We will introduce now the formalism described in ref. [20] in order to evaluate several quantities of interest appearing in the effective lagrangian. This formulation is based on the observation that, at very high-density, the energy spectrum of a massless fermion is described by states $|\pm\rangle$ with energies $E_\pm = -\mu \pm |\vec{p}|$ where $\mu$ is the quark number chemical potential. For energies much lower than the Fermi energy $\mu$, only the states $|+\rangle$ close to the Fermi surface. i.e. with $|\vec{p}| \approx \mu$, can be excited. On the contrary, the states $|-\rangle$ have $E_- \approx -2\mu$ and therefore they decouple.

This can be seen more formally by writing the four-momentum of the fermion as

$$p^\mu = \mu v^\mu + \ell^\mu, \tag{48}$$

where $v^\mu = (0, \vec{v}_F)$, and $\vec{v}_F$ is the Fermi velocity defined as $\vec{v}_F = \partial E/\partial\vec{p}|_{\vec{p}=\vec{p}_F}$. For massless fermions $|\vec{v}_F| = 1$. Since the hamiltonian for a massless Dirac fermion in a chemical potential $\mu$ is

$$H = -\mu + \vec{\alpha}\cdot\vec{p}, \quad \vec{\alpha} = \gamma_0\vec{\gamma}, \tag{49}$$

one has

$$H = -\mu(1 - \vec{\alpha}\cdot\vec{v}_F) + \vec{\alpha}\cdot\vec{\ell}. \tag{50}$$

Then, it is convenient to introduce the projection operators

$$P_\pm = \frac{1 \pm \vec{\alpha}\cdot\vec{v}_F}{2}, \tag{51}$$

such that

$$H|+\rangle = \vec{\alpha}\cdot\vec{\ell}\,|+\rangle, \quad H|-\rangle = (-2\mu + \vec{\alpha}\cdot\vec{\ell})\,|-\rangle. \tag{52}$$

We can define fields corresponding to the states $|\pm\rangle$ through the decomposition

$$\psi(x) = \sum_{\vec{v}_F} e^{-i\mu v\cdot x}\left[\psi_+(x) + \psi_-(x)\right], \tag{53}$$

where an average over the Fermi velocity $\vec{v}_F$ is performed. The velocity-dependent fields $\psi_\pm(x)$ are given by $(v^\mu = (0, \vec{v}_F))$

$$\psi_\pm(x) = e^{i\mu v\cdot x}\left(\frac{1 \pm \vec{\alpha}\cdot\vec{v}_F}{2}\right)\psi(x) \;=\; \int_{|\ell|<\delta}\frac{d^4\ell}{(2\pi)^4}e^{-i\,\ell\cdot x}\psi_\pm(\ell). \tag{54}$$

Since we are interested at physics near the Fermi surface we integrate out all the modes with $|\ell| > \delta$, where $\delta$ is a cut-off such that $\delta \ll \mu$. At the same time we will choose $\delta$ greater than the energy gap, $\Delta$. Since, as we shall see, physics around the Fermi surface is effectively two-dimensional, the results do not depend on the value of $\delta$. Substituting inside the Dirac part of the QCD lagrangian density one obtains $(V^\mu = (1, \vec{v}_f),\ \tilde{V}^\mu = (1, -\vec{v}_F))$

$$\mathcal{L} = \sum_{\vec{v}_F}\left[\psi_+^\dagger iV\cdot D\psi_+ + \psi_-^\dagger(2\mu + i\tilde{V}\cdot D)\psi_- + (\overline{\psi}_+ i\not{D}_\perp\psi_- + \text{h.c.})\right], \tag{55}$$

where $\not{D}_\perp = D_\mu\gamma_\perp^\mu$ and

$$\gamma_\perp^\mu \;=\; \frac{1}{2}\gamma_\nu\left(2g^{\mu\nu} - V^\mu\tilde{V}^\nu - \tilde{V}^\mu V^\nu\right). \tag{56}$$

We notice that the fields appearing in this expression are evaluated at the same Fermi velocity because off-diagonal terms are cancelled by the rapid oscillations of the exponential factor in the $\mu \to \infty$ limit. This behaviour can be referred to as the Fermi velocity superselection rule.

At the leading order in $1/\mu$ one has

$$iV\cdot D\psi_+ = 0, \qquad \psi_- = -\frac{i}{2\mu}\gamma_0\not{D}_\perp\psi_+, \tag{57}$$

showing the decoupling of $\psi_-$ for $\mu \to \infty$. The equation for $\psi_+$ shows also that only the energy and the momentum parallel to the Fermi velocity are relevant variables in the problem. We have an effective two-dimensional theory.

Eliminating the field $\psi_-$ we get

$$\mathcal{L} = \sum_{\vec{v}_F} \left[ \psi_+^\dagger iV \cdot D \psi_+ - \frac{1}{2\mu + i\tilde{V} \cdot D} \psi_+^\dagger (\not{D}_\perp)^2 \psi_+ \right]. \tag{58}$$

The previous remarks apply to any theory describing massless fermions at high density. The next step will be to couple this theory in a $SU(3)_L \otimes SU(3)_R \otimes SU(3)_c$ invariant way to Nambu-Goldstone bosons (NGB) describing the appropriate breaking for the CFL phase. Using a gradient expansion we get an explicit expression for the decay coupling constant of the Nambu-Goldstone bosons as well for their velocity.

# 5 Goldstone bosons self-energy

The invariant coupling between fermions and Goldstone fields reproducing the symmetry breaking pattern of eq. (30) is proportional to

$$\gamma_1 \, Tr[\psi_L^T \hat{X}^\dagger] \, C \, Tr[\psi_L \hat{X}^\dagger] + \gamma_2 \, Tr[\psi_L^T C \hat{X}^\dagger \psi_L \hat{X}^\dagger] + \text{h.c.}, \tag{59}$$

and analogous relations for the right-handed fields. Here the spinors are meant to be Dirac spinors. The trace is operating over the group indices of the spinors and of the Goldstone fields. Since the vacuum expectation value of the Goldstone fields is $\langle \hat{X} \rangle = \langle \hat{Y} \rangle = 1$, we see that this coupling induces the right breaking of the symmetry. In the following we will consider only the case $\gamma_2 = -\gamma_1 \propto \Delta/2$, where $\Delta$ is the gap parameter.

Since the transformation properties under the symmetry group of the fields at fixed Fermi velocity do not differ from those of the quark fields, for both left-handed and right-handed fields we get the effective lagrangian density [8]

$$\begin{aligned} \mathcal{L} &= \sum_{\vec{v}_F} \frac{1}{2} \Big[ \sum_{A=1}^{9} \left( \psi_+^{A\dagger} iV \cdot D \psi_+^A + \psi_-^{A\dagger} i\tilde{V} \cdot D \psi_-^A - \Delta_A \left( \psi_-^{AT} C \psi_+^A + \text{h.c.} \right) \right) \\ &- \Delta \sum_{I=1,3} \left( Tr[(\psi_- X_1^\dagger)^T C \epsilon_I (\psi_+ X_1^\dagger) \epsilon_I] + \text{h.c.} \right) \Big], \end{aligned} \tag{60}$$

where we have introduced the fields $\psi_\pm^A$:

$$\psi_\pm = \frac{1}{\sqrt{2}} \sum_{A=1}^{9} \lambda_A \psi_\pm^A. \tag{61}$$

Here $\lambda_a$ $(a = 1, ..., 8)$ are the Gell-Mann matrices normalized as follows: $Tr(\lambda_a\lambda_b) = 2\delta_{ab}$ and $\lambda_9 = \sqrt{2/3}\ \mathbf{1}$. Furthermore $\Delta_1 = \cdots = \Delta_8 = \Delta$, $\Delta_9 = -2\Delta$, and $X_1 = \hat{X} - 1$. Notice that the NGB fields couple to fermionic fields with opposite Fermi velocities. In this expression, as in the following ones, the field $\psi_-$ is defined as $\psi_+$ with $\vec{v}_F \to -\vec{v}_F$, and therefore it is not the same as the one defined in (54).

The formalism becomes more compact by introducing the Nambu-Gorkov fields

$$\chi = \begin{pmatrix} \psi_+ \\ C\psi_-^* \end{pmatrix}. \tag{62}$$

It is important to realize that the fields $\chi$ and $\chi^\dagger$ are not independent variables. In fact, since we integrate over all the Fermi surface, the fields $\psi_-^*$ and $\psi_+$, appearing in $\chi$, appear also in $\chi^\dagger$ when $\vec{v}_F \to -\vec{v}_F$. In order to avoid this problem we can integrate over half of the Fermi surface, or, taking into account the invariance under $\vec{v}_F \to -\vec{v}_F$, we can simply integrate over all the sphere with a weight $1/8\pi$ instead of $1/4\pi$:

$$\sum_{\vec{v}_F} = \int \frac{d\vec{v}_F}{8\pi}. \tag{63}$$

Then the first three terms in the lagrangian density (60) become

$$\mathcal{L}_0 = \int \frac{d\vec{v}_F}{8\pi}\ \frac{1}{2}\sum_{A=1}^{9} \chi^{A\dagger} \begin{bmatrix} iV\cdot D & \Delta^A \\ \Delta^A & i\tilde{V}\cdot D^* \end{bmatrix} \chi^A, \tag{64}$$

so that, in momentum space the free fermion propagator is

$$S_{AB}(p) = \frac{2\delta_{AB}}{V\cdot p\,\tilde{V}\cdot p - \Delta_A^2} \begin{bmatrix} \tilde{V}\cdot p & -\Delta_A \\ -\Delta_A & V\cdot p \end{bmatrix}. \tag{65}$$

We are now in position to evaluate the self-energy of the Goldstone bosons through their couplings to the fermions at the Fermi surface. There are two one-loop contributions [8], one from the coupling $\Pi\chi\chi$ and a tadpole from the coupling $\Pi\Pi\chi\chi$ arising from eq. (60). The tadpole diagram contributes only to the mass term and it is essential to cancel the external momentum independent term arising from the other diagram. Therefore, as expected, the mass of the NGB's is zero. The contribution at the second order in the momentum expansion is given by

$$i\,\frac{21 - 8\ln 2}{72\pi^2 F_T^2} \int \frac{d\vec{v}_F}{4\pi} \sum_{a=1}^{8} \Pi^a\, V\cdot p\,\tilde{V}\cdot p\,\Pi^a. \tag{66}$$

Integrating over the velocities and going back to the coordinate space we get

$$\mathcal{L}_{\rm eff}^{\rm kin} = \frac{21 - 8\ln 2}{72\pi^2 F_T^2} \sum_{a=1}^{8} \left( \dot{\Pi}^a\dot{\Pi}^a - \frac{1}{3}|\vec{\nabla}\Pi_a|^2 \right). \tag{67}$$

We can now determine the decay coupling constant $F_T$ through the requirement of getting the canonical normalization for the kinetic term; this implies

$$F_T^2 = \frac{\mu^2(21 - 8\ln 2)}{36\pi^2}, \tag{68}$$

a result obtained by many authors using different methods (for a complete list of the relevant papers see the first reference of [2]). We see also that $v^2 = 1/3$. The origin of the pion velocity $1/\sqrt{3}$ is a direct consequence of the integration over the Fermi velocity. Therefore it is completely general and applies to all the NGB's in the theory, including the ones associated to the breaking of $U(1)_V$ and $U(1)_A$ ($v_\phi^2 = v_\theta^2 = 1/3$); needless to say, higher order terms in the expansion $1/\mu$ could change this result.

The breaking of the Lorentz invariance exhibited by the pion velocity different from one, can be seen also in the matrix element $\langle 0|J_\mu^a|\Pi^b\rangle$. Its evaluation gives [8]

$$\langle 0|J_\mu^a|\Pi^b\rangle = iF_T\delta_{ab}\tilde{p}_\mu, \qquad \tilde{p}^\mu = (p^0, \vec{p}/3). \tag{69}$$

The current is conserved, as a consequence of the dispersion relation satisfied by the NGB's.

# 6 Gluons self-energy

The other couplings appearing in our effective lagrangian can be obtained via a direct calculation of $m_D$ and $m_M$ [8]. This is done evaluating the one-loop contribution to the gluon self-energy. Also in this case there are two contributions, one coming from the gauge coupling to the fermions, whereas the other arises from the second term (sea-gull like) appearing in the fermion effective lagrangian of eq. (58). The results we find are [8]

$$m_D^2 = g_s^2 F_T^2, \quad m_M^2 = \frac{1}{3}m_D^2. \tag{70}$$

Comparison with equation (45) shows that

$$\alpha_S = \alpha_T = 1. \tag{71}$$

Performing a gradient expansion of the gluon self-energy one finds that there is a wave function renormalization of order $g_s\mu/\Delta \gg 1$ [8]. In fact, considering the different components of the gluon field, the temporal, $g_0^a$ and the longitudinal, $g_L^{ia}$, and transverse, $g_T^{ia}$ ones, defined as

$$\begin{aligned} g_L^{ia} &= \frac{\vec{p}\cdot\vec{g}^a}{|\vec{p}|^2}\,p^i, \\ g_T^{ia} &= g^{ia} - g_L^{ia}\ , \end{aligned} \tag{72}$$

the following dispersion relations are obtained

$$\begin{aligned} g^{0a}: \quad & 3\alpha_1 E^2 - \alpha_1 |\vec{p}|^2 &= m_D^2, \\ g_L^{ia}: \quad & \alpha_1 E^2 - \alpha_2 \frac{|\vec{p}|^2}{3} &= m_M^2, \\ g_T^{ia}: \quad & \alpha_1 E^2 - \alpha_3 |\vec{p}|^2 &= m_M^2, \end{aligned} \tag{73}$$

where

$$\begin{aligned} \alpha_1 &= \frac{\mu^2 g_s^2}{216\Delta^2\pi^2}\left(7+\frac{16}{3}\ln 2\right), \\ \alpha_2 &= -\frac{\mu^2 g_s^2}{3240\Delta^2\pi^2}\left(59-\frac{688}{3}\ln 2\right), \\ \alpha_3 &= -\frac{\mu^2 g_s^2}{3240\Delta^2\pi^2}\left(41-\frac{112}{3}\ln 2\right) . \end{aligned} \tag{74}$$

The coefficients of the energy give just the square of the wave function renormalization (notice that we have neglected the term coming from the free equation of motion, since the renormalization part is much bigger than one). If we extrapolate in momenta up to order $\Delta$ we see that the physical masses of the gluons turn out to be of the order of the gap energy ($\approx 1.70\Delta$) [8]. The validity of this extrapolation has been recently confirmed in ref. [21]. Wave function renormalization of order $g_s\mu/\Delta$ for gauge fields in a dense fermionic medium appears to be a rather general phenomenon. For instance, consider the 2SC phase. The low energy degrees of freedom are 3 gluons and the almost free quarks of color 3. The symmetries determining the effective lagrangian are: the gauge symmetry $SU(2)_c$ and rotation invariance (Lorentz is broken being at finite density). For the gluons one gets [22]

$$\mathcal{L}_{\rm eff} = \frac{\epsilon}{2}\vec{E}^a\cdot\vec{E}^a - \frac{1}{2\lambda}\vec{B}^a\cdot\vec{B}^a, \tag{75}$$

with a propagation velocity for the gluons given by $v = 1/\sqrt{\epsilon\lambda}$. Values of $\epsilon$ and $\lambda$ different from 1 originate from wave function renormalization. One finds [22]

$$\epsilon = 1 + \frac{g_s^2\mu^2}{18\pi^2\Delta^2} \approx \frac{g_s^2\mu^2}{18\pi^2\Delta^2}, \quad \lambda = 1. \tag{76}$$

The strong coupling constant gets modified

$$\alpha_s \;\to\; \alpha_s' = \frac{g_{\rm eff}^2}{4\pi v} = \frac{g_s^2}{4\pi\sqrt{\epsilon}} = \frac{3}{2\sqrt{2}}\frac{g_s\Delta}{\mu}, \tag{77}$$

due to the changes in the propagation velocity and in the Coulomb force

$$g_s^2/r \to g_s^2/(\epsilon r) \quad \Rightarrow \quad g_s^2 \to g_{\rm eff}^2 = g_s^2/\epsilon. \tag{78}$$

Similar results hold for the massive gluons of type 4, 5, 6 and 7 which acquire a mass of order $\Delta$. Exceptions are the spatial components (but not the time one) of the gluon 8. In this case there is no wave function renormalization of the time derivative and the mass is of order $g_s\mu$ [23]. Also the em dielectric constant gets modified by the in-medium effects both in the CFL and in the 2SC phases [24]

$$\tilde{\epsilon} = 1 + \frac{r}{18\pi^2}\frac{\tilde{e}^2\mu^2}{\Delta^2}, \tag{79}$$

where $\tilde{e}$ is the in-medium rotated electric charge, and

$$r = 4 \text{ in CFL}, \quad r = 1 \text{ in 2SC}. \tag{80}$$

**Acknowledgments**

I would like to thank R. Gatto, M. Mannarelli and G. Nardulli for their precious collaboration in the works originating this contribution.

# References

[1] B. Barrois, Nucl. Phys. B **129**, 390 (1977); S. Frautschi, *Proceedings of workshop on hadronic matter at extreme density*, Erice 1978; D. Bailin and A. Love, Phys. Rep. **107** (1984) 325.

[2] K. Rajagopal and F. Wilczek, hep-ph/0011333;

[3] S.D.H. Hsu, hep-ph/0003140; D.K. Hong, Acta Phys. Pol. **B32** (2001) 1253, hep-ph/0101025; M. Alford, hep-ph/0102047.

[4] N. Isgur and M.B. Wise, Phys. Lett. **B232** (1989) 113 ; *ibidem* Phys. Lett. **B237** (1990) 527; E. Eichten and B. Hill, Phys. Lett. **B234** (1990) 511; H. Georgi, Phys. Lett. **B240** (1990) 447; for a recent review see A. V. Manohar and M.B. Wise *Heavy Quark Physics*, Cambridge University Press (2000).

[5] J. Polchinski, Lectures presented at TASI 92, hep-th/9210046.

[6] D. T. Son, Phys. Rev. D **59** (1999) 094019, hep-ph/9812287.

[7] K. Rajagopal and E. Shuster, Phys. Rev. D **62** (2000) 085007, hep-ph/0004074.

[8] R. Casalbuoni, R. Gatto and G. Nardulli, Phys. Lett. B **498** (2001) 179, hep-ph/0010321.

[9] M. Alford, K. Rajagopal and F. Wilczek, Phys. Lett. B **422**, 247 (1998), hep-ph/9711395; R. Rapp, T. Schäfer, E.V. Shuryak and M. Velkovsky, Phys. Rev. Lett. **81**, 53 (1998), hep-ph/9711396.

[10] M. Alford, K. Rajagopal and F. Wilczek, Nucl. Phys. B **537**, 443 (1999), hep-ph/9804403.

[11] T. Schäfer and F. Wilczek, Phys. Rev. Lett. **82**, 3956 (1999), hep-ph/9811473.

[12] R. Casalbuoni, Z. Duan and F. Sannino, Phys. Rev. D **62**, 094004 (2000), hep-ph/0004207; *ibidem* D **63**, 114026 (2001), hep-ph/0011394.

[13] R. Rapp, T. Schäfer , E.V. Shuryak and M. Velkovsky, Ann. of Phys. **280**, 35 (2000), hep-ph/9904353.

[14] T. Schäfer, Nucl. Phys. B **575**, 269 (2000), hep-ph/9909574.

[15] D.T. Son and M.A. Stephanov, Phys. Rev. D **61**, 074012 (2000), hep-ph/9910491; *ibidem* Erratum D **62**, 059902 (2000), hep-ph/0004095.

[16] I.A. Shovkovy and L.C. Wijewardhana, Phys. Lett. B **470**, 189 (1999), hep-ph/9910225.

[17] R. Casalbuoni and R. Gatto, Phys. Lett. B **464**, 111 (1999) , hep-ph/9908227.

[18] D.K. Hong, M. Rho and I. Zahed, Phys. Lett. B **468**, 261 (1999), hep-ph/9906551.

[19] T.Schäfer and F. Wilczek, Phys. Rev. Lett. **82**, 3956 (1999), hep-ph/9811473.

[20] D.K. Hong, Phys. Lett. B **473**, 118 (2000), hep-ph/9812510; D.K. Hong *Nuclear Physics* B **582**, 451 (2000), hep-ph/9905523; S.R. Beane, P.F. Bedaque and M.J. Savage, Phys. Lett. B **483**, 131 (2000), hep-ph/0002209.

[21] V. P. Gusynin and I. A. Shovkovy, hep-ph/0108175.

[22] D. H. Rischke, D. T. Son and M. A. Stephanov, Phys. Rev. Lett. **87** (2001) 062001, hep-ph/0011379.

[23] R. Casalbuoni, R. Gatto, M. Mannarelli and G. Nardulli, hep-ph/0107024.

[24] D. F. Litim and C. Manuel, hep-ph/0105165.

# Effective Theory for QCD in the LOFF Phase

*Giuseppe Nardulli*
*Dipartimento Interateneo di Fisica, Università di Bari,*
*I.N.F.N., Sezione di Bari*
*I-70126 Bari, ITALY*

## 1 Introduction

Recently, the old idea of color superconductivity [1] has been given a new life [2], after the discovery that QCD at high density and low temperature can undergo a phase transition to a color super-conducting state characterized, for three light quarks, by Color Flavor Locking: CFL (for recent reviews see [3]). In this talk I wish to examine a different phase of QCD also present at low temperature and high baryonic chemical potential [4]; for two flavors this phase is characterized by isospin breaking and the emergence of a crystalline pattern of the diquark condensate. In a recent paper [5] it has been shown that in this phase there exists a quasi particle (phonon) associated to spontaneous breaking of rotational and translational invariance. Its properties can be studied by an effective lagrangian approach [6], [7], [8]; they will be reviewed here together with a short discussion on possible astrophysical implications.

## 2 Crystalline colour superconductive phase

In any possible application of the color superconductivity, for instance in the inner core of neutron stars, flavor symmetry is likely to be broken not only explicitly by quark mass terms, but also by weak interactions. For example in compact stars, considering only two flavors, isospin is broken by $\delta\mu = \mu_u - \mu_d \neq 0$, due to the process:

$$d \to ue\nu \ . \tag{1}$$

When the two quarks in the Cooper pair have different chemical potentials, the vacuum is characterized, for certain values of $\delta\mu$, by a non vanishing expectation value of a quark bilinear breaking translational and rotational invariance. The appearance of this condensate is a consequence of the fact that in a given range of $\delta\mu$ [4], the formation of a Cooper pair with a total momentum

$$\vec{p}_1 + \vec{p}_2 = 2\vec{q} \neq \vec{0} \tag{2}$$

is energetically favored. A similar phenomenon was already observed many years ago in the context of the BCS theory for superconducting materials in presence of magnetic impurities by Larkin, Ovchinnikov, Fulde and Ferrel and the corresponding phase is named LOFF state [9].

The exact form of the order parameter (diquark condensate) breaking space-time symmetries in the crystalline phase is not yet known. In [4] the following ansatz is made:

$$\Delta(\vec{x}) = \Delta e^{i2\vec{q}\cdot\vec{x}} = \Delta e^{i2q\vec{n}\cdot\vec{x}} \ . \tag{3}$$

The value of $|\vec{q}|$ is fixed by the dynamics, while its direction $\vec{n}$ is spontaneously chosen. In the sequel I will assume the ansatz (3) as well. The order parameter (3) induces a lattice structure given by parallel planes perpendicular to $\vec{n}$:

$$\vec{n}\cdot\vec{x} = \frac{\pi k}{q} \qquad (k = 0, \pm 1, \pm 2, ...) \ . \tag{4}$$

We can give the following physical picture of the lattice structure of the LOFF phase: Due to the interaction with the medium, the Majorana masses of the red and green up and down quarks have a periodic modulation in space, reaching on subsequent planes maxima and minima. For the Cooper pair to be formed one needs a color attractive channel, which is the antisymmetric channel; therefore it must be in antisymmetric flavor state if it is in antisymmetric spin state ($S = 0$). The condensate has therefore the form

$$- < 0|\epsilon_{ij}\epsilon_{\alpha\beta 3}\psi^{i\alpha}(\vec{x})C\psi^{j\beta}(\vec{x})|0 >= 2\Gamma_A^L e^{2i\vec{q}\cdot\vec{x}} \ . \tag{5}$$

The analysis of [4] shows that, besides the condensate (5) (scalar condensate), another different condensate is possible, i.e. one characterized by total spin 1 (vector condensate) and by a symmetric flavor state:

$$i < 0|\sigma_{ij}^1\epsilon_{\alpha\beta 3}\psi^{i\alpha}(\vec{r})C\sigma^{03}\psi^{j\beta}(\vec{x})|0 >= 2\Gamma_B^L e^{2i\vec{q}\cdot\vec{x}} \ . \tag{6}$$

Note that in the BCS state the quarks forming the Cooper pair have necessarily $S = 0$.

It goes without saying that the hypotheses of [4] are rather restrictive, as these authors assume only two flavors and make the ansatz of a plane wave behavior, Eq. (3). In any event their results are as follows. Assuming a pointlike interaction as the origin of the Fermi surface instability, the LOFF state is energetically favored in a small range of values of $\delta\mu$ around $\delta\mu \sim 0.7\Delta$. The actual value of the window range compatible with the presence of the LOFF state depends on the calculation by which the crystalline color state is computed. While the small interval is based on a local interaction, assuming gluon exchange, as in [10], the window opens up considerably.

The order parameters (5) and (6) spontaneously break rotational and translational symmetries. Associated with this breaking there will be Nambu Goldstone Bosons (NGB) as in a crystal; these quasi-particles are known as phonons. Let us discuss them in some detail.

# 3 Phonons in the LOFF phase

For a generic lattice structure it is known that there are three phonons associated to the breaking of space symmetries. However one can show [5] that in order to describe the spontaneous breaking of space symmetries induced by the condensates (5) and (6) one NGB is sufficient. The argument (see Fig. 1) is as follows: Rotations and translations are not independent transformations, because the result of a translation plus a rotation, at least locally, can be made equivalent to a pure translation. The NGB

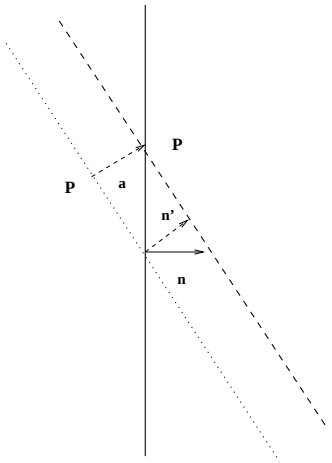


Figure 1: In the point P the effect of the rotation $\vec{n} \to \vec{n}'$ and the effect of the translation $\vec{x} \to \vec{x} + \vec{a}$ tend to compensate each other.

is a long wavelength small amplitude variation of the condensate $\Delta(\vec{x}) \to \Delta(\vec{x})e^{i\phi/f}$, with

$$\phi/f \;=\; 2q(\vec{n}+\delta\vec{n})\cdot(\vec{x}+\delta\vec{x}) - 2q\vec{n}\cdot\vec{x} \;=\; 2q\vec{R}\cdot\vec{x} + T - 2q\vec{n}\cdot\vec{x}\;, \tag{7}$$

where we have introduced the auxiliary function $T$, given by $T \;=\; 2\,q\,\vec{R}\cdot\delta\vec{x}$.

Now the lattice fluctuations $\phi/f$ must be small; from this it follows that $T$ and $\vec{R}$ are not independent fields and therefore $T$ must depend functionally on $\vec{R}$, i.e. $T = F[\vec{R}]$, which, using again (7), means that

$$\Phi \equiv 2q\vec{n}\cdot\vec{x} + \phi/f = 2q\vec{R}\cdot\vec{x} + F[\vec{R}] \equiv G[\vec{R},\,\vec{x}]\;. \tag{8}$$

The solution of this functional relation has the form

$$\vec{R} = \vec{h}[\Phi] \tag{9}$$

where $\vec{h}$ is a vector built out of the scalar function $\Phi$. By this function one can only[1]

[1]In principle there is a second vector, $\vec{x}$, on which $\vec{R}$ could depend linearly, but this possibility is excluded because $\vec{R}$ is a vector field transforming under translations as $\vec{R}(\vec{x}) \to \vec{R}'(\vec{x}') = \vec{R}(\vec{x})$.

form the vector $\vec{\nabla}\Phi$ ; therefore we get

$$\vec{R} = \frac{\vec{\nabla}\Phi}{|\vec{\nabla}\Phi|}\,, \tag{10}$$

which satisfies $|\vec{R}| = 1$ and $< \vec{R} >_0 = \vec{n}$. In terms of the phonon field $\phi$ the field $\vec{R}$ is given at the first order in $\phi$ by the expression

$$\vec{R} = \vec{n} + \frac{1}{2fq}\left[\vec{\nabla}\phi - \vec{n}(\vec{n}\cdot\vec{\nabla}\phi)\right]\,. \tag{11}$$

The interaction term between the NGB and the quarks is contained in

$$\mathcal{L}_{int} = -\frac{1}{2}\,e^{i\Phi}\sum_{\vec{v}}\left[\Delta^{(s)}\epsilon_{ij} + \Delta^{(v)}(\vec{v}\cdot\vec{R})\sigma^1_{ij}\right]\epsilon^{\alpha\beta 3}\psi_{i,\alpha,\vec{v}}\,C\,\psi_{j,\beta,-\vec{v}} + h.c. - (L\to R)\;; \tag{12}$$

from this lagrangian, following the same bosonization procedure of [7], one can obtain the effective lagrangian for the massless scalar field $\phi$ [5] and derive its dispersion law. It is worth observing that the fields $\psi_{j,\beta,\pm\vec{v}}$ in (12) are velocity dependent fields; they are computed at opposite velocities, as off-diagonal terms in the average over velocities cancel out.

# 4 Glitches and the LOFF phase

The pulsars are rapidly rotating stellar objects, characterized by the presence of strong magnetic fieds and by an almost continuous conversion of rotational energy into electromagnetic radiation. The rotaton periods can vary in the range $10^{-3}$ sec up to a few seconds; these periods increase slowly and never decrease except for occasional glitches, when the variation of frequency can be $\delta\Omega/\Omega \approx 10^{-6}$ or smaller.

Glitches are a typical phenomenon of the pulsars, in the sense that probably all the pulsar have glitches. The ordinary explanation of the glitches is based on the idea that these sudden jumps of the rotational frequency are due to the movements outwards of rotational vortices in the neutron superfluid and their interaction with the crust. This is one of the main reasons that allow the identification of pulsars with neutron stars, as only neutron stars are supposed to have a metallic crust. A schematic diagram of glitches is shown in Fig. 2

The interesting aspect of the LOFF phase discussed in this talk is that even in quark stars, provided one is in a color superconductivity phase, one can have a crystal structure given by a lattice characterized by a geometric array where the gap parameter varies periodically. Therefore also these stars might have glitches and the possibility arises that some of the pulsars are indeed quark stars [11]. In a more conservative vein one can also imagine that the LOFF phase be realized in the inner

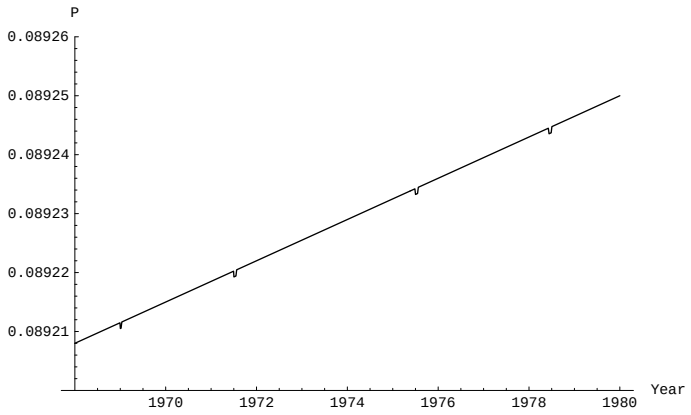


Figure 2: Schematic view of the period $P$ of the PSR 0833-45 (Vela) showing four glitches in the years 1969-1980.

core of neutron star; in this case the crystalline color superconductivity could be partly responsible for the glitches of the pulsar. A detailed analysis of this scenario is however premature as one should first complete the study of the LOFF phase in two directions, first by including the strange quark and, second, by sorting out the exact form of the color lattice.

I am grateful to R. Casalbuoni, R. Gatto, M. Mannarelli for their precious collaboration in the work on which this contribution is based and to I. Bombaci and K. Rajagopal for enlightening discussions on the subject of my talk.

# References

[1] For earliest papers on colour superconductivity see B. Barrois, Nucl. Phys. B **129**, 390 (1977); S. C. Frautschi, in *C78-10-13.7* CALT-68-701 *Presented at Workshop on Hadronic Matter at Extreme Energy Density, Erice, Italy, Oct 13-21, 1978.* See also: D. Bailin and A. Love, Phys. Rept. **107**, 325 (1984) and references therein.

[2] M. G. Alford, K. Rajagopal and F. Wilczek, Phys. Lett. B **422**, 247 (1998) [arXiv:hep-ph/9711395]; M. G. Alford, K. Rajagopal and F. Wilczek, Nucl. Phys. B **537**, 443 (1999) [arXiv:hep-ph/9804403].

[3] K. Rajagopal and F. Wilczek, arXiv:hep-ph/0011333; M. G. Alford, arXiv:hep-ph/0102047.

[4] M. G. Alford, J. Bowers and K. Rajagopal, Phys. Rev. D **63**, 074016 (2001) [arXiv:hep-ph/0008208].

[5] R. Casalbuoni, R. Gatto, M. Mannarelli and G. Nardulli, Phys. Lett. B **511**, 218 (2001) [arXiv:hep-ph/0101326].

[6] D. K. Hong, Phys. Lett. B **473**, 118 (2000) [arXiv:hep-ph/9812510]; D. K. Hong, Nucl. Phys. B **582**, 451 (2000) [arXiv:hep-ph/9905523]; S. R. Beane, P. F. Bedaque and M. J. Savage, Phys. Lett. B **483**, 131 (2000) [arXiv:hep-ph/0002209].

[7] R. Casalbuoni, R. Gatto and G. Nardulli, Phys. Lett. B **498**, 179 (2001) [Erratum-ibid. B **517**, 483 (2001)] [arXiv:hep-ph/0010321].

[8] R. Casalbuoni, these proceedings [arXiv:hep-ph/0110107].

[9] A. I. Larkin and Yu. N. Ovchinnikov, Zh. Eksp. Teor. Fiz. **47**, 1136 (1964): Sov. Phys. JETP **20**, 762 (1965); P. Fulde and R. A. Ferrell, Phys. Rev. **135**, A550 (1964).

[10] A. K. Leibovich, K. Rajagopal, E. Shuster, Phys. Rev. D **64**, 094005 (2001) [arXiv:hep-ph/0104073].

[11] I. Bombaci, talk given at this workshop.

# Discussion

**J. Madsen (University of Aarhus):** How would you visualize the LOFF phase? I.e.: What are the "ions" in the crystal and how are they organized?

**Nardulli:** In the LOFF phase the condensate varies periodically in space with minima and maxima. Maxima are places where the condensate is bigger and therefore the fermions have the largest Majorana mass. The lattice of "ions" could be visualized as parallel planes where the Cooper pairs are more tightly bounded.

**D. K. Hong (Pusan National University):** When you derived the effective theory of the LOFF phase, you used the same Fermi velocity for up and down quarks. But it would be much easier to analyze the effective theory using different Fermi velocities that satisfy the constraint $\mu_u \vec{v}_u + \mu_d \vec{v}_d = 2\vec{q}$.

**Nardulli:** The use of one velocity has the advantage of a Fermi velocity superselection rule, which reduces the complexity of the loop integrals. It arises because in the $\mu \to \infty$ limit the rapid oscillations of the exponential factor in the lagrangian cancel all the contributions except those satisfying $\vec{v}_u + \vec{v}_d = 0$.

# Confinement and domain walls in high density quark matter

*Dam T. Son*
*Physics Department*
*Columbia University*
*New York, NY 10027, USA*

In this talk I will review some recent progress in our understanding of properties of high density quark matter. This talk is based mainly on the papers [1]–[4], done in collaboration with D. Rischke, M. Stephanov, and A. Zhitnitsky.

In recent years, our knowledge of dense quark matter has considerably expanded. We now understand that, quark matter at high densities exhibits the phenomenon of color superconductivity, which determines the symmetry of the ground state and its infrared dynamics. In the simplest case of $N_f = 2$ massless quarks, the ground state of at high baryon densities is the 2SC state [5], characterized by the condensation of diquark Cooper pairs. These pairs are antisymmetric in spin $(\alpha, \beta)$, flavor $(i, j)$ and color $(a, b)$:

$$\begin{aligned} \langle q^{ia}_{L\alpha} q^{jb}_{L\beta} \rangle^* &= \epsilon_{\alpha\beta} \epsilon^{ij} \epsilon^{abc} X^c \,, \\ \langle q^{ia}_{R\alpha} q^{jb}_{R\beta} \rangle^* &= \epsilon_{\alpha\beta} \epsilon^{ij} \epsilon^{abc} Y^c \,. \end{aligned} \tag{1}$$

$X^c$ and $Y^c$ are complex color 3-vectors. In the ground state, they align along the same direction in the color space and break the color $\mathrm{SU}(3)_c$ group down to $\mathrm{SU}(2)_c$. Thus, five of the original eight gluons acquire "masses" by the Meissner effect, similar to the Higgs mechanism. The remaining three gluons are massless (perturbatively). Because of Cooper pairing, the spectrum of quark excitations carrying SU(2) color charge has a gap $\Delta$.

The physics below the energy scale $\Delta$ is governed by the pure gluodynamics in the remaining unbroken SU(2) sector. As shown in Ref. [1], the process of high-density "deconfinement" is quite nontrivial in this case: the quarks are *always* confined, however, the confinement radius grows *exponentially* with increasing density.

Below the scale $\Delta$, heavy (gapped) degrees of freedom decouple and the remaining fields can be described by a local effective Lagrangian. The absence of quarks carrying SU(2) charges below $\Delta$ (all are bound into SU(2) singlet Cooper pairs) implies that the medium is transparent to the SU(2) gluons: there is no Debye screening and Meissner effect for these gluons. Mathematically, the gluon polarization tensor $\Pi^{\mu\nu}_{ab}(q)$ vanishes at $q = 0$, which can be checked by a direct calculation of $\Pi$ at small $q$ [6]. However,

although a static SU(2) charge cannot be completely Debye screened by SU(2) neutral Cooper pairs, it can still be *partially* screened if the medium is polarizable, i.e., if it has a *dielectric constant* $\epsilon$ different from unity. Analogously, the medium can, in principle, have a magnetic permeability $\lambda \neq 1$.

The requirements of locality, gauge and rotational invariance, and parity fixes the effective action below the scale $\Delta$ in the following form

$$S_{\text{eff}} = \frac{1}{g^2} \int d^4x \left( \frac{\epsilon}{2} \mathbf{E}^a \cdot \mathbf{E}^a - \frac{1}{2\lambda} \mathbf{B}^a \cdot \mathbf{B}^a \right), \tag{2}$$

where $E_i^a \equiv F_{0i}^a$ and $B_i^a \equiv \frac{1}{2}\epsilon_{ijk} F_{jk}^a$. Explicit calculations [1] gives

$$\epsilon = 1 + \kappa = 1 + \frac{g^2 \mu^2}{18\pi^2 \Delta^2}, \tag{3}$$

$$\lambda = 1. \tag{4}$$

Since at high densities, the gap $\Delta$ is exponentially suppressed compared to the chemical potential $\mu$ [7], $\epsilon \gg 1$, i.e., the dielectric constant of the medium is very large. This can be interpreted as a consequence of the fact that the Cooper pairs have large size (of order $1/\Delta$) and so are easy to polarize. The magnetic permeability, in contrast, remains close to 1 due to the absence of mechanisms that would strongly screen the magnetic field.

The effective strong coupling constant $\alpha_s'$ in the theory (2), the equivalence of $\alpha_s = g^2/(4\pi\hbar c)$ in the vacuum, is very small at the matching scale with the microscopic theory (i.e., $\Delta$). In our dielectric medium, the Coulomb potential between two static charges separated by $r$ is $g^2/(\epsilon r)$. Thus, we have to replace $g^2$ by $g_{\text{eff}}^2 = g^2/\epsilon$. The velocity of light $c$ also needs to be replaced by the velocity of gluons $v = 1/\sqrt{\epsilon}$. This gives

$$\alpha_s' = \frac{g_{\text{eff}}^2}{4\pi\hbar v} = \frac{g^2}{4\pi\sqrt{\epsilon}} = \frac{3}{2\sqrt{2}} \frac{g\Delta}{\mu}. \tag{5}$$

The coupling increases logarithmically as one moves to lower energies, since pure SU(2) Yang-Mills theory is asymptotically free. This coupling becomes large at the confinement scale $\Lambda_{\text{QCD}}'$, which is the mass scale of SU(2) glueballs. Since $\alpha_s'$ is tiny (because $\Delta/\mu \ll 1$), it takes long to grow, and the scale $\Lambda_{\text{QCD}}'$ is thus very small. Using the one-loop beta function, one can estimate

$$\Lambda_{\text{QCD}}' \sim \Delta \exp\left(-\frac{2\pi}{\beta_0 \alpha_s'}\right) \sim \Delta \exp\left(-\frac{2\sqrt{2}\pi}{11} \frac{\mu}{g\Delta}\right), \tag{6}$$

where $\beta_0 = 22/3$ in SU(2) gluodynamics. The possible relevance of the light glueballs for astrophysics was discussed by Ouyed and Sannino [8].

In Ref. [2] we show that at high baryon densities QCD must have domain walls. The simplest case allowing for domain walls is again $N_f = 2$ massless flavors. In

perturbation theory, there is a degeneracy of the ground state with respect to the relative U(1) phase between $X^a$ and $Y^a$ in Eq. (1). This is due to the $\mathrm{U(1)_A}$ symmetry of the QCD Lagrangian at the classical level. This fact implies that the $\mathrm{U(1)_A}$ symmetry is spontaneously broken by the color-superconducting condensate. Since this is a global symmetry, its breaking gives rise to a Goldstone boson, which carries the same quantum numbers as the $\eta$ boson in vacuum.

The field corresponding to $\eta$ boson can be constructed explicitly. Indeed

$$\Sigma = XY^\dagger \equiv X^a Y^{a*}\,, \tag{7}$$

in contrast to $X$ and $Y$, is a gauge-invariant order parameter. Furthermore $\Sigma$ carries a nonzero $\mathrm{U(1)_A}$ charge. Under the $\mathrm{U(1)_A}$ rotations

$$q \to e^{i\gamma_5\alpha/2} q\,, \tag{8}$$

the fields (1) transform as $X \to e^{-i\alpha}X$, $Y \to e^{i\alpha}Y$, and therefore $\Sigma \to e^{-2i\alpha}\Sigma$. Thus, the color-superconducting ground state, in which $\langle\Sigma\rangle \neq 0$, breaks the $\mathrm{U(1)_A}$ symmetry. The Goldstone mode $\eta$ of this symmetry breaking is described by the phase $\varphi$ of $\Sigma$,

$$\Sigma = |\Sigma| e^{-i\varphi}\,. \tag{9}$$

Under the $\mathrm{U(1)_A}$ rotation (8), $\varphi$ transforms as

$$\varphi \to \varphi + 2\alpha\,. \tag{10}$$

At low energies, the dynamics of the Goldstone mode $\varphi$ is described by an effective Lagrangian, which must take the following form,

$$L = f^2[(\partial_0\varphi)^2 - u^2(\partial_i\varphi)^2]\,. \tag{11}$$

Two free parameters of this Lagrangian are the decay constant $f$ of the $\eta$ boson, and its velocity $u$. In general, $u$ may be different from 1 since the Lorentz invariance is violated by the dense medium. For large chemical potentials $\mu \gg \Lambda_{\mathrm{QCD}}$, the leading perturbative values for $f$ and $u$ have been determined by Beane *et al.* [9]:

$$f^2 = \frac{\mu^2}{8\pi^2}\,, \qquad u^2 = \frac{1}{3}\,. \tag{12}$$

In particular, the velocity of the $\eta$ bosons, to this order, is equal to the speed of sound. The fact that $f \sim \mu$ plays an important role in our further discussion.

It is well known that the $\mathrm{U(1)_A}$ symmetry is not a true symmetry of the quantum theory, even when quarks are massless. The violation of the $\mathrm{U(1)_A}$ symmetry is due to non-perturbative effects of instantons. Since at large chemical potentials the instanton density is suppressed (see below), the $\eta$ boson still exists but acquires a

finite mass. In other words, the anomaly adds a potential energy term $V_{\rm inst}(\varphi)$ to the Lagrangian (11),

$$L = f^2[(\partial_0\varphi)^2 - u^2(\partial_i\varphi)^2] - V_{\rm inst}(\varphi)\,. \tag{13}$$

The curvature of $V_{\rm inst}$ around $\varphi = 0$ determines the mass of the $\eta$.

A standard symmetry argument determines periodicity of $V_{\rm inst}(\varphi)$. One can formally restore the $\mathrm{U}(1)_{\rm A}$ symmetry by accompanying (8) by a rotation of the $\theta$-parameter

$$\theta \to \theta + N_f\alpha = \theta + 2\alpha\,. \tag{14}$$

This symmetry must be preserved in the effective Lagrangian, so the latter is invariant under (10) and (14). This means that the potential $V_{\rm inst}$ is a function of the variable $\varphi - \theta$, unchanged under $\mathrm{U}(1)_{\rm A}$. Since we know that the physics is periodic in $\theta$ with period $2\pi$, we can conclude that, at the physical value of the theta angle $\theta = 0$, $V_{\rm inst}$ is a periodic function of $\varphi$ with period $2\pi$.

Moreover, at large $\mu$, $V_{\rm inst}$ can be found from instanton calculations explicitly. The infrared problem that plagues these calculations in vacuum disappears at large $\mu$: large instantons are suppressed due to Debye screening. As a result, most instantons have small size $\rho \sim \mathcal{O}(\mu^{-1})$ and the dilute instanton gas approximation becomes reliable. One-instanton contribution, proportional to $\cos(\varphi - \theta)$, dominates in $V_{\rm inst}$. Therefore,

$$V_{\rm inst}(\varphi) = -a\mu^2\Delta^2\cos\varphi\,, \tag{15}$$

where $\Delta$ is the BCS gap, and $a$ is a dimensionless function of $\mu$ estimated in Ref. [2]. Here we only note that $a$ vanishes in the limit $\mu \to \infty$. This is an important fact, since it implies that the mass of the $\eta$ boson,

$$m = \sqrt{\frac{a}{2}}\,\frac{\mu}{f}\Delta = 2\pi\sqrt{a}\Delta\,, \tag{16}$$

becomes much smaller than the gap $\Delta$ at large $\mu$. In this case the effective theory (13) is reliable, since meson modes other than $\eta$ have energy of order $\Delta$, i.e., are much heavier than $\eta$ and decouple from the dynamics of the latter.

The Lagrangian (13) with the potential (15) is just the sine-Gordon model, in which there exist domain-wall solutions to the classical equations of motion. The profile of the wall parallel to the $xy$ plane is

$$\varphi = 4\arctan e^{mz/u}\,, \tag{17}$$

so the wall interpolates between $\varphi = 0$ at $z = -\infty$ and $\varphi = 2\pi$ at $z = \infty$. The tension of the domain wall is

$$\sigma = 8\sqrt{2a}\,uf\mu\Delta\,. \tag{18}$$

A good analog of this domain wall is the $N = 1$ axion domain wall, which also interpolates between the same vacuum.

Another phase with domain walls is that of kaon condensation. The likelihood of this phase was recently emphasized by Schäfer and other authors [10]. The crucial observation is that kaons have small masses [11] in the color-flavor locked phase (CFL) [12] of high-density QCD. A relatively small strangeness chemical potential is thus sufficient to drive kaon condensation. Moreover, it was argued that the mass of the strange quark also works in favor of kaon condensation. In contrast to the conventional charge kaon condensation in nuclear matter, in the CFL phase it is the neutral kaons which are more likely to condense. This is due to the inverse mass ordering [11] of mesons in the CFL phase, which makes the neutral kaons lighter than the charge kaons, at least at very high densities.

In a recent paper [3] we show that the $K^0$-condensed phase has in its spectrum an extremely light bosonic particle, whose presence implies the existence of non-topological metastable domain walls. Again, this feature can be understood easily from symmetry arguments. The $K^0$ condensate spontaneously breaks a global U(1) symmetry: the strangeness. The phase of this condensate becomes a Goldstone boson. However, since strangeness is violated by weak processes, the would-be Goldstone boson acquires a very small mass proportional to $G_F^{1/2}$. At very low energies, the effective Lagrangian for $\varphi$ must have the form of the sine-Gordon theory, which possesses domain wall solutions interpolating between $\varphi = 0$ and $\varphi = 2\pi$. More recently, vortons were discussed by Kaplan and Reddy [13].

It is interesting to note that if baryon number is violated, the superfluid Goldstone mode also acquires a mass. Since the superfluid order parameter is a dibaryon, the mass square of the superfluid Goldstone boson is proportional to the amplitudes of the $\Delta B = 2$ transitions. The experimental bound on $n\overline{n}$ oscillations, $\tau_{n\leftrightarrow\overline{n}} > 10^8$ s, put an upper limit on the mass of the Goldstone boson, $m < 10^{-7}$ eV. The thickness of the corresponding domain wall is larger than about 1 m, and still might be less than the radius of neutron stars. However, unless the neutron star under consideration rotates very slowly, a domain wall that thick is unlikely to exist because of the high density of vortices, which are separated by distances of order $10^{-2}$ cm.

Finally, domain walls of the type discussed above also exist in two-component Bose-Einstein condensates (BEC) [4]. Recently, two different hyperfine spin states of $^{87}$Rb, which were condensed in the same trap by the technique of sympathetic cooling [14]. A similar state has been observed for sodium gas [15]. Binary BEC breaks spontaneously *two* global U(1) symmetries. It is moreover possible to couple two condensates by a driving electromagnetic field tuned to the transition frequency. In this case atoms can be interconverted between the two spin states and the numbers of atoms of each species are not conserved separately anymore; only the total number of atoms is constant. In this case, only one U(1) symmetry remains exact, the other one is explicitly violated. The violated U(1) group corresponds to the relative phase between the two condensate. The Goldstone boson arising from the spontaneous breaking of this U(1) symmetry acquires a gap and gives rise to the domain walls.

I am grateful to R. Ouyed and F. Sannino for organizing this meeting, and thank D. Rischke, M. Stephanov and A. Zhitnitsky for fruitful collaboration.

# References

[1] D. H. Rischke, D. T. Son, and M. A. Stephanov, Phys. Rev. Lett. **87**, 062001 (2001) [hep-ph/0011379].

[2] D. T. Son, M. A. Stephanov, and A. R. Zhitnitsky, Phys. Rev. Lett. **86**, 3955 (2001) [hep-ph/0012041].

[3] D. T. Son, hep-ph/0108260.

[4] D. T. Son and M. A. Stephanov, cond-mat/0103451.

[5] M. G. Alford, K. Rajagopal, and F. Wilczek, Phys. Lett. B **422**, 247 (1998) [hep-ph/9711395]; R. Rapp, T. Schafer, E. V. Shuryak, and M. Velkovsky, Phys. Rev. Lett. **81**, 53 (1998) [hep-ph/9711396].

[6] D. H. Rischke, Phys. Rev. D **62**, 034007 (2000) [nucl-th/0001040].

[7] D. T. Son, Phys. Rev. D **59**, 094019 (1999) [hep-ph/9812287].

[8] R. Ouyed and F. Sannino, astro-ph/0103022.

[9] S. R. Beane, P. F. Bedaque, and M. J. Savage, Phys. Lett. **B483**, 131 (2000) [hep-ph/0002209].

[10] T. Schäfer, Phys. Rev. Lett. **85**, 5531 (2000) [nucl-th/0007021]; P. F. Bedaque and T. Schäfer, hep-ph/0105150; D. B. Kaplan and S. Reddy, hep-ph/0107265.

[11] D. T. Son and M. A. Stephanov, Phys. Rev. D **61**, 074012 (2000) [hep-ph/9910491]; *ibid.* **62**, 059902(E) (2000) [hep-ph/0004095].

[12] M. G. Alford, K. Rajagopal, and F. Wilczek, Nucl. Phys. B **537**, 443 (1999) [hep-ph/9804403].

[13] D. B. Kaplan and S. Reddy, hep-ph/0109256.

[14] C. J. Myatt, E. A. Burt, R. W. Ghrist, E. A. Cornell, and C. E. Wieman, Phys. Rev. Lett. **78**, 586 (1997).

[15] J. Stenger, S. Inouye, D. M. Stamper-Kurn, H.-J. Miesner, A. P. Chikkatur, and W. Ketterle, Nature **396**, 345 (1998) [cond-mat/9901072]

# Crystalline Color Superconductivity in Dense Matter

*Deog Ki Hong*
*Department of Physics*
*Pusan National University*
*Pusan 609-735, KOREA*

## 1 Introduction

In this talk I will discuss a recently proposed color superconducting phase of asymmetric quark matter where the up and down quark have different chemical potential, being in chemical equilibrium with electrons. Using Schwinger-Dyson equations derived from an effective theory of low-energy quasiparticles, we examine both the case of an effective four Fermi interaction (appropriate for intermediate densities, such as those found in a neutron star) and Landau-damped one gluon exchange (appropriate for asymptotic density) [1]. We then briefly discuss patching together regions of plane-wave (LOFF) condensation.

One of the most intriguing problems in QCD is to understand how matter behaves at extreme densities, densities much higher than the nuclear density, $\rho_0 = 0.16$ fm$^{-3}$, as expected in the core of compact stars like neutron stars or in the relativistic heavy ion collision (RHIC). According to QCD, which is now firmly believed to be the theory of strong interaction, the interaction among quarks becomes weaker and weaker as they get closer and closer. Therefore, when nucleons are closely packed, the wavefunctions of quarks inside nucleons will overlap with each other at high nucleon density and hadronic matter will turn into quark matter. The physical properties of quark matter are questions we wish to answer.

In general, weakly interacting fermion matter will be a Fermi liquid, forming a Fermi surface. However, according the Cooper theorem, the IR fixed point of the system of weakly interacting fermions will be very different from the Fermi liquid, if there exists an attraction between fermions with opposite momentum, even for an arbitrarily weak attraction. For quark matter, quarks attract not only holes but also quarks themselves if scattering occurs in the color anti-triplet channel. This can be seen by calculating the Coulomb potential due to one-gluon exchange interaction, which is valid at high density;

$$V(r) = -i \int \frac{\mathrm{d}^3\mathrm{q}}{(2\pi)^3}\, T^A D_{00}^{AB}(\vec{q}, q_0 = 0) T^B e^{i\vec{q}\cdot\vec{x}}, \tag{1}$$

where $T^A$'s are $SU(3)_c$ generators and $D^{AB}_{\mu\nu}$ is the gluon propagator. In perturbative QCD, $D^{AB}_{00} = i\delta^{AB}/\vec{q}^2$ and we see that the sign of the Coulomb potential depends on the initial (or final) color states $i, j$ (or $k, l$) of quarks:

$$T^A_{ik}T^A_{jl} = -\frac{2}{3}\delta_{[ij]}\delta_{[kl]} + \frac{1}{3}\delta_{(ij)}\delta_{(kl)}. \tag{2}$$

Of course, the Coulomb potential by one-gluon exchange interaction would not apply at intermediate density where the strong coupling constant is no longer small. However, it is quite reasonable to assume that the color exchange interation is attractive even at the intermediate density for the color anti-triplet channel since it reduces the color Coulomb energy among quarks. Since attraction occurs in the color anti-triplet channel for the diquark scattering and in the color singlet channel for the quark-hole scattering, the candidates for the condensates are therefore either diquark condensates in color anti-triplet channel or quark-hole condensates in color singlet channel, given as

$$\langle \psi_i(\vec{p})\psi_j(-\vec{p})\rangle\, \widetilde{\chi}^0_0 \quad \text{or} \quad \langle \overline{\psi}_i(-\vec{p})\psi_j(\vec{p})\rangle\, \widetilde{\chi}^0_0. \tag{3}$$

Note that the quark-hole condensate (or density wave) carries a momentum $2\vec{p}$. If it were translationally invariant condensate, it would involve antiquarks and thus energetically not prefered to form such a condensate. Since the diquark condensate has zero total momentum, the whole Fermi surface can contribute to the diquark scattering amplitude, while the phase space of quark-hole scattering is only a small fraction of the Fermi surface due to the momentum conservation. Indeed, it is shown that the diquark condensate is energetically more preferred to density waves, though the color exchange attration is weaker, due to the big difference in the phase space [2].

Depending on the density, the diquark condensate in quark matter takes two different forms. At the intermediate density, where the strange quark is too heavy to participate in Cooper pairing, the condensate takes

$$\langle \psi^a_{Li}(\vec{p})\psi^b_{Lj}(-\vec{p})\rangle = -\langle \psi^a_{Ri}(\vec{p})\psi^b_{Rj}(-\vec{p})\rangle = \epsilon_{ab}\epsilon^{ij3}\Delta, \tag{4}$$

where $a, b$ are the flavor indices, running from up and down quarks. In this phase, called the two-flavor superconducting (2SC) phase, the condensate is flavor singlet but color anti-triplet. The condensate does not break any flavor symmetry except the $U(1)$ baryon number, while breaking the $SU(3)$ color gauge group down to a $SU(2)$ subgroup. Since the Cooper-paring quarks should have equal and opposite momenta, the minimal energy needed to Cooper-pair a strange quark with up or down quarks is, if we neglect the interaction energy,

$$\delta E = \sqrt{p_F^2 + m_s^2} - p_F \simeq \frac{m_s^2}{2\mu}, \tag{5}$$

where $p_F \simeq \mu$ is the Fermi momentum of light quarks, almost equal to the quark chemical potential. We therefore see that the energy we gain by pairing the strange quark with light quarks, which is called Cooper-pair gap, $\Delta_0$, has to be bigger than the minimal energy $\delta E$ we have to provide for strange quarks to participate in Cooper-pairing.

On the other hand, at high density, where $\mu > m_s^2/(2\Delta_0)$, it is energetically prefered for the strange quarks to form Cooper pairs with light quarks. At such high density, it is shown that the condensate takes a so-called color-flavor locking (CFL) form [3, 4, 5]

$$\left\langle \psi_{Li}^a(\vec{p})\psi_{Lj}^b(-\vec{p})\right\rangle = -\left\langle \psi_{Ri}^a(\vec{p})\psi_{Rj}^b(-\vec{p})\right\rangle = k_1\delta_i^a\delta_j^b + k_2\delta_j^a\delta_i^b,$$

which breaks not only the color symmetry but also the chiral symmetry, leaving only the diagonal subgroup $SU(3)_V$ unbroken.

A natural place to look for the signature of color superconductivity is a dense object like compact stars. However, since the stars are electrically neutral, the chemical potentials of $u, d, s$ quarks are not equal if electrons are present. One therefore must take into account the effect of flavor asymmetry in Cooper pairing among different flavors. At weak interaction equilibrium, $u + e^- \leftrightarrow d\,(s) + \nu$, the up and down quarks have different chemical potentials, $\mu_d - \mu_u (\equiv 2\delta\mu) = \mu_e$, if the electron chemical potential is nonzero, $\mu_e \widetilde{\chi}_0^0$. When the Fermi surface mismatch becomes large enough, the input energy to make the momentum of pairing quarks equal and opposite exceeds the Cooper gap and the BCS pairing breaks down. The critical chemical potential, at which the BCS pairing breaks, is shown to be $\delta\mu = \Delta_0/\sqrt{2}$ [6]. However, as shown by Larkin and Ovchinnikov [6], and also by Fulde and Ferrell [7], even at $\delta\mu > \Delta_0/\sqrt{2}$, diquark condensate is possible, if we allow the diquark pair to carry a momentum [8], $2\vec{q} = \vec{p}_u + \vec{p}_d$, $\left\langle \psi_u^i(\vec{p}_u)\psi_d^j(\vec{p}_d)\right\rangle = \epsilon^{ij3}\Delta(\vec{q})$.

For such pairing, the (effective) four-Fermi interaction is not marginal and thus does not lead to Landau pole or dynamical mass unless the interaction is strong enough, which is a characteristic feature in dimensions higher than (1+1) [9]. As we will see later, LOFF pairing indeed occurs in dense QCD with light flavors when the couplings are bigger than critical values for both high and intermediate density.

## 2 Intermediate Density

At intermediate densities, where the effective QCD coupling is large and long-range interactions are likely to be screened, we take the Lagrangian to be

$$\mathcal{L} = \overline{\psi}\left(i\partial\!\!\!/ + \mu\gamma^0\right)\psi + \frac{G}{2}\left(\overline{\psi}\psi\right)^2. \tag{6}$$

Following the high density effective theory [10], we introduce the Fermi-velocity ($\vec{v}_F$) dependent field, defined as

$$\psi(\vec{v}_F, x) \equiv e^{-i\mu\vec{v}_F\cdot\vec{x}}\psi(x), \tag{7}$$

to rewrite the Lagrangian in terms of particles near the Fermi surface:

$$\mathcal{L} = \sum_{\vec{v}_F} \psi^\dagger(\vec{v}_F, x) iV\cdot\partial\psi(\vec{v}_F, x) + \sum_{\vec{v}_F^u, \vec{v}_F^d} \frac{G}{2}\overline{\psi}\psi(\vec{v}_F^u, x)\overline{\psi}\psi(\vec{v}_F^d, x) + \cdots \tag{8}$$

where $V^\mu = (1, \vec{v}_F)$, and the ellipse denotes other four-Fermi operators involving different Fermi velocities and higher order terms in $1/\mu$ expansion. Note that the velocity dependent field carries the residual momentum $l^\mu$, if the quark carries momentum $p^\mu = (l_0, \mu\vec{v}_F + \vec{l})$.

Introducing auxiliary fields, $\sigma(x)$, we rewrite the interaction Lagrangian as

$$\mathcal{L}_{4F} = \sigma(\vec{q}, x)\psi(\vec{v}_F^d, x)\psi(\vec{v}_F^u, x) - \frac{1}{2G}\sigma^2, \tag{9}$$

where $2\vec{q} = \mu_u\vec{v}_F^u + \mu_d\vec{v}_F^d$ is a fixed vector. The vacuum is a stationary point of the effective action, obtained by integrating over the fermions only.

$$S_{\text{eff}} = -\frac{1}{2G}\int d^4x\sigma^2 - i\text{Tr}\ln\gamma_0\begin{pmatrix} iV_d\cdot\partial & -\sigma(\vec{q}, x) \\ -\sigma^\dagger(\vec{q}, x) & iV_u\cdot\partial \end{pmatrix}. \tag{10}$$

At the stationary points, the auxiliary field is given as $\sigma_0(\vec{q}, x) = \left\langle\psi(\vec{v}_F^u, x)\psi(\vec{v}_F^d, x)\right\rangle \equiv \Delta(\vec{q})$. Since we are looking for a plane-wave condensate with a wave vector $2\vec{q}$, $\sigma_0$ is translationally invariant. The free energy density for the LOFF phase is then given in the Euclidean space as

$$V(\Delta) = +\frac{1}{2G}\Delta^2 - \frac{1}{2}\int\frac{d^4l}{(2\pi)^4}\ln\left[1 + \frac{\Delta^2}{(l_0 - il_u)(l_0 - il_d)}\right], \tag{11}$$

where we introduced new variables $l_u \equiv \vec{v}_F^u\cdot\vec{l}$ and $l_d \equiv \vec{v}_F^d\cdot\vec{l}$. Minimizing the free energy, we get the LOFF gap equation;

$$0 = \frac{\partial V}{\partial\Delta(\vec{q})} = \frac{\Delta(\vec{q})}{G} - \int\frac{\mathrm{d}^4l}{(2\pi)^4}\frac{\Delta(\vec{q})}{(l_0 - il_u)(l_0 - il_d) + \Delta^2}. \tag{12}$$

The characteristic feature of the gap equation (12) for the LOFF paring is that the quark propagator is a function of three independent momenta, $l_0$, $\vec{l}\cdot\vec{v}_F^u(\equiv l_u)$, and $\vec{l}\cdot\vec{v}_F^d(\equiv l_d)$, while in BCS pairing it is a function of two, $l_0$ and $\vec{l}\cdot\vec{v}_F$. In general, we may decompose $\vec{l}$ as $\vec{l} = \vec{l}_\perp + l_u\vec{v}_u^* + l_d\vec{v}_d^*$, where $\vec{v}_{u,d}^*$ are dual to $\vec{v}_F^{u,d}$, satisfying $\vec{v}_F^a\cdot\vec{v}_b^* = \delta_b^a$ with $a, b = u, d$. Though the magnitude of the Fermi velocity is $\vec{v}_F^a = 1$

for massless quarks, its dual has a magnitude $|\vec{v}_a^*| = (\sin\beta)^{-1}$, where $\beta$ is the angle between $\vec{v}_F^d$ and $-\vec{v}_F^u$.

Since the quark propagator is independent of $\vec{l}_\perp$, it just labels the degeneracy in the LOFF pairing. The perpendicular momentum $\vec{l}_\perp$ forms a circle on the Fermi surface, whose radius is given as $\mu_d \sin\alpha_d$ $(= \mu_u \sin\alpha_u)$, where $\alpha_{d,u}$ are the angles between $\vec{q}$ and $\vec{v}_F^{d,u}$, respectively. Upon integrating over $\vec{l}_\perp$, the gap equation (12) becomes a (2+1) dimensional gap equation. This is in sharp contrast with the gap equation in the BCS pairing, which is (1+1) dimensional after integrating over the $\vec{l}_\perp$, namely over the whole Fermi surface.

Integrating over $\vec{l}_\perp$, we find the gap equation in Euclidean space to be

$$1 = \int_{l_0,l_u,l_d} \frac{2G\mu_d \sin\alpha_d (3\sin\beta)^{-1}}{(l_0 - il_d)(l_0 - il_u) + \Delta^2} \simeq \frac{2G\mu_d \sin\alpha_d}{3\sin\beta} \int_\Delta^{\Lambda'} \frac{\mathrm{d}l_0}{2\pi^3} \left[\frac{1}{2}\ln\left(\frac{l_0^2+\Lambda^2}{l_0^2}\right)\right]^2, \quad (13)$$

where $(\sin\beta)^{-1}$ arises from the Jacobian and we introduced $\Lambda$ as the cutoff for $l_u, l_d$ and $\Lambda'$ for $l_0$. In the high density effective theory, the expansion parameter is $|l^\mu|/\mu$. From the condition that $|l^\mu| < l^2/\overline{\mu}$, where $2\overline{\mu}^2 = \mu_u^2 + \mu_d^2$, we find the ultraviolet cutoff for $l_{u,d}$ is $\Lambda = \overline{\mu}\sin^2\beta$. We also take $\Lambda' = \Lambda$, since the main contribution to the gap comes from nearly on-shell quarks. Finally, integrating over $l_0$, the gap equation becomes

$$1 - \frac{G_c}{G} = \frac{1}{2}\left(\frac{\Delta}{\overline{\mu}\sin^2\beta}\right)\left[\ln\left(\frac{\Delta}{\overline{\mu}\sin^2\beta}\right)\right]^2, \quad (14)$$

where the critical coupling for the LOFF gap $G_c = 3\pi^3 \sin\beta/(4\mu_d\overline{\mu}\sin\alpha_d)$. For a given $\delta\mu$ and $G$, the LOFF gap exists only when $G > G_c$.

The best $q$, or equivalently the critical coupling for the LOFF pairing, is determined by minimizing the Free energy, obtained by integrating the gap equation (14) after doing the momentum integration,

$$V(\Delta) = \int_0^\Delta \frac{\partial V}{\partial\Delta'} d\Delta' \simeq \frac{1}{6G}\Delta^2\left(1 - \frac{G}{G_c}\right). \quad (15)$$

For $\overline{\mu} = 400$ MeV, $\delta\mu = 30$ MeV, $\Delta_0 = 40$ MeV, we have $\cos\beta = 0.82$, from which we obtain $\Delta = 0.076\overline{\mu}$ and $V = -1.9 \times 10^{-5}\ \overline{\mu}^2/G$.

# 3 Asymptotic Density

For the one-gluon exchange case, the calculation goes in parallel. The Schwinger-Dyson (SD) equation for the quark two-point function is given in the leading order in the hard-dense loop (HDL) approximation as

$$\Delta(\vec{q},l) = (-ig_s)^2 \int \frac{\mathrm{d}^4k}{(2\pi)^4} V_u^\mu D_{\mu\nu}(l-k) V_d^\nu \frac{T^a \Delta(\vec{q},k) T^a}{k\cdot V_d k\cdot V_u - \Delta^2(\vec{q},k)}, \quad (16)$$

where $T^a$ is the color generator in the fundamental representation and $D_{\mu\nu}$ is the gluon propagator in the HDL approximation. Since the Landau-damped magnetic gluons give the dominant contribution, the SD equation becomes in Euclidean space as

$$\Delta(\vec{q}) = \frac{2}{3} g_s^2 \cot\beta \int \frac{\mathrm{d}l_0}{2\pi} \frac{\mathrm{d}l_\perp}{2\pi} \frac{\mathrm{d}l_u \mathrm{d}l_d}{(2\pi)^2} \frac{1}{\vec{l}^2 + \frac{\pi}{4} M^2 |l_0|/|\vec{l}|} \cdot \frac{\Delta(\vec{q})}{l \cdot V_E^u l \cdot V_E^d + \Delta^2}, \tag{17}$$

where the factor 2/3 is due to the color factor and $V_E^\mu \equiv (1, -i\vec{v}_F)$. Since the high energy region $\Lambda_0 > |l_0| > 2\Lambda_u$ does not contribute the integration in Eq. (17) much, the $l_0$ integration is regulated by the UV cutoff of $l_u$ or $l_d$ integration. We then note that when $l_u^2/(\sin\beta)^2 > \alpha_s \overline{\mu}^2 |l_0|/|\vec{l}|$ the $l_u$ integration converges rapidly. Hence for small coupling ($\alpha_s < 4\sin\beta$) we have a new UV cut-off for $l_u$ that satisfies $\overline{\Lambda}_u = \overline{\mu}\alpha_s \sin\beta$. Integrating over $\vec{l}_\perp$, $l_u$ and $l_d$, we get

$$1 = \frac{8\cot\beta}{9\sqrt{3}\pi^2} \alpha_s^{2/3} \overline{\mu}^{-2/3} \int_\Delta^{\overline{\Lambda}_u} \frac{dl_0}{l_0^{1/3}} \left[\frac{1}{2} \ln\left(1 + \frac{\overline{\Lambda}_u^2}{l_0^2}\right)\right]^2 = \left(\frac{\alpha_s}{\alpha_c}\right)^{4/3} \left[1 - \frac{2}{9}\left(\frac{\Delta}{\overline{\Lambda}_u}\right)^{2/3} \left(\ln\frac{\Delta}{\overline{\Lambda}_u}\right)^2\right] \tag{18}$$

where the critical coupling for the LOFF pairing by one-gluon exchange interaction is $\alpha_c = \left(\pi^2/2\sqrt{3}\right)^{3/4} \left(\sin\beta/\cos^3\beta\right)^{1/4}$.

Now, let us calculate the vacuum energy to find the pair momentum $2\vec{q}$ or the angle $\beta$ for a given parameters $\alpha_s$, $\overline{\mu}$, and $\delta\mu$. We find the vacuum energy is given as in the HDL approximation $V(\Delta) \simeq -\Delta^3/(6\pi^3)\left(\mu_d q/\overline{\mu}\right)$. The best $q$ or the angle $\beta$ is determined by minimizing the vacuum energy for a given $\alpha_s$. For $\alpha_s = 1$, we find $\cos\beta = 0.915$ and $V = -8.5 \times 10^{-4} \alpha_s \overline{\mu}^4$. To find $\delta\mu_2$ for a given $\alpha_s$, we minimize the vacuum energy with respect to $\beta$ and $\delta\mu$. At the leading order the vacuum energy is minimized for large $\delta\mu$. Therefore, to determine the correct $\delta\mu_2$ we need to go beyond the current approximations and include the $\delta\mu/\overline{\mu}$ corrections in the gap equation. This result is consistent, at least qualitatively, with the observation in [15] that the LOFF window widens considerably in the one gluon exchange regime.

# 4 Patching

In the preceding analysis we assumed a simple plane wave condensate $\Delta(\vec{q}) \propto e^{2iq\cdot x}$. Kinematical constraints require that quarks which participate in this condensation lie on a ring-like region of volume $\sim \Delta^2 \mu_i \sin\alpha_i$, where i = u,d. However, due to the rotaional invariance of the system any direction of the pair momentum $2\vec{q}$ is possible. Thus, one needs to patch condensates carrying same momentum but different direction to increase the binding energy The up and down quarks which pair in a LOFF condensate lie in rings of radius $\mu_i \sin\alpha_i$, where $i = u, d$. These rings lie in a plane perpendicular to $\vec{q}$, and have thickness of order $\Delta$. If we sum over patches associated

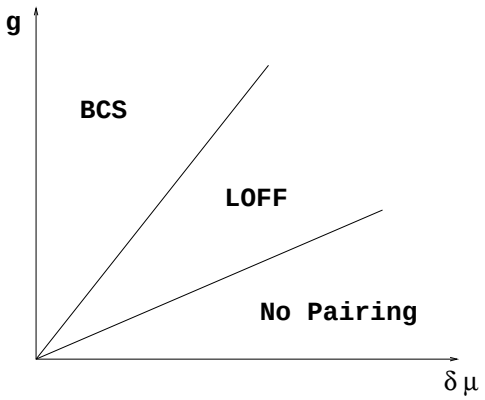


Figure 1: A (schematic) phase diagram in the coupling-$\delta\mu$ plane.

with planar rotations of $\vec{q}$ without overlap, we will recover a fraction Fermi surface which scales like $\mu^2$ and thus LOFF phase can be compatible with BCS pairing.

# 5 Conclusions

We have used high density effective theory to study crystalline superconductivity, using a local four fermion interaction to model the interaction at intermediate density, and one gluon exchange for the asymptotic regime. We obtained analytic results for the condensate and vacuum energy, and conclude that the LOFF phase is quite plausibly favored $\Delta_0/\sqrt{2} < \delta\mu < \delta\mu_2$. We also discussed how disjoint regions of condensate could be patched together to obtain a lower vacuum energy. The optimal patching configuration has yet to be determined for generic $\beta$, but it seems possible that the binding energy of crystalline superconductivity scales as the area of the Fermi surface ($\sim \mu^2$) rather than as $\mu$ in the case of a plane wave LOFF condensate.

I would like to thank F. Sannino and R. Ouyed for the wonderful workshop. I am grateful to M. alford, S. Hsu, K. Rajagopal, and Y. J. Sohn for discussions and collaboration, upon which this talk is based upon. This work is supported by Korea Research Foundation Grant (KRF-2000-015-DP0069).

# References

[1] D. K. Hong and Y. J. Sohn, hep-ph/0107003; D. K. Hong and S. D. H. Hsu, to appear.

[2] E. Shuster and D. T. Son, Nucl. Phys. B **573** (2000) 434; B. Y. Park, M. Rho, A. Wirzba and I. Zahed, Phys. Rev. D **62** (2000) 034015.

[3] M. G. Alford, K. Rajagopal and F. Wilczek, Nucl. Phys. B **537** (1999) 443.

[4] N. Evans, J. Hormuzdiar, S. D. Hsu and M. Schwetz, Nucl. Phys. B **581** (2000) 391.

[5] D. K. Hong, Nucl. Phys. B **582** (2000) 451.

[6] A. I. Larkin and Yu. N. Ovchinnikov, Zh. Eksp. Teor. Fiz. **47**, 1136 (1964) [Sov. Phys. JETP **20**, 762 (1965)].

[7] P. Fulde and R. A. Ferrell, Phys. Rev. **135**, A550 (1964).

[8] M. Alford, J. Bowers and K. Rajagopal, Phys. Rev. D **63**, 074016 (2001); J. A. Bowers, J. Kundu, K. Rajagopal and E. Shuster, Phys. Rev. D **64**, 014024 (2001); R. Casalbuoni, R. Gatto, M. Mannarelli and G. Nardulli, hep-ph/0101326.

[9] Y. Nambu and G. Jona-Lasinio, Phys. Rev. **122** (1961) 345; *ibid.* **124**, 246 (1961); D. K. Hong and S. H. Park, Phys. Rev. D **49**, 5507 (1994).

[10] D. K. Hong, Phys. Lett. B **473**, 118 (2000) [hep-ph/9812510];

[11] A. K. Leibovich, K. Rajagopal and E. Shuster, hep-ph/0104073.

# Discussion

**M. Mannarelli (INFN-Bari):** You say that the LOFF phase appears for $g > g_c$ (in asymmetric quark matter). Is this the reason why in ordinary BCS it has not been observed a LOFF phase?

**Hong:** For a given coupling $g$, there is always a window for LOFF as $\delta\mu$ changes. However the window is larger for a stronger coupling. It is therefore much easier to find a LOFF phase in strongly coupled systems.

**M. Alford (Glasgow University):** Just to clarify, for any coupling strength there is a range of $\delta\mu$ in which LOFF pairing is favored. This means that since $\delta\mu$ is a function of $r$ in a neutron star, there is a reasonable chance of seeing a shell of LOFF matter somewhere inside it.

**Hong:** For a given $\delta\mu$, the coupling between fermions has to be larger than $g_c$ for a LOFF phase to exist. This is the point I was trying to emphasize during my talk. However, as the coupling becomes larger than $g_{c1}$ ($> g_c$), the BCS gap becomes large

enough to win against a LOFF phase. A schematic phase diagram[1] as a function of the coupling $g$ and $\delta\mu$ can be given as Fig. 1:

[1] I thank M. Alford for helping me to understand the diagram in Fig. 1.

# A Colored Zoo of Quasi-particles and Light Glueballs

*Francesco Sannino*
NORDITA,
*Blegdamsvej 17, DK-2100*
*Copenaghen O, DENMARK*

## 1 Electroweak for CFL

Here I present a compendium of the effective Lagrangians for three and two flavors QCD describing the relevant color superconductive light degrees of freedom and their electroweak interactions. However I will not consider some more recent developments involving new phases which are presented by other participants in this conference. Possible phenomenological applications include the description of quark stars, neutron star interiors, the physics near the core of collapsing stars and supernova explosions [1, 2, 3].

At high density, in the 3 flavor case, the symmetry group $SU_L(3)\times SU_R(3)\times SU_c(3)$ breaks spontaneously to $SU_{c+L+R}(3)$ leaving behind 16 Goldston bosons. However, being $SU_c(3)$ a gauge group 8 Goldstone bosons are absorbed in the longitudinal components of the massive gluons. So we are left with 8, not colored, physical massless Goldstone bosons. They can be encoded in the unitary matrix [4] transforming linearly under the left-right flavor rotations $U \to g_L U g_R^\dagger$ with $g_{L/R} \in SU_{L/R}(N_f)$. $U$ satisfies the non linear realization constraint $UU^\dagger = 1$. We also require $\det U = 1$. In this way we avoid discussing the axial $U_A(1)$ anomaly at the effective Lagrangian level. (See Ref. [5] for a general discussion of trace and $U_A(1)$ anomaly). We have $U = \exp[i\Phi/F]$ with $\Phi = \sqrt{2}\Phi^a t^a$ representing the 8 Goldstone bosons and $\mathrm{Tr}\left[t^a t^b\right] = \delta^{ab}/2$. $F$ is the Goldstone bosons decay constant at finite density.

The effective Lagrangian, for massless quarks, globally invariant under chiral rotations (up to two derivatives) and invariant only under the rotational subgroup of the Lorentz group is:

$$L = \frac{F^2}{2}\,\mathrm{Tr}\left[\dot{U}\dot{U}^\dagger - v^2\vec{\nabla}U\cdot\vec{\nabla}U^\dagger\right] \ . \tag{1}$$

Clearly by rescaling the vector coordinates $\vec{x} \to \vec{x}/v$ we can recast the previous Lagrangian in the form $L = \frac{F^2}{2}\,\mathrm{Tr}\left[\partial_\mu U \partial^\mu U^\dagger\right]$.

We now augment the theory by the time-honored Wess-Zumino term which is compactly written using the language of differential forms. It is useful to introduce the algebra valued Maurer-Cartan one forms:

$$\alpha = (\partial_\mu U)\, U^{-1}\, dx^\mu \equiv (dU)\, U^{-1} \ , \qquad \beta = U^{-1} dU = U^{-1} \alpha U \ , \tag{2}$$

which transform, respectively, under the left and right $SU(N_f)$ flavor group. The Wess-Zumino effective action is

$$\Gamma_{WZ}[U] = C \int_{M^5} \mathrm{Tr}\left[\alpha^5\right] \ , \qquad C = -i \frac{N_c}{240\pi^2} \ . \tag{3}$$

$C$ assumes the same value then the one used at zero density and $N_c$ is the number of colors (fixed to be 3 in this case). The coefficient is fixed by saturating the global anomalies at the effective Lagrangian level [6]. The 3 flavor case respects the 't Hooft global anomaly matching conditions at non zero density. A relevant feature is that $\alpha$, being a differential form, is unaffected by coordinate rescaling (actually topological terms being independent on the metric are unaffected by medium effects), and hence the Wess-Zumino term is not modified at finite matter density.

At this point it is important to note[1] that in reference [7] the coefficient of the Wess-Zumino term actually agrees with the one presented here [8, 6] while it is the one presented/computed in [9] which disagrees by a factor three. A relevant consequence of our results is associated to the solitonic (Skyrme) sector of the effective Lagrangian theory. In fact now we have the same winding number as for ordinary QCD and hence we get massive excitations, which after collective quantization, describe spin half particles with the same quantum numbers of ordinary baryons.

Next we extend the previous effective Lagrangian by incorporating the electroweak intermediate vector mesons as external fields.

$$\begin{aligned} DU &= \partial U - i\frac{g}{\sqrt{2}}\left[W^+\tau^+ + W^-\tau^-\right] U - i\frac{g}{\cos\theta_W} Z^0 \left[\tau^3 U - \sin^2\theta_W \left[Q, U\right]\right] \\ &\quad -i\widetilde{e}\,\widetilde{A}\,[Q,U] - i\widetilde{e}\,\tan\theta \widetilde{G}^8\,[Q,U] \end{aligned} \tag{4}$$

where $\theta_W$ is the electroweak angle and

$$\tau^+ = \begin{pmatrix} 0 & 1 & 0 \\ 0 & 0 & 0 \\ 0 & 0 & 0 \end{pmatrix} \ , \qquad \tau^- = \begin{pmatrix} 0 & 0 & 0 \\ 1 & 0 & 0 \\ 0 & 0 & 0 \end{pmatrix} \ , \qquad \tau^3 = \frac{1}{2}\begin{pmatrix} 1 & 0 & 0 \\ 0 & -1 & 0 \\ 0 & 0 & -1 \end{pmatrix} \ . \tag{5}$$

The last two terms in Eq. (4) describe the, non anomalous, interaction of the Goldstone bosons with respectively the physical massless photon and the physical massive

[1] I thank D.K. Hong for helping me clarifying this point.

eight gluon. The physical photon and eight gluon states are related to the, in vacuum, ones via:

$$\widetilde{G}^8 = \cos\theta G^8 + \sin\theta A \ , \qquad \widetilde{A} = -\sin\theta G^8 + \cos\theta A \ , \tag{6}$$

with $\cos\theta = \sqrt{3}g_s/\sqrt{3g_s^2+4e^2}$. Clearly $\widetilde{e} = e\cos\theta$ is the finite density new electric charge.

The $\pi^0 \to \gamma\gamma$ Lagrangian term is obtained by gauging the Wess-Zumino action [6] and is given by:

$$\mathcal{L}_{\pi^0\to\gamma\gamma} = -\frac{30}{4}e^2\, C\, i\mathrm{Tr}\left[t^3Q^2\right]\pi^0\frac{\sqrt{2}}{F}\epsilon^{\mu\nu\rho\sigma}F_{\mu\nu}F_{\rho\sigma} \ , \tag{7}$$

and $\pi^0 = \Phi^3$. After substituting the, in vacuum, photon field with its expression as function of the physical photon and gluon [6] we discover that the process is identical to the in the vacuum one when replacing the, in vacuum, electric charge with $\widetilde{e}$. It is also worth noticing that since the mass of the physical eight gluon is larger than the pion mass the process $\pi^0 \to \widetilde{G}^8\widetilde{G}^8$ is barred kinematically.

# 2 Electroweak for 2SC

Here I summarize the effective low energy Lagrangian for two flavors (when a 2SC phase sets is) which contains all of the relevant degrees of freedom.

In 2SC the diquark condensate leaves invariant the following symmetry group:

$$[SU_c(2)] \times SU_L(2) \times SU_R(2) \times \widetilde{U}_V(1) \ , \tag{8}$$

where $[SU_c(2)]$ is the unbroken part of the gauge group. The $\widetilde{U}_V(1)$ generator $\widetilde{B}$ is the following linear combination of the previous $U_V(1)$ generator $B = \frac{1}{3}\mathrm{diag}(1,1,1)$ and the broken diagonal generator of the $SU_c(3)$ gauge group $T^8 = \frac{1}{2\sqrt{3}}\,\mathrm{diag}(1,1,-2)$: $\widetilde{B} = B - \frac{2\sqrt{3}}{3}T^8$. The quarks with color 1 and 2 are neutral under $\widetilde{B}$ and consequently the condensate too ($\widetilde{B}$ is $\sqrt{2}\widetilde{S}$ of Ref. [10]). The superconductive phase for $N_f = 2$ possesses the same global symmetry group of the confined Wigner-Weyl phase [8]. In Reference [8], it was shown that the low-energy spectrum, at finite density, displays the correct quantum numbers to saturate the 't Hooft global anomalies. In Reference [11] it was then seen, by using a variety of field theoretical tools, that global anomaly matching conditions hold for any cold but dense gauge theory.

The lowest lying excitations are protected from acquiring a mass by the aforementioned constraints and dominate the low-energy physical processes. Here, see [10], the relevant coset space is $G/H$ with $G = SU_c(3) \times U_V(1)$ and $H = SU_c(2) \times \widetilde{U}_V(1)$ is parameterized by

$$\mathcal{V} = \exp(i\xi^i X^i) \ , \tag{9}$$

where $\{X^i\}$ $i = 1, \cdots, 5$ belong to the coset space $G/H$ and are taken to be $X^i = T^{i+3}$ for $i = 1, \cdots, 4$ while $X^5 = B + \frac{\sqrt{3}}{3} T^8 = \mathrm{diag}(\frac{1}{2}, \frac{1}{2}, 0)$. $T^a$ are the standard generators of $SU(3)$. The coordinates

$$\xi^i = \frac{\Pi^i}{f} \quad i = 1, 2, 3, 4 \ , \qquad \xi^5 = \frac{\Pi^5}{\widetilde{f}} \ , \tag{10}$$

via $\Pi$ describe the Goldstone bosons.

$\mathcal{V}$ transforms non linearly

$$\mathcal{V}(\xi) \to u_V \, g \mathcal{V}(\xi) h^\dagger(\xi, g, u) h^\dagger_{\widetilde{V}}(\xi, g, u) \ , \tag{11}$$

with $u_V \in U_V(1)$, $g \in SU_c(3)$, $h(\xi, g, u) \in SU_c(2)$ and $h_{\widetilde{V}}(\xi, g, u) \in \widetilde{U}_V(1)$. It is, also, convenient to define:

$$\omega_\mu = i \mathcal{V}^\dagger D_\mu \mathcal{V} \quad \text{with} \quad D_\mu \mathcal{V} = (\partial_\mu - i g_s G_\mu) \mathcal{V} \ , \tag{12}$$

with gluon fields $G_\mu = G^m_\mu T^m$. Following [10] we decompose $\omega_\mu$ into

$$\omega^{\parallel}_\mu = 2 S^a \mathrm{Tr}\left[S^a \omega_\mu\right] \quad \text{and} \quad \omega^{\perp}_\mu = 2 X^i \mathrm{Tr}\left[X^i \omega_\mu\right] \ , \tag{13}$$

where $S^a$ are the unbroken generators of $H$ with $S^{1,2,3} = T^{1,2,3}$, $S^4 = \widetilde{B}/\sqrt{2}$. Summation over repeated indices is assumed.

To be able to include the in medium fermions in the picture we define:

$$\widetilde{\psi} = \mathcal{V}^\dagger \psi \ , \tag{14}$$

transforming as $\widetilde{\psi} \to h_{\widetilde{V}}(\xi, g, u) h(\xi, g, u) \widetilde{\psi}$ and $\psi$ possesses an ordinary quark transformations (as Dirac spinor).

The simplest non-linearly realized effective Lagrangian describing in medium fermions, the five gluons and their self interactions, up to two derivatives and quadratic in the fermion fields is:

$$\begin{aligned} \mathcal{L} = & \quad f^2 a_1 \mathrm{Tr}\left[\, \omega_0^\perp \omega_0^\perp - \alpha_1 \vec{\omega}^\perp \vec{\omega}^\perp \,\right] + f^2 a_2 \left[\mathrm{Tr}\left[\, \omega_0^\perp \,\right] \mathrm{Tr}\left[\, \omega_0^\perp \,\right] - \alpha_2 \mathrm{Tr}\left[\, \vec{\omega}^\perp \,\right] \mathrm{Tr}\left[\, \vec{\omega}^\perp \,\right]\right] \\ & + \quad b_1 \overline{\widetilde{\psi}} i \left[\gamma^0 (\partial_0 - i \omega_0^{\parallel}) + \beta_1 \vec{\gamma} \cdot \left(\vec{\nabla} - i \vec{\omega}^{\parallel}\right)\right] \widetilde{\psi} + b_2 \overline{\widetilde{\psi}} \left[\gamma^0 \omega_0^\perp + \beta_2 \vec{\gamma} \cdot \vec{\omega}^\perp\right] \widetilde{\psi} \\ & + \quad m_M \overline{\widetilde{\psi}^C} \gamma^5 (i T^2) \widetilde{\psi} + \text{h.c.} \ , \end{aligned} \tag{15}$$

where $\widetilde{\psi}^C = i \gamma^2 \widetilde{\psi}^*$, $i, j = 1, 2$ are flavor indices and

$$T^2 = S^2 = \frac{1}{2} \begin{pmatrix} \sigma^2 & 0 \\ 0 & 0 \end{pmatrix} \ , \tag{16}$$

$a_1,\ a_2,\ b_1$ and $b_2$ are real coefficients while $m_M$ is complex. The breaking of Lorentz invariance to the $O(3)$ subgroup, following [4], has been taken into account by providing different coefficients to the temporal and spatial indices of the Lagrangian, and it is encoded in the coefficients $\alpha$s and $\beta$s.

To construct the low energy effective theory for the electroweak sector we need to generalize the one form $\omega_\mu = i\mathcal{V}^\dagger D_\mu \mathcal{V}$ by introducing the new covariant derivative:

$$D_\mu \mathcal{V} = (\partial_\mu - i g_s G_\mu - i g' Y\, B^y_\mu)\mathcal{V} = (\partial_\mu - i g_s G_\mu - i g' \frac{B}{2}\, B^y_\mu)\mathcal{V}\ . \tag{17}$$

$B^y_\mu$ is the standard hypercharge gauge field and is a linear combination of the electroweak eigenstates associated to the photon field $A_\mu$ and the neutral massive vector boson $Z^0_\mu$, i.e.:

$$B^y_\mu = \cos\theta_W A_\mu - \sin\theta_W Z^0_\mu\ , \tag{18}$$

with $\theta_W$ the standard electroweak angle.

After diagonalizing the full quadratic terms the new massless eigenstate is interpreted as the, in medium, photon and is a linear combination of the in vacuum photon and eight gluon:

$$\widetilde{A}_\mu = \cos\theta_Q A_\mu - \sin\theta_Q G^8_\mu\ , \tag{19}$$

with $\cos\theta_Q = \sqrt{3}\frac{g_s}{\sqrt{3g_s^2+e^2}}$. The massive state orthogonal to $\widetilde{A}_\mu$ is $\widetilde{G}^8_\mu = \cos\theta_Q G^8_\mu + \sin\theta_Q A_\mu$ and further mixes with $Z^0$ of, in vacuum, mass $m_Z$. The new eigenstates are:

$$\hat{G}^8_\mu = \cos\theta_M \widetilde{G}^8_\mu + \sin\theta_M Z^0_\mu\ , \qquad \widetilde{Z}^0_\mu \ = \ \cos\theta_M Z^0_\mu - \sin\theta_M \widetilde{G}^8_\mu, \tag{20}$$

with $\tan 2\theta_M \approx \frac{2f^2\tan\theta_W}{9m_Z^2}\,(a_1+2a_2)\,\sqrt{3g_s^2+e^2}$ and we considered the physical limit $m_Z^2 \gg f^2$. In the same limit, as expected, $\widetilde{G}^8$ and $Z^0$ do not mix much and we can use them as physical eigenstates.

Having identified the correct physical eigenvalues and eigenvectors we now turn to the quark sector. We have $Q = \tau^3 + \frac{B-L}{2}$ with $\tau = \tau_L + \tau_R$ and $\widetilde{e} = e\cos\theta_Q$ is the new electric charge while $\widetilde{Q}$ is the associated electric charge operator associated with the field $\widetilde{A}_\mu$:

$$\widetilde{Q} = \tau^3 \times \mathbf{1} + \frac{\tilde{B}-L}{2} = Q\times\mathbf{1} - \frac{1}{\sqrt{3}}\mathbf{1}\times T^8\ . \tag{21}$$

By expanding around $\mathcal{V} = 1$ the relevant interaction terms we derive [6] the following full modified quark coupling to the neutral weak current:

$$b_1 \frac{g}{\cos\theta_W}\, Z^0_\mu \overline{\psi}\gamma^\mu \left[T^3_L - \sin^2\theta_W Q - \frac{b_2-b_1}{3\,b_1}\sin^2\theta_W (B+Q-\widetilde{Q})\right]\psi\ , \tag{22}$$

where we used Eq. (21) and $X^5 = B + Q - \widetilde{Q}$. Hence we discover that the neutral weak current is directly affected by finite density effects even when neglecting the small physical mixing between the eighth gluon $\widetilde{G}^8$ and $Z^0$. We also observe that the modified electroweak coupling only emerges for quarks with color indices 1 and 2, since $X^5 = \frac{1}{2}\mathrm{diag}(1,1,0)$. We expect relevant phenomenological consequences of our result for the cooling history of compact objects [12] (see Ref. [6] for more details).

# 3 The $SU_c(2)$ Glueball Effective Lagrangian

The $SU_c(2)$ gauge symmetry does not break spontaneously and confines. If the new confining scale [13] is lighter than the superconductive quark-quark gap the associated confined degrees of freedom (light glueballs) [14] can play, together with the massless quarks a relevant role for the physics of Quark Stars featuring a 2SC superconductive surface layer [3].

Defining by $H$ the mass-scale dimension 4 composite field describing, upon quantization, the scalar glueball [15] we can construct the simplest light glueball action, in medium, for the SU(2) color theory:

$$S_{G-ball} = \int d^4x \left\{ \frac{c}{2}\sqrt{b}\, H^{-\frac{3}{2}} \left[\partial^0 H \partial^0 H - v^2 \partial^i H \partial^i H\right] - \frac{b}{2} H \log\left[\frac{H}{\hat{\Lambda}^4}\right] \right\} . \qquad (23)$$

This Lagrangian correctly encodes the underlying $SU_c(2)$ trace anomaly [14]. The glueballs move with the same velocity $v$ as the underlying gluons in the 2SC color superconductor. $\hat{\Lambda}$ is the intrinsic scale associated with the theory and can be less than or of the order of few MeVs [13, 14] while $c$ is a constant of order unity. The glueballs are light (with respect to the gap) and barely interact with the ungapped fermions. They are stable with respect to the strong interactions unlike ordinary glueballs. We define the mass-dimension one glueball field $h$ via $H = \langle H\rangle \exp\left[h/F_h\right]$. By requiring a canonically normalized kinetic term for $h$ one finds $F_h^2 = c\sqrt{b\langle H\rangle}$, while the glueball mass term is $M_h^2 = \sqrt{b}\sqrt{\langle H\rangle/2c} = \sqrt{b}\hat{\Lambda}^2/2c\sqrt{e}$, which is clearly of the order of $\hat{\Lambda}$.

Once created, the light $SU_c(2)$ glueballs are stable against strong interactions but not with respect to electromagnetic processes. The following decay width, at non zero baryon density, was obtained by saturating the electromagnetic trace anomaly in [14]:

$$\Gamma\left[h \to \gamma\gamma\right] \approx 1.2 \times 10^{-2} \cos\theta_Q^4 \left[\frac{M_h}{1\ \mathrm{MeV}}\right]^5\ \mathrm{eV}\ , \qquad (24)$$

where $\alpha = e^2/4\pi \simeq 1/137$. For illustration purposes we consider a glueball mass of the order of 1 MeV which leads to a decay time $\tau \sim\ 5.5 \times\ 10^{-14} s$. We used $\cos\theta_Q \sim\ 1$ since $\theta_Q \sim 2.5^\circ$ [14].

The present light glueball analysis is limited to the zero temperature and high matter density case. However it is interesting to investigate the effects of a non zero temperature.

It is a pleasure for me to thank R. Casalbuoni, Z. Duan, S. D. Hsu, R. Ouyed and M. Schwetz for sharing part of the work on which this talk is based. This work is supported by the Marie-Curie fellowship under contract MCFI-2001-00181.

# References

[1] For reviews see K. Rajagopal, F. Wilczek hep-ph/0011333; M. Alford, hep-ph/0102047 ; S. D. Hsu, hep-ph/0003140; D. K. Hong, hep-ph/0101025, and references therein.

[2] D. K. Hong, S. D. Hsu and F. Sannino, Phys. Lett. B**516**, 362, (2001).

[3] R. Ouyed and F. Sannino, A&A, in press [astro-ph/0103022].

[4] R. Casalbuoni and R. Gatto, Phys. Lett. B**464**, 11 (1999); Phys. Lett. B**469**, 213 (1999).

[5] F. Sannino and J. Schechter, Phys. Rev. D**60**, 056004, (1999).

[6] R. Casalbuoni, Z. Duan and F. Sannino, hep-ph/0011394. Phys. Rev. D**63**, 114026, (2001).

[7] D. K. Hong, M. Rho and I. Zahed, Phys. Lett. B**468**, 261 (1999).

[8] F. Sannino, Phys. Lett. B**480**, 280, (2000).

[9] M.A. Nowak, M. Rho, A. Wirzba, I. Zahed, Phys. Lett. B**497**,85 (2001).

[10] R. Casalbuoni, Z. Duan and F. Sannino, Phys. Rev. D**62**, 094004, (2000).

[11] S. Hsu, F. Sannino and M. Schwetz, Mod. Phys. Lett. A**16**, 1871, (2001).

[12] S. L. Shapiro, S. A. Teukolsky, *Black Holes, White Dwarfs, and Neutron Stars*, "A Wiley-Interscience publication" , 1983.

[13] D.H. Rischke, D.T. Son, M.A. Stephanov, Phys. Rev. Lett. **87**, 062001, (2001).

[14] R. Ouyed and F. Sannino, Phys. Lett. B**511**, 66, (2001).

[15] J. Schechter, Phys. Rev. **D21**, 3393 (1980).

From Left to Right: Joseph Schechter, Holger Bech Nielsen, Roberto Casalbuoni and Dam Thanh Son in a discussion.

Felix Ryde (first from left) and Gulli Bjornsson (second from left) during the coffee break.

From Left to Right: Arun V. Thampan, Fridolin Weber and Ignazio Bombaci enjoying the last drops of coffee.

Ahmet Mecit, Öztaş (left) and Sverker Fredriksson during the coffee break.

Stephen Hsu (left) and Francesco Sannino in a heated debate.

Vladimir Usov (left) entertaining Mark Alford.

Students Nils Marchal (left) and Massimo Mannarelli taking a break.

Back to session.

# Color Superconductivity in Compact Stars

# Color superconducting quark matter in compact stars

*Mark Alford*
*Physics and Astronomy Department*
*Glasgow University*
*Glasgow G12 8QQ, UK*

## 1 Introduction

Matter just above nuclear density presents special challenges, both observational and theoretical. It is the densest state of which we have evidence in nature, but in terrestrial laboratories it can only be produced fleetingly and at high temperature over small volumes. We must therefore rely on astrophysical observations of compact stars to gather more indirect experimental information. Theoretically, it falls between the domain of nuclear physics, where models have been tested against scattering data, and the asymptotically high energy domain, where the relevant theory, QCD, becomes tractable.

We expect that somewhat above nuclear density, the nucleons will overlap so much as to lose their separate identities, and merge into quark matter. In this talk I will review some of theoretical expectations and speculations about quark matter, focusing on the phenomenon of quark pair condensation (color superconductivity).

indexFermi surface Since QCD is asymptotically free, one expects that at high enough densities and low temperatures, matter will consist of a Fermi sea of quarks, and the ones at the Fermi surface will be almost free. The residual gluon-mediated interaction is attractive in the color $\overline{\mathbf{3}}$ channel, so BCS quark pair condensation will take place, breaking the $SU(3)$ color gauge symmetry. his was first appreciated in the 1970s, and revived more recently [1, 2, 3, 4, 5]. It is discussed in more detail in the review articles [6]. The quark pairs play the same role here as the Higgs particle does in the standard model: the color-superconducting phase can be thought of as the Higgsed (as opposed to confined) phase of QCD.

t is important to remember from the outset that the breaking of a gauge symmetry cannot be characterized by a gauge-invariant local order parameter which vanishes on one side of a phase boundary. The superconducting phase can be characterized rigorously only by its global symmetries. In electromagnetism there is a non-local order parameter, the mass of the magnetic photons, that corresponds physically to

the Meissner effect and distinguishes the free phase from the superconducting one. In QCD there is no free phase: even without pairing the gluons are not states in the spectrum. No order parameter distinguishes the Higgsed phase from a confined phase or a plasma, so we have to look at the global symmetries.

# 2 Patterns of color superconductivity

In the real world there are two light quark flavors, the up ($u$) and down ($d$), with masses $\lesssim 10$ MeV, and a medium-weight flavor, the strange ($s$) quark, with mass $\sim 100$ MeV. It is convenient to treat the $u$ and $d$ as massless, and study the effect of varying the $s$ quark mass between zero and infinity.

## 2.1 Three flavors: color-flavor locking

In the three flavor case, $m_s = m_u = m_d = 0$, the structure of the quark pair condensate is particularly simple and elegant, because the number of flavors and colors is equal. The favored condensation pattern is "color-flavor locking",

$$\text{CFL phase:} \quad \Delta_{ij}^{\alpha\beta} = \langle q_i^\alpha q_j^\beta \rangle_{1PI} \propto C\gamma_5[(\kappa+1)\delta_i^\alpha\delta_j^\beta + (\kappa-1)\delta_j^\alpha\delta_i^\beta], \tag{1}$$

where color indices $\alpha, \beta$ and flavor indices $i, j$ all run from 1 to 3, Dirac indices are suppressed, and $C$ is the Dirac charge-conjugation matrix. The term multiplied by $\kappa$ corresponds to pairing in the $(\mathbf{6}_S, \mathbf{6}_S)$, which although not highly favored energetically breaks no additional symmetries and so $\kappa$ is in general small but not zero [7, 8, 9].

Eq. (1) exhibits the color-flavor locking property of this ground state. The Kronecker deltas connect color indices to flavor indices, so that the VEV is not invariant under color rotations, nor under flavor rotations, but only under simultaneous, equal and opposite, color and flavor rotations. Since color is only a vector symmetry, this VEV is only invariant under vector flavor rotations, and breaks chiral symmetry.

The pattern of symmetry breaking is therefore (with gauge symmetries in square brackets)

$$[SU(3)_{\text{color}}] \times \underbrace{SU(3)_L \times SU(3)_R}_{\supset [U(1)_Q]} \times U(1)_B \longrightarrow \underbrace{SU(3)_{C+L+R}}_{\supset [U(1)_{\tilde{Q}}]} \times \mathbb{Z}_2 \tag{2}$$

Note that electromagnetism is not a separate symmetry, but corresponds to gauging one of the flavor generators.

This pattern of condensation has many interesting features. (1) The color gauge group is completely broken, so all eight gluons become massive. This ensures that there are no infrared divergences associated with gluon propagators. (2) All the quark modes are gapped. The nine quasiquarks (three colors times three flavors)

fall into a smaller-gap octet and a larger-gap singlet of the unbroken global $SU(3)$. (3) Electromagnetism is replaced by a "rotated electromagnetism", namely a linear combination $\tilde{Q}$ of the original photon and one of the gluon. 4) Two global symmetries are broken, he chiral symmetry and baryon number, so there are two gauge-invariant order parameters that distinguish the CFL phase from the QGP, with corresponding Goldstone bosons which are long-wavelength disturbances of the order parameter. (5) Quark-hadron continuity. It is striking that the symmetries of the 3-flavor CFL phase are the same as those one might expect for 3-flavor hypernuclear matter [10]. This means the spectrum may evolve continuously from hypernuclear matter to the CFL phase of quark matter—there need be no phase transition.

## 2.2 Two flavors

If the strange quark is heavy enough to be ignored, then the up and down quarks pair in the color $\overline{\mathbf{3}}$ flavor singlet channel, a pattern that we call the two-flavor superconducting (2SC) phase,

$$\text{2SC phase:} \quad \Delta_{ij}^{\alpha\beta} = \langle q_i^\alpha q_j^\beta \rangle_{1PI} \propto C\gamma_5 \varepsilon_{ij} \varepsilon^{\alpha\beta 3}, \tag{3}$$

where color indices $\alpha, \beta$ run from 1 to 3, flavor indices $i, j$ run from 1 to 2. Four-fermion interaction calculations agree on the magnitude of $\Delta$: around 100 MeV. This is found to be roughly independent of the cutoff, although the chemical potential at which it is attained is not. Such calculations are based on calibrating the coupling to give a chiral condensate of around 400 MeV at zero density, and turning $\mu$ up to look for the maximum gap.

As with any spontaneous symmetry breaking, one of the degenerate ground states is arbitrarily selected. In this case, quarks of the first two colors (red and green) participate in pairing, while the third color (blue) does not. The ground state is invariant under an $SU(2)$ subgroup of the color rotations that mixes red and green, but the blue quarks are singled out as different. The pattern of symmetry breaking is therefore

$$\begin{array}{rl} & [SU(3)_{\text{color}}] \times [U(1)_Q] \times SU(2)_L \times SU(2)_R \\ \longrightarrow & [SU(2)_{\text{color}}] \times [U(1)_{\tilde{Q}}] \times SU(2)_L \times SU(2)_R \end{array} \tag{4}$$

The features of this pattern of condensation are (1) The color gauge group is broken down to $SU(2)$, so five of the gluons will become massive, with masses of order $g\mu$. The remaining three gluons are associated with an unbroken $SU(2)$ red-green gauge symmetry, whose confinement distance scale rises exponentially with density [11]. (2) The red and green quark modes acquire a gap $\Delta$. There is no gap for the blue quarks in this ansatz, and it is an interesting question whether they find some other channel in which to pair. The available attractive channels appear to be weak so the gap will be much smaller, perhaps in the keV range [4]. We will ignore such pairing

here. (3) A rotated electromagnetism ("$\tilde{Q}$") survives unbroken. It is a combination of the original photon and one of the gluons. 4) No global symmetries are broken, although additional condensates that break chirality have been suggested [12], so the 2SC phase has the same global symmetries as the quark-gluon plasma (QGP).

# 3 Two massless + one massive quark flavors

A nonzero strange quark mass explicitly breaks the flavor $SU(3)_L \times SU(3)_R$ symmetry down to $SU(2)_L \times SU(2)_R$. If the strange quark is heavy enough then it will decouple, and 2SC pairing will occur. For a sufficiently small strange quark mass we expect a reduced form of color-flavor locking in which an $SU(2)$ subgroup of $SU(3)_{\rm color}$ locks to isospin, causing chiral symmetry breaking and leaving a global $SU(2)_{\rm color+V}$ group unbroken.

As $m_s$ is increased from zero to infinity, there has to be some critical value at which the strange quark decouples, color and flavor rotations are unlocked, and the full $SU(2)_L \times SU(2)_R$ symmetry is restored [13]. On the way, however, other interesting phenomena may occur. Where differing masses or chemical potentials obstruct the pairing of one species of quark with another (eg in the 2SC+s phase) we expect regions of crystalline superconductivity [14], which grow larger at high chemical potential where forward scattering dominates the quark-quark interactions [15]. This could lead to interesting phenomena such as glitches in quark stars [14]. It is also possible that the CFL condensate responds to the strange quark mass by rotating in a direction that reduces the strangeness content. This corresponds to a condensation of $K_0$ mesons [16] yielding a "CFL-$K^0$" phase.

| symmetry: | gauged | baryon number | hyper-charge | isospin | chiral | axial $U(1)$ |
|---|---|---|---|---|---|---|
| broken by: | | | weak | electromag $m_u \neq m_d$ | $m_{u,d} \neq 0$ | instanton |
| QGP | $[SU(3) \times U(1)_Q]$ | $U(1)_B$ | $U(1)_Y$ | $SU(2)_V$ | $SU(2)_A$ | $U(1)_A$ |
| 2SC | $[SU(2) \times U(1)_{\tilde{Q}}]$ | $U(1)_B$ | $U(1)_Y$ | $SU(2)_V$ | $SU(2)_A$ | $U(1)_A$ |
| CFL | $[U(1)_{\tilde{Q}}]$ | $\{1\}$ | $U(1)_Y$ | $SU(2)_V$ | $\{3\}$ | $\{1\}$ |
| CFL-$K^0$ | $[U(1)_{\tilde{Q}}]$ | $\{1\}$ | $\{1\}$ | $\{2\}$ | $\{3\}$ | $\{1\}$ |

Table 1: Symmetry breaking of the high-density QCD phases in various approximations. For broken symmetries, the number of Goldstone bosons is given in curly brackets. Gauged symmetries are in square brackets. The strongest explicit breaking of each of the global symmetries is given: only baryon number is a global symmetry of the real world. The QGP is assumed to have the symmetries of the Lagrangian.

The CFL-$K^0$ phase is expected to occur if the strange quark mass is large enough, and the up and down are light enough. Calculations at asymptotically high density,

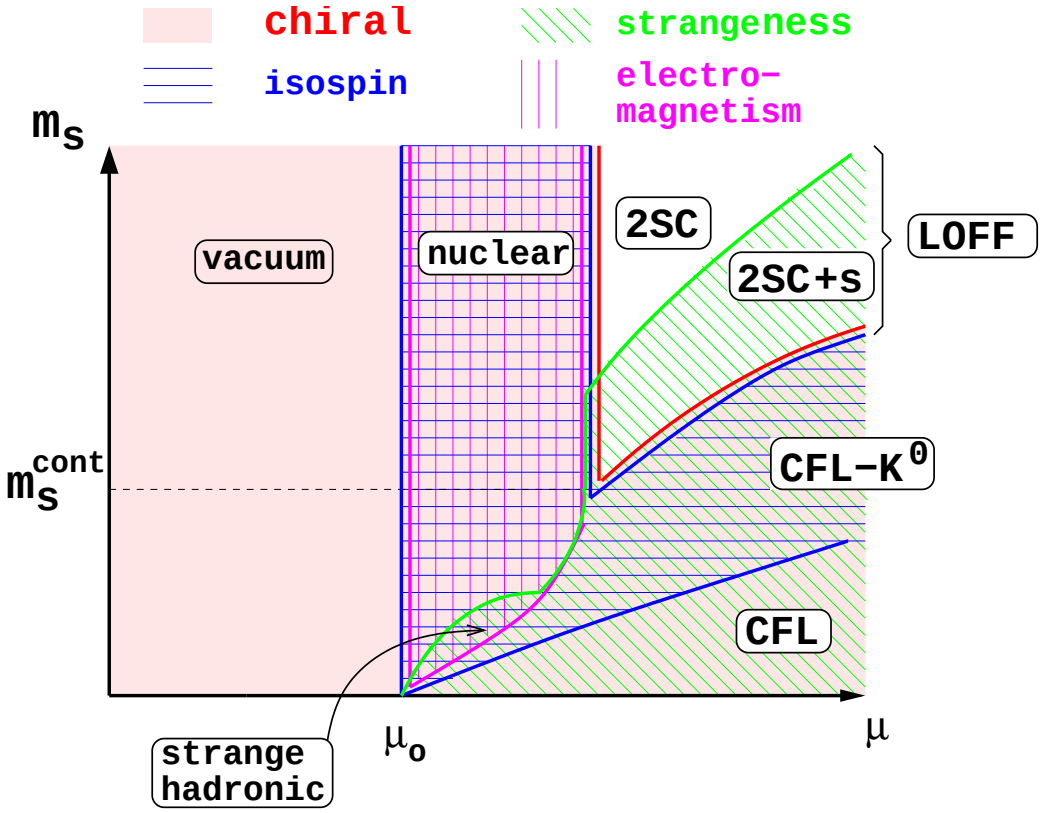


Figure 1: Possible phase diagram for 2+1 flavor QCD at $T = 0$. In the blue (horizontal) shaded area, isospin is broken. In the magenta (vertical) shaded area, electromagnetism is broken. In the green (top-left to bottom-right) shaded area, strangeness is broken. Chiral symmetry is broken in the whole densely (pink) shaded area, i.e. everywhere except in the wedge at top right. Small print: most of these symmetries are approximate, and potentially important physics has been ignored—see the text.

extrapolated back to around nuclear density, indicate that it is favored for quark matter at a few times nuclear density [17]. This estimate ignores terms that split the gaps corresponding to different flavor pairings [13] and $U(1)_A$-breaking terms induced by instantons that are expected to become important in that regime. In table 1 we show the symmetries broken by the various phases. In the real world, the only relevant true global symmetry is baryon number, and both CFL and CFL-$K^0$ break it, so they both have one massless superfluid mode. However, we expect a number of pseudo-Goldstone bosons arising from spontaneously broken near-symmetries. These are different in the CFL and CFL-$K^0$ phases. It has recently been noted that the breaking of isospin in the CFL-$K^0$ phase leads to 2 not 3 pseudo-Goldstone bosons, [18], and that the breaking of $U(1)_Y$ by the $K^0$-condensate may lead to long-lived axion-type domain walls [19].

In Fig. 1 we give one possibility for the resultant QCD phase diagram in the $\mu$-$m_s$ plane. The complications relating to the CFL-$K^0$ phase have been ignored, and most of the symmetries shown in the figure are approximate, so the "symmetry breaking" shaded areas actually correspond to regions where some pseudo-Goldstone states become very light, and the border lines are crossovers. The exceptions are electromagnetism, which is a gauge symmetry, with the mass of the photon as an order parameter, and baryon number. Electromagnetism is broken in the magenta (vertical) shaded region. Baryon number is a combination of electric charge, isospin, and strangeness, and is broken in all the shaded regions, leading to an exactly massless superfluid mode.

The low-$\mu$ part of the CFL phase is the region of quark-hadron continuity [10], where the whole baryon octet self-pairs in an isospin-respecting way [13]. The low-$\mu$ part of the CFL-$K^0$ phase can also be given a hadronic interpretation, in which there is $n$-$n$ and $p$-$\Sigma^-$ pairing, which breaks isospin amd strangeness, but leaves electromagnetism unbroken.

# 4 The transition to color superconducting quark matter in compact stars

The only place in the universe where we expect very high densities and low temperatures is compact stars (for a recent review, see [20]). These typically have masses close to $1.4M_\odot$, and are believed to have radii of order 10 km. Their density ranges from around nuclear density near the surface to higher values further in, although uncertainty about the equation of state leaves us unsure of the value in the core.

Color superconductivity gives mass to excitations around the ground state: it opens up a gap at the quark Fermi surface, and makes the gluons massive. One would therefore expect its main consequences to relate to transport properties, such as mean free paths, conductivities and viscosities. he influence of color superconductivity on the equation of state is an $\mathcal{O}((\Delta/\mu)^2)$ (few percent) effect, which is probably not phenomenologically interesting given the existing uncertainty in the equation of state at the relevant densities.

## 4.1 The transition region

There are two possibilities for the transition from nuclear matter to quark matter in a neutron star: a mixed phase, or a sharp interface. The surface tension of the interface determines which is favored. To be concrete, we will consider the case where the strange quark is light enough so that quark pairing is always of the CFL type. Figure 2 shows the $\mu_B$-$\mu_e^{\rm eff}$ phase diagram, ignoring electromagnetism. The lightly (yellow) shaded region is where nuclear matter (NM) has higher pressure. The darker

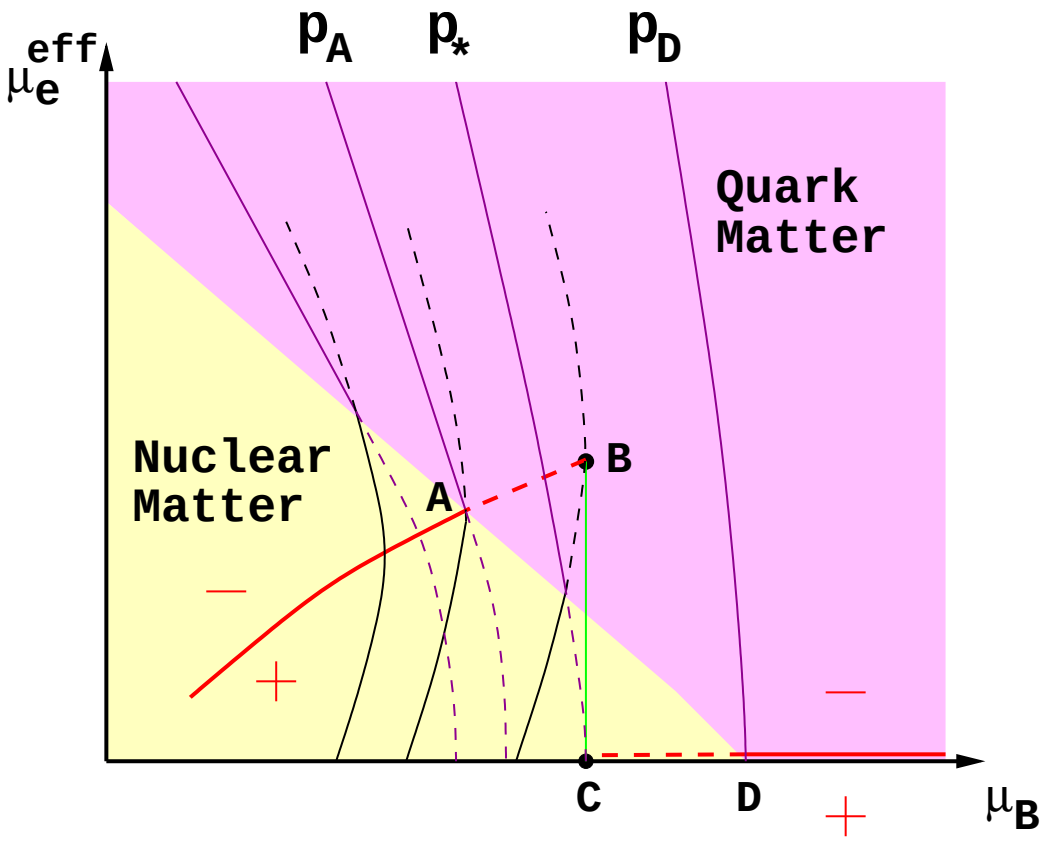


Figure 2: A schematic form of the $\mu_B$-$\mu_e$ phase diagram for nuclear matter and CFL quark matter, ignoring electromagnetism. For an explanation see the text.

(magneta) region is where quark matter (QM) has higher pressure. Where they meet is the coexistence line. The medium solid lines labelled by values of the pressure are isobars. Below the coexistence line they are given by the NM equation of state, above it by the QM equation of state. he thick (red) lines are the neutrality lines. Each phase is negatively charged above its neutrality line and positively charged below it. Dotted lines show extensions onto the unfavored sheet (NM above the coexistence line, QM below it).

The electric charge density is

$$Q = -\left.\frac{\partial p}{\partial \mu_e}\right|_{\mu_B} \tag{5}$$

so the neutrality line goes through the right-most extremum of each isobar, since there the derivative of pressure with respect to $\mu_e$ is zero. For the CFL phase, the neutrality line is $\mu_e = 0$ [21].

Two possible paths from nuclear to CFL matter as a function of increasing $\mu$ are

shown. In the absence of electromagnetism and surface tension, the favored option is to progress along the coexistence line from A to D, giving an overall neutral phase made of appropriate relative volumes of negatively charged CFL matter and positively charged nuclear matter.

If, on the other hand, Coulomb and surface energies are large, then the system remains on the nuclear neutrality line up to $B$, where there is a single interface between nuclear matter at $B$ and CFL matter at $C$. This minimal interface, with its attendant charged boundary layers [22], occurs between phases with the same $\mu_e$, $\mu = \mu_B = \mu_C$, and pressure $P_*$. The effective chemical potential $\mu_e^{\rm eff}$ changes across the interface, though, as a result of the presence of the electric field. For more details see Ref. [22].

As yet, not much work has been done on signatures related to these features. The single interface creates a dramatic density discontinuity in the star: CFL quark matter at about four times nuclear density floats on nuclear matter at about twice nuclear density. This may affect the mass vs. radius relationship for neutron stars with quark matter cores. It may also have qualitative effects on the gravitational wave profile emitted during the inspiral and merger of two compact stars of this type. The mixed phase has distinctively short neutrino mean free paths, due to coherent scattering [23]. Also, the droplets form a crystal lattice that could pin vortices, leading to glitches.

## 4.2 Latent heat

If there is a first-order phase transition between nuclear matter and quark matter, then there is the possibility that heat could be released when the center of a gravitationally compressed neutron star converts to quark matter [24].

A proper treatment requires the construction of solutions to the TOV equations, and a comparison of the masses of the resultant stars. To get an idea of the energy scales involved, however, one can study the statistical mechanics of a simplified system consisting of a lump of nuclear matter, slowly being compressed in a piston. We assume the system remains at zero temperature throughout. Since the compression is slow, the system will remain in equilibrium at all times, which means it can be characterized by a chemical potential $\mu$ for quark number. This is true in spite of the fact that the system as a whole has a fixed quark number: since it is in equilibrium, any subsystem has the same intensive properties as the whole system, and the rest of the system acts as a particle reservoir for the subsystem.

Under slow compression of nuclear matter, the pressure $p$ and chemical potential $\mu$ rise, until we reach a point in phase space where quark matter with the same

chemical potential $\mu_*$ would have the same pressure $p_*$.

$$\begin{aligned} -p_* &= \frac{F_{NM}}{V_{NM}} = \frac{E_{NM}}{V_{NM}} - \mu_* \frac{N_{NM}}{V_{NM}} \\ -p_* &= \frac{F_{QM}}{V_{QM}} = \frac{E_{QM}}{V_{QM}} - \mu_* \frac{N_{QM}}{V_{QM}} \end{aligned} \tag{6}$$

Under continued compression, the system contracts and $\mu$ and $p$ remain constant for a while, as the nuclear matter is converted to the denser quark matter phase. When the conversion is complete, further compression causes $\mu$ and $p$ to start rising again. From (6) we see that the quark matter phase has higher energy density, so the latent heat per unit volume is negative,

$$\frac{E_{NM}}{V_{NM}} - \frac{E_{QM}}{V_{QM}} = \mu_* \Big( \frac{N_{NM}}{V_{NM}} - \frac{N_{QM}}{V_{QM}} \Big) \tag{7}$$

The relevant quantity, however, is the amount of energy liberated per quark, since the quark number $N = N_{NM} = N_{QM}$ is constant, and the two phases have different volumes $V_{NM} > V_{QM}$. From (6) the latent heat per quark is

$$\Delta E/N = \frac{E_{NM}}{V_{NM}} \frac{V_{NM}}{N} - \frac{E_{QM}}{V_{QM}} \frac{V_{QM}}{N} = p_* \Big( \frac{V_{QM}}{N} - \frac{V_{NM}}{N} \Big) \tag{8}$$

which is again negative. The energy required comes from the mechanism that maintains the pressure by doing work on the piston. In the case of a compact star, this is the gravitational field, and the transition to quark matter is driven by the higher gravitational binding energy of the denser quark matter phase. The work done per quark is

$$\Delta W/N = -pdV/N = \frac{p_*}{N}(V_{NM} - V_{QM}) \tag{9}$$

which is just the negative of (8): the work done by the gravitational field provides exactly the energy needed to convert the nuclear matter to quark matter.

It is clear that as long as the microscopic processes that convert quark matter into nuclear matter occur on a much faster timescale than the compression, no energy will be liberated. It is possible for energy to be liberated if the compression to happens fast enough that the center goes out of equilibrium and becomes supercompressed, i.e. metastable.

## 4.3 Mixed phase vs sharp interface

If the surface tension $\sigma_{QCD}$ and the electrostatic forces are ignored, then a mixed phase is favored over a sharp interface. [25, 26, 27]. If we treat $\sigma_{\rm QCD}$ as an independent parameter, we can estimate the surface and Coulomb energy cost of the mixed phase

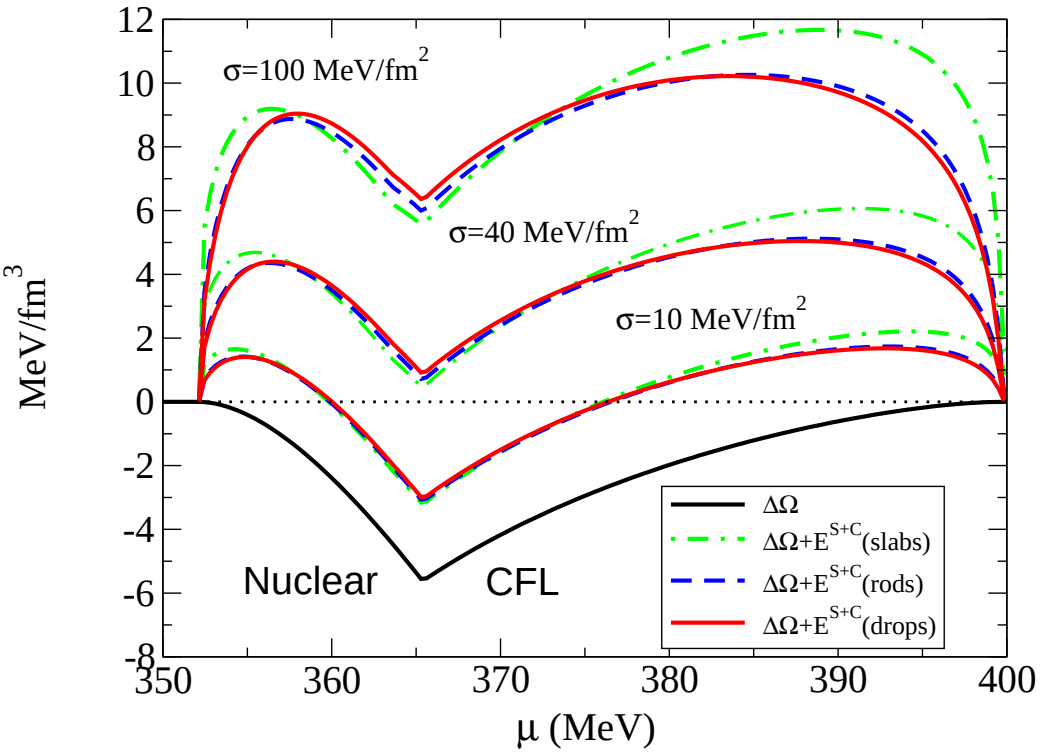


Figure 3: The free energy difference between the mixed phase and the homogeneous neutral nuclear and CFL phases. In the lowest curve, the surface and Coulomb energy costs of the mixed phase are neglected, do the mixed phase always has the lower free energy. Other curves include surface and Coulomb energy for different values of $\sigma_{\rm QCD}$ and different mixed phase geometry. As $\sigma_{\rm QCD}$ increases, the surface and Coulomb price paid by the mixed phase increases.

[27, 22]. In Fig. 3 we see how the competition between sharp interface and mixed phase depends on the $\sigma_{\rm QCD}$. The curves show the difference of free-energy between various kinds of mixed phase and the sharp interface (which occurs at $\mu = 365$ MeV, hence the kink there). For any value of $\sigma_{\rm QCD}$, the mixed phase progresses from drops to rods to slabs of CFL matter within nuclear matter to slabs to rods to drops of nuclear matter within CFL matter.

For any given $\sigma_{\rm QCD}$, the mixed phase has lower free energy than homogeneous neutral CFL or nuclear matter wherever one of the curves in Fig. 3 for that $\sigma_{\rm QCD}$ is negative. We see that much of the mixed phase will survive if $\sigma_{\rm QCD} \simeq 10$ MeV/fm$^2$ while for $\sigma_{\rm QCD} \gtrsim 40$ MeV/fm$^2$ the mixed phase is not favored for any $\mu$. This means that if the QCD-scale surface tension $\sigma_{\rm QCD} \gtrsim 40$ MeV/fm$^2$, the single sharp interface with its attendant boundary layers, described in previous sections, is free-energetically favored over the mixed phase.

# 5 Conclusions

The reawakening of interest in the color superconducting nature of quark matter has led us to appreciate that the QCD phase diagram is much richer than previously thought. I have outlined some of the structure in this paper. There has naturally been much speculation about observable consequences in compact star phenomenology. In spite of the limited nature of our observational knowledge of compact stars, there have been many suggestions, and these are discussed in the review articles [6] and in other contributions to these proceedings. Although we are still in the early stages of such phenomenology, we can take inspiration from high-temperature QCD, where great progress has been made in overcoming similar obstacles. At the same time as heavy-ion colliders map the high-temperature region of the QCD phase diagram, we hope that astrophysical observations and calculations will complement it by filling in details of the high-density region.

**Acknowledgements**. I am grateful to the organizers of Compact QCD, F. Sannino and R. Ouyed. I thank J. Bowers, S. Hsu, K. Rajagopal, S. Reddy, D. Son, F. Wilczek for discussions and collaboration on the topics discussed here.

# References

[1] B. C. Barrois, Nucl. Phys. B **129** (1977) 390. S. Frautschi, "Asymptotic Freedom And Color Superconductivity In Dense Quark Matter", in *Proceedings of 1978 Erice workshop "Hadronic matter at extreme density", Erice, Italy, Oct 13-21, 1978*, ed. by N. Cabibbo and L. Sertorio, (Plenum, New York, 1980) pp. 19-27

[2] B. Barrois, "Nonperturbative effects in dense quark matter", Cal. Tech. PhD thesis, UMI 79-04847-mc (1979)

[3] D. Bailin and A. Love, Phys. Rept. **107** (1984) 325.

[4] M. G. Alford, K. Rajagopal and F. Wilczek, Phys. Lett. B **422** (1998) 247 [hep-ph/9711395].

[5] R. Rapp, T. Schafer, E. V. Shuryak and M. Velkovsky, Phys. Rev. Lett. **81** (1998) 53 [hep-ph/9711396].

[6] M. G. Alford, hep-ph/0102047. D. K. Hong, Acta Phys. Polon. B **32** (2001) 1253 [hep-ph/0101025]. K. Rajagopal and F. Wilczek, hep-ph/0011333. T. Schafer and E. V. Shuryak, nucl-th/0010049. D. H. Rischke and R. D. Pisarski, Proceedings of the "Fifth Workshop on QCD", Villefranche, Jan. 3-7, 2000 [nucl-th/0004016].

[7] M. G. Alford, K. Rajagopal and F. Wilczek, Nucl. Phys. B **537** (1999) 443 [hep-ph/9804403].

[8] R. D. Pisarski and D. H. Rischke, "Why color-flavor locking is just like chiral symmetry breaking". To be published in, *Proceedings of the Judah Eisenberg Memorial Symposium, "Nuclear Matter, Hot and Cold"*, Tel Aviv, April 14 - 16, 1999 [nucl-th/9907094].

[9] T. Schafer, Nucl. Phys. B **575** (2000) 269 [hep-ph/9909574].

[10] T. Schafer and F. Wilczek, Phys. Rev. D **60** (1999) 074014 [hep-ph/9903503].

[11] D. H. Rischke, D. T. Son and M. A. Stephanov, Phys. Rev. Lett. **87** (2001) 062001 [hep-ph/0011379]; R. Ouyed and F. Sannino, Phys. Lett. B **511** (2001) 66 [hep-ph/0103168].

[12] J. Berges, Phys. Rev. D **64** (2001) 014010 [hep-ph/0012013].

[13] M. G. Alford, J. Berges and K. Rajagopal, Nucl. Phys. B **558** (1999) 219 [hep-ph/9903502].

[14] M. G. Alford, J. Bowers and K. Rajagopal, Phys. Rev. D **63** (2001) 074016 [hep-ph/0008208].

[15] A. K. Leibovich, K. Rajagopal and E. Shuster, hep-ph/0104073.

[16] P. F. Bedaque and T. Schafer, hep-ph/0105150.

[17] D. B. Kaplan and S. Reddy, hep-ph/0107265.

[18] V. A. Miransky and I. A. Shovkovy, hep-ph/0108178. T. Schafer, D. T. Son, M. A. Stephanov, D. Toublan and J. J. Verbaarschot, hep-ph/0108210.

[19] D. T. Son, hep-ph/0108260.

[20] H. Heiselberg and V. Pandharipande, Ann. Rev. Nucl. Part. Sci. **50** (2000) 481 [astro-ph/0003276].

[21] K. Rajagopal and F. Wilczek, Phys. Rev. Lett. **86** (2001) 3492 [hep-ph/0012039].

[22] M. G. Alford, K. Rajagopal, S. Reddy and F. Wilczek, hep-ph/0105009.

[23] S. Reddy, G. Bertsch and M. Prakash, Phys. Lett. B **475**, 1 (2000) [nucl-th/9909040].

[24] D. K. Hong, S. D. Hsu and F. Sannino, hep-ph/0107017.

[25] N. K. Glendenning, Phys. Rev. D **46**, 1274 (1992).

[26] M. Prakash, J. R. Cooke and J. M. Lattimer, Phys. Rev. D **52**, 661 (1995).

[27] N. K. Glendenning and S. Pei, Phys. Rev. C **52**, 2250 (1995).

# Color Superconductivity and Blinking Proto-Neutron Stars

*Greg W. Carter*
*Department of Physics and Astronomy*
*State University of New York*
*Stony Brook, NY 11794-3800*

## 1 Introduction

Due to instabilities at the Fermi surface, matter composed of deconfined quarks is believed to be a color superconductor at low temperatures (see Refs. [1] and other reviews). While the precise value of the energy gap at astrophysical densities is yet indeterminate, calculations using models of vacuum physics generally predict a gap in the neighborhood of 100 MeV for densities at and above three times that of equilibrium nuclear matter. This implies that quark matter with a chemical potential fixed around 400 MeV undergoes a phase transition between a quark-gluon plasma state and one of paired quarks at a critical temperature near 50 MeV. In this talk I discuss how this could lead to a variation in the neutrino signal emanating from a proto-neutron star formed in the wake of a supernova.

Our current understanding of Type II (core collapse) supernovae, based on a handful of observations and quite a bit of theoretical modeling, begins with the implosion of the inner core of star of mass 8–20 solar masses (see Ref. [2] for a recent review). The evolution of the remnant proto-neutron star is driven by the diffusion of neutrinos, which make their way through the hot ($T \sim 25$ MeV) and dense ($n_B \sim 3n_0$) core matter before a few are eventually detected on Earth. The temporal characteristics of this signal are determined for the most part by the neutrino mean free path through this core.

For temperatures much lower than the superconducting energy gap, $T \ll \Delta$, quark states are replaced by diquark quasi-particles and neutrino-quark cross sections are exponentially suppressed. Thus at late times, when $T \sim 1$ KeV, the neutrino mean free path in quark matter is practically infinite. But within the first minute after core collapse, deleptonization heats the dense core to $T \simeq 50$ MeV before thermal neutrino emission cools the system. It is during this time that transitions between states of strongly-interacting matter would occur. While the phase transition from hadronic matter to a quark plasma is likely first order (but poorly understood), a slightly later

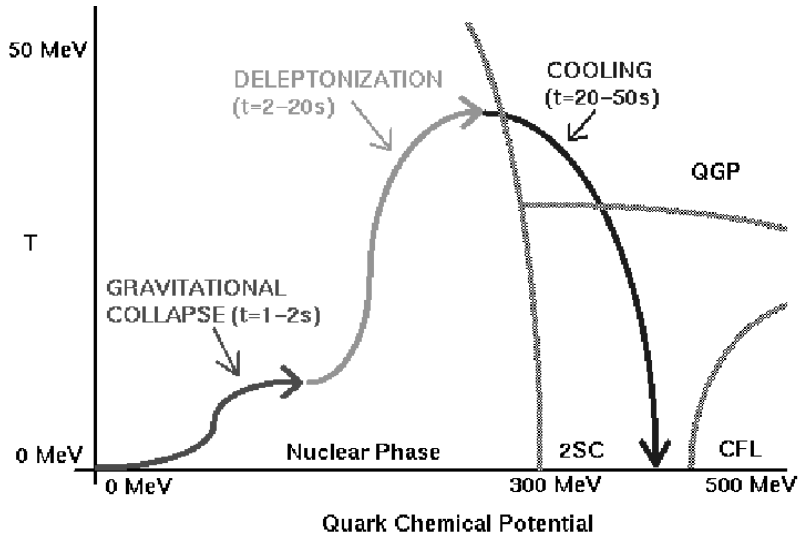


Figure 1: A tour of the phase diagram via a proto-neutron star.

transition from quark to superconducting quark matter might be second order, as in BCS theory. The associated critical behavior of the latter would lead to a slowdown in cooling, followed by a burst of streaming neutrinos as the temperature eventually falls below the quark energy gap. In what follows I will discuss inelastic neutrino-quark scattering in a simplified proto-neutron star environment in order to quantify this possible phenomena and speculate on an observable signal.

We are concerned here with the period in the proto-neutron star's evolution during which the matter is at its hottest and most dense, immediately following the Joule heating due to primordial lepton release. The ambient conditions are a temperature near 50 MeV and a density around four times that of nuclear matter, or equivalently a quark chemical potential of 400 MeV. This is the final period (Cooling) in the evolution mapped on the generic phase diagram for nuclear matter in Figure 1.

## 2 Neutrino Mean Free Path in a Color Superconductor

Thermal neutrino diffusion is the primary means of heat escape from the dense core. While noting that the neutrino production rate will also differ from that of normal matter [3], in the diffusive regime the dominant critical behavior will be a change in the *inelastic* quark-neutrino cross section, since here neutrino production rates decouple from the transport equation and depend only on the neutrino mean free path. We thus calculated the differential and total cross sections in order to compute the neutrino

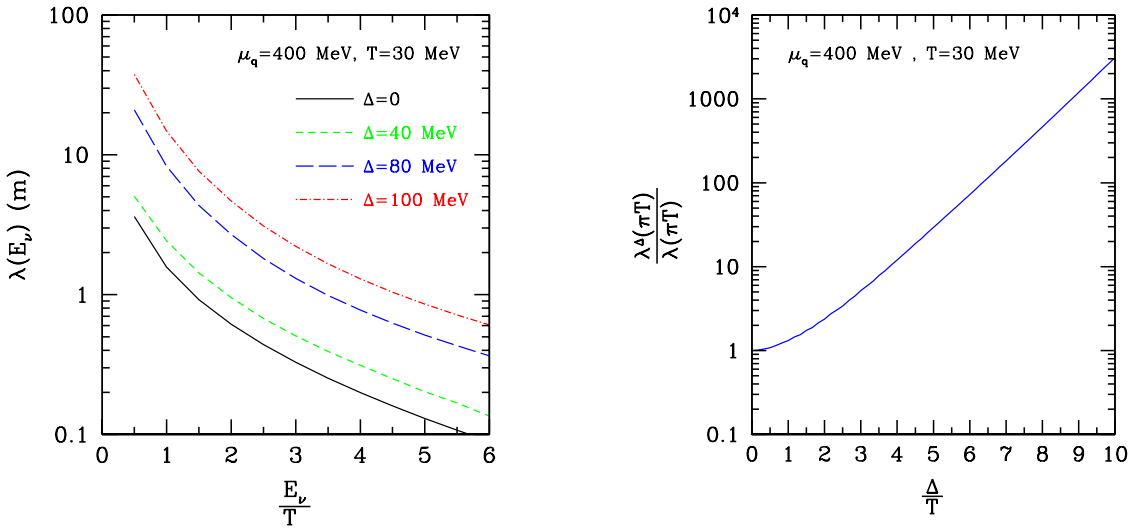


Figure 2: Left Panel: Neutrino mean free path as a function of neutrino energy. Right Panel: The neutrino mean free path for neutrino energy $E_\nu = \pi T$, plotted as a function of the gap $\Delta$.

mean free path in two-flavor quark matter. The magnitude of the superconducting gap, $\Delta$, was taken as arbitrary within a range of values found in recent literature. Closely following BCS theory, we assumed the gap to be a constant, and calculated the response functions and neutrino cross sections in the weak coupling approximation.

Details, including polarization operators, differential and total cross sections, and limiting behavior can be found in Ref. [4]. The essential physical difference between neutrinos scattering in superconducting quark matter as opposed to free quark matter is that, in the quasi-particle phase, the incident neutrino must transfer energy greater than twice the gap, or $E_\nu \geq 2\Delta$, to excite a quark pair. Stated equivalently, when the gap becomes large ($\Delta \gtrsim T \sim 30$ MeV) the spacelike response functions ($q_0 < |\vec{q}|$) are substantially suppressed, and the inelastic cross section is greatly diminished.

The mean free path, $\lambda = (\sigma/V)^{-1}$, therefore grows with energy gap. This main result is shown in Figure **??**. The left panel assumes a constant energy gap $\Delta$ at a constant temperature $T = 30$ MeV. As expected, the mean free path grows substantially when $T < \Delta$ for all neutrino energies. In the right panel an average thermal neutrino energy of $E_\nu = \pi T$ has been assumed, and the superconducting gap is varied for fixed $T$. The expected exponential behavior is clear for $\Delta \gtrsim 3T$ and, combining information from the two plots, one can deduce that for low temperatures the neutrinos are able to pass through kilometers of superconducting quark matter with only an occasional collision. These results are essentially independent of temperature for all $T \lesssim 50$ MeV.

# 3 Cooling of an Idealized Quark Star

The theoretical state of the art in modeling proto-neutron star cooling involves complex computer simulations of multi-phase environments. To explore the consequences of the onset of superconductivity in a macroscopic core of deconfined quark matter, we will simply assume the existence of such a system and approximate it by a sphere of quark matter. We furthermore consider the relatively simple case of two massless flavors with identical chemical potentials and disregard for now any non-superconducting quarks which might be present in the system. We also make the (safer) assumption that the neutrino mean free path is much smaller than the dimensions of the astrophysical object and several orders of magnitude greater than the quark mean free path, meaning that the system cools by neutrino diffusion.

In a such a sphere of quark matter, the diffusion equation for energy transport is

$$C_V \frac{dT}{dt} = -\frac{1}{r^2}\frac{\partial L_\nu}{\partial r}\,, \tag{1}$$

where $C_V$ is the specific heat per unit volume of quark matter, $T$ is the temperature, and $r$ is the radius. The neutrino energy luminosity for each neutrino type, $L_\nu$, depends on the neutrino mean free path and the spatial gradients in temperature. It is approximated by

$$L_\nu \cong -6\int dE_\nu \, \frac{c}{6\pi^2}\, E_\nu^3 r^2 \lambda(E_\nu)\frac{\partial f(E_\nu)}{\partial r}\,, \tag{2}$$

where $c$ denotes the speed of light in vacuum. In our analysis we assume that neutrino interactions are dominated by the neutral current scattering common to all neutrino types. Consequently, we take the same neutrino and anti-neutrino mean free path for every neutrino flavor, giving rise to the factor of six in Eq. (2). The equilibrium Fermi distribution, $f(E_\nu)$, and the (scattering) mean free path, $\lambda(E_\nu)$, are integrated over all neutrino energies, $E_\nu$.

The solution to the diffusion equation will also depend on the size of the system, the radius $R \sim 10$ km. The temporal behavior is characterized by a time scale $\tau_c$, which is proportional to the inverse cooling rate and can hence be deduced from Eq. (1). The characteristic time

$$\tau_c(T) = C_V(T)\frac{R^2}{c\langle\lambda(T)\rangle}\,, \tag{3}$$

is a strong function of the ambient matter temperature since it depends on the matter's specific heat and the neutrino mean free path. This applies to a system characterized by the radial length $R$ and the energy-weighted average of the mean free path, $\langle\lambda(T)\rangle$. Following our general treatment of the superconducting gap, we assume

that the temperature dependence of the specific heat is described by BCS theory. We will then use the scattering results to calculate $\langle\lambda(T)\rangle$. Furthermore, since neutrinos are in thermal equilibrium for the temperatures of interest, we may assume $\langle\lambda(T)\rangle \simeq \lambda(E_\nu = \pi T)$. Finally, we note that the diffusion approximation is only valid when $\lambda \ll R$ and will thus fail for very low temperatures, when $\lambda \sim R$.

# 4 A Signal of Color Superconductivity?

The results of our calculations are summarized in Figure **??**. We have taken the temperature dependence of the gap (long dashed curve) from BCS theory, $\Delta(T)/\Delta_0 = \sqrt{1-(T/T_c)^2}$, where $\Delta_0$ is the zero-temperature gap at a given density. The specific heat (dot-dashed curve) is also taken from the mean-field result, and is peaked around $T = T_c$ as expected in a second-order phase transition. With our result for the neutrino mean free path (short dashed curve), we combine factors to obtain the characteristic diffusion time (solid line), shown as a ratio to that found in a system of free quarks.

The consequences of these results are interpreted as follows. The early cooling rate, around $T_c$, is influenced mainly by the peak in the specific heat associated with the second order phase transition (the neutrino mean free path is not strongly affected when $\Delta \ll T$). Subsequently, as the matter cools, both $C_V$ and $\lambda^{-1}$ decrease in a non-linear fashion for $\Delta \sim T$. Upon further cooling, when $\Delta \gg T$, both $C_V$ and $\lambda^{-1}$ decrease exponentially. Both of these effects accelerate the cooling process at later times.

We conclude that if the core of a neutron star formed in the aftermath of a supernova contains a large amount of quark matter at sufficiently high temperature and density, and if the associated neutrino signal can be detected on Earth, a unique temporal profile would be observed. Specifically, we expect a brief interval during which the cooling would slow around $T \sim T_c$, signified by a period of reduced neutrino detection. This would be followed by a brief burst of neutrinos after the temperature falls well below $T_c$ and the quasi-quarks decouple from the thermal neutrinos.

We note that many real-world complications would weaken or disrupt this signal, as explained in Ref. [4]. Primary among them are the presence of strange quarks and the likely existence of a hadronic shell of nuclear matter covering the core, opaque to neutrinos, which would even out a sharp signal. Furthermore, ours is in fact a generic prediction for any second-order phase transition, applied here to color superconductivity given our understanding of proto-neutron star evolution and the phase diagram of QCD. However, given the real prospect of detecting neutrinos emitted from a future supernova event, transport processes like the ones we discuss here might someday serve as a reliable probe of the properties of extremely dense matter.

I am pleased to thank Sanjay Reddy, my collaborator in the work described here.

I am also grateful to the organizers of this conference and the staff of Nordita for their hospitality and support. This work was also supported by USDOE Grant DE-FG02-88ER40388.

# References

[1] K. Rajagopal and F. Wilczek, hep-ph/0011333; T. Schafer and E. V. Shuryak, nucl-th/0010049.

[2] M. Prakash, J. M. Lattimer, J. A. Pons, A. W. Steiner, and S. Reddy, astro-ph/0012136.

[3] P. Jaikumar and M. Prakash, Phys. Lett. B **516**, 345 (2001).

[4] G. W. Carter and S. Reddy, Phys. Rev. D **62**, 103002 (2000).

# Color-flavor locking in strange stars, strangelets, and cosmic rays

*Jes Madsen*
*Institute of Physics and Astronomy*
*University of Aarhus*
*DK-8000 Århus C, DENMARK*

## 1 Introduction

Three topics with relation to color superconductivity in strange quark matter are discussed. 1) The $r$-mode instability in strange stars, which is consistent with the existence of "ordinary" strange quark matter stars but inconsistent with strange stars in a pure color-flavor locked state. 2) Color-flavor locked strangelets, which are more bound than normal strangelets, and have a different charge-mass relation. 3) Estimates of the strangelet flux in cosmic rays, which is relevant for strangelet detections in upcoming cosmic ray space experiments.

## 2 $r$-mode instabilities in strange stars

As discussed in several talks during this conference, it is not an easy task to distinguish observationally between neutron stars and strange stars, and it is even more difficult to tell the difference between "ordinary" strange stars and strange stars composed of color-flavor locked (CFL) quark matter and/or quark matter with a two-flavor color superconducting phase (2SC). Precise mass and radius measurements may offer a way because strange stars are generally more compact than neutron stars. Differences in neutrino cooling properties could be another possibility. While some data can be interpreted as being in favor of at least a few objects being strange stars, the situation is still not convincingly settled [1, 2].

Another phenomenon in compact stars has turned out to be a sensitive probe of quark matter properties. This is the $r$-mode instability, which is a generic instability in all rotating compact stars in the absence of viscous forces [3, 4, 5]. The instability involves horisontal mass-currents in the stellar fluid. These currents couple to gravitational wave emission (like magnetic quadropole radiation). In a rotating star there are $r$-modes which are counter-rotating as seen from the stellar rest frame, but forward-rotating as seen from infinity. Gravitational wave emission taps positive

energy and angular momentum from the mode, which strengthens the mode in the stellar frame, so the mode is inherently unstable for any rate of rotation.

Viscosity may, however, prevent the mode from growing. In ordinary neutron stars, the combination of shear and bulk viscosities, and in particular the effect of "surface rubbing" [6] between the inner fluid and the solid part of the stellar crust dampens the $r$-mode instability significantly, leaving an interesting regime only for very high temperature and rotation rates close to the mass-shedding limit (the so-called Kepler limit, where the equatorial centripetal and gravitational accelerations are equal).

"Ordinary" strange stars may also have solid crusts of nuclear matter, held afloat by a strong electrostatic potential at the surface of the quark phase (the electrons are not as strongly bound as the quarks, so they form a thin "atmosphere", corresponding to a strong outward directed electrostatic potential), but the maximal crust density is much smaller than for neutron stars, only $\approx 10^{11}$g cm$^{-3}$, and therefore the surface rubbing is far less important.

In fact, data on pulsar rotation are consistent with the strange star hypothesis if the quark matter is non-superfluid [7, 8], and if the strange stars are either completely bare (making them invisible in x-rays), or have a very thick crust (to assure an internal temperature much higher than the surface temperature; otherwise the most rapid millisecond pulsars would be in a regime with significant spin-down due to the $r$-mode instability, contrary to observations).

In contrast strange stars purely in a color-flavor locked phase are not permitted by pulsar data [8]. The main contribution to bulk viscosity in strange quark matter is the weak reaction u+d $\leftrightarrow$ s+u, whereas shear viscosity is governed by strong quark-quark scattering. If the quark pairing energy gap is $\Delta$, the characteristic time-scales for viscous damping of $r$-modes are exponentially increased by factors of $\exp(2\Delta/T)$ and $\exp(\Delta/(3T))$ respectively for bulk and shear viscosity. As the relevant temperature regime in pulsars is $T \ll 1$ MeV (except in the first few seconds after the supernova explosion) this means that viscous damping of $r$-modes essentially disappears for $\Delta > 1$ MeV, and all color-flavor locked strange matter pulsars would spin down within hours in sharp contrast to observations. Figure 1 illustrates the situation for $\Delta = 1$ MeV. Values of $\Delta$ as high as 100 MeV are often assumed; for such values the entire diagram would be $r$-mode unstable.

Thus, the $r$-mode instability seems to firmly rule out that pulsars are color-flavor locked strange stars. (In [8] I showed how electron shear viscosity and/or surface rubbing on a CFL strange star crust might stop the spin-down at rotation periods of order 10 milliseconds at intermediate temperatures. This would still be far too slow to be consistent with observations of pulsars and low-mass x-ray binaries, but even these viscous mechanisms are ruled out by the realisation, that CFL strange quark matter is charge neutral [9], with equal numbers of up, down, and strange quarks, and no electrons. Such a system is without the electron "atmosphere" needed to sustain

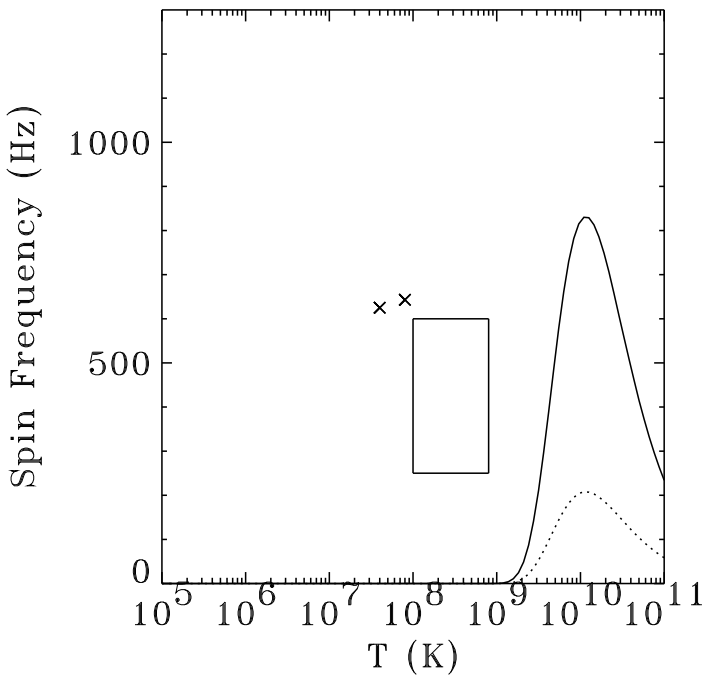


Figure 1: Critical rotation frequencies in Hz as a function of internal stellar temperature for CFL strange stars with an energy gap as small as $\Delta = 1$ MeV. Full curve is for $m_s = 200$ MeV; dotted curve for $m_s = 100$ MeV. The box marks the positions of most low-mass x-ray binaries (LMXB's), and the crosses are the most rapid millisecond pulsars known (the temperatures are upper limits). All strange stars above the curves (i.e. essentially all over the diagram) would spin down on a time scale of hours due to the $r$-mode instability, in complete contradiction to the observation of millisecond pulsars and LMXB's. Thus CFL strange stars are ruled out.

a crust; thus color-flavor locked strange stars would only exist in a "bare" variety, but these would not be able to rotate at all because of the $r$-mode instability, and are therefore not the pulsars or low-mass x-ray binaries observed).

For strange quark matter in the 2SC phase the situation is less conclusive. Now only some of the strong and weak reaction channels responsible for shear and bulk viscosities are exponentially suppressed, and the resulting viscous timescales for $r$-mode damping are increased in a much less dramatic fashion than for the CFL-phase, by factors of 9 and $(9/5)^{1/3}$ respectively for bulk and shear viscosity [8]. As seen in Figure 2 it becomes difficult to reconcile pulsar and LMXB data with 2SC-calculations, but it would be premature to rule it out.

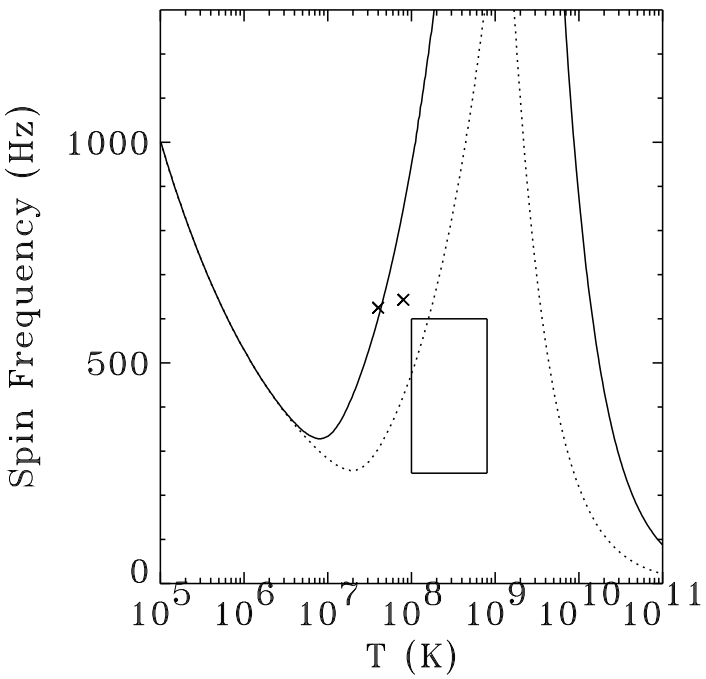


Figure 2: As Figure 1, but for 2SC-stars. Rapid spin-down happens above the parabola-like curves. The rapid millisecond pulsars are uncomfortably close to the instability regime, in particular because the temperatures are upper limits, but it would not seem appropriate to rule out 2SC strange stars on this basis alone.

The discussion above focused on strange stars, i.e. on the assumption of absolutely stable strange quark matter. If quark matter is only metastable CFL and/or 2SC phases could exist in the interior of hybrid stars, with mixed phases and ordinary hadronic matter in the outer parts. While no explicit $r$-mode studies have been performed for such systems, it is clear that the results will resemble those for ordinary neutron stars. This is because $r$-modes are located mainly in the outer parts of the star, and they are significantly damped by the boundary condition stemming from the fact that the $r$-modes cannot propagate in a solid crust.

Even pure quark matter stars could have significant substructure which could make them resemble neutron or hybrid stars in terms of $r$-mode instabilities. For instance, if the density profile of the star is such that only the central region is in the CFL phase, but the outer part in 2SC, then crystalline like structures like the LOFF-phase could form [10], and a surface rubbing effect might appear, suppressing the $r$-modes.

Finally magnetic fields and the exact nature of the superfluid vortices could be important. However, the conclusion that pure CFL strange stars are ruled out by the $r$-mode studies appears to be robust.

# 3 Color-flavor locked strangelets

If quark matter is in a color-flavor locked phase, it is because this phase has lower energy than other possible phases. In particular, this means that metastability or even absolute stability of strange quark matter becomes more likely than hitherto assumed, based on calculations for "ordinary" strange quark matter [1, 2]. For relevant ranges of strange quark mass, the gain in energy per baryon for bulk strange quark matter is roughly 100 MeV at fixed bag constant for $\Delta = 100$ MeV.

This also makes it relevant to reconsider the properties of finite size quark matter lumps, strangelets, for color superconducting strange quark matter. A first attempt in this direction was a study of color-flavor locked strangelets within the framework of the multiple-reflection expansion of the MIT bag model [11]. In this approach the total energy (mass) of a strangelet can be written as

$$E = \sum_i (\Omega_i + N_i \mu_i) + (\Omega_{\mathrm{pair},V} + B)V, \tag{1}$$

where the sum is over flavors, $B$ is the bag constant, $N_i$ and $\mu_i$ are quark number and chemical potential, $\Omega_{\mathrm{pair},V} \approx -3\Delta^2\mu^2/\pi^2$ is the binding energy from pairing ($\mu$ is the average quark chemical potential), and the thermodynamic potential of quark flavor $i$ is a sum of volume, surface, and curvature terms derived from a smoothed density of states.

Apart from the pairing energy another crucial difference relative to non-CFL strangelet calculations is the equality of all quark Fermi momenta in CFL strange quark matter. This property, which leads to charge neutrality in bulk without any need for electrons [9], is due to the fact that pairing happens between quarks of different color and flavor, and opposite momenta $\vec{p}$ and $-\vec{p}$, so it is energetically favorable to fill all Fermi seas to the same Fermi momentum, $p_F$.

As illustrated in Figure 3, color-flavor locked strangelets have an energy per baryon, $E/A$, that behaves much like that of ordinary strangelets as a function of $A$. For high $A$ a bulk value is approached, but for low $A$ the finite-size contributions from surface tension and curvature significantly increases $E/A$, making the system less stable. The main difference from ordinary strangelet calculations is the overall drop in $E/A$ due to the pairing contribution, which is of order 100 MeV per baryon for $\Delta \approx 100$ MeV for fixed values of $m_s$ and $B$. Since $\Omega_{\mathrm{pair},V} \propto \Delta^2$, the actual energy gain is of course quite dependent on the choice of $\Delta$.

A significant distinction between the properties of ordinary strangelets and CFL strangelets lies in the charge properties. They have in common a very small charge

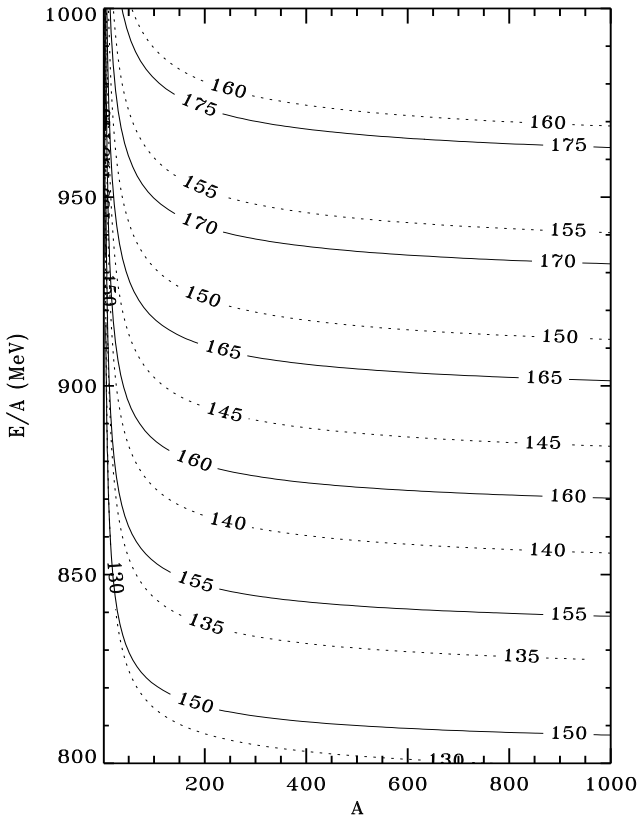


Figure 3: Energy per baryon in MeV as a function of $A$ for ordinary strangelets (dashed curves) and CFL strangelets (solid curves) for $B^{1/4}$ in MeV as indicated, $m_s = 150$ MeV, and $\Delta = 100$ MeV.

per mass unit relative to nuclei, but the exact relation is quite different, and this may provide a way to test color-flavor locking experimentally if strangelets are found in accelerator experiments or (perhaps more likely) in cosmic ray detectors. Ordinary strangelets have (roughly) [12, 13, 14]

$$Z \approx 0.1 \left(\frac{m_s}{150 \text{ MeV}}\right)^2 A; \quad A \ll 10^3; \tag{2}$$

$$Z \approx 8 \left(\frac{m_s}{150 \text{ MeV}}\right)^2 A^{1/3}; \quad A \gg 10^3. \tag{3}$$

In contrast, CFL strangelets are described by [11]

$$Z \approx 0.3 \left(\frac{m_s}{150 \text{ MeV}}\right) A^{2/3}. \tag{4}$$

This relation can easily be understood in terms of the charge neutrality of bulk CFL strange quark matter [9] with the added effect of the suppression of s-quarks near the surface, which is responsible for (most of) the surface tension of strangelets. This leads to a reduced number of negatively charged s-quarks in the surface layer; thus a total positive quark charge proportional to the surface area or $A^{2/3}$.

In fact, a similar effect becomes important even in ordinary strangelets, meaning that the standard $A^{1/3}$-result breaks down at very high $A$ [15]. And even more important, this effect is large enough to rule out a potential disaster scenario, where negatively charged strangelets produced in heavy ion colliders could grow by nucleus absorption and swallow the Earth. While ordinary strange quark matter can be negatively charged in bulk if the one-gluon exchange $\alpha_S$ is very prominent [12], the added positive surface charge due to massive s-quark suppresssion is sufficient to make the overall quark charge positive for a large range of $A$, thus preventing any such disaster [15].

Naturally, only first steps have been made in the effort to describe properties of color-flavor locked strangelets. First of all, the MIT bag model is a phenomenological approximation to strong interaction physics; it is not QCD. Secondly, while finite-size effects were included in the free quark energy calculations, such (unknown) higher order terms were not taken into account in the pairing energy. This approximation seems warranted as long as $\Omega_{\rm pair}$ itself is a perturbation to $\Omega_{\rm free}$. And thirdly, quark level shell effects were only taken into account in an average sense via the smoothed density of states described as a sum of volume, surface and curvature terms. While this is an excellent approximation to the average strangelet properties [16], it misses the interesting stabilizing effects near closed shells [17, 18] that could make certain baryon number states longer lived than one might expect from a glance at Figure 3. A first attempt at approaching finite size effects in 2SC quark matter in a completely different manner is discussed in [19].

# 4 Strangelet flux in cosmic rays

Two cosmic environments could in principle harbor strangelet formation. The cosmological quark-hadron phase transition $10^{-5}$ seconds after the Big Bang, and the high density conditions in compact supernova remnants, which may be strange stars composed of quark matter rather than neutron stars.

Cosmologically produced strangelets were for a time believed to be natural dark matter candidates [17]. In that case a significant background of largely neutral strangelets (quark core charge neutralized by electrons) would be moving in our galactic halo at typical speeds of 3–400 km/sec, corresponding to the depth of the galactic gravitational potential. Several experiments have placed limits on the abundance of these nonrelativistic strangelets (sometimes called quark nuggets), but it now seems

unlikely that they could form in or survive from the very hot ($T \approx 100$ MeV) environment in the early Universe. A similar problem faces strangelet production in ultrarelativistic heavy ion collisions; it has been compared to making ice cubes in a furnace.

## 4.1 Strangelet production in collisions of strange stars

A more likely origin of cosmic ray strangelets is from collisions of binary compact star systems containing strange stars. If strange quark matter is the ground state of hadronic matter at zero pressure, it will be energetically favorable to form strange stars rather than neutron stars, and it would be expected that all the objects normally associated with neutron stars (pulsars and low-mass x-ray binaries) would actually be strange stars.

Several pulsars are observed in binary systems containing another compact star; the most famous such system called PSR1913+16 delivered convincing evidence for gravitational wave emission. Such binaries typically move in elliptical orbits, spiraling closer to each other because the system loses energy by gravity wave emission. The remaining lifetime can be estimated, and combined with estimates of the number of these binaries in our galaxy, the expected rate of binary collisions is of order $10^{-4}$ year$^{-1}$.

Several numerical studies have been performed in the literature to follow the late stages of inspiral in systems composed of two neutron stars or neutron stars orbiting black holes or white dwarfs, especially to derive the gravitational wave signatures, which are of importance for upcoming gravity wave detection experiments. No detailed calculations have been done for systems containing strange stars, and since there are significant differences in the equation of state it may be dangerous to rely on existing models. Nevertheless, certain features seem robust. While details depend on assumptions about the orbit, most collisions seem to release a fraction of the total mass (of order $10^{-4}$–$10^{-1} M_\odot$, where $M_\odot$ is the solar mass) in connection with the actual collision and via tidal disruption in the late stages of inspiral.

No realistic estimates exist at present of the mass spectrum of quark matter lumps released during the actual collision. Lumps of matter released during the tidal disruption phase are expected to be very large. Balancing the tidal force trying to disrupt the star with the surface tension force of strange quark matter leads to a typical fragment baryon number of $A \approx 4 \times 10^{38} \sigma_{20} a_{30}^3$, where $\sigma_{20} \approx 1$ is the surface tension in units of 20 MeV/fm$^3$ and $a_{30}$ is the distance between the stars in units of 30 km.

A significant fraction of the tidally released material is originally trapped in orbits around the binary stars. The typical orbital speeds of the lumps are here $0.1c$, and collisions among lumps are abundant. Assuming the kinetic energy in these collisions mainly goes to fragmentation of the lumps into smaller strangelets (i.e. that the kinetic

energy is used to the extra surface and curvature energies necessary for forming $N$ lumps of baryon number $A/N$ from the original baryon number $A$), it can be shown for typical bag model parameters that the resulting strangelet distribution peaks at mass numbers from a few hundred to about $10^3$. This is well within the interesting regime for the upcoming cosmic ray experiment Alpha Magnetic Spectrometer AMS-02 on the International Space Station [21] (a prototype AMS-01 was flown on the Space Shuttle mission STS-91 in 1998). AMS-02 is a roughly 1 m$^2$ sterad detector which will analyze the flux of cosmic ray nuclei and particles in unprecedented detail for three years or more following deployment in 2005. It will be sensitive to strangelets in a wide range of mass, charge and energy [22].

## 4.2 Strangelet flux at AMS-02

Strangelet propagation in the Milky Way Galaxy is in many ways expected to be similar to that of ordinary cosmic ray nuclei. Except for a possible background of slow-moving electrically neutral quark nuggets confined solely by the gravitational potential of the Galaxy, strangelets are charged and are therefore bound to the galactic magnetic field. They lose kinetic energy by electrostatic interactions with the interstellar medium, and they gain energy by Fermi acceleration in shock waves, for example from supernovae. Even if accelerated to relativistic speeds, scatterings on impurities in the magnetic field makes the motion resemble a diffusion process. The solar wind as well as the Earth's magnetic field become important for understanding the final approach to the detector. Also, strangelets may undergo spallation in collisions with cosmic ray nuclei, nuclei in the interstellar medium, or other strangelets.

Detailed studies of all of these phenomena have recently been started in order to understand strangelet propagation in more detail. Much depends on the charge-to-mass relation, but the details of propagation are not even well understood for ordinary nuclei, so clearly some uncertainty in the expectations for the strangelet flux at AMS is inevitable.

In the following it will be assumed that strangelets share two of the features found experimentally for nuclei, namely a powerlaw energy distribution: $N(E)dE \propto E^{-2.5}$, and an average confinement time in the galaxy of $10^7$ years. Assuming strangelets to move close to the speed of light, and ascribing one baryon number, $A$, to them all, the strangelet flux at AMS-02 would be

$$F = 3 \times 10^{12} A^{-1} (\mathrm{m}^2 \text{ y sterad})^{-1} \times R_{-4} \times M_{-2} \times V_{100}^{-1} \times t_7 \times \mathrm{GCfraction} \quad (5)$$

where $R_{-4}$ is the number of strange star collisions in our Galaxy per $10^4$ years, $M_{-2}$ is the mass of strangelets ejected per collision in units of $10^{-2} M_\odot$, $V_{100}$ is the effective galactic volume in units of 100 kpc$^3$ over which strangelets are distributed, and $t_7$ is the average confinement time in units of $10^7$ years. All these factors are of order unity if strange matter is absolutely stable, though each with significant uncertainties.

Finally, GCfraction is the fraction of strangelets surviving the geomagnetic cutoff. Taking this cutoff to be at rigidity 6 GeV/c, assuming the standard $E^{-2.5}$ powerlaw for the energy distribution with a cutoff at $\beta \equiv v/c = 0.01$, and assuming a charge-mass relation $Z = 0.3A^{2/3}$ as derived for color-flavor locked strangelets, the resulting strangelet flux at AMS-02 becomes

$$F = 5 \times 10^5 (\mathrm{m}^2 \text{ y sterad})^{-1} \times R_{-4} \times M_{-2} \times V_{100}^{-1} \times t_7. \quad (6)$$

By coincidence, this result (valid for $A < 6 \times 10^6$; for larger $A$ GCfraction equals 1 and the previous expression applies) is independent of strangelet mass.

As should be evident from the discussion above, there are many uncertainties involved in the calculation of the strangelet flux at AMS-02. A systematic study of these issues has been initiated and should significantly improve our understanding of the strangelet production and propagation. But ultimately we must rely on experiment. So far it is reassuring, that the simple flux estimates above lead us to expect a very significant strangelet flux in the AMS-02 experiment.

A discovery of strangelets would of course be a very significant achievement in itself. Getting data on the charge-to-mass relation may even allow an experimental test of color-flavor locking in quark matter.

This work was supported in part by The Danish Natural Science Research Council, and The Theoretical Astrophysics Center under the Danish National Research Foundation. I thank Jack Sandweiss and Dick Majka for discussions and collaboration on strangelet detection with AMS-02.

# References

[1] For a review and references on the physics and astrophysics of "ordinary" strange quark matter, see J. Madsen, Lecture Notes in Physics **516**, 162 (1999) [arXiv:astro-ph/9809032].

[2] For reviews and references on color superconducting quark matter, see M. Alford, Annu. Rev. Nucl. Part. Sci. **51**, 131 (2001) [arXiv:hep-ph/0102047]; K. Rajagopal and F. Wilczek, arXiv:hep-ph/0011333.

[3] N. Andersson, Astrophys. J. **502**, 708 (1998).

[4] J. L. Friedman and S. M. Morsink, Astrophys. J. **502**, 714 (1998).

[5] For a review on $r$-mode instabilities, see N. Andersson and K. D. Kokkotas, Int. J. Mod. Phys. **D10**, 381 (2001).

[6] L. Bildsten and G. Ushomirsky, Astrophys. J. **529**, L33 (2000).

[7] J. Madsen, Phys. Rev. Lett. **81**, 3311 (1998).

[8] J. Madsen, Phys. Rev. Lett. **85**, 10 (2000).

[9] K. Rajagopal and F. Wilczek, Phys. Rev. Lett. **86**, 3492 (2001).

[10] M. Alford, J. Bowers and K. Rajagopal, Phys. Rev. D **63**, 074016 (2001).

[11] J. Madsen, Phys. Rev. Lett. **87**, 172003 (2001).

[12] E. Farhi and R. L. Jaffe, Phys. Rev. D **30**, 2379 (1984).

[13] M. S. Berger and R. L. Jaffe, Phys. Rev. C **35**, 213 (1987); **44**, 566(E) (1991).

[14] H. Heiselberg, Phys. Rev. D **48**, 1418 (1993).

[15] J. Madsen, Phys. Rev. Lett. **85**, 4687 (2000).

[16] J. Madsen, Phys. Rev. D **50**, 3328 (1994).

[17] E. P. Gilson and R. L. Jaffe, Phys. Rev. Lett. **71**, 332 (1993).

[18] J. Schaffner-Bielich, C. Greiner, A. Diener and H. Stöcker, Phys. Rev. C **55**, 3038 (1997).

[19] P. Amore, M. C. Birse, J. A. McGovern and N. R. Walet, arXiv:hep-ph/0110267.

[20] E. Witten, Phys. Rev. D **30**, 272 (1984).

[21] The AMS homepage is http://ams.cern.ch.

[22] A. Chikanian, J. Madsen, R. Majka and J. Sandweiss, work in progress.

# Discussion

**F. Weber (Notre Dame):** In your flux determination, did you assume that all neutron stars are in fact strange stars or that there exist two separate families of compact stars?

**Madsen:** All compact stars were assumed to be strange stars. Coexistence of two separate families is very unlikely if strange matter is the ground state at zero external pressure, since the Galaxy would be "polluted" by quark lumps from binary pulsar collisions. These lumps would trigger transition to strange stars in supernova cores.

**F. Sannino (Nordita):** How do you disentangle (CFL) or strange droplets experimentally? What is the signature?

**Madsen:** Strangelets have very low charge for a given baryon number compared to nuclei. CFL-strangelets have a charge-mass relation that differs from "ordinary" strangelets.

**J.E. Horvath (Sao Paulo):** A low charge-to-mass ratio for strangelets would not allow substantial acceleration in supernova shocks, thus the spectrum (and also the confinement time) is not necessarily the one measured in cosmic rays. How does this change the estimates of the rates in the expected range of center-of-mass energies?

**Madsen:** Clearly the propagation in the Galaxy requires further study, and we are trying to address the relevant mechanisms in detail. One should keep in mind, though, that these issues are not fully understood even for ordinary cosmic ray nuclei.

# Diquark Properties and the TOV Equations

*David Blaschke*[a,1], *Sverker Fredriksson*[b,2] *and Ahmet Mecit Öztaş*[b,c,3]

[a] *Department of Physics, University of Rostock*
[b] *Department of Physics, Luleå University of Technology*
[c] *Department of Physics, Hacettepe University*

## 1 Introduction: Diquarks

This is a status report of our work on quark/diquark effects inside compact astrophysical objects. It goes somewhat in excess of the results shown at the workshop.

The word diquark is due to Gell-Mann in 1964 [1]. The idea of a two-quark correlation has now spread to many areas of particle physics, motivated by phenomenology, lattice calculations, QCD or instanton theory. Now there are some 1200 papers on diquarks, some of which were covered by a review in 1993 [2]. The speaker (S.F.) has an updated database with diquark papers.

Although there is no consensus about diquark details, it seems certain that a $(ud)$ quark pair experiences some attraction when in total spin-0 and colour-$\mathbf{3^*}$. Nuclear matter should also be subject to such pairing, maybe in some new way, *e.g.*, as in the nuclear EMC effect [3]. Quark pairing should also affect a (hypothetical) quark-gluon plasma (QGP), and by now there are more than 300 papers built on this idea. Many of these assume that the correlation is like the one between electrons in a superconductor, with diquarks being the Cooper pairs of QCD [4]. The notion of "superconducting quark matter" is due to Barrois in 1977 [5]. Current efforts owe much to the review paper by Bailin and Love [6], and to work by Shuryak, Wilczek and collaborators [7, 8]. Diquarks in a QGP have also been analysed "classically", with thermodynamics, or field theory [9, 10].

*Astrophysical* diquarks gained popularity about a decade ago, when they were suggested to influence the supernova collapse and "bounce-off" [11, 12, 13, 14], and to enhance the neutrino cooling of quark-stars. The latter effect is now subject to much research [15, 25].

[1]Postal address: D-18051 Rostock, Germany; E-mail: david@darss.mpg.uni-rostock.de
[2]Postal address: SE-97187 Luleå, Sweden; E-mail: sverker@mt.luth.se
[3]Postal address: TR-06532 Ankara, Turkey; E-mail: oztas@hacettepe.edu.tr

Here we study some features of compact objects that would be sensitive to diquark condensation in a QGP. The form factor of the diquark correlation and the quark isospin (a)symmetry due to presence of electrons will be given special attention.

There are many situations where a QGP with diquarks might play a role: (i) In a *quark star*, which might appear as dark matter [17, 18]; (ii) In a *hybrid/neutron star*, surrounded by a hadronic crust; (iii) In a *supernova*, or a *'hypernova' gamma-ray burster*, where diquarks might trigger neutrino bursts and the bounce-off; (iv) In the *primordial plasma* at the Big Bang, where diquarks might have delayed the hadronisation.

## 2 Formalism and Results

We use the BCS theory of colour superconductivity [6, 7, 8]. The gap $\Delta$ can be seen as the gain in energy due to the diquark correlation. Another gap, $\phi$, is related to the quark-antiquark condensate. The thermodynamical grand canonical potential, $\Omega$, is minimised in its variables, resulting in an equation of state (EOS) and other relations. We follow the approach of [19] for the $\Omega$ and generalise it for isospin asymmetry between $u$ and $d$ quarks [20]

$$
\begin{aligned}
&\Omega(\phi,\Delta;\mu_B,\mu_I,\mu_e;T) = \\
&= \frac{\phi^2}{4G_1} + \frac{\Delta^2}{4G_2} - \frac{1}{12\pi^2}\mu_e^4 - \frac{1}{6}\mu_e^2 T^2 - \frac{7}{180}\pi^2 T^4 \\
&-2\int_0^\infty \frac{q^2 dq}{2\pi^2}(N_c-2)\times\Big\{2E_\phi + \\
&+T\ln\left[1+\exp\left(-\frac{E_\phi-\mu_B-\mu_I}{T}\right)\right] + T\ln\left[1+\exp\left(-\frac{E_\phi-\mu_B+\mu_I}{T}\right)\right] \\
&+T\ln\left[1+\exp\left(-\frac{E_\phi+\mu_B-\mu_I}{T}\right)\right] + T\ln\left[1+\exp\left(-\frac{E_\phi+\mu_B+\mu_I}{T}\right)\right]\Big\} \\
&-4\int_0^\infty \frac{q^2 dq}{2\pi^2}\times\Big\{E_- + E_+ + \\
&+T\ln\left[1+\exp\left(-\frac{E_- -\mu_I}{T}\right)\right] + T\ln\left[1+\exp\left(-\frac{E_- +\mu_I}{T}\right)\right] \\
&+T\ln\left[1+\exp\left(-\frac{E_+ -\mu_I}{T}\right)\right] + T\ln\left[1+\exp\left(-\frac{E_+ +\mu_I}{T}\right)\right]\Big\} + C\ , \qquad (1)
\end{aligned}
$$

where the subtraction $C = -\Omega((\phi_0^{vac})^2, 0; 0, 0, 0; 0)$ has been introduced to make (1) finite and to assure that pressure and energy density of the vacuum at $T = \mu = 0$ vanish. Thus at the boundary of a compact quark matter object, where the quark-condensate $\phi_0$ changes, a pressure difference arises, which is necessary for confining the system, at least for small masses.

Instead of the chemical potentials $\mu_u$, $\mu_d$ of $u$ and $d$ quarks, one uses [20] those of baryon number, $\mu_B = (\mu_u + \mu_d)/2$, and isospin asymmetry, $\mu_I = (\mu_u - \mu_d)/2$. Then, if beta equilibrium with electrons holds, $\mu_e = -2\mu_I$. The particle densities are given by $n_B = n_u + n_d = -\partial\Omega/\partial\mu_B$, $n_I = n_u - n_d = -\partial\Omega/\partial\mu_I$ and $n_e = -\partial\Omega/\partial\mu_e = -\mu_e^3/(3\pi^2)$. Charge neutrality means $n_B + 3n_I - 6n_e = 0$, and isospin symmetry $n_I = 0$.

The dispersion relations are

$$E_\phi = \sqrt{q^2 + (m + F^2(q)\phi)^2} \quad \text{and} \quad E_\pm = (E_\phi \pm \mu_B)\sqrt{1 + \frac{F^4(q)\Delta^2}{(E_\phi \pm \mu_B)^2}}, \qquad (2)$$

where $F(q)$ is a form factor for two-quark correlations.

We use $T = 0$ and $m = 0$, and start by finding the gaps $\phi_0$ and $\Delta_0$ that minimise $\Omega$. These values give the EoS as

$$\Omega(\phi_0, \Delta_0; \mu_B, \mu_I, \mu_e; T = 0) = \epsilon - \mu_B n_B - \mu_I n_I - \mu_e n_e = -P, \qquad (3)$$

where $\epsilon$ is the energy density and $P$ the pressure.

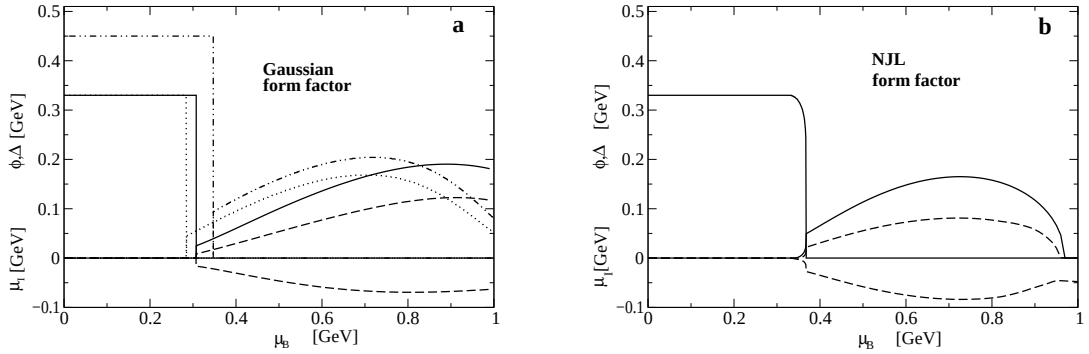


Figure 1: The gaps $\phi$, $\Delta$ and the isospin asymmetry chemical potential $\mu_I$ as functions of $\mu_B$ for (a) Gaussian, and (b) NJL form factors. *Solid lines* are with isospin symmetry (and no electrons), *Dashed lines* are with beta equilibrium. *Dotted lines* in (a) are with isospin symmetry for $\Lambda_G = 0.8$ GeV and $\phi_0^{vac} = 0.33$ GeV. *Dashed double-dotted lines* in (a) are with isospin symmetry for $\Lambda_G = 0.8$ GeV and $\phi_0^{vac} = 0.45$ GeV (giving the same vacuum pressure as with the solid lines).

We use the form factors suggested by Schmidt *et al.* [21], who fitted those to masses and decay properties of light mesons. The following special cases are consid-

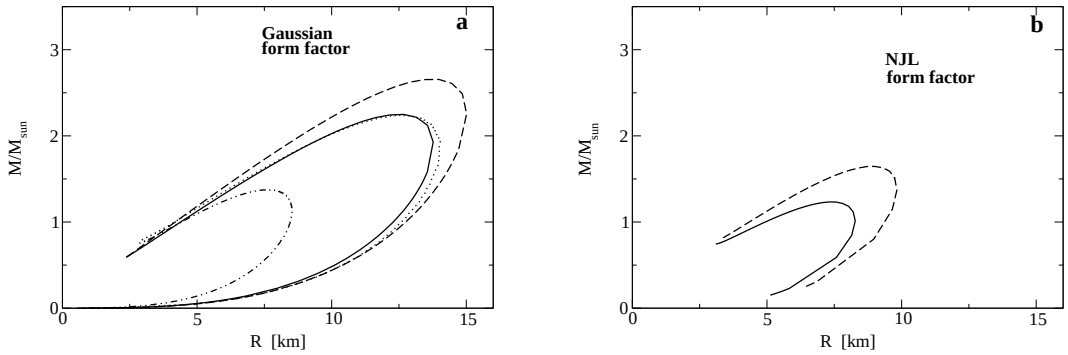


Figure 2: a) The mass ratio $M/M_{sun}$ *vs.* the radius $R$ of a compact object according the the TOV equation. The curves correspond to the same situations as in Fig. 1.

ered: (i) Gaussian: $F^2(q) = \exp(-q^2/\Lambda_G^2)$; (ii) Lorentzian: $F^2(q) = 1/[1 + (q/\Lambda_L)^4]$; (iii) cutoff NJL: $F^2(q) = \Theta(1 - q/\Lambda_{NJL})$. Here $\phi_0 = 0.33$ GeV, $\Lambda_G = 1.025$ GeV, $\Lambda_L = 0.8937$ GeV and $\Lambda_{NJL} = 0.9$ GeV [21]. We contrast this to $\Lambda_G = 0.8$ GeV used in [19]. Fig. 1 shows our results for the Gaussian and NJL form factors, and for two extreme cases: (i) isospin symmetry (equal numbers of $u$ and $d$ quarks), and (ii) beta equilibrium and charge neutrality. In the former case charge is balanced *outside* the object. In the latter, the electron fraction is small, and $n_d \approx 2n_u$. Here $\mu_I$ is given in the lower part of the figures. We also test the sensitivity on the parameter $\Lambda_G$. There is now the choice to either keep $\phi_0^{vac}$ fixed, or to change it so that the vacuum pressure $(\phi_0^{vac})^2/(4G_1)$ is kept fixed.

The EoS is used as input to the standard Tolman-Oppenheimer-Volkoff equations [22] for an equilibrium (spherical) fluid (see also [23]):

$$\frac{dP(r)}{dr} = -\frac{[\epsilon(r) + P(r)][m(r) + 4\pi r^3 P(r)]}{r[r - 2m(r)]}, \tag{4}$$

$$m(r) = 4\pi \int_0^r \epsilon(r') r'^2 dr'. \tag{5}$$

The equations are iterated in $r$, starting with some value $\epsilon_0$ at $r = 0$. The procedure stops when $P = 0$, which defines the radius $R$ of the object, and $M = m(R)$ is plotted *vs.* $R$, see Fig. 2. Each $\epsilon_0$ value results in one point in the plot, with unique values also of $\mu_B$ and $\mu_I$. The graph becomes a backbending spiral, with $\epsilon_0$ and $\mu_B$ increasing along the curve. Solutions on left-going parts of the curve are unstable.

# 3 Conclusions and Outlook

The diquark form factor and the isospin (a)symmetry are important inside a quark/ diquark star. They can make a difference of up to two solar masses, as for its maximal mass.

We now have results also for $0 < T < \Delta$, where condensate-free states can occur in intervals of $\mu_B$ [24]. These correspond to an interaction-free plasma, and appear as "bumps" in the TOV curves. They might be relevant as phase transitions inside a collapsing system (supernova). The QGP might suddenly enter a diquark phase, whereafter it again becomes a free-quark state just before the bouncing [31]. We also intend to study such events for the Big Bang plasma. Maybe a transition into a diquark phase resulted in a release of neutrinos, just as with the cosmic microwave background. The neutrino energy would have been of the order of $\Delta$, but now cooled to keV energies.

**Acknowledgements**

SF and AÖ are grateful to the Organisers for providing a very inspiring atmosphere. SF would like to thank the University of Rostock, and DB and AÖ the Luleå University of Technology for hospitality during visits. Some of these have been supported by the European Commission within the Erasmus programme.

# References

[1] M. Gell-Mann, Phys. Lett. **8**, 214 (1964).

[2] M. Anselmino *et al.*, Rev. Mod. Phys. **65**, 1199 (1993).

[3] S. Fredriksson, Phys. Rev. Lett. **52**, 724 (1984).

[4] S. Fredriksson, M. Jändel and T.I. Larsson, Phys. Rev. Lett. **81**, 2179 (1983).

[5] B.C. Barrois, Nucl. Phys. **B129**, 390 (1977).

[6] D. Bailin and A. Love, Phys. Rep. **107**, 325 (1984).

[7] R. Rapp *et al.*, Phys. Rev. Lett. **81**, 53 (1988).

[8] M. Alford, K. Rajagopal and F. Wilczek, Phys. Lett. **B450**, 325 (1999).

[9] S. Ekelin, in *Strong Interactions and Gauge Theories*, p. 559, Ed. J. Tran Thanh Van (Editions Frontières, Gif-sur-Yvette, 1986).

[10] J.F. Donoghue and K.S. Sateesh, Phys. Rev. **D38**, 360 (1988); K.S. Sateesh, Phys. Rev. **D45**, 866 (1992).

[11] S. Fredriksson, in *Workshop on Diquarks*, p. 22, Eds. M. Anselmino and E. Predazzi (World Scientific, Singapore, 1989).

[12] D. Kastor and J. Traschen, Phys. Rev. **D44**, 3791 (1991).

[13] J.E. Horvath, O.G. Benvenuto and H. Vucetich, Phys. Rev. **D44**, 3797 (1991); O.G. Benvenuto, H. Vucetich and J.E. Horvath, Nucl. Phys. Proc. Suppl. **24B**, 160 (1991); J.E. Horvath, Phys. Lett. **B294**, 412 (1992); J.E. Horvath, J.A. de Freitas Pacheco and J.C.N. de Araujo, Phys. Rev. **D46**, 4754 (1992).

[14] P. Sahu, Int. J. Mod. Phys. **E2**, 647 (1993).

[15] D. Blaschke, T. Klähn and D.N. Voskresensky, Astrophys. J. **533**, 406 (2000); D. Blaschke, H. Grigorian and D.N. Voskresensky, A & A **368**, 561 (2001).

[16] G.W. Carter and S. Reddy, Phys. Rev. **D62**, 103002 (2000); P. Jaikumar and M. Prakash, Phys. Lett. **B516**, 345 (2001).

[17] E. Witten, Phys. Rev. **D30**, 272 (1984).

[18] S. Fredriksson *et al.*, in *Dark Matter in Astrophysics and Particle Physics*, p. 651, Eds. H.V. Klapdor-Kleingrothaus and L. Baudis (Inst. of Physics, Bristol & Philadelphia, 1998).

[19] J. Berges and K. Rajagopal, Nucl. Phys. **B538**, 215 (1999).

[20] O. Kiriyama, S. Yasui and H. Toki, hep-ph/0105170 (2001).

[21] S. Schmidt, D. Blaschke and Yu. Kalinovsky, Phys. Rev. **C50**, 435 (1994).

[22] J.R. Oppenheimer and G. Volkoff, Phys. Rev. **55**, 377 (1939).

[23] N.K. Glendenning, *Compact Stars* (Springer, New York & London, 2000).

[24] D. Blaschke, S. Fredriksson, H. Grigorian and A. Öztas, in preparation.

[25] D.K. Hong, S.D. Hsu and F. Sannino, Phys. Lett. **B516**, 362 (2001).

# Discussion

**A. Thampan:** Should one not see a signature (say in terms of phase transitions or so) in the $P$ *vs.* $\rho$ (EoS) relationships?

**Fredriksson:** For some extreme parameter values bumps occur in, *e.g.*, $M$ *vs.* $R$ and $P$ *vs.* $\epsilon$, and certainly also in a $P$ *vs.* $\rho$, although we did plot the latter. For the case of beta equilibrium, these transitions are smoother in the TOV graphs. The bumps are clearer for $T > 0$, as mentioned above.

**J.E. Horvath:** Do diquarks disappear suddenly in this model? Could you identify what makes the matter self-bound?

**Fredriksson:** Not suddenly in time, because these are equilibrium solutions. But diquarks disappear "suddenly" when other parameters change, *e.g.*, $\mu_B$ (see "NJL"). A strange star is self-bound by gravity at high masses, but also due to our "vacuum pressure" ($C$).

**Unknown:** Are the stars beyond the mass peak stable?

**Fredriksson:** Our approach does not tell, but states with $\frac{\partial M}{\partial \epsilon} < 0$ are usually prescribed to be unstable [23].

# Diquark degrees of freedom in the EOS and the compactness of compact stars

*J. E. Horvath, G. Lugones*
*Instituto Astronômico e Geofísico/Universidade de São Paulo*
*Av. M. Stéfano 4200, Agua Funda, 04301-904 São Paulo SP, BRAZIL*
and *J.A. de Freitas Pacheco*
*Observatoire de la Côte d'Azur*
*BP 4229, F-06304, Nice Cedex 4, FRANCE*

## 1 Introduction

"Old" questions of relativistic astrophysics, like the internal structure of compact stars, have received a lot of attention recently since they are very important for a solid knowledge of the QCD diagram in the low-$T$ , high $\mu$ region as discussed along this Workshop. Among the most simple forms of investigating (indirectly) the nature of high-density matter, more precisely of the equation of state connecting the pressure and the energy density; is by obtaining accurate determinations of masses and radii. A comparison of the static models generated by integration of the Tolman-Oppenheimer-Volkoff equations with observed data should reveal a great deal of information about the equation of state.

While astronomers and physicists alike have longely dreamed of such determinations we have only recently achieved sufficient accuracy to perform some key tests on selected objects, although it should be acknowledged that three decades of compact star astrophysics had produced quite clever arguments to determine masses and radii, even in the cases in which they proved to be wrong.

A paradigmatic example of the above assertions is the celebrated determination of the binary pulsar mass PSR 1913+16, believed to be accurate to the fourth decimal place [7]. Methods based on combinations of spectroscopic and photometric techniques have been recently perfectioned, and have confirmed that at least one X-ray source is significantly above the "canonical" 1.44 $M_{\odot}$; namely Vela X-1 for which a value of $1.87^{+0.23}_{-0.17}\,M_{\odot}$ has been obtained [7].

It is also possible that at least some compact stars are extremely compact, or in other words, that their radii are $\sim 30-40\%$ less than the cherished $10\,km$ for $M \sim 1\,M_{\odot}$. Indeed, this is the claim of the analysis of [4] of the binary Her X-1 ($M = 0.98 \pm 0.12\,M_{\odot}$ and $R = 6.7 \pm 1.2\,km$) and [11] in the case of the isolated

nearby RX J1856-37 ($M = 0.9 \pm 0.2\ M_\odot$ and $R = 6^{-1}_{+2}\, km$). In fact, such compactness is extremely difficult (impossible?) to model using underlying equations of state based on hadrons alone, and a "natural" alternative would be to consider deconfined matter. Naturally, these results will be checked and scrutinized for confirmation.

Could this be related to high-density deconfined matter ? Perhaps, since there is hope to achieve deconfinement densities inside compact stars. Also, there is some evidence that diquarks (e. g. a spin-0, color-antitriplet bound state of two quarks) might occur as a component in the QCD plasma (see [9] and references therein for a review). Such diquarks would be expected to be favoured by Bose statistics and they are quit helpful to model the low-energy hadronic properties. Of course, at very high densities, characterized by interquark distances less than $(10GeV^2)^{-1/2}$, diquarks lose their identity and must eventually dissolve into quarks, even if there is no clear consensus about the onset of the asymptotic regime.

According to this picture we may regard a diquark as any system of two quarks considered collectively. Diquark correlations arise in part from spin-dependent interactions between two quarks. Regardless of the exact mechanism for their origin, it is imperative to have some gain of energy (binding) for the stellar models to work (see below). The bound state is a quite strong assumption, and is not easy to prove (or disprove) in the absence of a reliable way of performing sensible calculations. As a working hypothesis (quite analogous to the well known strange matter), we shall assume simply that this bound state actually exists.

## 2 Bag-inspired quark-diquark Model

Some time ago it was the interesting controversy about the compactness of Her X-1 that prompted us [3] to consider models in which diquarks are considered fundamental digrees of freedom and treated as effective bosons. The results were derived using an effective $\lambda\phi^4$ model and a derived equation of state given in [10], shown to be valid in this case. We shall not repeat the analysis here, but just point out that (as expected) a self-bound quark-diquark mixture indeed produced very compact models (see Fig.1, curve A). In those models there are two quantities that had to be treated parametrically: the diquark mass $m_D$ and the vacuum energy density $B$. There is no relation between the two included and therefore other possibilities than the $m_D = 575MeV\ B = 57MeVfm^{-3}$ could be considered. However, it is desirable to reduce the freedom in the parameters to see whether the compactness can be altered.

## 3 QMDD Model

In a more recent attempt we have modeled the quark - diquark plasma as a relativistic gas of $u$ and $d$ quarks, and $(ud)$ diquarks. We treated non-perturbative effects in the

quark mass-density-dependent model of confinement (QMDD model) extended for the diquarks assuming $m_D = m_{D0} + C/n_B^{1/3}$, analogously to quarks. Some information on the parameter $C$ to describe absolutely stable SQM has been found in the range (155-171)$^2$ $MeV^2$ [2] based on known stability arguments. The expression for the thermodynamic potential $\Omega$ was derived in the thermodynamic limit for the QMDD model extended for bosons, and the usual thermodynamical quantities derived from $\Omega$ with some care(see [2]).

Because $\Omega$ depends on the baryon number $n_B$ through the masses $m_i$; the standard relation $P = -\Omega$ [2, 1] is not valid and we have an extra term generated by this density dependence; namely $P = -\frac{\partial(V\Omega)}{\partial V} = \sum_i \Big( -\Omega_i + n_B \frac{\partial m_i}{\partial n_B}\frac{\partial \Omega_i}{\partial m_i}\Big)$. As stressed in previous works [1], the term $n_B \frac{\partial m_i}{\partial n_B}\frac{\partial \Omega_i}{\partial m_i}$ allows the pressure to be zero at finite baryon number, playing the role of the Bag Constant B in the MIT Bag Model. Needless to say, this is a property related to the parametrization of the mass only, and does not depend on the particle statistics of the particles. However, in the case of bosons this extra term does not contribute at zero temperature. As in the standard case of massive bosons at $T = 0$ the energy density reduces to $E = \sum_i n_i m_i$. Diquarks do not contribute to the pressure as they are all in the ground state, but do contribute to the energy density, the equation of state is expected to be quite soft.

These equations have been supplemented with the conditions of equilibrium between $D$, $u$ and $d$. By imposing very general stability and equilibrium conditions we found an absolute lower limit on $m_{D0}$ $m_{D0,lim} = \frac{C}{n_b^{1/3}} = 230\Big(\frac{n_0}{n_B}\Big)^{1/3} MeV$. Electrical charge neutrality and baryon number conservation were enforced to calculate the equation of state for each $n_B$ once the parameters $(C, m_{D0})$ were given. The numerical results were scanned for stability of the mixture . Stability (and hence self-binding [14]) occurs inside a pretty large region in the $(C^{1/2}, M_{D0})$ plane. This region of absolute stability allows the existence of pure quark-diquark stars.It is curious to remark that the *same* parametrization used for simulating the confinement produces a behaviour of the diquark mass that mimics the uprising part of a gap curve (i.e. increasing binding) and thus energetically favoured diquarks as the density increases. This is *not* inconsistent with the idea of dissociation of the diquarks at still higher densities, but in any case it is not expected that a mass density-dependent model can solve the complicated structure of a theory at higher densities (see [8] for a through discussion of this and other details of the model).

# 4 Discussion

Three examples of the QMDD diquark model are shown in Fig. 1. The resulting equations of state are very soft (models B and C), as expected, but fall short to explain the claimed compactness by at least $\Delta R \sim 1\, km$, even in the most favourable

case (model B). When compared with the equation of state for quark-diquark matter presented in [3] (model A) and the softest models of MIT bag models [12] (model D) we may assert that the stellar sequences are in between the former and the latter. Diquarks may be relevant for compact star structure because they allow the existence of stable compact stars with masses of $\sim 1 M_{\odot}$ and very small radii. For comparison, the inferred radius and mass of both Her X-1 and RX J1856-37 are shown with their respective error bars. Li *et al.* models SS1 and SS2 [13](not shown in the figure) are examples of other self-bound models of the equation of state which do produce very compact stars, in fact also capable of matching the values of Her X-1 claimed in [4] and of RX J1856-37 [11]. We may state that if evidence for extreme compactness holds, diquarks may be relevant for model building .

G. Lugones acknowledges the IAG-São Paulo for hospitality and the financial support received from the Fundação de Amparo à Pesquisa do Estado de São Paulo. J.E. Horvath wishes to acknowledge the CNPq Agency (Brazil) for partial financial support. The Scientific Organizers of the meeting and Mrs. Ana Rey are acknowledged for making JEH stay in Copenhaguen a very pleasant experience and partial financial support to attend the event. I. Bombaci, S. Balberg and S. Fredricksson have shared with him several interesting discussions.

# References

[1] O. G. Benvenuto and G. Lugones, Phys. Rev D 51, 1989 (1995); G. Lugones and O. G. Benvenuto, Phys. Rev D 52, 1276 (1995)

[2] G. X. Peng, H. C. Chiang, J. J. Yang, L. Li and B. Liu, Phys. Rev. C 61, 015201 (2000).

[3] J. E. Horvath and J. A. de Freitas Pacheco, Int. J. of Mod. Phys. D 7, 19 (1998).

[4] X. -D. Li, Z. -G. Lai and Z. -R. Wang, Astro. Astrophys. 303, L1 (1995)

[5] V. M. Belyaev and Ya. I. Kogan, Phys. Lett. B 136, 273 (1984); K. D. Born, E. Laermann, N. Pirch, T. F. Walsh and P. M. Zerwas, Phys. Rev D 40, 1653 (1989).

[6] N. Isgur and J. Paton, Phys. Lett. B 124, 273 (1983); Phys. Rev D 31, 2910 (1985).

[7] M.H. van Kerkwijk, in *Proceedings of the ESO Workshop on Black Holes in Binaries and Galactic Nuclei*, eds. L. Kaper, E.M. van den Heuvel and P.A. Woudt (Springer-Verlag, 2001).

[8] G. Lugones and J.E. Horvath, in preparation.

[9] M. Anselmino, E. Pedrazzi, S. Elkin, S. Fredriksson and D.B. Litchemberg, Rev. Mod. Phys. 65, 1199 (1993).

[10] M. Colpi, S. L.Shapiro and I. Wasserman, Phys. Rev. Lett. 57, 2485 (1986).

[11] J.A. Pons, F.M. Walter, J.M. Lattimer, M. Prakash, R. Neuhäuser and Penghui An, astro-ph/0107404 (2001).

[12] O.G. Benvenuto and J.E. Horvath, MNRAS 241, 43 (1989).

[13] X-D. Li, I. Bombaci, M. Dey, J. Dey and E. P. J. van den Heuvel, Phys. Rev. Lett. 83, 3776 (1999).

[14] J.E. Horvath, Phys. Lett. B 242, 419 (1993).

## Discussion

**Dmitri Diakonov(NORDITA):** The spin-0 diquark mass in vacuum has been measured in lattice computer simulations has been measured by the Bielefeld group (M.Hess *et al.*) and claimed to be around $700\,MeV$. It seems that it is unbound.

**J.E. Horvath:** The $m_D$ appearing in the effective Lagrangian is not necessarily the vacuum mass to which calculations refer, but if the scalar diquark is indeed unbound the possibility of self-bound stars will be gone. Then diquark models may even be useful, although not for explaining small radii.

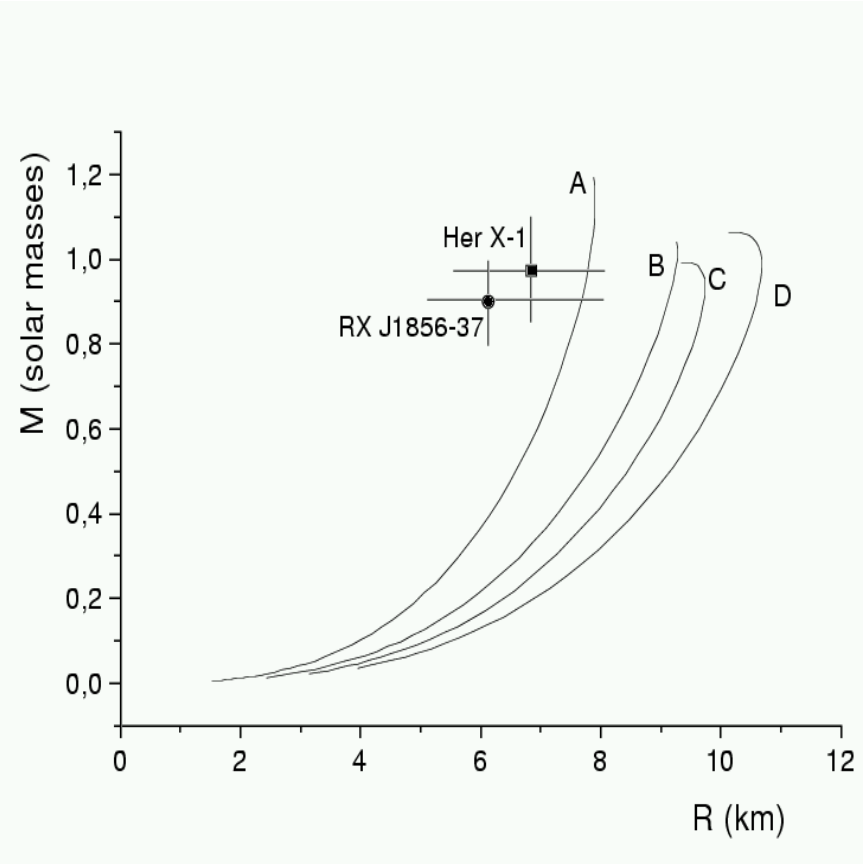


Figure 1: The mass-radius plane, stellar sequences labeled as indicated in the text.


Francesco Sannino on a tour of his colorful Zoo.

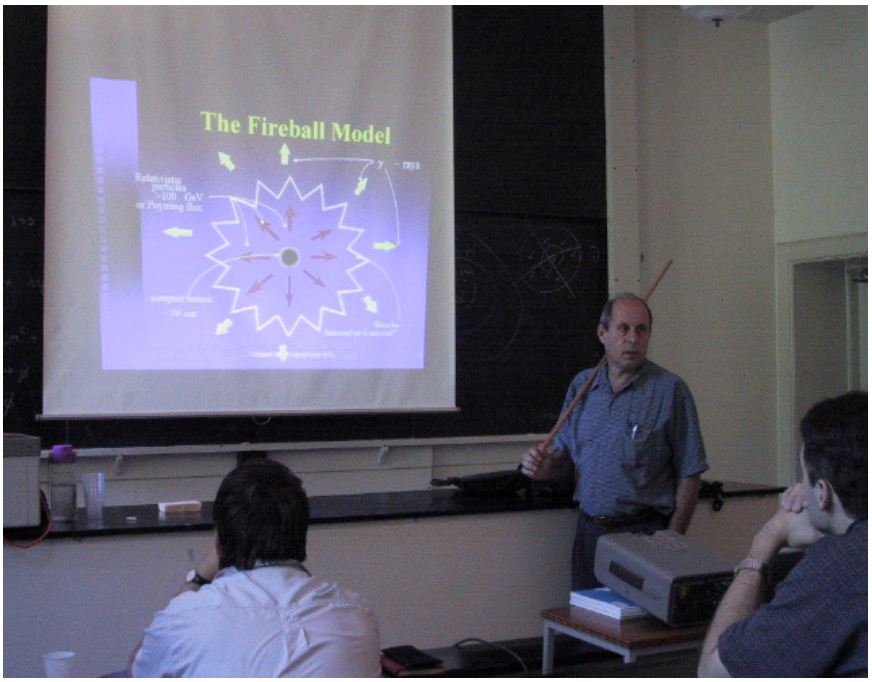


Tsvi Piran about to describe the Fireball model in Gamma Ray Bursts session.

# The Gamma Ray Burst Connection

# How to Construct a GRB Engine?

*Tsvi Piran and Ehud Nakar*
*Racah Institute for Physics*
*The Hebrew University*
*Jerusalem, ISRAEL*

## 1 Introduction

Our understanding of Gamma-Ray Bursts (GRBs) was revolutionized during the last ten years. According to the generally accepted Fireball model (see e.g. [1, 2]) the gamma-rays and their subsequent multiwavelength afterglow are produced when an ultra-relativistic flow is slowed down. All current observations, from prompt emission to late afterglow, from $\gamma$-rays via X-ray optical and IR to radio, are consistent with this model.

Observations of GRB host galaxies revealed the association of (long) GRBs (there is no information on the positions of short GRBs) with star forming Galaxies [3] and that these (long) GRBs follow the star formation rate [4, 5, 6]. There is evidence (still inconclusive) that some long bursts are associated with Supernovae [7, 8, 9, 10]. These observations suggest that the progenitors of GRBs are massive stars. There are some reasonable ideas how does a collapsing star [11, 12, 13] or a merging binary [14] produce the required $\sim 10^{51}$ergs. But it is not clear how does the GRB's "inner engine" accelerates and collimated the relativistic flow. Today this is the most interesting (and most difficult) open question concerning GRBs. This is also the most relevant question for this conference where the possibility that transitions to strange stars power GRBs has been discussed [15].

We summarize, here, the known constrains on the "inner engines" of GRBs. These constrains arise mostly from the temporal structure of GRBs. Several years ago Sari and Piran [16] have shown that variable GRBs can be generated only by internal interactions[1] within the flow. To produce internal shocks the central engine must produce a long and variable wind. This leads to a powerful **NO GO** theorem:
**Variable GRBs cannot be produced from a single explosion.**
This NO GO theorem rules out explosive GRB models that produce the relativistic flow in a single explosion. Kobayashi et al [17] have shown that the observed

[1] This interaction is usually considered as a collisionless shock. However the exact nature of the interaction is unimportant for most of our arguments.

internal shocks light curve reflects almost directly the temporal activity of the inner engine. This is the best direct evidence on what is happening at the center of the GRB.

We review the arguments leading to these conclusions. We also discuss new observational results [18, 19, 20] and a new theoretical toy model [21] that explains these observations within the internal shocks paradigm. This toy model suggests that the "inner engine" is producing a variable Lorentz factor wind by modulating the mass ejection of a roughly constant energy flow. The other alternative of modulating the energy of a constant mass flow is ruled out. We conclude by summarizing the various constrains on the "inner engines". We leave to the reader the task of examining the implications of these results to his/hers favorite model[2].

## 2 Energetics and Beaming

The most important factor in any model is the total amount of energy that it releases. Redshift measurements have lead to alarming estimates of more than $10^{54}$ergs in some bursts [23]. When factoring in the efficiency the requirements exceed a solar rest mass energy.

However, these early estimates assumed isotropic emission. Jet breaks in afterglow light curves lead to estimates of the beaming factors. When those are taken into account we find a "modest" practically constant energy release of $\sim 10^{51}$ergs [24, 25, 26, 27]. This lower energy budget allows for many possible models. At the same time it introduces an additional requirement on the central engine. It has to collimate the relativistic flow to narrow beaming angles (at times or order of $1^o - 2^o$).

We cannot estimate directly the total energy released by the "inner engine". However, here are two possible estimates: $E_\gamma$, the energy released as $\gamma$-rays and $E_K$, the kinetic energy during the adiabatic afterglow phase. Remarkably both energies are comparable. This last observation implies that the conversion efficiency of the initial relativistic kinetic energy to $\gamma$-rays must be very high.

## 3 Time Scales In GRBs - Observations

Most GRBs are highly variable. Fig 1 depicts the light curve of a typical variable GRB (GRB920627). The variability time scale, $\delta t$, is determined by the width of the peaks. $\delta t$ is much shorter (in some cases by a more than a factor of 100) then $T$, the duration of the burst. Variability on a time scale of milliseconds is seen in some long bursts [20]. However, not all bursts are variable. We stress that our discussion applies to variable bursts and it is not applicable to the small subset of smooth ones.

[2]See [22] for a discussion of the implications for possible accretion models

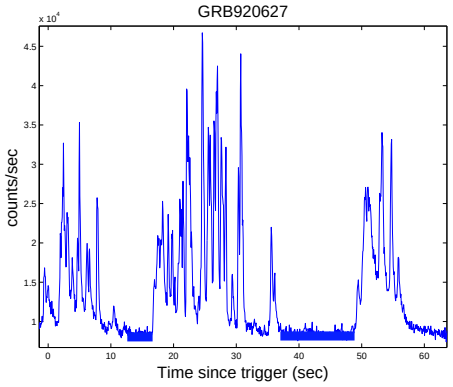


Figure 1: The light curve of GRB920627. The total duration of the burst is 52sec, while typical pulses are 0.8sec wide. Two quiescent periods lasting ∼10 seconds are marked by horizontal solid bold lines.

A comparison of the pulse width distribution and the pulse separation, $\Delta t$ , distribution, reveals an excess of long intervals [18, 19]. These long intervals can be classified as quiescent periods [28], relatively long periods of several dozen seconds with no activity. When excluding the quiescent periods we [18, 19] find that both distributions are lognormal with a comparable parameters: The average pulse interval, $\overline{\Delta t} = 1.3sec$ is larger by a factor 1.3 then the average pulse width $\overline{\delta t} = 1sec$. One also finds that the pulse widths are correlated with the preceding interval [18, 19].

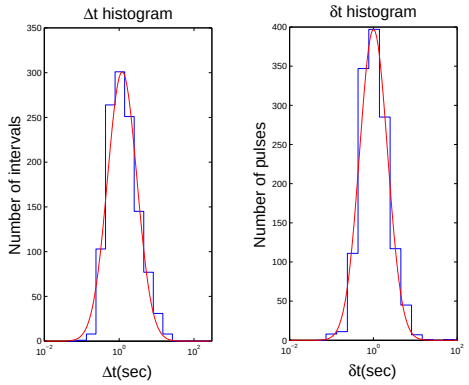


Figure 2: The pulse width distribution (right) and the distribution of intervals between pulses (left) (from [19]).

The results described so far are for long bursts. the variability of short ($T < 2$sec) bursts is more difficult to analyze. The duration of these bursts is closer to the limiting

resolution of the detectors. Still we find that most ($\sim 66\%$) short bursts are variable with $\delta t/T < 0.1$ [20].

# 4 Time Scales In GRBs - Theory

Consider a spherical relativistic emitting shell with a radius $R$, a width $\Delta$ and a Lorentz factor $\Gamma$. This can be a whole spherical shell or a spherical like section of a jet whose opening angle $\theta$ is larger than $\Gamma^{-1}$. Because of relativistic beaming an observer would observe radiation only from a region of angular size $\Gamma^{-1}$. Photons emitted by matter moving directly towards the observer (point A in Fig. 3) will arrive first. Photons emitted by matter moving at an angle $\Gamma^{-1}$ (point D in Fig. 3) would arrive after $t_{ang} = R/2c\Gamma^2$. This is also the time of arrival of photons emitted by matter moving directly towards the observer but emitted at $2R$ (point C in Fig. 3). Thus, $t_{rad} \approx t_{ang}$ [16, 29]. This coincidence is the first part of the NO GO theorem that rules out single explosions a sources of GRBs.

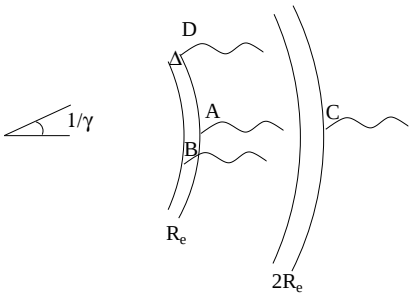


Figure 3: Different time scale from a relativistic expanding shell in terms of the arrival times ($t_i$) of various photons: $t_{ang} = t_D - t_A$, $t_{rad} = t_C - t_A$ and $T_\Delta = t_B - t_A$.

At a given point particles are continuously accelerated and emit radiation as long as the shell with a width $\Delta$ is crossing this point. The photons emitted at the front of this shell will reach the observer a time $T_\Delta = \Delta/c$ before those emitted from the rear (point B in Fig. 3). In fact photons are emitted slightly longer as it takes some time for the accelerated photons to cool. For most reasonable parameters the cooling time is much shorter from the other time scales [30] and we ignore it hereafter.

Light curves are divided to two classes according to the ratio between $T_\Delta$ and $t_{ang} \approx t_{rad}$. The emission from different angular points smoothes the signal on a time scale $t_{ang}$. If $T_\Delta \leq t_{ang} \approx t_{rad}$ the resulting burst will be smooth with a width $t_{ang} \approx t_{rad}$. The second part of the NO GO theorem follows from the hydrodynamics of external shocks. Sari and Piran [16] have shown that for external shocks $\Delta/c \leq R/c\Gamma^2 \approx t_{rad} \approx t_{ang}$. External shocks can produce only smooth bursts!

A necessary condition for the production of a variable light curve is that $T_\Delta = \Delta/c > t_{ang}$. This can be easily satisfied within internal shocks (see Fig 4). Consider an "inner engine" emitting a relativistic wind active over a time $T_\Delta = \Delta/c$ ($\Delta$ is the overall width of the flow in the observer frame). The source is variable on a scale $L/c$. The internal shocks will take place at $R_s \approx L\Gamma^2$. At this place the angular time and the radial time satisfy: $t_{ang} \approx t_{rad} \approx L/c$. Internal shocks continue as long as the source is active, thus the overall observed duration $T = T_\Delta$ reflects the time that the "inner engine" is active. Note that now $t_{ang} \approx L/c < T_\Delta$ is trivially satisfied. The observed variability time scale in the light curve, $\delta t$, reflects the variability of the source $L/c$. While the overall duration of the burst reflects the overall duration of the activity of the "inner engine".

Numerical simulations [17] have shown that not only the time scales are preserved but the source's temporal behaviour is reproduced on an almost one to one basis in the observed light curve. We will return to this point in section 6 in which we describe a simple toy model that explains this result.

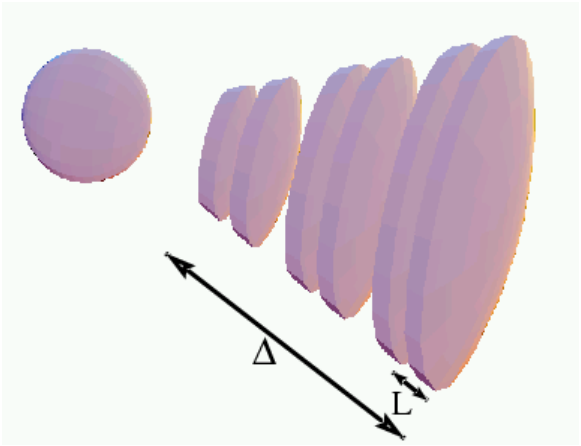


Figure 4: The internal shocks model (from [32]). Faster shells collide with slower ones and produce the observed $\gamma$ rays. The variability time scale is $L/c$ while the total duration of the burst is $\Delta/c$ .

# 5 Caveats and Complications

Clearly the way to get around the NO GO theorem is if $t_{ang} < t_{rad}$. In this case one can identify $t_{rad}$ with the duration of the burst and $t_{ang}$ as the variability time scale. The observed variability would require in this case that: $t_{ang}/t_{rad} = \delta t/T$.

One can imagine an inhomogeneous external medium which is clumpy on a scale $d \ll R/\Gamma$ (see Fig 5). Consider such a clump located at an angle $\theta \sim \Gamma^{-1}$ to the

direction of motion of the matter towards the observer. The resulting angular time, which is the difference in arrival time between the first and the last photons emitted from this region would be:$\sim d/c\Gamma$. Now $t_{ang} < t_{rad}$ and it seems that one can get around the NO GO theorem.

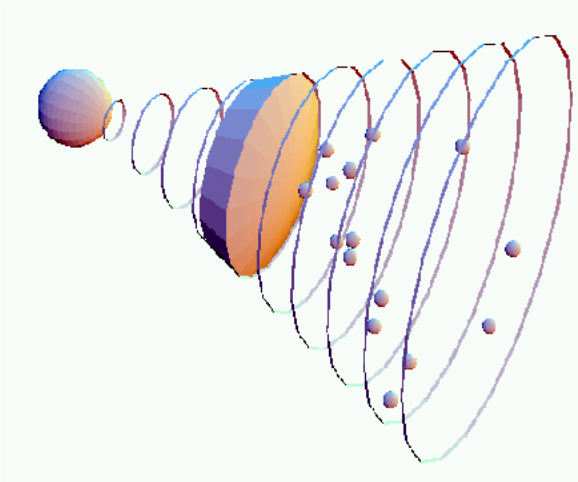

Figure 5: The clumpy ISM model (from [32]). Note the small covering factor and the resulting "geometrical" inefficiency.

Sari and Piran [16] have shown that such a configuration would be extremely inefficient. This third component of the NO GO theorem rules out this caveat. The observations limit the size of the clumps to $d \approx c\Gamma\delta t$ and the location of the shock to $R \approx cT\Gamma^2$. The number of clumps within the observed angular cone with an opening angle $\Gamma^{-1}$ equals the number of pulses which is of the order $T/\delta t$. The covering factor of the clumps can be directly estimated in terms of the observed parameters by multiplying the number of clumps $T/\delta t$ times their area $d^2 = (\delta t\Gamma)^2$ and dividing by the cross section of the cone $(R/\Gamma)^2$. The resulting covering factor equals $\delta t/T \ll 1$. The efficiency of conversion of kinetic energy to $\gamma$-rays in this scenario is smaller than this covering factor which for a typical variable burst could be smaller than $10^{-2}$.

We turn now to several attempts to find a way around this result. We will not discuss here the feasibility of the suggested models (namely is it likely that the surrounding matter will be clumpy on the needed length scale [31], or can an inner engine eject "bullets" [33] or "cannon balls" [34] with an angular width of $\sim 10^{-2}$ degrees and what keeps these bullets so small even when they are shocked and heated). We examine only the question whether the observed temporal structure can arise within these models.

## 5.1 External Shocks on a Clumpy Medium

Dermer and Mitman [31] claim that the simple efficiency argument of Sari and Piran [16] was flawed. They point out that if the direction of motion of a specific blob is almost exactly towards the observer the angular time would be of order $d^2/cR$. This is narrower by a factor $d\Gamma/R$ than the angular time across the same blob that is located at a typical angle of $\Gamma^{-1}$. These special blobs would produce strong narrow peaks and will form a small region along a narrow cone with a larger covering factor. Dermer and Mitman [31] present a numerical simulation of light curves produced by external shocks on a clumpy inhomogenous medium with $\delta t/T \sim 10^{-2}$ and efficiencies of up to $\sim 10\%$.

A detailed analysis of the light curve poses, however, several problems for this model. While this result is marginal for bursts with $\delta t/T \sim 10^{-2}$ it is insufficient for bursts with $\delta t/T \sim 10^{-3}$. Variability on a time scale of milliseconds is observed [20] in many long GRBs (namely $\delta t/T$ can be as samll as $10^{-4}$.). Moreover, in this case we would expect that earlier pulses (that arise from blobs along the direction of motion) would be narrower than latter pulses. This is in a direct contradiction with the observations [35]. Finally there is no reason to expect the observed similarity between the pulse width and the pulse separation and the correlation between the pulse width and the preceding interval in this model.

## 5.2 The Shot-Gun and the Cannon Ball Models

Heinz and Begelman [33] suggested that the "inner engine" operates as a shot-gun emiting multiple narrow bullets with an angular size much smaller than $\Gamma^{-1}$ (see Fig 6). These bullets do not spread while propagating and they are slowed down rapidly by an external shock with a very dense circumburst matter. The pulses width is $t_{ang}$ or the slowing down time while the duration of the burst is determined by the time that the "inner engine" emits the bullets. While the cannon ball model of Dar and De Rujulla [34] is drastically different from a physical point of view it is rather similar in terms of its temporal features. Hence the following remarks apply to this model as well.

This model satisfies our NO GO theorem in the sense that also here the burst is not produced by a single explosion. Moreover the observed light curve represents also here the temporal activity of the source. However, it is based on external shocks.

The most serious problem is the fact that the width of the pulses here is determined by the angular time or the hydrodynamic time (which in turn depends on the external density profile of the circumburst matter) while the intervals between the pulses depend on the activity of the inner engine. There is no reason why the two distributions will be similar and why there should be a correlation between them.

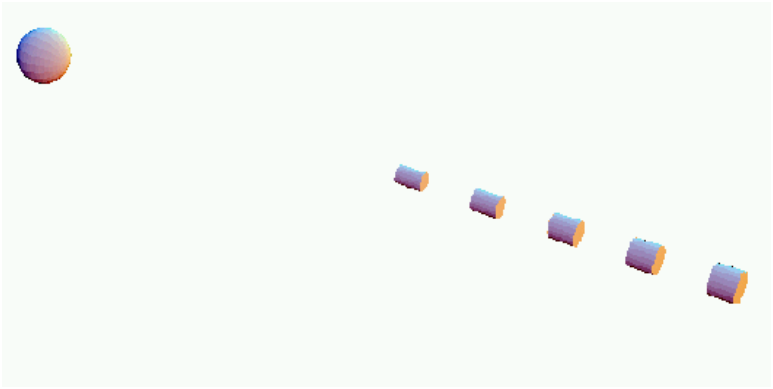

Figure 6: The shot-gun or the cannon-ball models (from [32]). The inner engine emits narrow "bullets" that collide with the ISM.

# 6 An Internal Shocks Toy Model

The discovery [18, 19] that the distribution of pulse widths and pulse separations are comparable and that there is a correlation between the pulse width and the preceding interval provides an independent evidence in favor of the internal shocks model. Furthermore it suggests that the different shells emitted by the internal engine are most likely "equal energy" rather than "equal mass" shells.

The similarity between the pulse width and the pulse separation distribution and the correlation is extremely unlikely to arise from a single shell passing thought a random distribution of clumps that surround the "central engine". In this case the arrival time of individual pulses will depend on the position of the emitting clumps relative to the observers. Two following pulses could arise from two different clumps that are rather distant from each other. There is no reason why the pulses and intervals should be correlated in any way. A similar problem arises in the "shot-gun" or the "cannon-ball" models in which the pulse duration is determined by one parameter and the separation by another.

Both features arise naturally within the internal shocks model [21] in which both the pulse duration and the separation between the pulses are determined by the same parameter. We outline here the main arguments showing that. Consider two shells with a separation $L$. The slower outer shell Lorentz factor is $\Gamma_1 = \Gamma$ and the inner faster shell Lorentz factor is $\Gamma_2 = a\Gamma$ ($a > 2$ for an efficient collision), both in the observer frame. The shells' are ejected at $t_1$ and $t_2 \approx t_1 + L/c$. The collision takes place at a radius $R_s \approx 2\Gamma^2 L$ (Note that $R_s$ does not depend on $\Gamma_2$). The emitted photons from the collision will reach the observer at time (omitting the photons flight time, and assuming transparent shells):

$$t_o \approx t_1 + R_s/(2c\Gamma^2) \approx t_1 + L \approx t_2 \ . \tag{1}$$

The photons from this pulse are observed almost simultaneously with a (hypothetical) photon that was emitted from the "inner engine" together with the second shell (at $t_2$). This explains why Kobayashi et al [17] find numerically that for internal shocks the observed light curve replicates the temporal activity of the source.

Consider now four shells emitted at times $t_i$ $(i = 1, 2, 3, 4)$ with a separation of the order of $L$ between them. Assume that there are two collisions - between the first and the second shells and between the third and the fourth shells. The first collision will be observed at $t_2$ while the second one will be observed at $t_4$. Therefore, $\Delta t \approx t_4 - t_2 \approx 2L/c$. Now assume a different collision scenario, the second and the first shells collide, and afterward the third shell takes over and collide with them (the forth shell does not play any roll in this case). The first collision will be observed at $t_2$ while the second one will be observed at $t_3$. Therefore, $\Delta t \approx t_3 - t_2 \approx L/c$. Numerical simulations [21] show that more then 80% of the efficient collisions follows one of the two scenarios described above. Therefore we can conclude:

$$\Delta t \approx L/c \ . \tag{2}$$

Note that this result is independent of the shells' masses.

The pulse width is determined by the angular time (ignoring the cooling time): $\delta t = R_s/(2c\Gamma_s^2)$ where $\Gamma_s$ is the Lorentz factor of the shocked emitting region. If the shells have an equal mass $(m_1 = m_2)$ then $\Gamma_s = \sqrt{a}\Gamma$ while if they have equal energy $(m_1 = am_2)$ then $\Gamma_s \approx \Gamma$. Therefore:

$$\delta t \approx \begin{cases} R_s/2a\Gamma^2 c \approx L/ac & \text{equal mass,} \\ R_s/2\Gamma^2 c \approx L/c & \text{equal energy.} \end{cases} \tag{3}$$

The ratio of the Lorentz factors $a$, determines the collision's efficiency. For efficient collision the variations in the shells Lorentz factor (and therefore $a$) must be large.

It follows from Eqs. 2 and 3 that for equal energy shells the $\Delta t$-$\delta t$ similarity and correlation arises naturally from the reflection of the shells initial separation in both variables. However, for equal mass shells $\delta t$ is shorter by a factor of $a$ than $\Delta t$. Since $a$ has a large variance this would wipes off the $\Delta t$-$\delta t$ correlation. This suggests that equal energy shells are more likely to produce the observed light curves.

# 7 Conclusions

We cannot provide a recipe for a GRB "inner engine". However we can list the specifications of this engine (for a long variable GRB). It must satisfy the following conditions:

- It should accelerate $\sim 10^{51}$ergs to a variable relativistic flow with $\Gamma > 100$.
- It should collimate this flow, with a varying degree of collimation (up to $1^o$).
- It should be active from several seconds up to several hundred seconds (according to the duration of the observed burst).
- It should vary on a time scale of seconds or less (corresponding to the duration of a typical pulse within the burst).
- Different shells of matter should have a comparable energy and their different Lorentz facors should arise due to a modulation of the accelerated mass.
- At times the engine should stop for several dozen seconds (resulting in a quiescent periods).

Before concluding we stress that these specification are for long variable burst (which compose the majority of the observed bursts). Many of these (but not all) apply also to short variable bursts (about two thirds of the short bursts). These specifications do not apply to smooth bursts (either short or long ones).

This research was supported by a grant from the US-Israel Binational Science Foundation.

# References

[1] T. Piran, Physics Reports, **314**, 575 (1999).

[2] T. Piran, Physics Reports, **333**, 529 (2000).

[3] A. S. Fruchter, et al., ApJ, **516**, 683, (1999).

[4] R. Wijers, J. Bloom, J. Bagla and P. Natarjan, MNRAS, **294**, L13, (2000).

[5] T. Totani, ApJ, **511**, 41 (1999).

[6] A. Blain and P. Natarajan, MNRAS, **312**, L35, (2000).

[7] T. Galama et al., Nature, **395**, 70, (1998).

[8] Bloom, J. S. et al., Nature, **401**, 453 (1999).

[9] Reichart, D. E. 1999, ApJ, **521**, L111, (1999).

[10] Galama, T. J. et al., ApJ, **536**, 185 (2000).

[11] S. E. Woosley, Astrophys. J. **405**, 273 (1993).

[12] B. Paczynski, Ap. J. Lett., **494**, L45 (1998).

[13] A. I. MacFadyen and S. E. Woosley, Astrophys. J. **524**, 262 (1999).

[14] D. Eichler, M. Livio, T. Piran, and D. N. Schramm, Nature **340**, 126 (1989).

[15] R. Ouyed, "Quark Stars and Color Superconductivity: A GRB connection?" this volume, astro-ph/0201408 (2002).

[16] R. Sari and T. Piran, Astrophys. J. **485**, 270 (1997).

[17] S. Kobayashi, T. Piran, and R. Sari, Astrophys. J. **490**, 92 (1997).

[18] E. Nakar and T. Piran, astro-ph/0103011, GRBs in the Afterglow Era, Eds. E. Costa, F. Fronteira and K. Hjorth,NK01,NK02a (Springer) (2001).

[19] E. Nakar and T. Piran, MNRAS, in press, astro-ph/0103210 (2002)

[20] E. Nakar and T. Piran, MNRAS, in press, astro-ph/0103192 (2002)

[21] E. Nakar and T. Piran, submitted astro-ph/0202404 (2002).

[22] R. Narayan, T. Piran and P. Kumar, Astrophys. J. **557**, 949, (2001).

[23] S. R. Kulkarni *et al.*, Nature **398**, 389 (1999).

[24] T. Piran, P. Kumar. A. Panaitescu and L. Piro, Ap. J. Lett., **560**, L167, (2001).

[25] T. Piran, astro-ph/0111314 talk given at the J. van Paradijs Memorial Symposium, June 6-8 Amsterdam, (2001).

[26] A. Panaitescu and P. Kumar, Ap. J. Lett., **560**, L49, (2001).

[27] D. A. Frail *et al.*, Ap. J. Lett., **562**, L55 (2001).

[28] E. Ramirez-Ruiz, and A Melroni, MNRAS, **320**, K25 (2001).

[29] E. E. Fenimore, C. D. Madras, and S. Nayakshin, Astrophys. J. **473**, 998, (1996).

[30] R. Sari, R. Narayan and T. Piran, Astrophys. J. **473**, 204, (1996).

[31] C. D. Dermer, and K. E., Mitman, Astrophys. J. **513**, 5, (1999)

[32] R. Sari, PhD thesis, (1998)

[33] S. Heinz, and M. C. Begelman, Ap. J. Lett., **527**, L35, (1999).

[34] A. Dar and A. De Rujula, unpublished astro-ph/0008474 (2000).

[35] E. Ramirez-Ruiz, and E. E. Fenimore A & A.S. **132**, 521, (1999).

# Prompt Emission and Early Afterglows of Gamma-Ray Bursts

*Andrei M. Beloborodov*
*Canadian Institute for Theoretical Astrophysics*
*University of Toronto, 60 St. George Street*
*Toronto, M5S 3H8 Ontario, CANADA*

## 1 Introduction

Gamma-ray bursts (GRBs) are extremely bright ($10^{50} - 10^{53}$ erg/s) and short ($10^{-2} - 10^{2}$ s) emission events observed from distant parts of the Universe. Their redshifts are now measured in about 20 cases and typical $z \sim 1$ (up to 4.5) are found [1]. The burst were observed to occur with a rate of $\approx 1$ per day by the BATSE experiment [2] and even a higher rate would probably be detected with more sensitive instruments [3]. GRBs are very different from supernovae not only because of their short duration and high luminosity. Their most special feature is that the emission peaks in the gamma-ray band, at $h\nu$ of a few hundred keV or perhaps more. In many cases ($\approx 50\%$) the gamma-ray bursts are followed by afterglows — a much longer and softer emission that deacays in time and evolves from X-rays (hours) to radio (months) [4].

What triggers the bursts is still uncertain. The primary energy release occurs in a very compact region (probably within $10^7$ cm — from variability arguments) which is comparable to the size of compact objects — black holes and neutron stars. The energy output (assuming isotropic explosion) approaches a stellar rest-mass energy. This suggests a high efficiency of mass conversion into radiation and points to a relativistic collapse with a gravitational potential $\phi \sim c^2$ which agrees with the potential of compact objects. Yet the configuration of the progenitor system and the reason of the collapse are uncertain (see reviews [5, 6] and refs. therein). It can be (I) coalescence of a close binary consisting of two compact objects [7], (II) collapse of a massive star core [8], and (III) collapse of a white dwarf [9]. Also conversion of neutron stars into strange stars was proposed [10, 11]. Different scenarios can be tested against observations. In particular, massive stars spend their short lifes close to where they were born, and hence in the second scenario GRBs should occur in regions of active star formation. There is a growing evidence that this is indeed the case [1].

The afterglow is believed to come from a relativistic blast wave driven by the central explosion into an ambient medium. If GRBs are triggered by old stellar

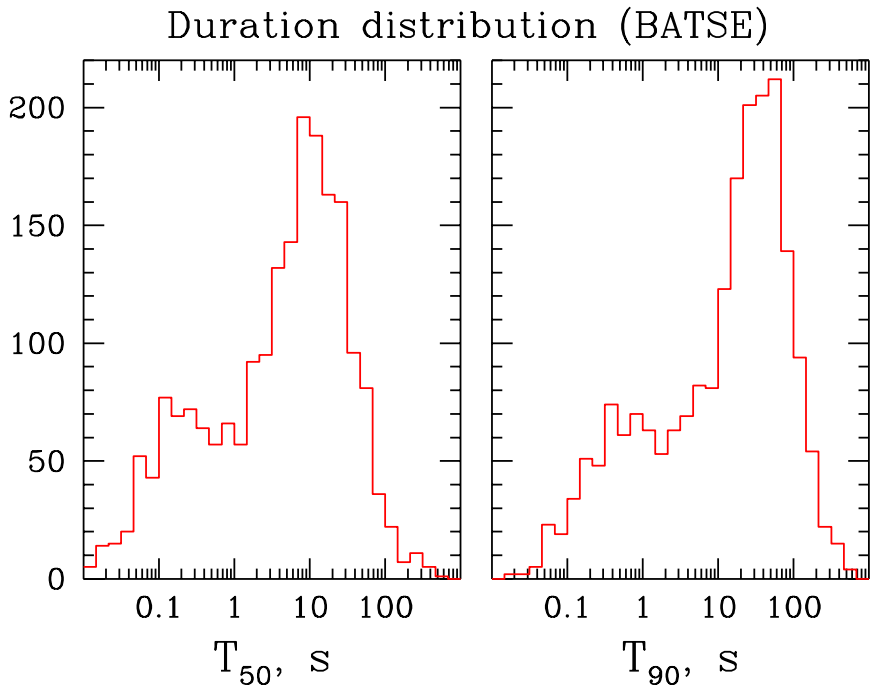


Figure 1: The duration distribution of 2041 GRBs from the current BATSE catalogue. Right panel: the duration is measured by T90, which is the time over which a burst emits from 5% of its total counts to 95%. Left panel: the duration is measured by $T_{50}$ — the time over which a burst emits from 25% of its total counts to 75%. The counts are summed over all 4 BATSE energy channels (photon energy $E > 20$keV).

remnants they are likely surrounded by an interstellar medium (ISM) of density $n \sim 1$ cm$^{-3}$ or even lower if the remnants are kicked out of the disk of the parent galaxy. In contrast, a GRB with a massive progenitor should occur inside a dense and strongly inhomogeneous star-forming cloud. Even more importantly, a massive progenitor emits a powerful wind all the time before it explodes, and this wind is the actual ambient medium of the GRB, with density scaling with radius as $R^{-2}$ out to a distance of a few parsecs [12]. The afterglow observations were supposed to reveal the nature of the ambient medium and thereby the progenitor. Yet after having observed many afterglows no definite conclusions are made. Perhaps the most surprising finding is that the afterglows are very diverse.

# 2 Prompt Emission: Observations

The prompt $\gamma$-ray emission (called prompt as opposed to the afterglow) displays a rich phenomenology which is poorly understood from a theoretical standpoint. In this section basic observed properties of the prompt GRBs are briefly summarized.

## 2.1 Time profiles: preferred timescales

The duration of GRBs varies by 4 orders of magnitude. The duration distribution is shown in Fig. 1. It has three clear features: (1) a break at short $T_{50} \approx 0.1$ s, (2) a break at long $T_{50} \approx 10$ s, and (3) a deficit of GRBs with $T_{50} \approx 1$ s. The three timescales are not explained yet.

Time profiles $C(t)$ of GRBs are very diverse. They show strong variations on all resolved timescales (the resolution $\Delta t = 64$ ms in the standard BATSE data). In long bursts the range $\Delta t < t < T_{50}$ spans three decades and Fourier transform $C(f)$ of the profile is useful: its power spectrum $P_f = C_f C_f^*$ shows how the variability power is distributed over timescales. It reveals an interesting special feature of GRBs: $P_f$ follows a power law with slope $\alpha \approx -5/3$ at frequencies $(2\pi T_{50})^{-1} < f < f_{\rm br} \approx 1$ Hz and breaks at $f_{\rm br}$ (Fig. 2). This Fourier spectrum is observed in individual GRBs and it becomes especially clear when $P_f$ of several GRBs are averaged: then the statistical fluctuations $\Delta P_f/P_f \sim 1$ are averaged out and a perfect power law with a sharp break is found [13]. The break is not an artifact of the 64 ms time binning; it rather indicates a timescale $\tau_{\rm br} \approx (1/2\pi)$ s below which the variability decreases.

Various techniques were used to study the GRB profiles, for example decomposition into separate pulses [15], construction of the average time profile [3], and construction of the average auto-correlation function (ACF) [16]. The results of different approaches are related. For example, the pulse decomposition gives a distribution of pulse widths with a break at a fraction of second, in agreement with the break in the power spectrum $P_f$. The ACF is just a Fourier transform of $P_f$ and it is perfectly fitted as a stretched exponential $\exp[-(\tau/\tau_0)^\beta]$ of index $\beta = \alpha - 1$ [13]. The ACF width $\tau_0$ is about the geometrical mean of $\tau_{\rm br}$ and $T_{50}$.

## 2.2 Spectra: a preferred photon energy?

The GRB energy spectrum is very difficult to study because it varies rapidly during the burst. The time-averaged spectrum is well fitted by a (smoothly) broken power law with a low-energy slope $\Gamma_s = -1 \pm 0.5$ and a high-energy slope $\Gamma_h = -2.3 \pm 0.5$ [17]. The spectral peak position $E_{\rm pk}$ was found to cluster around $\sim 200$ keV. This clustering is not understood. Theoretically, there is no convincing model that would reproduce it. Observationally, one may ask whether the results based on the BATSE data are conclusive, since the experiment had the highest sensitivity at $\sim 100$ keV. Statistical

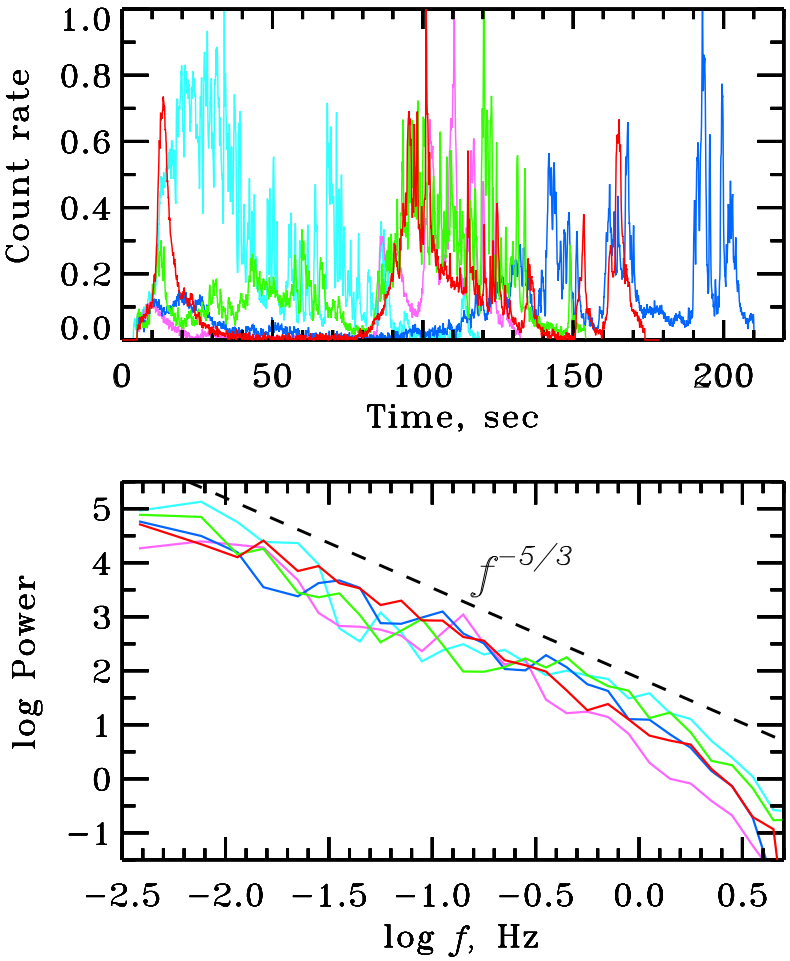


Figure 2: Peak-normalized time profiles and their power spectra for the 5 brightest BATSE bursts with $T_{90} > 100$ s (brightness is measured by the peak count rate).

studies point toward reality of the $E_{\rm pk}$ clustering [17], yet a confirmation by a future mission is desirable. One should also keep in mind that the time-average spectrum is normally far from the instantaneous one and its parameters do not give a direct information on the emission mechanism. Indeed, the instantaneous spectrum was fitted by a similar function yet with different (evolving) $E_{\rm pk}$ and slopes. $E_{\rm pk}$ can change during one burst by more than one order of magnitude. An interesting feature of spectral evolution is a positive correlation between the instantaneous $E_{\rm pk}$ and the energy flux $F$. In particular, the dependence $F \propto E_{\rm pk}^{\gamma}$ was found for the decay phase of GRB where $\gamma = 1 - 3$ varies from pulse to pulse and the average $\overline{\gamma} \approx 2$ [18].

The question of preferential energy can be reformulated: do GRB-like bursts occur in different energy bands? Recently, such bursts (X-ray flashes) were found

by BeppoSax [19]. These events have durations and time profiles similar to classical GRBs, but they emit most of their energy at softer energies (below 20 keV). The hardness ratio distribution of these soft bursts indicates that they extend continuously the population of the classical GRBs to lower energies.

# 3 Models for Prompt Emission

A basic constraint on GRB models is derived from their fast variability and enormous power: GRBs must be emitted by highly relativistic ejecta directed toward the observer. A lower bound on the ejecta Lorentz factor $\Gamma$ can be estimated as follows. Baryonic ejecta with kinetic luminosity $L_k \sim 10^{52}$ erg/s become transparent to electron scattering at a radius $R_* = L_k\sigma_{\rm T}/(8\pi m_p c^3\Gamma^3) \sim 10^{19}\Gamma^{-3}$ cm. The observed emission from the ejecta can vary on timescales $t_v \geq R_*/(2\Gamma^2 c) \sim 10^8\Gamma^{-5}$ s. The actual $t_v < 0.1$ s then requires $\Gamma \sim 10^2$.

A simple phenomenological model of a relativistic outflow envisions a central engine of size $r_0 \sim 10^7$ cm which deposits energy at a high rate $\sim 10^{52}$ erg/s at the base of the outflow; this causes high pressure and free expansion with increasing $\Gamma \propto R$ [20]. The engine operates much longer ($t_{\rm obs} \sim$ s) than its light-crossing time ($r_0/c \lesssim$ ms). It ejects a long sequence of blobs $\sim r_0$ that undergo free expansion (on timescale $r_0/c$) one after another and form a continuous outflow.

The high $\Gamma$ of the outflow implies that energy is ejected with a very low baryon "pollution". This energy must be carried by a highly relativistic plasma and frozen magnetic fields. Below we first describe outflows dominated by the plasma energy and then those dominated by magnetic energy.

## 3.1 Baryonic Outflow: Internal Shocks

Suppose the engine emits thermal energy into a solid angle $\Omega$ with rate $L(\Omega/4\pi)$. The energy density at the outflow base, $w = L/(4\pi r_0^2 c)$, is so high that the matter must be in complete thermodynamic equilibrium with radiation at a temperature $kT_0 \sim$ MeV. Here the matter is strongly dominated by $e^\pm$ pairs which maintain an equilibrium with radiation through reaction $\gamma + \gamma \leftrightarrow e^+ + e^-$, and $w$ is dominated by photons and $e^\pm$ [21]. The high-pressure material expands freely with acceleration. The expansion is accompanied by adiabatic cooling, eventually the temperature drops, and pairs annihilate.

A crucial parameter of the outflow is its baryonic rest-mass luminosity, $L_b$. If there are no baryons ($L_b = 0$) the outflow becomes transparent after $e^\pm$ annihilation and the radiation escapes. This happens when the temperature in the comoving frame drops to $kT_\pm \sim 10$ keV, at a radius $R = r_0(T_0/T_\pm)$ and $\Gamma = (T_0/T_\pm)$. Essentially all the explosion energy is carried away by the blackbody radiation with temperature $T =$

$\Gamma T_\pm = T_0$. Thus, a strong burst is produced at MeV energies. Only a small energy remains available for an afterglow; it is carried by an optically thin outflow of surviving $e^\pm$ with luminosity $L_\pm = 8\pi(r_0 m_e c^3/\sigma_{\rm T})(T_0/T_\pm)^4 \ll L$. In contrast, the observed afterglows are comparable in energy with the prompt GRB, and this is one reason why the outlined model is unfavorable. Besides, the blackbody exponential cutoff was not found in GRB spectra and a nonthermal emission mechanism is preferred.

A small baryonic pollution, $L_b \ll L$, can drastically change the model in that it keeps the outflow optically thick after $e^\pm$ annihilation. The radiation remains trapped, continues to accelerate the outflow, $\Gamma \propto R$, and cools down adiabatically. The kinetic luminosity of baryons $L_k = \Gamma L_b$ grows and approaches $L$ at $R_s = (L/L_b)r_0$. Now the explosion luminosity has been converted into $L_k$ and the Lorentz factor saturates at $\Gamma = L/L_b$.

The baryonic outflow was suggested to emit GRBs by internal shocks [22, 23, 24]. If $L_b/L$ varies during the outflow ejection, $\Gamma$ will fluctuate, which results in internal collisions (caustics). A minimum scale of the $\Gamma$-fluctuations is $\lambda_0 \sim r_0$ — the size of the central engine. First internal collisions will occur at a radius $R_0 = 2\overline{\Gamma}^2\lambda_0/A$ where $A = \Delta\Gamma/\overline{\Gamma}$ is the fluctuation amplitude (rms) and $A < 1$ is assumed [25]. At $R > R_0$ the collisions proceed on scales $\lambda > \lambda_0$ in a hierarchical manner. For a given initial spectrum of fluctuations one can compute the history of internal dissipation [25, 26].

The transparency radius of the baryonic outflow $R_* = L\sigma_{\rm T}/(8\pi m_p c^3 \Gamma^3)$ is comparable to $R_0$, and hence internal shocks can emit nonthermal spectra. Any time profiles of GRBs can be fitted by the model with properly chosen initial conditions. One would also like to know what fraction $\epsilon$ of the total bulk kinetic energy $E$ is dissipated internally. It is determined by an initial free energy $U_{\rm free}$ of the fluctuating outflow: $\epsilon = U_{\rm free}/E$. $U_{\rm free}$ is easily calculated analytically given an initial amplitude of fluctuations $A < 1$, leading to $\epsilon = A^2/2 < 0.5$ [25]. The case of $A > 1$ is also possible and it is more complicated. At high $A$ the Lorentz factors of colliding shells differ by a big factor $\Gamma_2/\Gamma_1$ up to $10^2 - 10^3$; then the outflow evolves in a non-linear way and $\epsilon$ could approach unity. A realistic $\Gamma_2/\Gamma_1$ is limited because a radiation-pressure-accelerated ejecta has $\Gamma \le (R/r_0)$ at any given $R$. A slow shell with $\Gamma_1$ is hit by a following fast shell with $\Gamma_2 \gg \Gamma_1$ at $R_0 = 2\Gamma_1^2\lambda_0$ (where $\lambda_0$ is their initial separation); since $\Gamma_2 \le R_0/r_0$ one gets a maximum $\Gamma_2/\Gamma_1 = 2\Gamma_1(\lambda_0/r_0)$. It may be much higher than $2\Gamma_1$ if the central engine "waits" before ejecting a very energetic shell ($\lambda_0 \gg r_0$) and the shell has space ahead to develop a high $\Gamma_2$ before colliding. Therefore, in the non-linear regime, $\epsilon$ is not a simple function of $A$ and it is sensitive to details of initial conditions. Additional complications are owing to possible $e^\pm$ production [27] which depends on the unknown spectrum of the produced $\gamma$-rays at $h\nu > 100$ MeV.

A major uncertainty of this scenario is the emission mechanism of internal shocks which remains to be a matter of controversy. The simplest model of synchrotron emission from shock-accelerated electrons predicts a broken power-law radiation spectrum

with a low energy slope $\Gamma_s > -2/3$ [5] and this is inconsistent with the data [17]. Possible modifications were discussed [29, 30, 31] yet the issue is not yet settled. Also the radiative efficiency $\eta$ of an internal shock is unknown and speculations range from $\eta \ll 1$ to $\eta = 1$. The net radiative efficiency of the outflow can be high even when $\eta \ll 1$ in each shock [28]. The fraction of the emitted radiation that appears in the BATSE spectral window depends on the model assumptions and may be small [32].

## 3.2 Magnetic Outflow: Field Dissipation

The central compact engine is likely to have a rotational energy $E_{\rm rot}$ comparable to the gravitational energy. Differential rotation can generate very strong magnetic fields, as high as $B \sim 10^{16}$ G. For example, neutron stars can be born strongly magnetized [9, 33]. When a compact binary merges or a massive star core collapses, a black hole forms and accretes debris. Then strong magnetic fields can be generated by the differentially rotating accretion disk. A magnetized rotator emits Poynting flux with luminosity $L_P \approx \mu^2\omega^4/c^3$ where $\mu$ is the magnetic moment and $\omega$ is the angular velocity of rotation. For expected $\mu \sim 10^{34}$ G cm$^3$ and $\omega \sim 10^4$ s$^{-1}$ one gets $L_P \sim 10^{52}$ erg/s and hence $E_{\rm rot}$ is emitted in a few seconds. The resulting Poynting-flux-dominated outflow was studied as a possible GRB source; we will describe here the scenario proposed in [34].

A fraction $\sigma$ of $E_{\rm rot}$ can be dissipated at the base of the Poynting outflow, loading it with baryon-free $e^\pm$ plasma and trapped blackbody radiation. The Poynting flux is "frozen" into the plasma whose early dynamics is similar to the scenario described in Section 3.1. The difference is that now only a fraction $\sigma$ of the total energy is thermalized and the initial temperature $T_0$ is lower by a modest factor $\sigma^{1/4}$. The magnetized outflow is accelerated by the thermal pressure until the temperature drops to $kT_\pm \sim 10$ keV. Here pairs annihilate to transparency, the thermal radiation decouples, and the Lorentz factor of the surviving $e^\pm$ plasma saturates at $\Gamma = T_0/T_\pm \sim 10^2$.

The coasting $e^\pm$ outflow carries the initially frozen magnetic field as long as the particle density $n$ is sufficient to ensure the MHD approximation. The toroidal field component $B_\phi$ is least suppressed in the expansion process and $B \approx B_\phi \propto R^{-1}$. The magnetic outflow (like the baryonic one) can be inhomogeneous on scales $\lambda \gtrsim r_0$, so that the field possesses a free energy $U_{\rm free}$ of currents $j = (c/4\pi)|\nabla \times \mathbf{B}| \approx (c/4\pi)(B/r_0) \propto R^{-1}$. The density of surviving $e^\pm$ at $R > R_\pm$ is $n_+ \sim \Gamma R_\pm/(\sigma_{\rm T} R^2) \propto R^{-2}$ and outside $\sim 10^{14}$ cm it is too small to support the currents. Then the displacement current $\dot{E}/c = j$ is generated and $U_{\rm free}$ is converted into large-amplitude electromagnetic waves. The waves have a low frequency, $c/r_0 \sim 10^4$ Hz, and they are quickly absorbed by the $e^\pm$ plasma, resulting in particle acceleration to a Lorentz factor $\gamma \sim L_P/L_\pm \sim 10^6$. The accelerated $e^\pm$ move in the residual magnetic field and the field of waves and emit photons of energy $h\nu \sim \gamma^2\hbar(c/r_0) \sim$ MeV. This mechanism may give rise to a GRB. Very strong bursts can naturally be produced

since the Poynting outflow carries a large energy $E_{\rm rot}$ and $U_{\rm free} \lesssim E_{\rm rot}$ is possible. Like the internal shock model, GRBs with arbitrary time profiles can be generated, depending on the initially frozen field structure in the outflow. The predicted energy spectrum is uncertain. After the prompt GRB (dissipation of $U_{\rm free}$) the magnetic fields outflows further with energy $E_{\rm ej} = E_{\rm rot} - U_{\rm free}$ until it passes the energy to an ambient medium. Here it gives rise to an afterglow.

# 4 Afterglow

There are a number of observations of GRB afterglows in X-rays, optical, IR, and radio (see [4] for a review). In many cases the afterglow spectral flux decays as a simple power law, $F_\nu(t) \propto \nu^{-\alpha} t^{-\beta}$. Clear deviations from this law are also observed, e.g. breaks or humps. The indexes $\alpha$ and $\beta$ change from burst to burst and can also change during one afterglow. Important early afterglow observations in X-rays were done by BeppoSax [35], SIGMA [36], and BATSE [37]. These observations showed that the afterglow starts immediately after or even overlaps with the prompt GRB. Chandra, BeppoSax, and ASCA detected spectral lines of iron in the afterglow, which places strong constraints on the GRB progenitors [38, 6].

## 4.1 Standard Afterglow Model

The energy source of the afterglows is easily explained. The ejecta with Lorentz factor $\Gamma$ runs into an ambient medium and its energy is dissipated when it sweeps a sufficient ambient mass $m$. Namely, half of the ejecta energy $E_{\rm ej}$ is dissipated when the swept inertial mass $m\Gamma$ (measured in the ejecta frame) reaches that of the ejecta itself, $E_{\rm ej}/(c^2\Gamma)$. The swept mass at a radius $R$ is given by $m(R) = \int_0^R 4\pi R^2 \rho {\rm dR}$ where $\rho(R)$ is the medium mass density. The characteristic $m_{\rm dec} = E_{\rm ej}/(c^2\Gamma^2)$ corresponds to a radius $R_{\rm dec}$. For example, $R_{\rm dec} = (3E_{\rm ej}/4\pi\rho c^2\Gamma^2)^{1/3}$ if $\rho(R) = const$. In the massive progenitor scenario, $\rho(R) = \dot{M}/(4\pi R^2 w)$ where $\dot{M}$ and $w$ are the mass loss and velocity of the progenitor wind. In this case $R_{\rm dec} = E_{\rm ej} w/(\Gamma^2 \dot{M} c^2)$. For the most likely Wolf-Rayet progenitors with $\dot{M} \sim 10^{-5} M_\odot$ yr$^{-1}$ and $w \approx 10^8$ cm/s, one gets $R_{\rm dec} \approx 10^{15}(E_{\rm ej}/10^{53})$ cm. (As we discuss in Section 4.2, this standard estimate neglects the impact of the $\gamma$-ray front and turns out invalid.)

The ejecta dynamics at $R > R_{\rm dec}$ depends on what happens faster — the dissipated heat is radiated away or the ejecta expands by a factor of two. If radiative losses dominate, $E_{\rm ej}$ is converted into radiation at $R \sim R_{\rm dec}$ and $\Gamma$ quickly decreases: $\Gamma \approx \Gamma_{\rm ej}(m/m_{\rm dec})^{-1}$ at $m > m_{\rm dec}$ [39]. If expansion is faster, the heat converts back into the bulk kinetic energy via adiabatic cooling; then $\Gamma \approx \Gamma_{\rm ej}(m/m_{\rm dec})^{-1/2}$.

The decelerating shell is made of the ejecta material and the swept ambient mass, with a contact discontinuity between them. The shell has a high pressure that drives

a forward shock into the medium. (A collisionless shock is expected to form if the Larmor radius of the reflected upstream ions $r_L = \Gamma^2 m_p c^2/eB_{\rm up} < R$; this condition may be not satisfied and then a different model is needed [40].) The emission from the forward shock gives rise to the observed afterglow. A simple emission model can fit the observations [41, 4]. It assumes that a fraction $\epsilon_e$ of the shocked ion energy goes to the electrons and accelerates them with a power-law energy spectrum $\mathrm{dN/dE_e} \propto \mathrm{E_e^{-p}}$. The electrons emit a synchrotron spectrum in a magnetic field behind the shock. The field is assumed to be strongly amplified compared to the upstream field and it is parametrized by $\epsilon_B = (B^2/8\pi)w_{\rm th}^{-1}$ where $w_{\rm th}$ is the energy density of the shocked medium. The model has six main fitting parameters and they are found to vary strongly from burst to burst [42]. Therefore it is not obvious whether the assumptions are justified by the data and the afterglow physics is well captured by the model. In any case the fits by the model provide a form for data representation; it is used commonly and referred to as a standard afterglow model.

The breaks sometimes observed in the afterglow light curves are thought to be indications of beaming of the GRB ejecta: a break should happen when $\Gamma^{-1}$ equals the beaming angle $\theta_{\rm ej}$ [43]. The beaming implies that the total GRB energy $E$ is reduced by a factor of $\theta_{\rm ej}^2/(4\pi)$ compared to what one deduces assuming isotropy. Intriguingly, when this correction is applied to GRBs with evaluated $\theta_{\rm ej}$, $E$ displays a much smaller dispersion and clusters around $\sim 10^{51}$ erg [42, 44].

The deceleration radius $R_{\rm dec}$ is especially interesting since here the main afterglow is emitted. The afterglow should peak early, at an observed time $t_{\rm obs} = t_{\rm peak} = R_{\rm dec}/(2\Gamma^2 c)$, and at $t_{\rm obs} > t_{\rm peak}$ the emission gets weaker and softer because it comes from the decelerated shell. Unfortunately, there are no direct observations of $R_{\rm dec}$. In one case the angular size of the afterglow source was inferred from radio observations at $t_{\rm obs} \approx 1$ month [45]: the scintillation amplitude died out at that time, giving an angular size that corresponds to the source radius $R \approx 10^{17}$ cm, in agreement with model expectations. Extrapolating $R(t)$ back in time one finds that $R_{\rm dec}$ is likely to be within $10^{16}$ cm. The $t_{\rm peak}$ should then be comparable to the prompt GRB duration and this agrees with the reported observations of hard X-ray afterglows already at the end of the prompt GRB [35, 36, 37]. These observations revealed a spectrally distinct and smoothly decaying emission component at the end of the burst and it was interpreted as the beginning of an afterglow. The standard model predicted this early afterglow in hard X-rays.

## 4.2 Revision of the Early Afterglow

Recently the physics of the early afterglow was revised. The new effect discovered is the strong impact of the prompt $\gamma$-rays on the afterglow blast wave. The presence of the violent radiation front ahead of the ejecta was neglected by the standard model while in fact it crucially changes the medium faced by the ejecta: the leading $\gamma$-rays

scatter off the medium, load it with $e^{\pm}$ pairs, and preaccelerate to a large Lorentz factor $\gamma$ [46, 47, 48]. These effects introduce three new characteristic radii into the problem: $R_{\rm gap} < R_{\rm acc} < R_{\rm load}$ [48]. At $R < R_{\rm gap} \approx 0.3R_{\rm acc}$ the $\gamma$-ray front sweeps the ambient medium out with $\gamma > \Gamma$ and opens a gap between the ejecta and the surfing medium. When the front passes radii $R_{\rm gap} < R < R_{\rm acc} = 0.7 \times 10^{16}(E_\gamma/10^{53})^{1/2}$ cm ($E_\gamma$ is the isotropic energy of the prompt GRB emission) $\gamma$ is decreasing from $\Gamma$ to unity and the ejecta is sweeping the preaccelerated and $e^{\pm}$ loaded medium behind the radiation front. At $R_{\rm acc} < R < R_{\rm load} \approx \sqrt{5}R_{\rm acc}$ the ejecta sweeps a static ($\gamma \approx 1$) medium dominated by loaded $e^{\pm}$. Not until $R > R_{\rm load} = 1.6 \times 10^{16}(E_\gamma/10^{53})^{1/2}$ cm the $e^{\pm}$ loading is shut down and the standard afterglow model applies.

The afterglow should start at $R = R_{\rm gap}$ when the gap is closed and a blast wave is formed. Initially, the shock Lorentz factor $\Gamma_{\rm sh} \approx \Gamma/\gamma$ is modest and $e^{\pm}$ density of the ambient medium exceeds the ion density by a very large factor $n_+/n_i \approx 10^3$. The energy per shocked $e^{\pm}$ particle is suppressed $\propto \gamma^{-1}(n_i/n_+)$, resulting in soft emission. In contrast to the standard model, one expects to see the very beginning of the afterglow in optical/UV. As the ejecta approaches $R_{\rm acc}$ the preacceleration $\gamma$ falls down steeply, $\Gamma_{\rm sh}$ rises, the emission hardens fast, and the afterglow appears in the X-ray band. This unusual soft-to-hard evolution of the early afterglow was detected in GRB 910402 [36]. At $R > R_{\rm load}$ the front effects become small and the afterglow gradually fades according to the standard model. The whole afterglow evolution is shown in Figure 3.

The $\gamma$-ray front can strongly impact the deceleration radius [48], especially in the massive progenitor scenario where the standard model predicts $R_{\rm dec} \ll R_{\rm acc}$. The ejecta cannot decelerate until it approaches $R_{\rm acc}$, and one finds $R_{\rm dec} \approx R_{\rm acc}$. Then the peak of the afterglow is predicted at $t_{\rm peak} = R_{\rm acc}/(2\Gamma^2 c) = 12(E_\gamma/10^{53})^{1/2}(\Gamma/100)^{-2}$ s. A measured $t_{\rm peak}$ and $E_\gamma$ would allow one to evaluate $\Gamma$. The isotropic energy $E_\gamma$ is now known for about 20 bursts, however $t_{\rm peak}$ was not determined. The peak can be clearly observed in soft bands where the prompt GRB is not seen. In short GRBs with duration $\ll t_{\rm peak}$ the afterglow should also be separated from the prompt emission in time, and the peak could be noticed even in the BATSE data (at $h\nu > 20$ keV). A possible detection of such a peak at tens of seconds (an excess in a time-averaged profile of 76 short GRBs) was recently reported [49].

The early soft afterglow can be studied in optical, UV, and soft X-ray bands on timescales less than one minute. Normally, GRB observations in soft bands start hours or days after the prompt burst when only the decaying emission from $R > R_{\rm dec}$ can be observed. Attempts were made to detect prompt optical emission at $t_{\rm obs} \gtrsim$ 10 s and in one case (GRB 990123) such emission was detected [50]. The observed optical flash was expected to come from a reverse shock in a baryonic ejecta [51, 52]. In [48] an alternative interpretation was suggested: the soft flash is produced by the forward shock at its early stage when it propagates in the preaccelerated and $e^{\pm}$-loaded environment. In contrast to the reverse shock interpretation, the ejecta is not

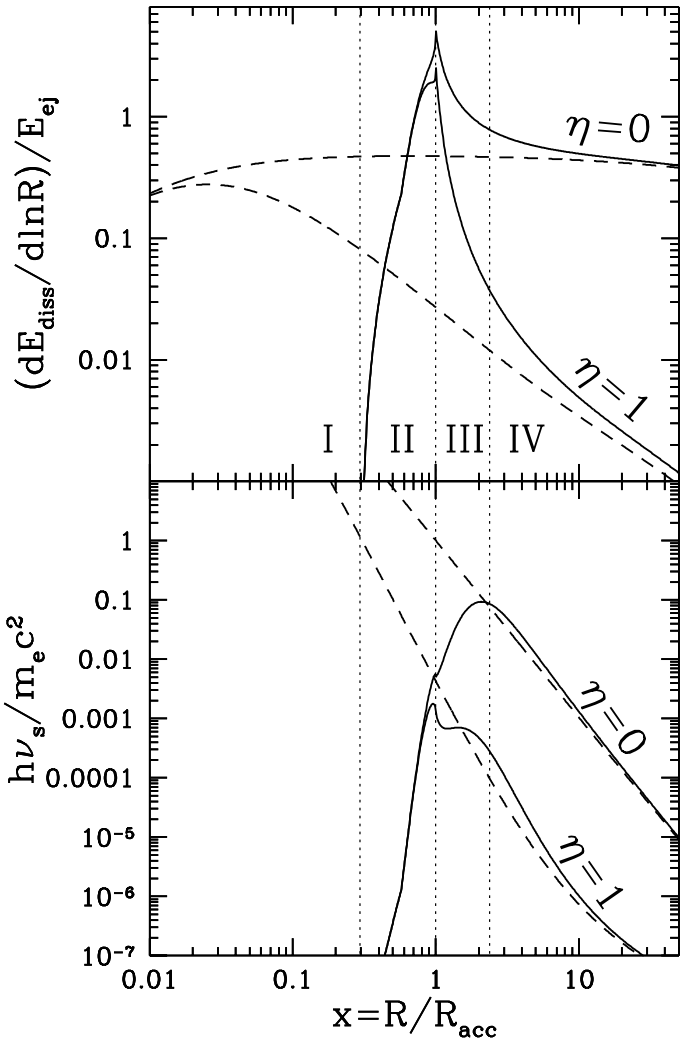


Figure 3: Afterglow from a GRB ejecta decelerating in a wind of a Wolf-Rayet progenitor with $\dot{M} = 2 \times 10^{-5} M_\odot$ yr$^{-1}$, $w = 10^3$ km s$^{-1}$. The GRB is modeled as an impulsive emission of a gamma-ray front (with isotropic energy $E_\gamma = 10^{53}$ erg) and a thin ejecta shell with kinetic energy $E_{\rm ej} = 10^{53}$ erg and Lorentz factor $\Gamma_{\rm ej} = 200$. Dashed curves show the prediction of the standard model that neglects the impact of the radiation front and solid curves show the actual behavior. Two extreme cases are displayed in the figure: $\eta = 0$ (adiabatic blast wave) and $\eta = 1$ (radiative blast wave). Four zones are marked: I — $R < R_{\rm gap}$ (the gap is opened), II — $R_{\rm gap} < R < R_{\rm acc}$ (the gap is closed and the ejecta sweeps the relativistically preaccelerated $e^\pm$-loaded ambient medium), III — $R_{\rm acc} < R < R_{\rm load}$ ($e^\pm$-loaded ambient medium with $\gamma \approx 1$), and IV — $R > R_{\rm load}$ (pair-free ambient medium with $\gamma \approx 1$). Radius is measured in units of $R_{\rm acc} = 0.7 \times 10^{16} (E_\gamma/10^{53})^{1/2}$ cm. *Top panel*: the dissipation rate. *Bottom panel*: the synchrotron peak frequency $\nu_s$ (assuming $\epsilon_B = 0.1$) in units of $m_e c^2/h$.

required to be baryonic — it may be a Poynting flux as well.

Prompt observations of GRBs in soft bands can help to understand the main early phase of the ejecta-medium interaction. A major future GRB mission is Swift (to be launched in 2003). It will provide optical/UV and soft X-ray data 20–70 s after the burst detection in hard X-rays. Unfortunately, this time may be too long to catch the early soft phase of afterglows. Quicker observations can be done with the proposed microsatellite ECLAIRs [53] which is devoted specifically to prompt GRB observations in optical and soft X-rays.

# 5 Concluding Remarks

Owing to the recent observational progress, the state of the GRB field has crucially transformed. In the beginning of 90s, $\sim 10^2$ theories did not contradict the data and were considered as principally possible; to a large extent the choice of a plausible theory was a matter of taste. The present situation is just opposite. GRBs have shown a mysterious complicated phenomenology with a number of well formulated observational facts. A successful theory is expected to make specific predictions that agree with the data on a quantitative level. The understanding of GRBs is far from such an ideal state, and the existing theories are rather naive and lacking a predictive power. Where models can fit the data (e.g. afterglow light curves) it is partially due to a large number of free parameters which ensure a sufficient flexibility of the model, and it does not make one confident that the simplifying assumptions are correct.

The difficulty of the GRB theory is well compensated by the recent observations which put more and more constraints. The observational progress may become even more impressive with additional channels of information such as neutrino and gravitational radiation. New exciting observations of electromagnetic radiation are expected from future missions — Swift and GLAST. It allows one to hope for a future theory that would clarify the physics of the explosion and answer the basic questions: (1) What is the progenitor and why does it collapse? (2) Where is the released gravitational energy channeled to before it starts to feed the outflow (energy of rotation, magnetic energy, heat?) (3) What is the composition of the ejecta ($e^{\pm}$, $p$, $n$, magnetic field?) and why are they so highly relativistic?

# References

[1] S. G. Djorgovski et al., in Gamma-Ray Bursts in the Afterglow Era: 2nd Workshop, N. Masetti et al., eds. (ESO Astrophysics Symposia, Berlin: Springer Verlag, in press, 2001), astro-ph/0107535

[2] G. J. Fishman, C. A. Meegan, ARA&A, **33**, 415 (1995)

[3] B. E. Stern, Ya. Tikhomirova, D. Kompaneets, R. Svensson, J. Poutanen, ApJ **563**, 80 (2001)

[4] J. van Paradijs, C. Kouveliotou, A. M. J. Wijers, ARA&A 38, 379 (2000)

[5] T. Piran, Phys. Rep. **314**, 575, 1999

[6] P. Mészáros, ARA&A **40** (2002, in press), astro-ph/0111170

[7] B. Paczynski, ApJ, **308**, L43 (1986)

[8] S. E. Woosley, ApJ **405**, 273 (1993)

[9] V. V. Usov, Nature **357**, 472 (1992)

[10] K. S. Cheng, Z. G. Dai, Phys. Rev. Lett. **77**, 1210 (1996)

[11] I. Bombaci, B. Datta, ApJ **530**, L69 (2000)

[12] Z.-Y. Li, R. A. Chevalier, in Supernovae and Gamma Ray Bursts, K. W. Weiler, ed. (Springer-Verlag, in press, 2002), astro-ph/0110002

[13] A. M. Beloborodov, B. E. Stern, R. Svensson, ApJ **535**, 158 (2000)

[14] B. E. Stern, ApJ **464**, L11 (1996)

[15] J. P. Norris et al., ApJ **459**, 393 (1996)

[16] E. E. Fenimore et al., ApJ **448**, L101 (1995)

[17] R. D. Preece et al., ApJS **126**, 19 (2000)

[18] L. Borgonovo, F. Ryde, ApJ **548**, 770 (2001)

[19] J. Heise, J. in't Zand, M. Kippen, P. Woods, in Gamma-Ray Bursts in the Afterglow Era, N. Masetti, ed. (Springer, in press, 2002), astro-ph/0111246

[20] B. Paczyński, ApJ **363**, 218 (1990)

[21] G. Cavallo, M. J. Rees, MNRAS **183**, 359 (1978)

[22] M. J. Rees, P. Mészáros, ApJ, **430**, L93 (1994)

[23] S. Kobayashi, T. Piran, R. Sari, ApJ **490**, 92 (1997)

[24] F. Daigne, R. Mochkovitch, MNRAS **296**, 275 (1998)

[25] A. M. Beloborodov, ApJ **539**, 25L (2000)

[26] A. M. Beloborodov, in Gamma-Ray Bursts in the Afterglow Era, N. Masetti, ed. (Springer, in press, 2002)

[27] D. Guetta, M. Spada, E. Waxman, ApJ, **559**, 10 (2001)

[28] S. Kobayashi, R. Sari, ApJ **551**, 934 (2001)

[29] G. Ghisellini, A. Celotti, ApJ **511**, 93L (1999)

[30] P. Mészáros, M. J. Rees, ApJ **530**, 292 (2000)

[31] N. M. Lloyd-Ronning, V. Petrosian, ApJ **565**, 182 (2002)

[32] M. Spada, A. Panaitescu, P. Mészáros, ApJ **537**, 824 (2000)

[33] C. Thompson, R. C. Duncan, ApJ **408**, 194 (1993)

[34] V. V. Usov, MNRAS **267**, 1035 (1994)

[35] F. Frontera et al., ApJS **127**, 59 (2000)

[36] A. Yu. Tkachenko et al., A&A **358**, L41 (2000)

[37] T. W. Giblin et al., ApJ **524**, L47 (1999)

[38] M. Vietri, G. Ghisellini, D. Lazzati, F. Fiore, L. Stella, ApJ **550**, L43 (2001)

[39] Blandford, R. D., & McKee, C. F. 1977, MNRAS, 180, 343

[40] Smolsky, M. V., & Usov, V. V. 2000, 531, 764

[41] R. Sari, T. Piran, R. Narayan, ApJ 497, L17 (1998)

[42] A. Panaitescu, P. Kumar, ApJ **560**, L49 (2001)

[43] J. E. Rhoads, ApJ **525**, 737 (1999)

[44] D. A. Frail et al., ApJ **562**, L55 (2001)

[45] D. A. Frail, S. R. Kulkarni, L. Nicastro, M. Feroci, G. B. Taylor, Nature **389**, 261 (1997)

[46] C. Thompson, P. Madau, ApJ **538**, 105 (2000)

[47] P. Mészáros, E. Ramirez-Ruiz, M. J. Rees, ApJ **554**, 660 (2001)

[48] A. M. Beloborodov, ApJ **565**, 808 (2002)

[49] D. Lazzati, E. Ramirez-Ruiz, G. Ghisellini, A&A **379**, L39 (2001)

[50] C. Akerlof et al., Nature **398**, 400 (1999)

[51] P. Mészáros, M. J. Rees, ApJ **418**, L59 (1993)

[52] R. Sari, T. Piran, ApJ **517**, L109 (1999)

[53] D. Barret et al., astro-ph/0109178

# Quark Stars and Color Superconductivity: A GRB connection ?

*Rachid Ouyed*
*Nordic Institute for Theoretical Physics (NORDITA)*
*Blegdamsvej 17*
*DK-2100 Copenhagen O, Denmark*

At this conference many interesting talks were presented on the plausible existence of Quark Stars. Other talks dealt with the exotic new phases of quark matter at very high density. Here, I show how combining these two elements might offer a new way of tackling the Gamma Ray Burst puzzle.

## 1 Introduction

It is widely accepted that the most conventional interpretation of the observed Gamma-ray bursts (GRBs) result from the conversion of the kinetic energy of ultra-relativistic particles to radiation in an optically thin region [1, 2, 3, 4]. The particles being accelerated by a fireball mechanism (or explosion of radiation) taking place near an unknown central engine [5, 6, 7]. The first challenge is to conceive of circumstances that would create a sufficiently energetic fireball. In the model presented in this talk, the approach is to make use of intrinsic properties of quark stars (where exotic phases of quark matter come into play) to account for the fireball.

Quark matter at very high density is expected to behave as a color superconductor (see Figure 1). A novel feature of such a phase (in the 2-flavor case; hereafter 2SC) is the generation of glueball like particles (hadrons made of gluons) which as demonstrated in [8] immediately decay into photons. If 2SC sets in at the surface of a quark star the glueball decay becomes a natural mechanism for a fireball generation; a mechanism which is fundamentally different from models where the fireball is generated via a collapse [9, 10, 11] or conversion (of neutron star to quark star [12, 13, 14]) processes. I will then show how and why quark stars might constitute new candidates for GRB inner engines [15].

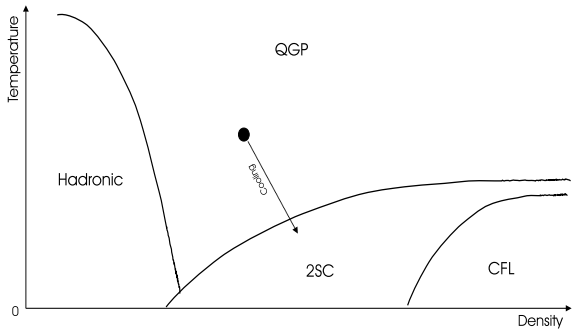


Figure 1: A schematic representation of a possible QCD phase diagram (see Alford in this volume). The arrow depicts a plausible cooling path of a quark star leading to the onset of color superconductivity in its surface.

# 2 Quark stars and the 2SC phase

We first assume that quark stars exists in nature (further discussed in §7.2; see also Heiselberg and Bombaci in this volume) and constitutes the first major assumption in our model.

## 2.1 Hot Quark stars

We are concerned with quark stars born with temperatures above $T_c$ (the critical temperature above which thermal fluctuations will wash out the superconductive state). We shall refer to these stars as "hot" quark stars (HQSs) in order to avoid any confusion with strange stars which are conjectured to exist even at zero pressure if strange matter is the absolute ground state of strong interacting matter rather than iron [16, 17, 18, 19, 20].

Among the features of HQSs relevant to our model [19, 21, 22, 23]:

i) The "surface" of a HQS is very different from the surface of a neutron star, or any other type of stars. Because it is bound by the strong force, the density at the surface changes abruptly from zero to $\rho_{HQS}$. The abrupt change (the thickness of the quark surface) occurs within about 1 fm, which is a typical strong interaction length scale.

ii) The electrons being bound to the quark matter by the electro-magnetic interaction and not by the strong force, are able to move freely across the quark surface extending up to $\sim 10^3$ fm above the surface of the star. Associated with this electron

layer is a strong electric field ($5 \times 10^{17}$ V/cm)- higher than the critical value ($1.3 \times 10^{16}$ V/cm) to make the vacuum region unstable to spontaneously create $(e^+, e^-)$ pairs.

iii) The presence of normal matter (a crust made of ions) at the surface of the quark star is subject to the enormous electric dipole. The strong positive Coulomb barrier prevents atomic nuclei bound in the nuclear crust from coming into direct contact with the quark core. The crust [24] is suspended above the vacuum region.

iv) One can show that the maximum mass of the crust cannot exceed $M_{crust} \simeq 5 \times 10^{-5} M_\odot$ set by the requirement that if the density in the inner crust is above the neutron drip density ($\rho_{drip} \simeq 4.3 \times 10^{11}$ g/cc), free neutrons will gravitate to the surface of the HQS and be converted to quark matter. This is due to the fact that neutrons can easily penetrate the Coulomb barrier and are readily absorbed.

## 2.2 2SC and Light GlueBalls (LGBs)

The 2SC phase is characterized by five out of the eight gluons acquiring mass. The 3 massless gluons bind into LGBs. In [8] we studied properties of these LGBs. Those relevant to our present study are :

i) The LGBs decay into photons with an associated lifetime of the order of $10^{-14}$ s.

ii) The mass of the LGBs is of the order of 1 MeV.

## 2.3 Cooling and 2SC layer formation

The HQS surface layer might enter the 2SC phase as illustrated in Figure 1. In the QCD phase diagram (Figure 2), ($\rho_{\mathbf{B_0}}$, $T_{\mathbf{B_0}}$) is the critical point beyond which one re-enters the Quark-Gluon-Plasma (QGP) phase - illustrating the extent of the 2SC layer into the star. The star consists of a QGP phase surrounded by a 2SC layer where the photons (from the LGB/photon decay) leaking from the surface of the star provides the dominant cooling source. This picture, as illustrated in Figure 2, is only valid if neutrino cooling in the 2SC phase is heavily suppressed as to become slower than the photon cooling. Unfortunately, the details of neutrino cooling in the 2SC phase is still a topic of debate and studies ([25, 26] to cite only few). One can only assume such a scenario which constitutes the second major assumption in our model. In §6.2, we discuss the remaining alternative when photon cooling is dwarfed by neutrino cooling.

## 2.4 LGB decay and photon thermalization

The photons from LGB decay are generated at energy $E_\gamma < T_c$ and find themselves immersed in a degenerate quark gas. They quickly gain energy via the inverse Compton process and become thermalized to $T_c$. We estimate the photon mean free path

to be smaller than few hundred Fermi [27, 28] while the 2SC layer is measured in meters (see §4.2). A local thermodynamic equilibrium is thus reached with the photon luminosity given by that of a black body radiation,

$$L_\gamma = 3.23 \times 10^{52} \text{ ergs s}^{-1} \ (\frac{R_{HQS}}{5 \text{ km}})^2 (\frac{T_c}{10 \text{ MeV}})^4 \ . \tag{1}$$

The energy for a single 2SC/LGBs event is thus

$$\Delta E_{LGB} = \delta_{LGB} M_{2SC} c^2, \tag{2}$$

where $M_{2SC} = \delta_{2SC} M_{HQS}$ is the portion of the star in 2SC. Here, $\delta_{2SC}$ depends on the star's mass while $\delta_{LGB}$ represent the portion of the 2SC that is in LGBs (intrinsic property of 2SC; see [8]). The photon emission/cooling time is then

$$\Delta t_{cool} = \frac{\epsilon M_{HQS} c^2}{L_\gamma} \ , \tag{3}$$

with $\epsilon = \delta_{2SC} \delta_{LGB}$.

# 3 Powering Gamma-Ray Bursts

## 3.1 Fireball and baryon loading

The fireball stems from the LGB decay and photon thermalization. The photons are emitted from the star's surface into the vacuum region beneath the inner crust ($\sim 10^3$ fm in size). Photon-photon interaction occurs in a much longer time than the vacuum region crossing time. Also, the cross-section for the creation of pairs through interactions with the electrons in the vacuum region is negligible ([27, 28]). The fireball energy is thus directly deposited in the crust. If its energy density, $aT_c^4$ (with $a$ being the radiation density constant), exceeds that of the gravitational energy density in the crust, energy outflow in the form of ions occurs. More specifically, it is the energy transfer from photons to electrons which drag the positively charged nuclei in the process. One can show that the condition

$$aT_c^4 > \frac{GM_{HQS}}{R_{HQS}} \rho_{crust} \ , \tag{4}$$

where $\rho_{crust}$ is the crust density and $G$ the gravitational constant, is equivalent to

$$(\frac{T_c}{30 \text{ Mev}})^4 > (\frac{M_{HQS}}{M_\odot})(\frac{5 \text{ km}}{R_{HQS}})(\frac{\rho_{crust}}{\rho_{drip}}) \ , \tag{5}$$

which is always true if $T_c > 30$ MeV. The fireball is thus loaded with nuclei present in the crust. Note that the 2SC layer is not carried away during the two-photon decay process because of the star's high gravitational energy density: $\rho_{HQS}/\rho_{drip} >> 1$.

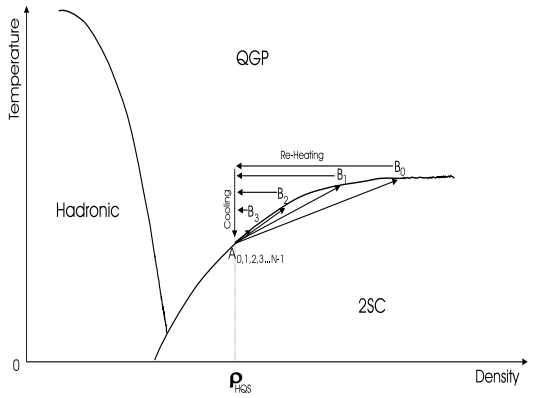


Figure 2: The episodic emission as illustrated in the QCD phase diagram. The 2SC front spreads deep inside the star and stops at $\mathbf{B_0}$ before re-entering the QGP phase. Following photon cooling, heat flows from the core and re-heats the surface. The star then starts cooling until $\mathbf{A_1}$ is reached at which point the stage is set for the 2SC/LGB/photon process to start all over again ($\mathbf{A_1} \rightarrow \mathbf{B_1}$) resulting in another emission.

## 3.2 Episodic behavior

The star's surface pressure is reduced following photon emission[1]. A heat and mass flux is thus triggered from the QGP phase to the 2SC layer re-heating (above $T_c$) and destroying the superconductive phase. The entire star is now in a QGP phase (5 gluons$\rightarrow$ 8 gluons at the surface) and hence the cooling process can start again. This corresponds to the transition $[\rho(\mathbf{B_0}), T(\mathbf{B_0})] \rightarrow [\rho_{HQS}, T(\mathbf{B_0})]$ in the QCD phase diagram (thermal adjustment). The stage is now set for the 2SC/LGB/photon process to start all over again resulting in another emission. For the subsequent emission, however, we expect the system to evolve to point $\mathbf{B_1}$ generally located at different densities and temperatures than $\mathbf{B_0}$. The cycle ends after $N$ emissions when $\rho(\mathbf{B_N}) \simeq \rho_{\rm HQS}$.

The time it takes to consume most of the star (the glue component) by this process is

$$t_{engine} \simeq \frac{M_{HQS}c^2}{L_\gamma} \simeq 1 \text{ s } (\frac{M_{HQS}}{M_\odot})(\frac{5 \text{ km}}{R_{HQS}})^2(\frac{30 \text{ MeV}}{T_c})^4 \ , \qquad (6)$$

which is representative of the engine's activity. The above assumes quick adjustment of the star following each event, but is not necessarily the case for the most massive

[1]The pressure gradient in the 2SC layer is $\Delta p \propto (8-5)T_c^4$ ([21]) where the massless gluons (3 out of 8) have been consumed by the LGB/photon process.

stars.

### 3.3 Multiple shell emission

The episodic behavior of the star together with the resulting loaded fireball (we call shell) offers a natural mechanism for multiple shell emission if $T_c < 30$ MeV. Indeed from eq(5) a higher $T_c$ value would imply extraction of the entire crust in a single emission and no loading of the subsequent fireballs. Clearly, $T_c < 30$ MeV must be considered if multiple ejections are to occur[2].

The fraction ($f$) of the crust extracted in a single event is,

$$\Delta M_{crust} = f M_{crust} \ . \tag{7}$$

The shell is accelerated with the rest of the fireball converting most of the radiation energy into bulk kinetic energy. The corresponding Lorentz factor we estimate to be,

$$\Gamma_{\rm shell} \simeq \frac{\epsilon M_{HQS}}{f M_{crust}} \ , \tag{8}$$

where we used eq(2) and eq(7). $\epsilon$ and $f$ depend on the star's mass and characterize the two emission regimes in our model.

## 4 The two regimes

When the inner crust density is the neutron drip value, one finds a minimum mass star of $\sim 0.015 M_\odot$. For masses above this critical value, the corresponding crusts are thin and light. They do not exceed few kilometers in thickness. Matter at the density of such crusts is a Coulomb lattice of iron and nickel all the way from the inner edge to the surface of the star ([24]). For masses below $0.015 M_\odot$, the crust can extend up to thousands of kilometers with densities much below the neutron drip. This allows us to identify two distinct emission regimes for a given $T_c$ ($< 30$ MeV).

### 4.1 Light stars ($M_{HQS} < 0.015 M_\odot$)

These are objects whose average density is $\sim \rho_{HQS}$ ($M_{HQS} \simeq \frac{4\pi}{3} R^3_{HQS} \rho_{HQS}$). The 2SC front extends deeper inside the star ($\delta_{2SC} \sim 1$). The star can be represented by

[2]Even if $T_c$ turns out to be greater than 30 MeV, in which case the entire crust will be blown away (eq(5)), one can imagine mechanisms where crust material is replenished. By accretion, for instance, if the HQS is part of a binary. There are also geometrical considerations where asymmetric emission/ejection can occur due to the rapid rotation of Quark Stars; here only a portion of the crust is extracted at a time. This aspect of the model requires better knowledge of the conditions and environments where HQSs are formed.

a system close to $\mathbf{A_0}$ in Figures 2. Each of the few emissions (defined by $\epsilon$) is thus capable of consuming a big portion of the star. Furthermore, the entire crust material can be extracted in a few 2SC/LGB/photon cycles ($\rho_{crust}/\rho_{drip} \ll 1$).

Using eq(6), the few emissions lead to

$$\begin{aligned} t_{tot} &\simeq \text{fraction} \times t_{engine} \\ &\simeq \text{fraction} \times 0.25 \text{ s } (\frac{M_{HQS}}{0.01\ M_\odot})(\frac{1 \text{ km}}{R_{HQS}})^2(\frac{30 \text{ MeV}}{T_c})^4 \ , \end{aligned} \tag{9}$$

where $t_{tot}$ is representative of the observable time which takes into account the presence of the crust.

## 4.2 Massive stars ($M_{HQS} \geq 0.015 M_\odot$)

The surface density of a massive star being that of a light star, defines a standard unit in our model. In other words, the mass of the 2SC layer in a massive star case is

$$\Delta M_{2SC,m} \simeq M_{2SC,l} \ , \tag{10}$$

where "$m$" and "$l$" stand for massive and light, respectively. It implies

$$\frac{\Delta R_{2SC,m}}{R_{2SC,m}} \simeq \frac{1}{3}(\frac{R_l}{R_m})^3 \simeq \frac{1}{3}(\frac{1 \text{ km}}{5 \text{ km}})^3 \simeq 0.003 \ . \tag{11}$$

For a typical star of 5 km in radius, we then estimate a 2SC layer of about 15 meters thick (much larger than the photon mean free path thus justifying the local thermal equilibrium hypothesis). Equivalently,

$$\overline{\epsilon} = \frac{M_l}{M_m} \simeq (\frac{1 \text{ km}}{5 \text{ km}})^3 \simeq 0.01 \ , \tag{12}$$

where $\overline{\epsilon}$ is the average value. This naturally account for many events (or $N$ fireballs). The average number of fireballs with which an entire star is consumed is thus

$$N \simeq \frac{1}{\overline{\epsilon}} \simeq 100 \ . \tag{13}$$

Since most of the crust is at densities close to the neutron drip value, eq(5) implies that only a tiny part of the crust surface material (where $\rho_{crust} << \rho_{drip}$) can be extracted by each of the fireballs. This allows for a continuous loading of the fireballs.

The total observable time in our simplified approach is thus,

$$t_{tot} \simeq t_{engine} = 1 \text{ s } (\frac{M_{HQS}}{M_\odot})(\frac{5 \text{ km}}{R_{HQS}})^2(\frac{30 \text{ MeV}}{T_c})^4 \ . \tag{14}$$

We isolated two regimes:

(i) Light stars $\Rightarrow$ short emissions.

(ii) Massive stars $\Rightarrow$ long emissions.

It appears, according to BATSE (Burst and Transient Source Experiment detector on the COMPTON-GRO satellite), that the bursts can be classified into two distinct categories: short ($< 2$ s) bursts and long ($> 2$ s, typically $\sim 50$ s) bursts. The black body behavior ($T_c^4$) inherent to our model puts stringent constraints on the value of $T_c$ which best comply with these observations. Using $T_c \simeq 10$ MeV, from eq(9) and eq(14) we obtain in the star's rest frame

$$t_{tot} \simeq 81 \text{ s } (\frac{M_{HQS}}{M_\odot})(\frac{5 \text{ km}}{R_{HQS}})^2 \ , \tag{15}$$

for massive stars (suggestive of long GRBs), and

$$t_{tot} \simeq 2 \text{ s } (\frac{M_{HQS}}{0.01 \ M_\odot})(\frac{1 \text{ km}}{R_{HQS}})^2 \ , \tag{16}$$

for light stars (suggestive of short GRBs). There is a clear correlation (almost one to one) between the observed burst time and the time at which the source ejected the specific shell (see Figure 3 in [**?**], for example). Note that $T_c \simeq 10$ MeV implies that only a portion of the crust is extracted. This is also consistent with our previous assumption ($T_c < 30$ MeV) and subsequent calculations.

Eq(15) and eq(16) is simply eq(6) rescaled to the appropriate object size. We separated two regimes due to intrinsic differences in the engine and the crust. From the engine point of view, massive stars generate many more emissions when compared to light ones, and no substantial reduction of the engine time is expected because of the omni-presence of the crust. Another important difference is related to the physics of the multiple re-adjustments following each event which is more pronounced for very massive stars. The latter among other factors is related to $\epsilon$ which can vary from one event to another.

# 5 Features and predictions

## 5.1 GRB energies

The maximum available energy is when the heaviest HQS ($M_{HQS,max} \simeq 2M_{\odot}$) is entirely consumed. That is,

$$E_{LGB,max} \simeq 4 \times 10^{54} \text{ ergs} . \tag{17}$$

The corresponding GRB energy is

$$E_{GRB,max} \simeq 1.6 \times 10^{54} \text{ ergs} , \tag{18}$$

where we used a fiducial conversion efficiency of 40%.

Since $M_{HQS,min} < 0.015 M_{\odot}$ we conclude that,

$$E_{LGB,min} < 3 \times 10^{52} \text{ ergs} , \tag{19}$$

implying

$$E_{GRB,min} < 1.2 \times 10^{52} \text{ ergs} . \tag{20}$$

## 5.2 GRB total duration

From eq(15) and eq(16) we have

$$t_{tot} \simeq 81 \text{ s} , \tag{21}$$

for typical massive stars, and

$$t_{tot} \simeq 2 \text{ s} , \tag{22}$$

for typical light stars.

Our estimate of the duration time for the massive star case should be taken as a lower limit. As we have said, a complete model should take into account star re-adjustments. Nevertheless, we can still account for a wide range in GRB duration by an appropriate choice of different values of the mass and radius.

# 6 Discussion and Conclusion

## 6.1 Existence and formation of HQSs

In the last few years, thanks to the large amount of fresh observational data collected by the new generation of X-ray and $\gamma$-ray satellites, new observations suggest that the compact objects associated with the X-ray pulsars, the X-ray bursters, particularly the SAX J1808.4-3658, are good quark stars candidates (see Bombaci in this volume

and [29]). If one assumes that these plausible quark stars form via the "standard" supernova mechanism or by conversion of neutron stars then the two regimes (Heavy and Light stars) discussed in our model are difficult to account for. It has been argued however that quark stars formation mechanisms may be numerous and "exotic" (early discussions can be found in [30, 23]). In the case of 4U 1728-34 (where a mass of less than $1.0M_{\odot}$ was derived; [14]), it seems that accretion-induced collapse of white dwarfs is a favored formation mechanism. If the quark star formed via the direct conversion mechanism then it required too much mass (at least $\sim 0.8M_{\odot}$ to be ejected during the conversion). Other formation scenarios are discussed in [31, 32].

## 6.2 Neutrino cooling and HQSs

If it turns out that neutrino cooling is still very efficient in the 2SC phase, one must consider the scenario where the entire HQS enters the 2SC phase (for comparison of cooling paths between quark stars and neutron stars and the plausible effects of 2SC on cooling we refer the interested reader to [26, 33, 34]). Here, the 2SC/LGB/photon process (the fireball) occurs only once and inside the entire star. Furthermore, one must involve more complicated physics (such as that of the crust) to account for the episodic emissions so crucial to any model of GRBs. It is not clear at the moment how to achieve this goal and is left as an avenue for future research.

## 6.3 2SC-II stars

The 2SC/LGB/photon process might proceed until one is left with an object made entirely of 2SC. We name such objects *2SC-II* stars[3] which are still bound by strong interactions (their density is constant $\sim \rho_{HQS}$). 2SC-II stars carry an Iron/Nickel crust left over from the GRB phase. The crust mass range is $0 < M_{2SC,crust} < 5 \times 10^{-5} M_{\odot}$ depending on the efficiency of crust extraction/ejection during the GRB phase.

BATSE observes on average one burst per day. This corresponds, with the simplest model - assuming no cosmic evolution of the rate - to about once per million years in a galaxy [3]. In the Milky way we thus expect up to $10^5$ of 2SC-II stars. Nevertheless, they are tiny enough ($M \leq 10^{-2} M_{\odot}$, $R \leq 1$ km) to be difficult to detect.

## 6.4 The Mass−Radius Plane

Take observed GRBs with known energies and total duration. From the burst total energy $E_{GRB} \simeq 0.4Mc^2$ we derive the mass while the burst total duration ($t_{tot}$) gives

[3]The "II" in 2SC is a simple reminder of the final state of the star, namely the 2SC with only 5 gluons.

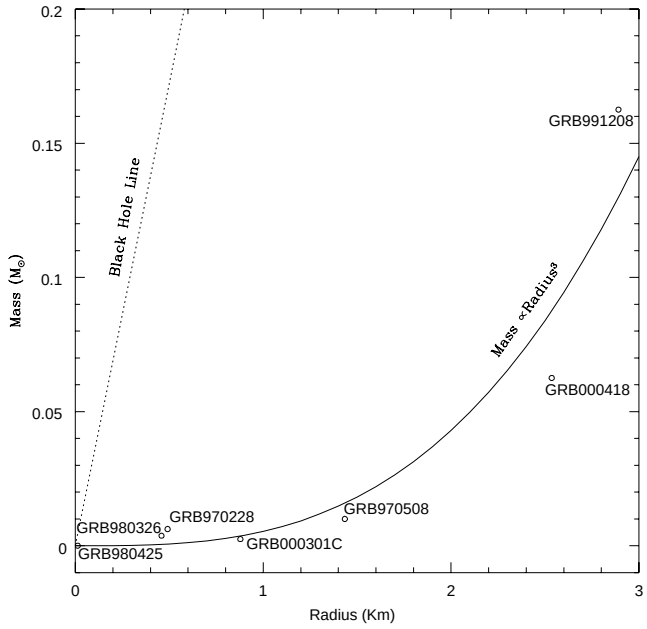


Figure 3: The Mass−Radius plane derived in our model using few existing GRBs with known energies and total duration. The solid curve shows the $M_{HQS} = \frac{4\pi}{3}\rho_{HQS}R^3_{HQS}$ equation for $\rho_{HQS} \simeq 9\rho_N$.

us the radius (using eq(14) with $T_c \simeq 10$ MeV). In Figure 3 we plot the resulting Mass−Radius. The solid curve shows the $M_{HQS} = \frac{4\pi}{3}\rho_{HQS}R^3_{HQS}$ equation which is a reasonable approximation for HQSs. While the GRB data set used is limited nevertheless it seems to support the idea that extremely compact objects ($M \propto R^3$) are behind GRBs activity within our model.

# References

[1] Kouveliotou, C., Briggs, M. S., and Fishman, G. J., (Eds), Gamma Ray Bursts, AIP Conf. Proc., 384 (AIP, New York, 1995)

[2] Kulkarni, S. R., et al., Nature, **398**, 389 (1999)

[3] Piran, T., Phys. Rev., **314**, 575 (1999a)

[4] Piran, T., in Gamma-Ray Bursts: The first three minutes, ASP Conference Series, Vol. 190, eds. J. Poutanen and R. Svensson, 3 (1999b)

[5] Goodman, J., ApJ, **308**, L47 (1986)

[6] Shemi, A., and Piran, T., ApJ, **365**, L55 (1990)

[7] Paczyński, B., ApJ, **363**, 218 (1990)

[8] Ouyed, R., and Sannino, F., Phys. Lett. **B511**, 66 (2001a)

[9] Blandford, R. D., and Znajek, R. L., MNRAS, **179**, 433 (1977)

[10] Ruffert, M., and Janka, H. -T., A&A, **344**, 573 (1999)

[11] Janka, H. -T., Eberl, T., Ruffert, M., and Fryer, C., ApJ, **527**, L39 (1999)

[12] Olinto, A., Phys. Lett. **B192**, 71 (1987)

[13] Cheng, K. S., and Dai, Z. G., Phys. Rev. Lett., **77**, 1210 (1996)

[14] Bombaci, I, and Datta, B., ApJ, **530**, L69 (2000)

[15] Ouyed, R., and Sannino, F., A&A, in press [astro-ph/0103022] (2001b)

[16] Bodmer, A. R., Phys. Rev. **D4**, 1601 (1971)

[17] Witten, E., Phys. Rev. **D30**, 272 (1984)

[18] Haensel, P., Zdunik, J. L., and Schaefer, R., A&A, **160**, 121 (1986)

[19] Alcock, C., Farhi, E., and Olinto, A., ApJ, **310**, 261 (1986)

[20] Dey, M., Bombaci, I., Dey, J., Ray, S., and Samanta, B. C., Phys. Lett. **B438**, 123 (1998)

[21] Farhi, E., and Jaffe, R. L., Phys. Rev. **D30**, 2379 (1984)

[22] Glendenning, N. K., and Weber, F., ApJ, **400**, 647 (1992)

[23] Glendenning, N. K., Compact stars (Springer, 1997)

[24] Baym, G., Pethick, C. J., and Sutherland, P. G., ApJ, **170**, 299 (1971)

[25] Carter, G. W., and Reddy, S., hep-ph/0005228

[26] Schaab, C., Hermann, B., Weber, F., and Manfred, K., ApJ, **480**, L111 (2000)

[27] Rybicki, G. B., and Lightman, A. P. Radiative processes in astrophysics (Wiley, 1979)

[28] Longair, M. S., High energy astrophysics (Cambridge Univ. Press, 1992)

[29] Li, et al., Phys. Rev. Lett., **83**, 3776 (1999)

[30] Alpar, A. M., Phys. Rev. Lett, **58**, 2152 (1987)

[31] Hong, D. K., Hsu, S. D. H., and Sannino, F., Phys. Lett. B, in press (hep-ph/0107017)

[32] Ouyed, R., Dey, J., and Dey, M., astro-ph/0105109

[33] Blaschke, D., Klähn, T., and Voskresensky, D. N., ApJ, **533**, 406 (2000)

[34] Blaschke, D., Grigorian, H., and Voskresensky, D. N., A&A, **368**, 561 (2001)

Axel Brandenburg enjoying the wine before dinner.

Paul Hoyer (right; NORDITA director) and Greg Carter in a conversation while Tsvi Piran and Shmulig Balberg (left) salute the photographer.

Wolfgang Schaefer (left) entertaining the students (from left to right) Jonas Larson, Miguel de ValBorro and Patrick Motylinski (right).


The editors: Rachid Ouyed (left) and Francesco Sannino.

Ignazio Bombaci (right) and Jorge Horvath (no comments!).

From Left to Right: Patrick Motylinski, Andrei Beloborodov Gulli Bjornsson and Lars Melwyn Jensen waiting for dessert.

Holger Bech Nielsen (left) and Rachid Ouyed caught on camera.

From Left to Right: Students Michael Svart Jorgensen, Jan Erling Staff.

# Program

# Compact Stars in the QCD Phase Diagram Scientific Program

Monday, August 15, 2001

| | | |
|---|---|---|
| *13:50* | *Welcome* | Dmitri Diakonov (NORDITA) |
| **From Neutron Stars to Quark Stars** | | **Chair**: Dmitri Diakonov |
| 14:00 | Neutron Star Masses, Radii and Equation of State | Henning Heiselberg (NORDITA) |
| 15:00 | Diquark properties and the TOV equations | Sverker Fredriksson (Lulea Tech.) |
| *15:30* | *Coffee Break* | |
| 16:00 | Strange star candidates in low mass X-ray binaries | Ignazio Bombaci (Pisa) |
| 16:30 | Diquarks degrees of freedom in the EOS and the compactness of compact stars | Jorge Horvath (Sao Paulo) |
| | | **Chair**: Jes Madsen |
| 09:00 | From Neutron Stars to Strange Stars | Fridolin Weber (Notre Dame) |
| 10:00 | Tensor correlations and Pions in dense nuclear matter | Chris J. Pethick (Nordita) |
| *10:30* | *Coffee Break* | |
| 11:00 | The observational appearance of strange stars | Vladimir V. Usov (Weizmann Inst.) |
| 12:00 | Structure of rapidly rotating strange stars: salient differences with neutron stars | Arun V. Thampan (SISSA) |
| *12:30* | *Lunch Break* | |
| **The QCD Phase Diagram** | | **Chair**: Francesco Sannino (NORDITA) |
| 14:00 | The QCD Phase Diagram and Explosive Astrophysics | Stephen D.H. Hsu (Oregon) |
| 15:00 | Crystalline Color Superconductivity in Dense Matter | Deog-Ki Hong (Pusan) |

*15:30 Coffee Break*

| | | |
|---|---|---|
| 16:00 | Effective description of QCD at high density | Roberto Casalbuoni (Firenze) |
| 16:30 | Effective Theory for QCD in the LOFF Phase | Giuseppe Nardulli (Bari) |

**Chair**: Roberto Casalbuoni

| | | |
|---|---|---|
| 09:00 | Color superconducting quark matter in compact stars | Mark Alford (Glasgow) |
| 10:00 | Color Superconductivity and Blinking Proto-Neutron Stars | Greg W. Carter (Stony Brook) |

*10:30 Coffee Break*

| | | |
|---|---|---|
| 11:00 | Color-flavor locking in strange stars, strangelets, and cosmic rays | Jes Madsen (Aarhus) |
| 12:00 | Confinement and domain walls in high density quark matter | Dam T. Son (Columbia) |

*12:30 Lunch Break*

Chair: Dam T. Son (Columbia)

| | | |
|---|---|---|
| 14:00 | Introduction to effecive Lagrangians for QCD | Joseph Schechter (Syracuse) |
| 15:00 | A Colored Zoo of Quasi-particles and Light Glueballs | Francesco Sannino (NORDITA) |

*15:30 Coffee Break*

16:00 Student Session

**The Gamma Ray Burst Connection**

**Chair**: Vladimir V. Usov

| | | |
|---|---|---|
| 09:00 | Gamma Ray Bursts | Tsvi Piran (Hebrew) |

*10:30 Coffee Break*

| | | |
|---|---|---|
| 11:00 | Prompt Emission and Early Afterglows of Gamma-Ray Bursts | Andrei M. Beloborodov (CITA) |
| 12:00 | Quark Stars and Color Superconductivity: A GRB connection ? | Rachid Ouyed (NORDITA) |

11:30 Student Session

*12:30* *Lunch Break*

14:00 Discussion Panel

# Contributed Papers

# Papers Contributed to Compact Stars in the QCD Phase Diagram

| | | |
|---|---|---|
| Mark, Alford | hep-ph/0110150 | Color superconducting quark matter in compact stars |
| Andrei, Beloborodov | astro-ph/0201321 | Prompt Emission and Early Afterglows of Gamma-Ray Bursts |
| Ignazio, Bombaci | astro-ph/0201369 | Strange star candidates |
| Greg, Carter | hep-ph/0111353 | Color Superconductivity and Blinking Proto-Neutron Stars |
| Roberto, Casalbuoni | hep-ph/0110107 | Effective description of QCD at high density |
| Sverker, Fredriksson | astro-ph/0111587 | Diquark Properties and the TOV Equations |
| Henning, Heiselberg | astro-ph/0201465 | Neutron Star Masses, Radii and Equation of State |
| Deog-Ka, Hong | hep-ph/0112028 | Crystalline Color Superconductivity in Dense Matter |
| Steve, Hsu | hep-ph/0111049 | The QCD Phase Diagram and Explosive Astrophysics |
| Jorge, Horvath | astro-ph/0112159 | Diquark degrees of freedom in the EOS and the compactness of compact stars |
| Jes, Madsen | hep-ph/0111417 | Color-flavor locking in strange stars, strangelets, and cosmic rays |
| Giuseppe, Nardulli | hep-ph/0111178 | Effective Theory for QCD in the LOFF Phase |
| Rachid, Ouyed | astro-ph/0201408 | Quark Stars and Color Superconductivity: A GRB connection ? |
| Chris, Pethick | astro-ph/0203011 | Tensor correlations and Pions in dense nuclear matter |
| Tsvi, Piran | astro-ph/0202403 | How to Construct a GRB Engine? |
| Francesco, Sannino | hep-ph/0112029 | A Colored Zoo of Quasi-particles and Light Glueballs |
| Joseph, Schechetr | hep-ph/0112205 | Introduction to effective Lagrangians for QCD |
| Dam Thanh, Son | hep-ph/0112068 | Confinement and domain walls in high density quark matter |
| Arun, Thampan | astro-ph/0111604 | Structure of rapidly rotating strange stars: salient differences from neutron stars |
| Vladimir, Usov | astro-ph/0111442 | The observational appearance of strange stars |
| Fridolin, Weber | astro-ph/0112058 | From Neutron Stars to Strange Stars |

# Participants

# Compact Stars in the QCD Phase Diagram Participants

| | |
|---|---|
| Shmulik, Balberg | Hebrew University |
| Andrei, Beloborodov | Stockholm Observatory |
| Gunnulaugur, Bjornsson | University of Iceland |
| Ignazio, Bombaci | Pisa University |
| Axel, Brandenburg | Nordita |
| Greg, Carter | Stony Brook |
| Roberto, Casalbuoni | Firenze University |
| Dmitri, Diakonov | Nordita |
| Wolfgang, Dobler | NewCastle University |
| Sverker, Fredriksson | Lulea Techincal University |
| Oskar, Halldorsson | Reykjavik University |
| Henning, Heiselberg | Nordita |
| Jens, Hjorth | Niels Bohr Institute |
| Deog-Ka, Hong | Pusan National University |
| Steve, Hsu | Oregon University |
| Jorge, Horvath | Sao Paulo University |
| Michael Svart, Jorgensen | Copenhagen University |
| Sushan, Konar | IUCAA |
| Jonas, Larson | Aarhus University |
| Jes, Madsen | Aarhus University |
| Massimo, Mannarelli | Bari University |
| Nils, Marchal | Nordita |
| Patrick, Motylinski | Aarhus University |
| Giuseppe, Nardulli | Bari University |
| Agnes, Nyiri | Bergen University |
| Chris, Pethick | Nordita |
| Tsvi, Piran | Hebrew University |
| Rachid, Ouyed | Nordita |
| Felix, Ryde | Stanford |
| Francesco, Sannino | Nordita |
| Wolfgang, Schaefer | Nordita |
| Joseph, Schechetr | Syracuse University |
| Dam Thanh, Son | Columbia University |
| Jan, Staff | Copenhagen University |
| Yasutaka, Takanishi | The Niels Bohr Institute |
| Arun, Thampan | IUCAA |
| Vladimir, Usov | Hebrew University |
| Fridolin, Weber | University of Notre Dame |
| Miguel, de Val Borro | Stockholm Observatory |

# Author Index